Title

Fuel Cell Handbook

Authors

Kinoshita, K
McLarnon, F R
Cairns, E J

Publication Date

1988-09-01

FUEL CELL HANDBOOK

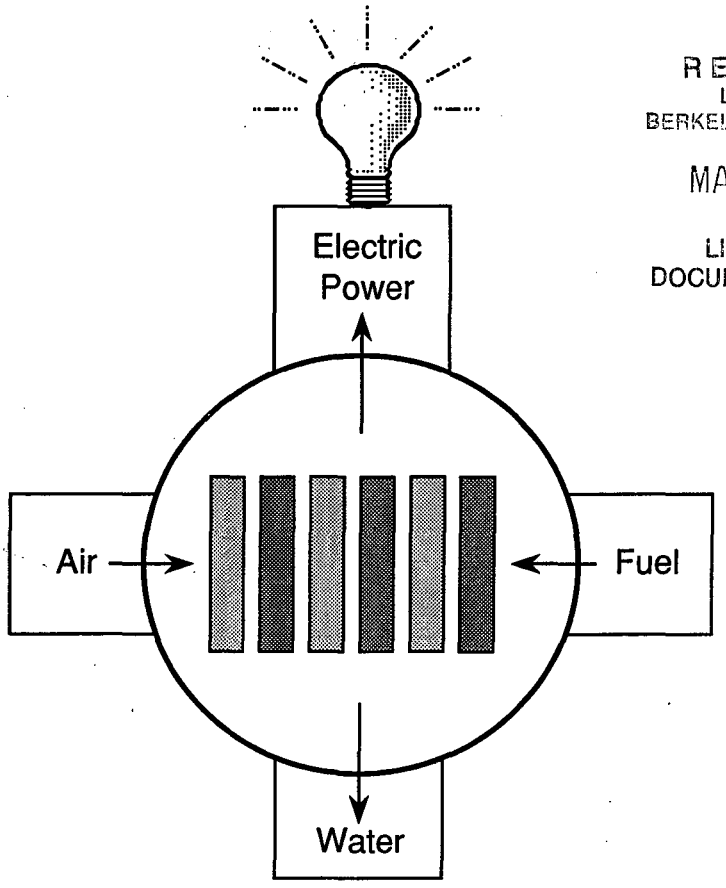

K. Kinoshita, F.R. McLarnon and E.J. Cairns

Applied Science Division
Lawrence Berkeley Laboratory
Berkeley, California 94720

September 1988

Prepared for the U.S. Department of Energy under Contract DE-AC03-76SF00098

DISCLAIMER

FUEL CELL HANDBOOK

by

K. Kinoshita
F.R. McLarnon
E.J. Cairns

Applied Science Division
Lawrence Berkeley Laboratory
1 Cyclotron Road
Berkeley, California 94720

for

U.S. Department of Energy
Office of Fossil Energy
Morgantown Energy Technology Center
P.O. Box 880
Morgantown, West Virginia 26505

This work was supported by the U.S. Department of Energy, Morgantown Energy Technology Center, Fuel Cell Projects Branch, through the Assistant Secretary for Fossil Energy, U.S. Department of Energy under Contract Number DE-AC03-76SF00098.

PREFACE

The past two decades have provided exciting opportunities for fuel cell technology. Both the alkaline and polymer electrolyte fuel cells have demonstrated their capabilities in the Apollo and Gemini Space Programs. Concurrently, major efforts were underway to develop fuel cells for terrestrial applications, with the early emphasis on the development of phosphoric acid fuel cells for generation of base-load power and on-site power. Now more recently, there is strong interest in fuel cells for transportation (propulsion) applications.

There are numerous opportunities where fuel cells could provide a feasible alternative to existing technologies. However, for fuel cells to displace existing technologies require that information on the characteristics and benefits of fuel cells be widely known before a rational decision can be made. Many avenues are available to disseminate public information on the various fuel cell technologies, among them are seminars, workshops, review meetings and technical society meetings. In addition various publications serve to document research and development activities on fuel cells. The purpose of the *Fuel Cell Handbook* is to present information that describes fuel cells which is helpful to scientists, engineers and technical managers who are not experienced in this technology, as well as to provide an update on the current technical status of the various types of fuel cells. Through this publication and related documents, it is hoped that a better appreciation of fuel cell technologies and their potential applications will be obtained.

In 1980 the Institute of Gas Technology published the *Handbook of Fuel Cell Performance* under the sponsorship of the U.S. Department of Energy. This publication served as the genesis for the current Handbook which updates the developments in fuel cell technology since about 1980. Much of the terminology and format in the original Handbook has been retained to provide continuity between the two versions. Several topics that were discussed in the original Handbook, such as the sample calculations and extensive discussion on fuel cell efficiencies were eliminated, and other topics, such as solid oxide, alkaline and polymer electrolyte fuel cells are presented in the updated Handbook.

ACKNOWLEDGEMENT

The authors would like to acknowledge the cooperation of the fuel cell community for their contributions to this Handbook. Many of our colleagues provided information, references, etc., valuable suggestions, and constructive comments which were incorporated in the Handbook. In addition the assistance of our colleagues who reviewed the chapters was helpful in updating the status of the various fuel cell technologies. In particular we would like to acknowledge the contributions of the following individuals: J. Appleby (Texas A&M Univ.), D. Fee (ANL), A. Fickett (EPRI), E. Gillis (EPRI), J. Giner (Giner, Inc.), G. Hagey (DOE), M. Hsu (ZTEK Corporation), J. Huff (LANL), V. Jalan (ElectroChem Inc.), A. Jones (Westinghouse Electric Co.), V. Kolba (ANL), M. Krumpelt (ANL), A. LaConti (Giner, Inc.), L. Marianowski (IGT), H. Maru (ERC), C. Pax (DOE), D. Pierce (ANL), A. Pigeaud (ERC), J. Rudnicki (LBL), D. Scarpiello (GRI), R. Selman (IIT), D. Shores (Univ. of Minnesota), S. Singhal (Westinghouse Electric Co.), K. Trimble (GRI), N. Vanderborgh (LANL), M. Warshay (NASA-Lewis) and G. Wilemski (Physical Sciences, Inc.). The assistance of Susan Lauer (LBL) at various stages of preparation of the manuscript is gratefully acknowledged.

The authors wish to thank Douglas Jewell of the Morgantown Energy Technology Center, U.S. Department of Energy (METC/DOE), for his support and encouragement, and for providing the opportunity to write this Handbook. Technical staff members at METC/DOE, David Berry, Edward Beyma, James Copley, Thomas George, William Huber, Gary Nelkin and Charles Zeh, are gratefully acknowledged for their suggestions and comments during this project.

This work was supported by the U.S. Department of Energy, Morgantown Energy Technology Center, Fuel Cell Projects Branch, through the Assistant Secretary for Fossil Energy, U.S. Department of Energy under Contract Number DE-AC03-76SF00098.

CONTENTS

List of Figures

List of Tables

List of Symbols

Abbreviations

AFC	alkaline fuel cell
COE	cost of electricity
DOE	Department of Energy
EVD	electrochemical vapor deposition
HHV	higher heating value
HR	heat rate
IRMCFC	internal-reforming molten carbonate fuel cell
LHV	lower heating value
MCFC	molten carbonate fuel cell
OS/IES	on-site/integrated energy systems
PAFC	phosphoric acid fuel cell
PC	phthalocyanines
PEFC	polymer electrolyte fuel cell
PTFE	polytetrafluoroethylene
SOFC	solid oxide fuel cell
TAA	tetraazaannulenes
TFMSA	trifluoromethane sulfonic acid
TMPP	tetramethoxyphenylporphyrins
TPP	tetraphenylporphyrins

Roman Letters

a	coefficient
a	$(-2.3RT/\alpha nF) \log i_o$
b	coefficient
b	$2.3RT/\alpha nF$
b	Tafel slope
C_B	bulk concentration
C_p	heat capacity
C_S	surface concentration
c	coefficient
D	diffusion coefficient
D	pore diameter
<D>	equilibrium pore size
E^o	standard potential
E	equilibrium (reversible) potential
ΔE	potential difference
E_a	activation energy

F	Faraday's constant
f	gas flow rate
ΔG	Gibbs free energy
ΔH_c	heat available from combustion of fuel gas
ΔH_r	enthalpy of reaction
I	current
i	current density
i_L	limiting current density
i_o	exchange current density
K	equilibrium constant
$k(T)$	constant, function of temperature
n	number of electrons participating in a reaction
n_{max}	maximum stoichiometric value
P	pressure
P_i	partial pressure
P_T	total pressure
R	cell resistance
R	gas constant
ΔS_r	entropy of reaction
T	temperature
t	electrolyte thickness
U	utilization
V	cell voltage
V	volume
V_c	voltage of single cell
v	rate at which reactant species are consumed
W_{el}	maximum electrical work
X	mole fraction

Greek Letters

α	transfer coefficient
β	hydrogen utilization
Γ	mole fraction
γ	interfacial surface tension
γ	oxidant utilization
δ	diffusion layer thickness
ε_c	Carnot efficiency
ε_E	electrochemical efficiency
ε_F	Faradaic efficiency
ε_{FC}	fuel cell efficiency
ε_H	heating value efficiency
ε_I	current efficiency
ε_S	fuel cell system efficiency
ε_{Th}	thermal efficiency

ε_V	voltage efficiency
η_{act}	activation polarization
η_{conc}	concentration polarization
η_{dohm}	ohmic polarization
θ	electrolyte contact angle
θ_{CO}	CO coverage

Subscript

a	anode
c	cathode
e	electrolyte
i	species i
in	cell inlet
out	cell outlet
p	pressure
T	temperature

1. INTRODUCTION TO FUEL CELLS

1.1 Objective and Scope of the Fuel Cell Handbook

Fuel cells are electrochemical devices that convert the chemical energy of a reaction directly into electrical energy. In a typical fuel cell, gaseous fuels are fed continuously to the anode (negative electrode) compartment and an oxidant (i.e., oxygen from air) is fed continuously to the cathode (positive electrode) compartment; the electrochemical reactions take place at the electrodes to produce an electric current. A fuel cell differs from a typical battery in several respects. The battery is an energy storage device, that is, the maximum energy that is available is determined by the amount of chemical reactant stored in the battery itself. Thus, the battery will cease to produce electrical energy when the chemical reactants are consumed (i.e., discharged). In a secondary battery, the reactants are regenerated by recharging, which involves putting energy into the battery from an external source. The fuel cell, on the other hand, is an energy conversion device, which theoretically has the capability of producing electrical energy for as long as the fuel and oxidant are fed to the electrodes. In reality, degradation or malfunction of components limits the practical operating life of fuel cells.

A variety of fuel cells have been developed, and they are usually classified according to the type of electrolyte used in the cells; these include (i) polymer electrolyte fuel cell (PEFC), (ii) alkaline fuel cell (AFC), (iii) phosphoric acid fuel cell (PAFC), (iv) molten carbonate fuel cell (MCFC) and (v) solid oxide fuel cell (SOFC). These fuel cells are listed in the approximate order of increasing operating temperature, ranging from ~80°C for PEFC, ~100°C for AFC, ~200°C for PAFC, ~650°C for MCFC and ~1000°C for SOFC. The fuel cells of current importance for near-term commercialization are the PAFC, MCFC and SOFC.

Fuel cells provide a new and exciting option for the efficient conversion of fossil fuels to electricity. Commercial development of fuel-cell technology has been underway in the United States for over 20 years, with the U.S. Government playing a prominent role. The Assistant Secretary for Fossil Energy of the U.S. Department of Energy (DOE) supports fuel-cell R&D for stationary power generation; three technologies are currently under serious development—PAFC, MCFC and SOFC. Through the combined efforts of government, private research institutes (i.e., the Electric Power Research Institute and the Gas Research Institute), and industry, fuel-cell technology has advanced to near commercialization. Further advancements in technology would be greatly aided by making information on the technical status of fuel cells readily available to the fuel-cell community. In the latter half of the 1970s, DOE supported a project to evaluate the technical status of PAFCs

and MCFCs for stationary energy generation. This study resulted in the publication of a fuel-cell handbook (1). This handbook provided an assessment of fuel-cell technology to about 1980. Since that time tremendous advances have been made in fuel-cell technology, thus an update of the technology status is timely.

The objective of this publication is to update the technical status of fuel-cell technologies for stationary power generation. The basic format of the original fuel-cell handbook will be retained, with the major emphasis being to update the technical advances in PAFC, MCFC and SOFC technology since about 1980. The emphasis of this handbook will be on these fuel-cell systems because they are currently the strongest contenders for commercial stationary power generation. AFCs and PEFCs may play a role in electrical power generation where relatively pure and inexpensive hydrogen is available, but they are not serious candidates at this time. Fuel cells are considered to be attractive candidates for mobile power sources, but these applications are outside the scope of this study.

1.2 Operating Principles

The basic element of a fuel cell consists of an electrolyte phase in contact with a porous anode and cathode on either side. A schematic representation of a fuel cell and the reactant/product gases and ion-conduction flow directions through the cell for PAFCs, MCFCs and SOFCs, are shown in Figure 1-1. The fuel and oxidant gases flow past the backside of the anode and cathode, respectively, and generate electrical energy by the electrochemical oxidation of fuel, usually hydrogen, and the electrochemical reduction of oxygen. A three-phase boundary is established in the region of the porous electrode/electrolyte/reactant interface. The nature of this interface plays a critical role in the electrochemical performance of a fuel cell, particularly in those fuel cells with liquid electrolytes (i.e., AFC, PAFC, MCFC). In such fuel cells, the reactant gases diffuse through a thin electrolyte film that wets portions of the porous electrode and react electrochemically on the electrode surface. If the porous electrode contains an excessive amount of electrolyte, the electrode may "flood" and restrict the transport of gaseous species in the electrolyte phase. The consequence is a reduction in the electrochemical performance of the porous electrode. Thus a delicate balance must be maintained among the electrode, electrolyte and gaseous phases in the porous electrode structure. Much of the recent effort in the development of fuel-cell technology has been devoted to refining and improving the electrode structure and the electrolyte phase, with the aim of obtaining a higher and more stable electrochemical performance.

The electrolyte not only transports dissolved reactants to the electrode, but it also conducts ionic charge between the electrodes and thereby completes the cell electric circuit, as illustrated in Figure 1-1. In low-temperature fuel cells (PEFC, AFC, PAFC), protons or hydroxyl ions are the major charge carriers in the electrolyte, whereas in the high-temperature fuel cells, MCFC and SOFC, carbonate ions and oxygen ions are the charge carriers, respectively. The SOFC must be operated at about 1000°C because the transport rate of oxygen ions in the solid oxide electrolyte in SOFCs is adequate for practical applications only at such high temperatures.

A fuel-cell stack usually consists of a number of individual cells connected in electrical series, as depicted by the schematic representation of the basic cell structure in Figure 1-2. Each cell contains an electrolyte matrix in contact with a porous anode and a porous cathode; the details of these cell components are presented in Chapters 3 to 6. The individual cells in Figure 1-2 are connected by a ribbed bipolar separator plate which has two major functions: (i) current collector—provides

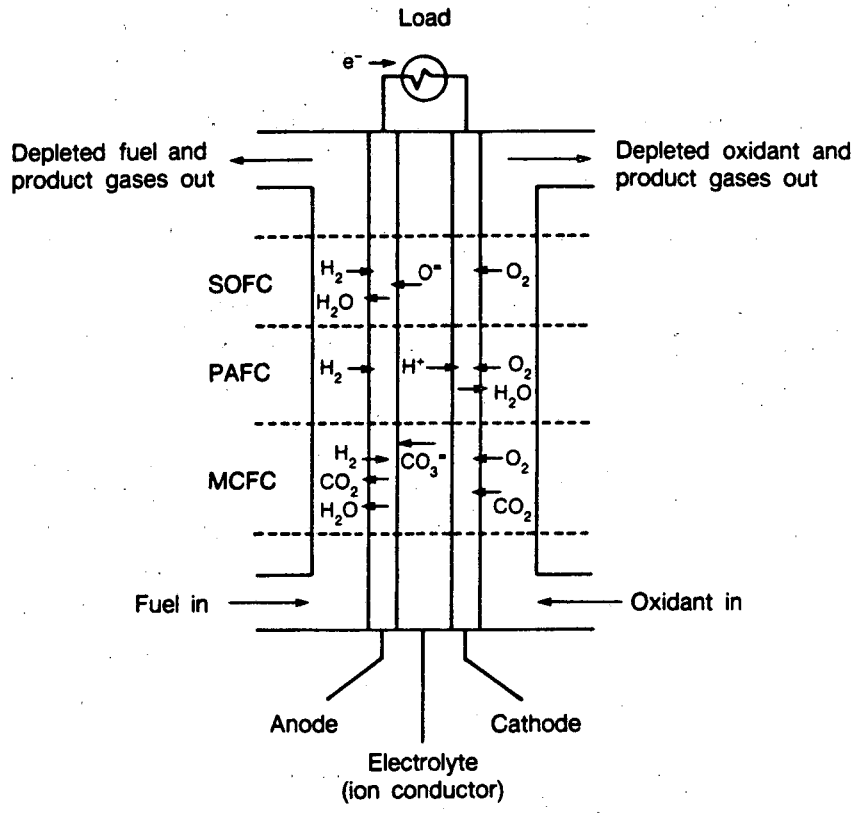

Figure 1-1. Schematic representation of a typical fuel cell showing the reactant/product gases and ion-conduction flow paths for PAFCs, MCFCs and SOFCs.

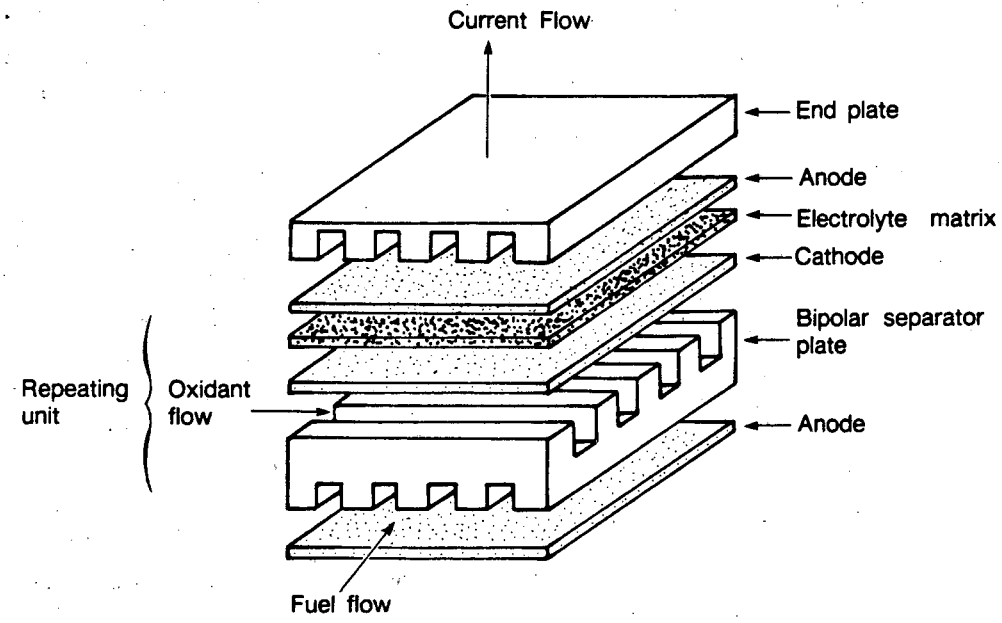

Figure 1-2. Expanded view of basic fuel-cell structure with the repeating unit in a fuel-cell stack.

the electrical series connection between cells and (ii) gas barrier—separates the fuel and oxidant streams in adjacent cells. Thus the bipolar plate must be both an electrical conductor and impermeable to gases. The ribbed channels provide a more uniform gas distribution to the backside of the electrodes and they also serve to mechanically support the porous electrode structures. In the representation shown in Figure 1-2, the fuel and oxidant streams flow perpendicular to each other (i.e., "crossflow") and the current flows perpendicular to the gas flow. Other arrangements of gas flow and current flow are used in fuel-cell stack designs, and these are mentioned in the following chapters.

The physicochemical and thermomechanical properties of materials used in the cell components (i.e., electrodes, electrolyte, separator, current collector, etc.) determine the practical operating temperature and useful life of a fuel cell. Aqueous electrolytes are limited to temperatures of about 200°C or lower because of their high water vapor pressure and/or rapid degradation at higher temperatures. The operating temperature also plays an important role in dictating the type of fuel that can be utilized in a fuel cell. The low-temperature fuel cells utilizing aqueous electrolytes are, in most practical applications, restricted to hydrogen as a fuel. In high-temperature fuel cells, the list of fuels is more extensive because of the inherently rapid electrode kinetics and the lesser need for high electrocatalytic activity at high temperature. These aspects will be discussed in the following section.

1.2.1 Electrode Reactions

The typical electrochemical reactions that occur with different fuels and oxidants in practical fuel cells are summarized in Table 1.1. CO and CH_4 are shown in the table as undergoing anodic oxidation, but in actuality, direct oxidation may not occur. Instead, these reactants are potential fuels because they undergo chemical reaction with H_2O to produce H_2 which is the oxidizable fuel. In MCFCs, CO and CH_4 are sources of H_2 from water-gas shift and steam-reforming reactions, respectively. The direct oxidation of CO and CH_4 in high-temperature SOFCs is feasible, but they are still not as easily oxidized as H_2. Low-temperature fuel cells (PEFC, AFC, PAFC) require electrocatalysts to achieve practical reaction rates at the anode and cathode, and hydrogen is the only acceptable fuel for large-scale fuel-cell power plants. With high-temperature fuel cells (MCFC, SOFC), the requirements for electrocatalysis are relaxed, and the number of potential fuels is increased. Carbon monoxide "poisons" the anode electrocatalyst in low-temperature fuel cells, but it serves as a potential source of H_2 in high-temperature fuel cells.

The overall electrochemical reactions corresponding to the individual electrode reactions listed in Table 1.1 are given in Table 1.2, along with the appropriate form of the Nernst equation. The Nernst equation provides a relationship between the standard potential (E^o) for the cell reaction and the equilibrium potential (E) at various temperatures and partial pressures (activities) of reactants and products. According to the Nernst equation, the equilibrium cell potential at a given temperature can be increased by operating at higher reactant pressures, and improvements in fuel-cell performance have, in fact, been observed at higher pressures (discussed in Chapter 2).

The electrochemical reactions of H_2 and O_2 in fuel cells produce H_2O. When a carbon-containing fuel is involved in the anode reaction, CO_2 is also produced. In the case of the MCFC, CO_2 is required in the cathode reaction to maintain an invariant carbonate concentration in the electrolyte. Because CO_2 is produced at the anode and consumed at the cathode in MCFCs, and the concentrations in the anode and cathode feed streams are not necessarily equal, the Nernst equation in Table 1.2 includes the CO_2 partial pressure for both electrode reactions.

Table 1.1 Typical Electrochemical Reactions in Fuel Cells

Fuel Cell	Anode Reaction	Cathode Reaction
Proton Exchange	$H_2 \rightarrow 2H^+ + 2e^-$	$O_2 + 4H^+ + 4e^- \rightarrow 2H_2O$
Alkaline	$H_2 + 2OH^- \rightarrow 2H_2O + 2e^-$	$O_2 + 2H_2O + 4e^- \rightarrow 4OH^-$
Phosphoric Acid	$H_2 \rightarrow 2H^+ + 2e^-$	$O_2 + 4H^+ + 4e^- \rightarrow 2H_2O$
Molten Carbonate	$H_2 + CO_3^= \rightarrow H_2O + CO_2 + 2e^-$	$O_2 + 2CO_2 + 4e^- \rightarrow 2CO_3^=$
	$CO + CO_3^= \rightarrow 2CO_2 + 2e^-$	
Solid Oxide	$H_2 + O^= \rightarrow H_2O + 2e^-$	$O_2 + 4e^- \rightarrow 2O^=$
	$CO + O^= \rightarrow CO_2 + 2e^-$	
	$CH_4 + 4O^= \rightarrow 2H_2O + CO_2 + 8e^-$	

Table 1.2 Fuel-Cell Reactions and the Corresponding Nernst Equations

Cell Reaction[a]	Nernst Equation
$H_2 + \frac{1}{2}O_2 \rightarrow H_2O$	$E = E^o + (RT/2F) \ln [P_{H_2}/P_{H_2O}] + (RT/2F) \ln [P_{O_2}^{1/2}]$
$H_2 + \frac{1}{2}O_2 + CO_2(c) \rightarrow H_2O + CO_2(a)$	$E = E^o + (RT/2F) \ln[P_{H_2}/P_{H_2O}(P_{CO_2})_a] + (RT/2F) \ln [P_{O_2}^{1/2}(P_{CO_2})_c]$
$CO + \frac{1}{2}O_2 \rightarrow CO_2$	$E = E^o + (RT/2F) \ln [P_{CO}/P_{CO_2}] + (RT/2F) \ln [P_{O_2}^{1/2}]$
$CH_4 + 2O_2 \rightarrow 2H_2O + CO_2$	$E = E^o + (RT/8F) \ln [P_{CH_4}/P_{H_2O}^2 P_{CO_2}] + (RT/8F) \ln [P_{O_2}^2]$

a = anode c = cathode

[a] The cell reactions are obtained from the anode and cathode reactions listed in Table 1.1.

1.2.2 Transport Processes

The transport processes involving the mass transfer of reactants/products play a prominent role in the performance of porous electrodes in fuel cells. Transport processes involving heat transfer and thermal management are important in fuel-cell systems, but these aspects will not be discussed here. The slow transport of reactant and product species through the porous electrode gives rise to the polarization discussed later in this chapter (section 1.3.2). A sequence of steps, involving both transport and rate processes, occurs when a reactant species undergoes electrochemical reaction in a porous electrode. One sequence suggested by Liebhafsky and Cairns (2) is presented in Table 1.3.

Table 1.3 Processes Involved in the Overall Electrochemical Reaction in Porous Fuel Cell Electrodes

Step	Process	Type
1	Transport of reactant to gas/electrolyte interface	Physical
2	Dissolution of reactant in electrolyte	Physical
3	Transport of reactant through electrolyte to electrode surface (double layer)	Physical
4	Pre-electrochemical homogeneous or heterogeneous chemical reaction	Chemical
5	Adsorption of electroactive species onto electrode	Chemical
6	Surface migration of adsorbed species	Physical
7	Electrochemical reaction involving electrically charged species	Electro-chemical
8	Post-electrochemical surface migration	Physical
9	Desorption of products	Chemical
10	Post-electrochemical reaction	Chemical
11	Transport of products away from electrode surface	Physical
12	Evolution of products from electrolyte	Physical
13	Transport of gaseous products from electrolyte/gas interface	Physical

Source: (Table 4.4-1) H.A. Liebhafsky and E.J. Cairns, *Fuel Cells and Fuel Batteries,* John Wiley and Sons, Inc., New York, NY (1968) p. 107.

With the exception of steps 2 and 12, each of the other steps can be associated with a polarization that could contribute to an increase in the inefficiency of the electrode reaction. It is outside the scope of this presentation to describe each of the steps in Table 1.3, and the details are found in Reference 2. The important point to note here is that not all of the steps contribute significantly to the total polarization, and those steps can be disregarded. Thus, efforts to improve the performance of porous fuel-cell electrodes can be directed at reducing the polarization associated with the remaining steps.

Transport processes involving diffusion, convection and migration can take place in the gas phase in the pores of the electrodes, or in the liquid (electrolyte) phase in the pores of the electrode. The relative contribution of these transport processes to the overall electrode polarization is affected by the porous electrode structure, electrolyte composition and temperature, and reactant gas composition and pressure.

The maximum rate of transport of reactant species to the electrode surface provides an upper limit to the rate of electrochemical reaction. Under these conditions a limiting current is reached. In a fuel cell with porous electrodes containing a liquid (electrolyte) layer, the diffusion of the reactant species through the electrolyte is usually the rate-limiting transport process.

1.2.3 Porous Gas Electrodes

The current densities that are obtained from smooth electrodes are usually in the range of a few mA/cm^2 or less because of rate-limiting processes such as the mass transport of reactants to the electrode surface. Porous electrodes that are commonly used in fuel cells are capable of achieving current densities (based on the projected area of the porous electrode) that are orders of magnitude higher, e.g., about 1 A/cm^2. These high current densities are possible because: (i) the electrode has a high specific surface area, and (ii) the optimized electrode structure has favorable mass-transport properties. In an idealized porous gas electrode for fuel cells, high current densities at reasonable polarization are obtained when the liquid (electrolyte) layer on the electrode surface is sufficiently thin so that it does not significantly impede the transport of reactants to the electroactive sites, and a stable three-phase (gas/electrolyte/electrode surface) interface is established. When an excessive amount of electrolyte is present in the porous electrode structure, the concentration polarization increases to a large value and the electrode is considered to be "flooded".

The porous electrodes that are used in low-temperature fuel cells consist of a composite structure that contains Pt electrocatalyst on a high-surface-area carbon black and a PTFE (polytetrafluoroethylene) binder. Such electrodes for acid and alkaline fuel cells are described by Kordesch et al. (3). In these porous electrodes, PTFE is hydrophobic (acts as a wet-proofing agent) and serves as the gas-permeable phase, and carbon black is an electron conductor that supports the electrocatalyst. The carbon black also has a certain degree of hydrophobicity, depending on the surface properties of the material. The composite structure of PTFE and carbon establishes an extensive three-phase interface in the porous electrode, which is the benchmark of PTFE-bonded electrodes. Recently, some interesting results have been reported by Japanese workers (4-9) on higher-performance gas diffusion electrodes for acid and alkaline fuel cells.

In MCFCs, which operate at relatively high temperature, there are no known materials that can serve to wet-proof a porous structure against ingress by molten carbonates. Consequently, the technology used to obtain a stable three-phase interface in MCFC porous electrodes is different from that used in PAFCs. In the MCFC, the stable interface is achieved in the electrodes by carefully

tailoring the pore structures of the electrodes and the electrolyte matrix ($LiAlO_2$) so that the capillary forces establish a dynamic equilibrium in the different porous structures. Pigeaud et al. (10) provide a discussion of porous electrodes for MCFCs.

In a SOFC, there is no liquid electrolyte present that is susceptible to movement in the porous electrode structure, and electrode flooding is not a problem. Consequently, the three-phase interface that is necessary for efficient electrochemical reaction involves two solid phases (solid electrolyte/electrode) and a gas phase. A critical requirement of porous electrodes for SOFC is that they are sufficiently thin and porous to provide an extensive electrode/electrolyte interfacial region for electrochemical reaction.

1.3 Thermodynamics[a]

The common energy conversion devices (i.e., heat engines), which rely on the combustion of fossil fuels to produce electrical energy, have an intrinsic efficiency limitation imposed by the Carnot cycle. That is, the maximum efficiency (ε_c) is set by the high temperature (T_h) of the heat source and the low temperature (T_l) of the heat sink, i.e.,

$$\varepsilon_c = \frac{T_h - T_l}{T_h} \tag{1-1}$$

Based on the Carnot cycle, the theoretical efficiency of a heat engine increases as the source temperature increases and the sink temperature decreases. If one takes for example T_h = 1000°K and T_l = 300°K, ε_c = 0.7, i.e., 70% of the enthalpy of reaction is theoretically converted into useful work. Unfortunately, the maximum efficiency of practical heat engines based on the Carnot cycle is usually ≤40%. An attractive feature of fuel cells is that their efficiency is not limited by the Carnot cycle, and most of the chemical energy in the fuel may be converted to electricity, along with heat that is useful in some applications.

1.3.1 Reversible Thermodynamics

The maximum electrical work (W_{el}) obtainable in a fuel cell operating at constant temperature and pressure is given by the change in Gibbs free energy (ΔG) of the electrochemical reaction

$$W_{el} = \Delta G = -nFE \tag{1-2}$$

where n is the number of electrons participating in the reaction, F is Faraday's constant and E is the reversible potential of the cell. If we consider the case of all reactants and products being in the standard state, then

$$\Delta G^\circ = -nFE^\circ \tag{1-3}$$

[a] See References 11 and 12 for discussion on fuel cell thermodynamics.

The overall reactions given in Table 1.2 can be utilized to produce both electrical energy and heat. The maximum work available from a fuel source is related to the free energy of reaction in the case of a fuel cell, whereas the enthalpy of reaction is the pertinent quantity for a heat engine, i.e.,

$$\Delta G_r = \Delta H_r - T\Delta S_r \tag{1-4}$$

where the difference between ΔG_r and ΔH_r is proportional to the change in entropy. This entropy change is manifested in changes in the degrees of freedom for the chemical system being considered. The maximum amount of electrical energy available is ΔG_r, as mentioned above, and the total energy available is ΔH_r. The amount of heat that is produced by a fuel cell operating reversibly is $T\Delta S_r$. Reactions in fuel cells that have negative entropy change generate heat, while those with positive entropy change may extract heat from their surroundings, if the irreversible generation of heat is smaller than the reversible absorption of heat.

The reversible potential of a fuel cell at temperature T is calculated from ΔG_T for the cell reaction at that temperature. This potential can be computed from the heat capacities (C_p) of the species involved as a function of T and using values of both ΔS^o and ΔH^o at one particular temperature, usually 298°K. Empirically, the heat capacity of a specie as a function of T can be expressed as

$$C_p = a + bT + cT^2 \tag{1-5}$$

and the difference in the heat capacities for the products and reactants involved in the stoichiometric reaction is given by

$$\Delta C_p = \Delta a + \Delta bT + \Delta cT^2 \tag{1-6}$$

Since

$$\Delta H_T = \Delta H^o_{298} + \int \Delta C_p dT \tag{1-7}$$

and, at constant pressure,

$$\Delta S_T = \Delta S^o_{298} + \int \frac{\Delta C_p}{T} dT \tag{1-8}$$

Then it follows that

$$\Delta H_T = \Delta H^o_{298} + \Delta a(T - 298) + \tfrac{1}{2}\Delta b(T - 298)^2 + \tfrac{1}{3}\Delta c(T - 298)^3 \tag{1-9}$$

and

$$\Delta S_T = \Delta S^o_{298} + \Delta a \ln \left(\frac{T}{298}\right) + \Delta b(T - 298) + \tfrac{1}{2}\Delta c(T - 298)^2 \tag{1-10}$$

The coefficients a, b and c (see Appendix 9.1), as well as ΔS°_{298} and ΔH°_{298}, are available from standard reference tables, and may be used to calculate ΔH_T and ΔS_T. From these values it is then possible to calculate ΔG°_T and E°_T.

For the general cell reaction

$$aA + bB \rightarrow cC + dD \tag{1-11}$$

the free energy change can be expressed by the equation

$$\Delta G = \Delta G^{\circ} + RT \ln \frac{[C]^c[D]^d}{[A]^a[B]^b} \tag{1-12}$$

When Equations 1-2 and 1-3 are substituted in Equation 1-12,

$$E = E^{\circ} + \frac{RT}{nF} \ln \frac{[A]^a[B]^b}{[C]^c[D]^d} \tag{1-13}$$

or

$$E = E^{\circ} + \frac{RT}{nF} \ln \frac{\Pi\ [\text{reactant activity}]}{\Pi\ [\text{product activity}]} \tag{1-14}$$

which is the general form of the Nernst equation. For the overall cell reaction, the cell potential increases with an increase in the activity of reactants and a decrease in the activity of products. Changes in temperature also influence the reversible cell potential, and the dependence of potential on temperature varies with the cell reaction. Figure 1-3 illustrates the change in the reversible standard potential for the reactions

$$H_2 + \tfrac{1}{2}O_2 \rightarrow H_2O \tag{1-15}$$

$$CO + \tfrac{1}{2}O_2 \rightarrow CO_2 \tag{1-16}$$

and

$$CH_4 + 2O_2 \rightarrow 2H_2O + CO_2 \tag{1-17}$$

as a function of temperature. It is apparent from Figure 1-3 that the standard potentials for the oxidation of H_2 and CO show a marked decrease with an increase in temperature, whereas the corresponding potential for the oxidation of CH_4 is nearly invariant with temperature. The significance of these results is that the reversible cell voltage of high-temperature fuel cells is usually lower than that of low-temperature fuel cells. In practical fuel cells, the theoretical advantage in cell voltage for MCFC over SOFC is about 0.1 V and about 0.15 V for PAFC over MCFC, with comparable gas compositions. The actual difference in cell voltages between these fuel cells are less than the differences in theoretical voltages (13). This point will be discussed in the next section.

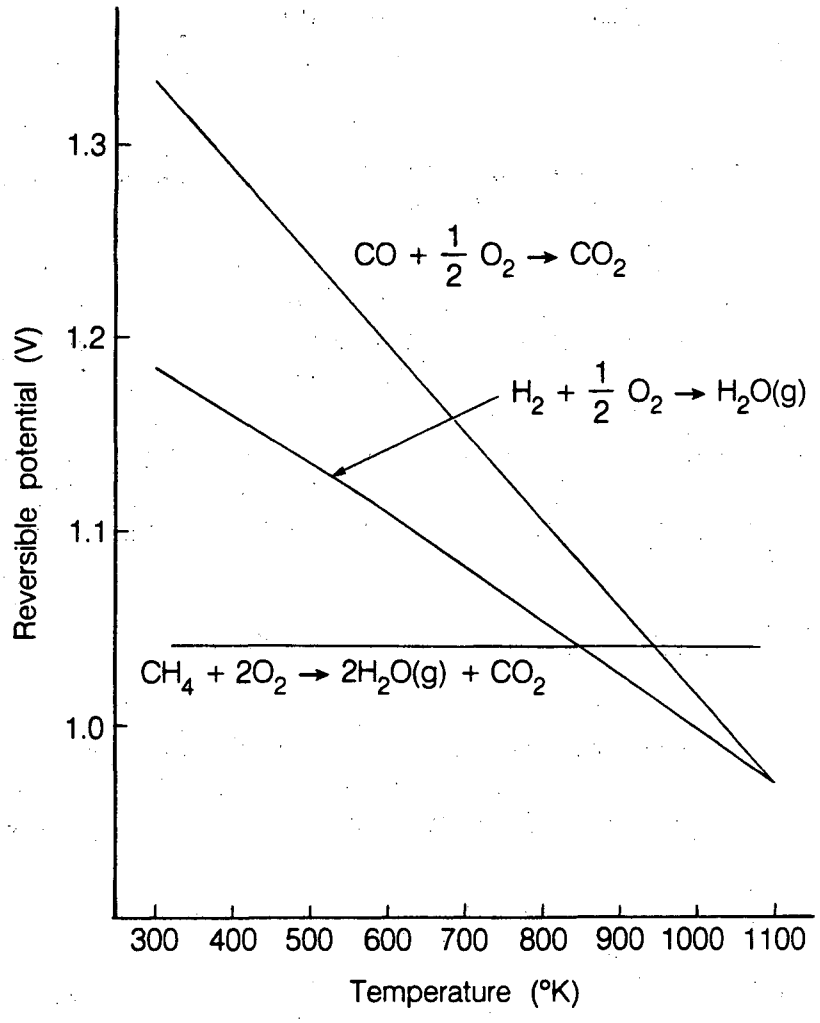

Figure 1-3. Reversible standard potential for fuel cell reactions as a function of temperature.

1.3.2 Irreversible Thermodynamics

Useful amounts of work (electrical energy) are obtained from a fuel cell only when a reasonably large current is drawn, but the cell potential will be decreased from its equilibrium potential because of irreversible losses. There are several sources that contribute to irreversible losses in a practical fuel cell. The losses, which are often called polarization, overpotential or overvoltage, originate primarily from three sources: (i) ohmic polarization (η_{ohm}), (ii) concentration polarization (η_{conc}) and (iii) activation polarization (η_{act}). These losses result in a cell voltage (V) for a fuel cell that is less than its reversible potential.

Ohmic Polarization: The ohmic losses occur because of resistance to the flow of ions in the electrolyte and resistance to flow of electrons through the electrode materials. The dominant ohmic losses through the electrolyte phase are reduced by decreasing the electrode separation and enhancing the ionic conductivity of the electrolyte. Because both the electrolyte and fuel-cell electrodes obey

Ohm's law, the ohmic losses can be expressed by the equation

$$\eta_{ohm} = IR \tag{1-18}$$

where I is the current flowing through the cell, and R is the total cell resistance, which includes electronic, ionic and contact resistances.

Concentration Polarization: As a reactant is rapidly consumed at the electrode by electrochemical reaction, concentration gradients will be established. Several processes may contribute to concentration polarization—slow diffusion in the gas phase in the electrode pores, solution/dissolution of reactants/products into/out of the electrolyte, or diffusion of reactants/products through the electrolyte to/from the electrochemical reaction site. At practical current densities, slow transport of reactants/products to/from the electrochemical reaction site is a major contributor to concentration polarization.

The rate of mass transport to an electrode surface in many cases can be described by Fick's first law of diffusion

$$i = \frac{nFD\ (C_B - C_S)}{\delta} \tag{1-19}$$

where D is the diffusion coefficient of the reacting species, C_B is its bulk concentration, C_S is its surface concentration and δ is the thickness of the diffusion layer. The limiting current (i_L) is a measure of the maximum rate at which a reactant can be supplied to an electrode, and occurs when $C_S = 0$, i.e.,

$$i_L = \frac{nFDC_B}{\delta} \tag{1-20}$$

By appropriate manipulation of Equations 1-19 and 1-20 we arrive at

$$\frac{C_S}{C_B} = 1 - \frac{i}{i_L} \tag{1-21}$$

The Nernst equation for the reactant species at equilibrium conditions, or when no current is flowing, is

$$E\,|_{i=o} = E^o + \frac{RT}{nF} \ln C_B \tag{1-22}$$

When current is flowing, the surface concentration becomes less than the bulk concentration, and the Nernst equation becomes

$$E = E^o + \frac{RT}{nF} \ln C_S \tag{1-23}$$

The potential difference (ΔE) produced by a concentration change at the electrode is called the concentration polarization

$$\Delta E = \eta_{conc} = \frac{RT}{nF} \ln \frac{C_S}{C_B} \tag{1-24}$$

Upon substituting Equation 1-21 in 1-24, the concentration polarization is given by the equation

$$\eta_{conc} = \frac{RT}{nF} \ln \left(1 - \frac{i}{i_L}\right) \tag{1-25}$$

In this analysis of concentration polarization, the activation polarization is assumed to be negligible. That is, the charge-transfer reaction has such a high exchange current density that the activation polarization is much smaller than the concentration polarization.

Activation Polarization: Activation polarization is present when the rate of an electrochemical reaction at an electrode surface is associated with sluggish electrode kinetics. In other words, activation polarization is directly related to the rates of electrochemical reactions. There is a close similarity between electrochemical and chemical reactions in that both involve an activation barrier that must be overcome by the reacting species. In the case of an electrochemical reaction with $\eta_{act} \geq$ 50-100 mV, η_{act} is described by the general form of the Tafel equation

$$\eta_{act} = \frac{RT}{\alpha nF} \ln \frac{i}{i_o} \tag{1-26}$$

where α is the transfer coefficient and i_o is the exchange current density. The usual form of the Tafel equation is

$$\eta_{act} = a + b \log i \tag{1-27}$$

where $a = (-2.3RT/\alpha nF) \log i_o$ and $b = 2.3RT/\alpha nF$. The term b is called the Tafel slope, and is obtained from the slope of a plot of η as a function of log i. The Tafel slope for an electrochemical reaction is about 100 mV/decade (log current density) at room temperature. Thus, a 10-fold increase in current density causes a 100-mV increase in the activation polarization. On the other hand, if the Tafel slope is only 50 mV/decade, then the same increase in current density produces a 50-mV increase in activation polarization. Clearly there exists a strong incentive to develop electrocatalysts that yield a lower Tafel slope for electrochemical reactions.

The simplified description presented here did not consider the processes that give rise to activation polarization, except for attributing it to sluggish electrode kinetics. A detailed discussion of the subject is outside the scope of this presentation, but processes involving adsorption of reactant species, transfer of electrons across the double layer, desorption of product species, and the nature of the electrode surface can all contribute to activation polarization.

Electrode Polarization: Activation and concentration polarizations can exist at both the positive (cathode) and negative (anode) electrodes in fuel cells. The total polarization at these electrodes is the sum of η_{act} and η_{conc}, or

$$\eta_{anode} = \eta_{act,a} + \eta_{conc,a} \tag{1-28}$$

and

$$\eta_{cathode} = \eta_{act,c} + \eta_{conc,c} \tag{1-29}$$

The effect of polarization is to shift the potential of the electrode ($E_{electrode}$) to a new value ($V_{electrode}$)

$$V_{electrode} = E_{electrode} \pm |\eta_{electrode}| \tag{1-30}$$

For the anode

$$V_{anode} = E_{anode} + |\eta_{anode}| \tag{1-31}$$

and for the cathode

$$V_{cathode} = E_{cathode} - |\eta_{cathode}| \tag{1-32}$$

The net result of current flow in a fuel cell is to increase the anode potential and to decrease the cathode potential, thereby reducing the cell voltage.

Cell Voltage: The cell voltage includes the contribution of the polarization and the anode and cathode potentials

$$V_{cell} = V_{cathode} - V_{anode} - IR \tag{1-33}$$

When Equations 1-31 and 1-32 are substituted in Equation 1-33

$$V_{cell} = E_{cathode} - |\eta_{cathode}| - (E_{anode} + |\eta_{anode}|) - IR \tag{1-34}$$

or

$$V_{cell} = \Delta E_e - |\eta_{cathode}| - |\eta_{anode}| - IR \tag{1-35}$$

where $\Delta E_e = E_{cathode} - E_{anode}$. Equation 1-35 shows that current flow in a fuel cell results in a decrease in the cell voltage because of losses by electrode and ohmic polarizations. The goal of fuel-cell developers is to minimize the polarization so that V_{cell} approaches ΔE_e. This goal is approached by modifications to the fuel-cell operating conditions (i.e., higher gas pressure, higher temperature, change in gas composition to lower the gas impurity concentration, etc.), improvement in electrode structures, better electrocatalysts, more-conductive electrolyte, etc. However, for any fuel cell, trade-offs exist between achieving higher performance by operating at higher temperature or pressure and the problems associated with the stability/durability of cell components encountered at the more severe conditions.

1.4 Types of Fuel Cells

Fuel cells can be classified by use of various parameters, depending on the combination of type of fuel and oxidant, whether the fuel is processed outside (indirect) or inside (direct) of the fuel cell, the type of electrolyte, the temperature of operation, etc. The common parameters that serve to classify the types of fuel cells are presented in Table 1.4, based on the analysis by Fickett (14). From this extensive list of parameters has emerged five major classes of fuel cells—PEFC (denoted as SPE in Table 1.4), AFC, PAFC, MCFC and SOFC—which are characterized by the type of electrolyte. A brief description of each of these fuel cells follows. A detailed discussion on each of these fuel cells was published recently (15).

Polymer Electrolyte Fuel Cell: The electrolyte in this fuel cell is an ion-exchange membrane (fluorinated sulfonic acid polymer) which is an excellent proton conductor. The only liquid in this fuel cell is water, thus corrosion problems are minimal. Water management in the membrane is critical for efficient performance; the fuel cell must operate under conditions where the by-product water does not evaporate faster than it is produced because the membrane must be hydrated. Because of the limitation on the operating temperature, usually less than 120°C, H_2-rich gas with little or no CO is used, and higher Pt loadings than those used in PAFCs are required in both the anode and cathode.

Table 1.4 Fuel Cell Parameters

Fuel				
Direct	Indirect	Oxidant	Temperature	Electrolyte
Hydrogen	Hydrides	Oxygen	Low (120°C)	Aqueous Acid
Hydrazine	Ammonia	Oxygen (air)	Intermediate	Sulfuric
Ammonia	Hydrocarbons	Hydrogen peroxide	(120-260°C)	Phosphoric
Hydrocarbons	Methanol		High (260-750°C)	Solid polymer electrolyte (SPE)
Methanol	Ethanol		Very high (>750°C)	
Coal gas	Coal			Aqueous alkaline
Coal				Molten alkaline
				Aqueous carbonate
				Molten carbonate
				Solid oxide

Source: (Table 41.3). A. Fickett, in *Handbook of Batteries and Fuel Cells,* Edited by D. Linden, McGraw-Hill Book Co., New York, NY (1984) p. 41-10.

Alkaline Fuel Cell: The electrolyte in this fuel cell is concentrated (85 wt%) KOH in fuel cells operated at high temperature (~250°C), or less concentrated (35-50 wt%) KOH for lower-temperature (<120°C) operation. The electrolyte is retained in a matrix (usually asbestos), and a wide range of electrocatalysts can be used (e.g., Ni, Ag, metal oxides, spinels and noble metals).

Phosphoric Acid Fuel Cell: Concentrated phosphoric acid is used for the electrolyte in this fuel cell, which operates at 150-220°C. At lower temperatures, phosphoric acid is a poor ionic conductor and CO poisoning of the Pt electrocatalyst in the anode becomes more severe. The relative stability of concentrated phosphoric acid is high compared to other common acids, consequently the PAFC is capable of operating at elevated temperatures. In addition, the use of concentrated acid (~100%) minimizes the water vapor pressure so water management in the cell is not difficult. The matrix used to retain the acid is usually SiC, and the electrocatalyst in both the anode and cathode is Pt.

Molten Carbonate Fuel Cell: The electrolyte in this fuel cell is usually a combination of alkali (Li, Na, K) carbonates, which is retained in a ceramic matrix of $LiAlO_2$. The fuel cell operates at 600-700°C where the alkali carbonates form a highly conductive molten salt, with carbonate ions providing ionic conduction. At the high operating temperatures in MCFCs, Ni (anode) and nickel oxide (cathode) are adequate electrode materials, and noble metals are not required.

Solid Oxide Fuel Cell: The electrolyte in this fuel cell is a solid, nonporous metal oxide, usually Y_2O_3-stabilized ZrO_2. The cell operates at 900-1000°C where ionic conduction by oxygen ions takes place. Typically, the anode is Co-ZrO_2 or Ni-ZrO_2 cermet, and the cathode is Sr-doped $LaMnO_3$.

A more detailed discussion of these fuel cells is presented in Chapters 3-6.

1.4.1 Characteristics

Fuel cells have many favorable characteristics for energy conversion devices; several of these general characteristics are:

- high energy conversion efficiency
- efficiency relatively independent of load
- modular design provides for rapid deployment
- flexibility in size of fuel cells
- very low chemical and acoustic pollution
- cogeneration capability
- ease of siting
- flexibility in fuel use
- rapid response

The general negative features of fuel cells for energy conversion include:

- sensitive to certain fuel contaminants
- relatively high cost
- endurance needs improvement for certain applications

One of the main attractive features of fuel cell systems is their expected high fuel-to-electricity efficiency (40-60%, based on lower heating value of the fuel), which is higher than that of many other energy conversion systems. In addition, fuel cells operate at a constant temperature, and the heat from the electrochemical reaction is available for cogeneration applications. Because fuel cells operate at near constant efficiency, independent of size, small fuel cells operate nearly as efficiently

as large ones.[b] Thus fuel-cell power plants can be configured in a wide range of electrical output, ranging from watts to megawatts. Fuel cells are quiet and operate with virtually no noxious emissions, but they are sensitive to certain fuel contaminants (see Table 1.5), which must be minimized in the fuel gas. The two major impediments to the widespread use of fuel cells are (i) high initial cost and (ii) short operational lifetime; it is these two aspects which are the major focus of technological effort.

Table 1.5 Projection of Allowable Fuel Gas Impurities in PAFC and MCFC

Gas Species	PAFC	MCFC
CO_2	Diluent	Diluent
CO	<4%	Fuel
CH_4	Diluent	Diluent
H_2O	Diluent	Diluent
H_2S + COS	200 ppm	1 ppm
Chlorides	0.1 ppm	0.1 ppm
Ammonia	0.1 ppm	0.1 ppm
C_2 & Heavier HC	100 ppm	100 ppm

Source: E.A. Gillis, *Chemical Engineering Progress,* 88 (October 1980).

1.4.2 Advantages/Disadvantages

The advantages and disadvantages of the five major classes of fuel cells are presented in Table 1.6. Two of these fuel cell systems, PEFC and AFC, despite their advantages, are not currently being considered for stationary baseload or dispersed power plant applications. Instead the current interest in these fuel cells is mainly for transportation and specialty applications (i.e., military, aerospace, undersea).

The advantages of the PEFC are that the solid polymer electrolyte is not volatile or subject to movement such as that encountered with liquid electrolytes, and that materials are not problematic, except for the electrocatalysts. Because the current technology restricts the practical operating temperature to about 120°C or lower, pure H_2 is the only suitable fuel. Consequently, PEFCs are not practical for stationary power plants that use reformed hydrocarbons for fuel.

The major advantages of AFCs are: (i) cathode performance is much better than that for acid fuel cells and (ii) materials of construction tend to be low cost. The primary disadvantage is that the

[b] The fuel-processor efficiency is size dependent, therefore, small fuel-cell power plants using externally reformed hydrocarbon fuels would have a lower overall system efficiency.

Table 1.6 Advantages and Disadvantages of Various Fuel Cells

Fuel Cell	Advantages	Disadvantages
PEFC	• CO_2-rejecting electrolyte • non-volatile polymer electrolyte • corrosion and materials problems are minimal	• requires high Pt loading • CO is an anode poison • H_2O management is a problem • requires high-cost ion-exchange membrane • H_2 is only suitable fuel for direct oxidation
AFC	• wide range of potential electrocatalysts • lower-cost electrocatalysts than PAFC • better O_2 electrode kinetics than PAFC	• does not reject CO_2 • carbonaceous fuels are not suitable
PAFC	• CO_2-rejecting electrolyte • high overall fuel efficiency in on-site cogeneration application	• H_2 is only suitable fuel for direct oxidation • CO is an anode poison • uses high-cost electrocatalysts • irreversible O_2 kinetics • low-conductivity electrolyte
MCFC	• electrode kinetics are fast • high-grade heat available • CO is a usable fuel • potential cost advantage over PAFC • high efficiency • direct reforming of fuel in cells is feasible	• materials problems related to life and mechanical stability • low sulfur tolerance • CO_2 source required for cathode
SOFC	• high-grade heat available • CO is a usable fuel • electrode kinetics are fast • external reforming of fuel not required • high system efficiency • CO_2 recycling not required • no electrolyte management problem • electrolyte composition is invariant	• high-cost fabrication process • high temperature presents severe constraints on cell materials • relatively high electrolyte resistivity

electrolyte reacts with carbon oxides to produce potassium carbonate. Thus, reformed hydrocarbons are not practical fuels for AFCs.

The other types of fuel cells—PAFC, MCFC and SOFC—possess the combination of advantages which make them attractive candidates for stationary power plant applications that utilize reformed hydrocarbon fuels. These aspects are discussed in the following section.

1.5 Applications

The above characteristic features and advantages of fuel cells led to their consideration for a variety of applications, which are summarized in Table 1.7. The high energy density obtained from fuel cells operating on pure H_2 and O_2 provide a useful power generator in remote applications where system weight and volume are important parameters (i.e., space, undersea). On the other hand, fuel-cell power plants operating on fossil fuels and air offer the potential for environmentally acceptable, highly efficient, and low-cost power generation. Thus fuel cells can be considered for terrestrial applications where environmental pollution or noise would be objectionable, and they can be located near their point of use, such as an urban site, rather than at a remote location. Applications for fuel cells have been reviewed by Fickett (16), Warshay (17), Srinivasan (18), and Maru (19, 20).

A fuel-cell power plant for the generation of electricity for industrial, commercial and residential use requires two major subsystems besides the fuel cell: (i) a power conditioner to convert dc power to ac power and (ii) a fuel processor unit to convert commercially available fuels into a fuel

Table 1.7 Applications of Fuel Cells

Application	Important Parameter	Typical Size
Utility • peaking • intermediate • baseload	Life-cycle cost	5-1000 MW
Cogeneration	Overall efficiency Quality of waste heat	1-50 MW
On-site	Reliability, cost	40-400 kW
Propulsion	Weight, initial cost	15-60 kW
Portable	Weight, ruggedness	<2 kW
Space	Weight, volume	25-100 kW

Source: (Table 2) H.C. Maru, in *Symposium Proceedings Fuel Cells Technology Status and Applications,* Edited by E.H. Camara, Institute of Gas Technology, Chicago, IL (1982) p. 10.

that is effectively utilized in the cell. The integration of the fuel processor, fuel cell, power conditioner and other ancillaries (e.g., turbocompressors and blowers, thermal management subsystem, bottoming cycle subsystem to generate additional electricity and/or heat recovery for other use) must be optimized to achieve the maximum efficiency from the system.

1.5.1 Stationary Baseload Power

The fuel-cell power systems are intended to compete with current thermal power systems, as well as proposed energy-conversion technologies, for electrical power generation by the electric utilities (16-21). The relative insensitivity of the fuel cell's efficiency to rate of electrical output (25 to 100% of rated output) makes them more competitive with other load-following electricity generators, which are usually less efficient at full load and become even more inefficient at lower rated output.

Three possible roles for fuel cells in utility applications are:

- central station (baseload) power plant—integrated with coal gasifier
- dispersed (substation) power plant—fueled by liquid/gases with option for waste heat recovery
- on-site power plant—fueled by natural gas with waste heat recovery.

In the near term, the PAFC is the closest to commercialization in electric utility applications. These fuel-cell systems will be in the 5 to 25-MW range for dispersed power plants to perform load-following duty, and petroleum- or coal-derived gas or liquid are suitable fuels. In the longer term, MCFCs and SOFCs (as well as PAFC), which use coal for the fuel source, are expected for central-station power plants in the 100 to 600-MW range and greater. An advantage of fuel cells for the electric utilities is that fuel-cell power plants can be sized to match load growth by the addition of fuel-cell modules.

1.5.2 Stationary On-Site Power

Low-temperature fuel cells, principally PAFCs, are being developed to operate at the application site (denoted as "on-site"), as well as the traditional electric utility application. The waste heat from the fuel cells can be utilized for industrial applications (called "cogeneration"), and for residential and commercial applications (called "on-site/integrated energy systems", OS/IES).

The fuel-cell systems for OS/IES are expected to range from 40 to 400 kW in size, and they are intended to meet the energy requirements of restaurants, retail stores, motels, apartment buildings, hospitals, etc. For these applications the waste heat will be utilized for heating water, space heating, low-pressure steam (up to 60 psig) and possibly for absorption chilling. Overall efficiencies approaching 90% have been projected for fuel cells of this type. Natural gas and coal-derived gases and liquids are suitable fuels for on-site fuel cells.

Most industrial cogeneration schemes require fuel cells in the megawatt rather than the kilowatt range. For this application, PAFC power plants of 4.5 to 11-MW power rating are under development, and they are expected to be used in municipal waste treatment plants, breweries, paper making, petroleum and metal refining, and chlor-alkali production. The on-site utilization of high-temperature fuel cells will most likely be greater in industrial cogeneration applications than in residential and commercial OS/IES applications. This is because better utilization of the high-quality waste heat is possible in most industrial applications than in residential or commercial applications.

1.5.3 Other Applications

Because of the modular nature of fuel cells, they are attractive for use in small portable units, ranging in size from 5 W or smaller to 1000-W power levels; different power levels are attained by appropriate electrical connection of the fuel cells. The application of fuel cells in the space program (1-kW PEFC in the Gemini program and 1.5-kW AFC in the Apollo program) was demonstrated in the 1960s. More recently, a 7-kW AFC based on KOH electrolyte was used in the Space Shuttle Orbiter. In these space applications, the fuel cells used pure reactant gases.

For terrestrial applications, small portable fuel cells (1 to 100 W) can be an attractive alternative to batteries for long-term operation (22). Pure O_2 is not required for terrestrial applications, instead air is used for the O_2 source. For these small fuel cells, elaborate fuel conditioning is not feasible, hence easily handled and readily oxidized fuels (e.g., liquid or gaseous fuels such as CH_3OH, N_2H_4, NH_3, and other fuels that provide H_2) are considered. Slightly larger fuel-cell units, 500 W to 5 kW, were developed for military application as silent, lightweight sources of electrical energy.

Fuel cells of about 20-kW power level and greater are being considered for terrestrial transportation applications. The PAFC and PEFC, using reformed CH_3OH for fuel, are both being evaluated for transportation use. There is also some effort on the development of AFC for electric vehicle application. A discussion on fuel cells for electric vehicles is presented in References 18 and 23.

References

1. T.G. Benjamin, E.H. Camara and L.G. Marianowski, *Handbook of Fuel Cell Performance,* prepared by the Institute of Gas Technology for the United States Department of Energy under Contract No. EC-77-C-03-1545, (May 1980).
2. H.A. Liebhafsky and E.J. Cairns, *Fuel Cells and Fuel Batteries,* John Wiley and Sons, Inc., New York, NY, (1968) p. 107.
3. K. Kordesch, J. Gsellmann, S. Jahangir and M. Schautz, in *Proceedings of the Symposium on Porous Electrodes: Theory and Practice,* Edited by H.C. Maru, T. Katan and M.G. Klein, The Electrochemical Society, Inc., Pennington, NJ, (1984), p. 163.
4. S. Mottoo, M. Watanabe and N. Furuya, *J. Electroanal. Chem.,* **160,** 351 (1984).
5. M. Watanabe, M. Tomikawa and S. Mottoo, *J. Electroanal. Chem.,* **182,** 193 (1985).
6. M. Watanabe, M. Tozawa and S. Mottoo, *J. Electroanal. Chem.,* **183,** 391 (1985).
7. M. Watanabe, M. Tomikawa and S. Mottoo, *J. Electroanal. Chem.,* **195,** 81 (1985).
8. M. Watanabe, K. Makita, H. Usami and S. Mottoo, *J. Electroanal. Chem.,* **197,** 195 (1986).
9. M. Watanabe, M. Uchida and S. Mottoo, *J. Electroanal. Chem.,* **199,** 311 (1986).
10. A. Pigeaud, H.C. Maru, L. Paetsch, J. Doyon and R. Bernard, in *Proceedings of the Symposium on Porous Electrodes: Theory and Practice,* Edited by H.C. Maru, T. Katan and M.G. Klein, The Electrochemical Society, Inc., Pennington, NJ, (1984), p. 234.
11. H.A. Liebhafsky, *J. Electrochem. Soc.,* **106,** 1069 (1959).
12. A.J. deBethune, *J. Electrochem. Soc.,* **107,** 937 (1960); *J. Electrochem. Soc.,* **108,** 608 (1961).
13. J.P. Ackerman, *Prog. Batteries & Solar Cells,* **5,** 13 (1984).
14. A.P. Fickett, in *Handbook of Fuel Cells and Batteries,* Edited by D. Linden, McGraw-Hill Book Co., New York, NY, (1984), p. 41-3.
15. *Assessment of Research Needs for Advanced Fuel Cells,* Edited by S.S. Penner, DOE/ER/30060-T1, prepared by the DOE Advanced Fuel Cell Working Group for the United States Department of Energy under Contract No. DE-AC01-84ER30060 (November 1985); Energy **11,** 1 (1986).
16. A.P. Fickett, in *Handbook of Fuel Cells and Batteries,* Edited by D. Linden, McGraw-Hill Book Co., New York, NY, (1984), p. 43-3.
17. M. Warshay, in *The Science and Technology of Coal and Coal Utilization,* Edited by B.R. Cooper and W.A. Ellingson, Plenum Press, New York, NY, (1984), p. 339.
18. S. Srinivasan, *J. Electroanal. Chem.,* **118,** 51 (1981).
19. H.C. Maru, in *Symposium Proceedings Fuel Cells Technology Status and Applications,* Edited by E.H. Camara, Institute of Gas Technology, Chicago, IL, (1982), p. 1.
20. H.C. Maru and B.S. Baker, reprint from International Power Generation (February 1981).
21. A.P. Fickett, *Int. J. Hydrogen Energy,* **8,** 617 (1983).
22. D. Linden, in *Handbook of Fuel Cells and Batteries,* Edited by D. Linden, McGraw-Hill Book Co., New York, NY, (1984), p. 42-1.
23. *Power Sources for Electric Vehicles,* Edited by B.D. McNicol and D.A.J. Rand, Elsevier Science Publishers B.V., Amsterdam, The Netherlands (1984).

2. FUEL CELL PERFORMANCE VARIABLES

The performance of fuel cells is affected by the operating variables (e.g., temperature, pressure, gas composition, utilization) that influence the reversible cell potential and the magnitude of the irreversible voltage losses described in Chapter 1. The following discussion is based partially on the descriptions in the fuel-cell handbook by Benjamin et al. (1).

2.1 Temperature and Pressure

Changing the operating parameters, temperature and pressure, to more-extreme conditions can have either a beneficial or detrimental impact on fuel-cell performance. In practice, a compromise in the operating parameters is necessary to obtain optimum fuel-cell performance and acceptable cell life.

The effect of temperature and pressure on the reversible potential (E) of a fuel cell can be analyzed on the basis of changes in the Gibbs free energy with temperature and pressure. Differentiating Equation 1-4 with respect to temperature or pressure, and substituting into Equation 1-2, yields

$$\left[\frac{\partial E}{\partial T}\right]_P = \frac{\Delta S}{nF} \tag{2-1}$$

and

$$\left[\frac{\partial E}{\partial P}\right]_T = \frac{-\Delta V}{nF} \tag{2-2}$$

Because the entropy change for the H_2/O_2 reaction is negative, the reversible potential of a H_2/O_2 fuel cell decreases with an increase in temperature by 0.84 mV/°C (reaction product is liquid water). For the same reaction, the volume change is negative, therefore, the reversible potential increases with an increase in pressure.

The practical effect of temperature on the voltage of fuel cells is illustrated schematically in Figure 2-1, which presents initial (i.e., early in life) performance data from typical operating cells and the dependence of the reversible potential of H_2/O_2 fuel cells on temperature (2). The cell voltages of AFCs, PEFCs, PAFCs and MCFCs show a strong dependence on temperature. The

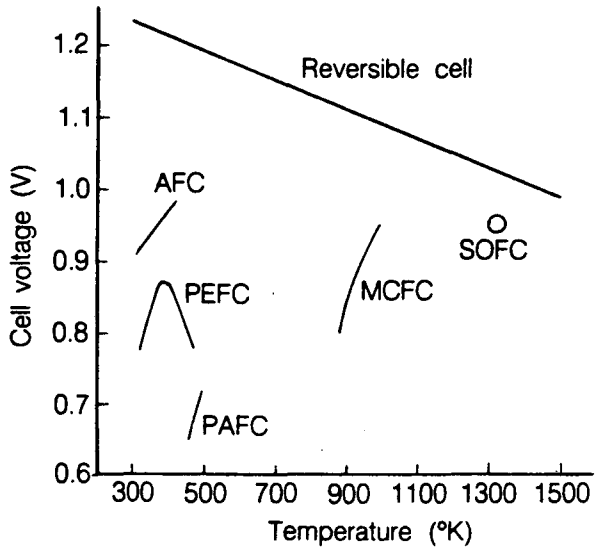

Figure 2-1. Dependence of the initial operating cell voltage of typical fuel cells on temperature. *Source*: (Figure 1, p. 46) S.N. Simons, R.B. King and P.R. Prokopius, in *Symposium Proceedings Fuel Cells Technology Status and Applications*, Edited by E.H. Camara, Institute of Gas Technology, Chicago, IL (1982) p. 45.

operating voltages of these fuel cells increase with an increase in operating temperature, with PEFCs exhibiting a maximum in operating voltage.[a] The operating temperature of SOFCs is limited to about 1000°C because the ohmic resistance of the solid electrolyte increases rapidly as the temperature decreases. Furthermore, with the exception of SOFCs, the other types of fuel cells typically operate at voltages considerably below the reversible cell voltage. An increase in the operating temperature is beneficial to fuel-cell performance because of the increase in reaction rate, higher mass-transfer rate, and usually lower cell resistance arising from the higher ionic conductivity of the electrolyte. In addition, the CO tolerance of electrocatalysts in low-temperature fuel cells improves as the operating temperature increases. These factors all combine to reduce the polarization at higher temperatures. On the negative side, materials problems related to corrosion, electrode degradation, electrocatalyst sintering and recrystallization, and electrolyte loss by evaporation are all accelerated at high temperature.

An increase in operating pressure has several beneficial effects on fuel-cell performance because the reactant partial pressure, gas solubility and mass transfer rates are higher. In addition, electrolyte loss by evaporation is reduced at higher operating pressures. These benefits must be balanced against hardware and materials problems, as well as power costs, imposed at higher operating pressure. In particular, pressure differentials in MCFCs must be minimized to prevent reactant gas leakage through the electrolyte and seals, and high pressure favors carbon deposition and methane formation in the fuel gas.

[a] The cell voltage of PEFCs goes through a maximum as a function of temperature because of the difficulties with water management at higher temperature.

2.2 Reactant Utilization and Gas Composition

Both the reactant utilization and gas composition have a major impact on fuel-cell efficiency. It is apparent from the discussion in Chapter 1 that fuel and oxidant gases containing a higher concentration of electrochemical reactants will produce a higher fuel-cell voltage.

Utilization (U) refers to the fraction of the total fuel or oxidant introduced into a fuel cell that reacts electrochemically. In low-temperature fuel cells, determining the fuel utilization is relatively straightforward when H_2 is the fuel because it is the only reactant that is involved in the electrochemical reaction,[b] i.e.,

$$U = \frac{H_{2,in} - H_{2,out}}{H_{2,in}} = \frac{H_2 \text{ consumed}}{H_{2,in}} \tag{2-3}$$

where $H_{2,in}$ and $H_{2,out}$ are the concentration of H_2 at the inlet and outlet of the fuel cell, respectively. However, hydrogen can be consumed by various other pathways, such as by chemical reaction (i.e., with O_2 and cell components) and loss via leakage out of the cell. These pathways increase the apparent utilization of hydrogen without contributing to the electrical energy derived from the fuel cell. A similar type of calculation is used to determine the oxidant utilization. For the cathode in MCFCs, two reactant gases, O_2 and CO_2, are utilized in the electrochemical reaction. The oxidant utilization should be based on the limiting reactant. Frequently O_2, which is readily available from make-up air, is present in excess and CO_2 is the limiting reactant.

A significant advantage of high-temperature fuel cells such as MCFCs is their ability to utilize CO as a fuel. The anodic oxidation of CO in an operating MCFC is slow compared to the anodic oxidation of H_2, thus the direct oxidation of CO is not likely. However the water-gas shift reaction

$$CO + H_2O = H_2 + CO_2 \tag{2-4}$$

reaches equilibrium rapidly in MCFCs at 650°C to produce H_2. As H_2 is consumed, the reaction is driven to the right since both H_2O and CO_2 are produced in equal quantities in the anodic reaction. Because of the shift reaction, fuel utilization in MCFCs can exceed the value for H_2 utilization, based on the inlet H_2 concentration. Take for example a typical anode gas composition of 34% H_2/22% H_2O/13% CO/18% CO_2/12% N_2. A fuel utilization of 80% (i.e., equivalent to 110% H_2) can be achieved with this gas composition even though this would require 10% more H_2 (total of 37.6%) than is available in the original fuel. The high fuel utilization is possible because the shift reaction provides the necessary additional H_2 that is oxidized at the anode. In this case the fuel utilization is given by

$$U = \frac{H_2 \text{ consumed}}{H_{2,in} + CO_{in}} \tag{2-5}$$

where the H_2 consumed originates from the H_2 present at the fuel cell inlet ($H_{2,in}$) and any H_2 produced in the cell by the water-gas shift reaction (CO_{in}).

[b] Assumes no gas cross-over or leakage out of the cell.

Gas composition changes between the inlet and outlet of a fuel cell, caused by the electrochemical reaction, lead to reduced cell voltages. This voltage reduction arises because the cell voltage adjusts to the lowest electrode potential given by the Nernst equation for the various gas compositions at the exit of the anode and cathode chambers. Since electrodes are usually good electronic conductors and isopotential surfaces, the cell voltage may not exceed the minimum (local) value of the Nernst potential. In the case of a fuel cell with the flow of fuel and oxidant in the same direction (i.e., co-flow), the minimum Nernst potential occurs at the cell outlet. When the gas flows are counter-flow or cross-flow, determining the location of the minimum potential is not straightforward.

The MCFC provides a good example to illustrate the influence of the extent of reactant utilization on the electrode potential. An analysis of the gas composition at the fuel-cell outlet as a function of utilization at the anode (β) and cathode (γ) is presented in Appendix 9.2. The Nernst equation can be expressed in terms of the mole fraction of the gases (X_i) at the fuel-cell outlet,

$$E = E^{o} + \frac{RT}{2F} \ln \frac{X_{H_2} X_{O_2}^{1/2} X_{CO_2,cathode} P^{1/2}}{X_{H_2O,anode} X_{CO_2,anode}} \tag{2-6}$$

where P is the cell gas pressure. The second term on the right-hand side of Equation 2-6, the so-called Nernst term, reflects the change in the reversible potential as a function of reactant utilization, gas composition and pressure. Figure 2-2 illustrates the change in reversible cell potential calculated as a function of utilization using Equation 2-6. The reversible potential at 650°C and 1-atm pressure

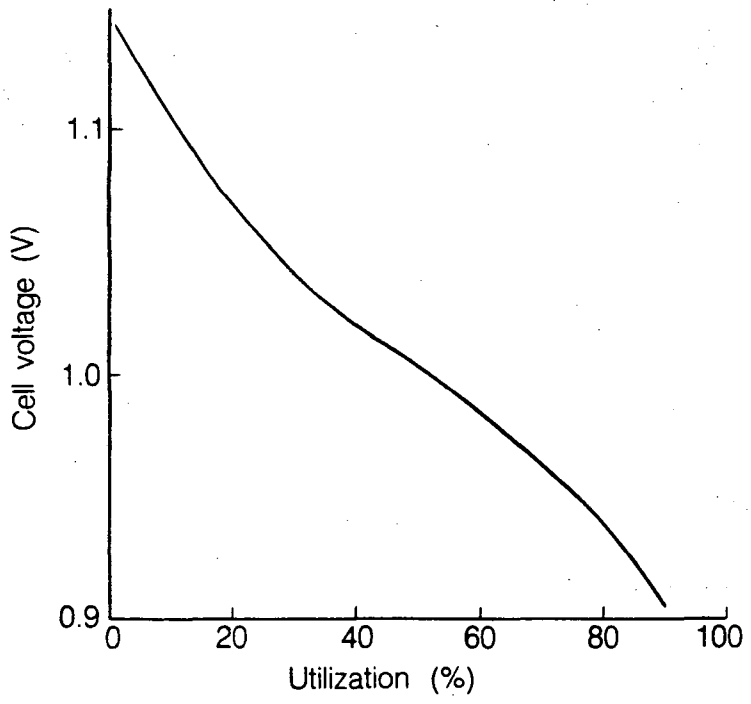

Figure 2-2. The variation in the reversible cell voltage as a function of reactant utilization (fuel and oxidant utilizations equal) in a MCFC at 650°C and 1 atm. Fuel gas: H_2/20% CO_2 saturated with H_2O at 25°C; oxidant gas: 60% CO_2/30% O_2/10% inert.

is plotted as a function of reactant utilization ($\beta = \gamma$) for inlet gas compositions of 80% H_2/20% CO_2 saturated with H_2O at 25°C (fuel gas[c]) and 60% CO_2/30% O_2/10% inerts (oxidant gas); gas compositions and utilizations are listed in Table 2.1. The mole fractions of H_2 and CO in the fuel gas decrease as the utilization increases and the mole fractions of H_2O and CO_2 show the opposite trend. At the cathode the mole fractions of O_2 and CO_2 decrease with an increase in utilization because they are both consumed in the electrochemical reaction. The reversible cell potential plotted in Figure 2-2 is calculated from the equilibrium compositions for the water-gas shift reaction at the cell outlet. An analysis of the data in the figure indicates that a change in the utilization from 20 to 80% will cause a decrease in the reversible potential of about 0.158 V, or roughly 0.0026 V/% utilization. These results show that MCFCs operating at high utilization will suffer a large voltage loss because of the magnitude of the Nernst term.

An analysis by Cairns and Liebhafsky (3) for a H_2/air fuel cell shows that a change in the gas composition that produces a 60-mV change in the reversible cell potential at near room temperature corresponds to a 300-mV change at 1200°C. Thus, gas composition changes are more serious in high-temperature fuel cells.

Table 2.1 Outlet Gas Composition as a Function of Utilization in MCFC at 650°C

Gas	Utilization[a] (%)				
	0	25	50	75	90
Anode[b]					
X_{H_2}	0.645	0.410	0.216	0.089	0.033
X_{CO_2}	0.064	0.139	0.262	0.375	0.436
X_{CO}	0.130	0.078	0.063	0.033	0.013
X_{H_2O}	0.161	0.378	0.458	0.502	0.519
Cathode[c]					
X_{CO_2}	0.600	0.581	0.545	0.461	0.316
X_{O_2}	0.300	0.290	0.273	0.231	0.158

[a] Same utilization for fuel and oxidant. Gas compositions are given in mole fractions.

[b] 80% H_2/20% CO_2 saturated with H_2O at 25°C. Fuel gas compositions are based on compositions for water-gas shift equilibrium.

[c] 30% O_2/60% CO_2/10% inert gas.

[c] Anode inlet composition is 64.5% H_2/6.4% CO_2/13% CO/16.1% H_2O after equilibration by water-gas shift reaction.

2.3 Fuel-Cell Efficiency

In this section, the concept of fuel-cell efficiency will be introduced. Various definitions of efficiencies have been applied to operating fuel cells, and they are compiled in Table 2.2. A more-detailed analysis of the various efficiency parameters is provided by Benjamin et al. (1), and so they are only summarized here. Additional details on the efficiencies of fuel cells are presented by Gilvarry and Slaughter (4).

Table 2.2 Fuel-Cell Efficiency Definitions

Efficiency Parameter	Symbol	Remarks
Thermal	$\varepsilon_{Th} = \frac{\Delta G_r}{\Delta H_r}$	$\frac{\text{Gibbs free energy change}}{\text{enthalpy change}}$
Voltage	$\varepsilon_V = \frac{V}{E}$	$\frac{\text{actual cell voltage}}{\text{thermodynamic cell voltage}}$
Current	$\varepsilon_I = \varepsilon_F U$	$\frac{\text{actual current}}{\text{current equivalent of reactant molar flow rate}}$
Electrochemical	$\varepsilon_E = \varepsilon_{Th}\varepsilon_V\varepsilon_F U$	$\frac{\text{dc energy produced}}{\text{enthalpy change}}$
Heating Value	$\varepsilon_H = \frac{\Delta H_r}{\Delta H_c}$	$\frac{\text{enthalpy change of combustible species}^a}{\text{heat energy available by combustion of fuel}}$
Fuel Cell	$\varepsilon_{FC} = \varepsilon_E\varepsilon_H$	$\frac{\text{dc energy produced}}{\text{LHV of gaseous fuel to fuel cell}}$
Fuel Processor	ε_{FP}	$\frac{\text{LHV of gaseous fuel from fuel processor}}{\text{HHV of raw fuel into fuel processor}}$
Power Conditioner	ε_{PC}	$\frac{\text{AC power out}}{\text{DC power in}}$
Fuel Cell System[b]	$\varepsilon_S = \varepsilon_{FP}\varepsilon_{FC}\varepsilon_{PC}$	$\frac{\text{AC energy out}}{\text{HHV of raw fuel into fuel processor}}$
Fuel Cell System[c]	$\varepsilon_{S/H}$	$\frac{\text{total electrical energy + cogeneration heat}}{\text{HHV of raw fuel into fuel processor}}$

[a] combustible species involved in electrochemical reaction

[b] without waste heat utilization

[c] with waste heat utilization for additional electricity and cogeneration heat

HHV = higher heating value
LHV = lower heating value
U = fuel utilization

2.3.1 Thermal Efficiency

The comparative thermal efficiency (ε_{Th}), or maximum efficiency of an ideal electrochemical energy converter, is equal to the ratio of the free energy change to the enthalpy change, i.e.,

$$\varepsilon_{Th} = \frac{\Delta G_r}{\Delta H_r} = \frac{\Delta H_r - T\Delta S_r}{\Delta H_r} \tag{2-7}$$

where $T\Delta S_r$ is the reversible heat that is produced. For a combustion reaction, ΔH_r is the heat of combustion or heating value,[d] and it represents the maximum heat energy that can be produced isothermally and isostatically.

For fuels containing less than 100% H_2,

$$\Delta H_r = LHV_{H_2}\Gamma_{H_2}(\text{cal/g–mol feed gas}) \tag{2-8}$$

where Γ_{H_2} is the mole fraction of H_2 available in the fuel cell or from chemical equilibrium. For the PAFC operating at about 200°C, the amount of H_2 formed by chemical reactions (water-gas shift and methane reforming) in the fuel cell is negligible, thus only the feed H_2 (X_{H_2}) participates in the electrochemical reaction, i.e.,

$$\Gamma_{H_2} = X_{H_2} \tag{2-9}$$

On the other hand, additional H_2 is produced in high-temperature fuel cells such as MCFCs by the water-gas shift reaction (Equation 2-4) and the CH_4-reforming reactions

$$CO + H_2O = H_2 + CO_2 \tag{2-10}$$

and

$$CH_4 + H_2O = 3H_2 + CO \tag{2-11}$$

Therefore, the total H_2 mole fraction is equal to

$$\Gamma_{H_2} = X_{H_2} + X_{CO} + X_{CH_4} \tag{2-12}$$

where X_{CO} and X_{CH_4} are the mole fractions of H_2 obtained from CO and CH_4 by Reactions 2-10 and 2-11.

The Gibbs free energy change used in Equation 2-7 must be obtained for the cell operating temperature. Although thermodynamic data can be used, a more convenient approach is to use the

[d] In the combustion of H_2 to produce H_2O, the higher heating value (HHV) is obtained if water is condensed to a liquid. If the water is not condensed, the lower heating value (LHV) is obtained. The difference between HHV and LHV is the heat of condensation of water (i.e., 10.54 kcal/mole).

Nernst equation to determine the open-circuit voltage (E). Then ΔG_r is calculated from the equation

$$\Delta G_r = -nFE\Gamma_{H_2}(\text{cal/g–mol feed gas}) \tag{2-13}$$

Because E is a function of the gas partial pressure, ΔG_r is a function of the cell operating pressure and gas composition.

The thermal efficiency can be greater or less than 100%, depending on the chemical reaction (reactions with positive entropy change may result in $\varepsilon_{Th} > 100\%$). For example, η_{Th} at 25°C for the reactions

$$H_2\,(g) + \tfrac{1}{2}O_2\,(g) \rightarrow H_2O\,(l) \tag{2-14}$$

and

$$C\,(s) + \tfrac{1}{2}O_2\,(g) \rightarrow CO\,(g) \tag{2-15}$$

is 83% and 124%,[e] respectively, based on the HHV. The thermal efficiency for a fuel cell utilizing H_2 and O_2 (Reaction 2-14) decreases with an increase in temperature. Thus, the thermal efficiency of a high-temperature H_2/O_2 fuel cell is less than that of a low-temperature H_2/O_2 fuel cell, but the higher operating temperature reduces polarization to such an extent that the fuel-cell efficiency is higher. In general, ΔH_r is larger than ΔG_r for reactions of interest in fuel cells, i.e., η_{Th} is less than 100% and is usually in the range of 90%. However, in practice a part of the free energy, ΔG_r, as well as $T\Delta S_r$, is transformed into heat rather than electrical energy because of polarization.

2.3.2 Voltage Efficiency

The voltage efficiency (ε_V) is the ratio of the actual cell voltage (V) to the thermodynamic cell voltage (E), which is based on the inlet compositions for the fuel and oxidant. Because of polarization, the actual cell voltage of an operating fuel cell is less than the thermodynamic cell voltage. The voltage efficiency increases as the current decreases because of the decrease in polarization (see Chapter 1).

2.3.3 Current Efficiency

The Faradaic efficiency (ε_F) can be defined by the relationship

$$\varepsilon_F = \frac{I}{n_i F v} \tag{2-16}$$

where I is the current, n_i is the valence change for the electrochemical reaction, and v is the rate (moles/s) at which the reactant specie is consumed.[f] From Equation 2-16 it is apparent that the

[e] A hypothetical fuel cell based on the oxidation of carbon to CO would theoretically yield more electrical energy than obtained from the difference in enthalpy change of the products and reactants.

[f] For example, H_2 gas (1 atm, 298°K) which is completely consumed in an electrochemical reaction at the anode at a rate of $v = 6.8 \times 10^{-5}$ moles/s (equivalent to a flow rate of 100 cm^3/min) produces a current of I = 13 A.

highest current is obtained when $\varepsilon_F = 100\%$ and n_i is the maximum stoichiometric value (n_{max}), if multiple electrochemical reactions are possible. However, if an electrochemical reaction occurs with the formation of several products, the Faradaic efficiency will be less than 100%. To illustrate this point, consider the electrochemical oxidation of methanol to produce CO_2,

$$CH_3OH + H_2O \rightarrow CO_2 + 6H^+ + 6e^- \quad (2\text{-}17)$$

This reaction occurs with $n_{max} = 6$, but other products (i.e., formaldehyde, formic acid) are possible by electrochemical oxidation involving $n < 6$. When the electrochemical oxidation of CH_3OH occurs by several oxidation pathways to form different products, the Faradaic efficiency is less than 100%.

The current efficiency (ε_I) is defined by the ratio of the current obtained by electrochemical reaction to the total current available from complete electrochemical conversion of the reactant, which can be expressed in the form

$$\varepsilon_I = \varepsilon_F U \quad (2\text{-}18)$$

In general, U refers to the utilization of the fuel gas. When $\varepsilon_F = 100\%$, Equation 2-18 reduces to

$$\varepsilon_I = U \quad (2\text{-}19)$$

which is essentially the same definition used by Benjamin et al. (1) for current efficiency. For a simple reactant such as H_2 undergoing electrochemical oxidation, ε_F is close to 100% if there are no side reactions, gas leaks or inter-electrode diffusion. In general, the Faradaic efficiency of electrochemical reactions in typical fuel cells is high. On the other hand the reactant utilization varies greatly, depending on the operating conditions and the design of the cell; but, reactant utilizations exceeding 85% are generally not practical in fuel cells because of the high polarization that is encountered. The net result is that the current efficiency of fuel cells is dictated mainly by the reactant utilization and not the Faradaic efficiency, consequently fuel cells must operate at high utilization to obtain high current efficiency.

The current efficiencies for the anode and cathode should be considered separately because they usually are different at the two electrodes. If only one electrode operates at less than 100% Faradaic efficiency, then ε_F in Equation 2-18 should refer to this electrode. In the case where both the anode and cathode operate at ε_F less than 100% then Equation 2-18 should be modified by combining each ε_F with the corresponding closed-circuit half-cell potential for each electrode. These situations are discussed in more detail by Eisenberg (5).

2.3.4 Electrochemical Efficiency

The electrochemical efficiency (ε_E) of a fuel cell is the product of several efficiency parameters (i.e., thermodynamic, voltage and current)

$$\varepsilon_E = \varepsilon_{Th}\, \varepsilon_V\, \varepsilon_F\, U \quad (2\text{-}20)$$

When $\varepsilon_F = 100\%$, Equation 2-20 reduces to

$$\varepsilon_E = \varepsilon_{Th}\, \varepsilon_V\, U \tag{2-21}$$

which is the same equation presented earlier by Benjamin et al. (1). For a fuel cell operating on a fuel gas containing only inert gases and electrochemically active reactants, Equation 2-20 is sufficient to determine the efficiency of fuel conversion to electrical power. When other combustible species are present in the fuel cell, an additional efficiency term must be considered.

2.3.5 Heating Value Efficiency

A mixture of inert gases (e.g., N_2, CO_2), impurities (e.g., S, COS) and combustible (e.g., H_2, CO, CH_4) gases are products from most practical fuel processors. A heat engine is capable of converting these combustible gases into heat energy, whereas a fuel cell is able to electrochemically oxidize only H_2 directly into electrical energy, although CO and CH_4 are consumed indirectly at high temperature after they are converted to H_2. The heating value efficiency (ε_H) provides a measure of the ratio of ΔH_r, which includes only those combustible species involved in the electrochemical reaction, to the amount of heat available from combustion of all combustible species in the fuel gas (ΔH_c)

$$\varepsilon_H = \frac{\Delta H_r}{\Delta H_c} \tag{2-22}$$

To calculate ΔH_c requires the summation of LHV for each of the combustible species i

$$\Delta H_c = \Sigma\, LHV_i\, X_i \tag{2-23}$$

The lower heating value is used because the combustion product H_2O is generally not condensed in the fuel cell.

2.3.6 Fuel Cell Efficiency

The fuel cell efficiency (ε_{FC}) is defined as

$$\varepsilon_{FC} = \varepsilon_E\, \varepsilon_H \tag{2-24}$$

and is proportional to the ratio of the energy produced in the fuel cell to the LHV of the fuel. Only the efficiency of the fuel-cell power section is included in ε_{FC}, and not those associated with the fuel processor, power conditioner, and the utilization of waste heat.

2.3.7 Fuel Cell System Efficiency

A fuel-cell power plant consists of other subsystems, besides the fuel-cell subsystem, which contribute to the overall efficiency. These include the fuel-processor and power-conditioner subsystems, which along with the fuel-cell subsystem and an optional bottoming cycle or cogeneration subsystem, make up a fuel-cell power plant. The overall efficiency of a fuel-cell power plant without

waste heat utilization is given by

$$\varepsilon_S = \varepsilon_{FP}\, \varepsilon_{FC}\, \varepsilon_{PC} \tag{2-25}$$

where ε_{FP} and ε_{PC} are defined in Table 2.2. If the waste heat is utilized in a bottoming cycle and/or cogeneration scheme, the fuel-cell system efficiency becomes

$$\varepsilon_{S/H} = \frac{\text{total ac energy + cogeneration heat}}{\text{HHV raw fuel into fuel processor}} \tag{2-26}$$

The total ac power is the sum of the power obtained from the fuel cell and the bottoming cycle.

A rough estimate of the efficiency (%) of a total fuel-cell power plant, from fuel to alternating-current power, is given by Fickett (6):

$$\text{Efficiency} = 59V_c \tag{2-27}$$

where V_c is the voltage of a single cell. The error in this estimate is about 5%, and the equation illustrates the importance of the voltage of single cells in establishing the overall efficiency of a fuel-cell power plant.

2.3.8 Heat Rate and Calculated Fuel Cell Efficiency

From the above definitions, it follows that

$$\varepsilon_{FC} = \frac{n_i FVU}{\Delta H_c} \tag{2-28}$$

when ε_F = 100%. Equation 2-28 is useful for calculating ε_{FC} when a fuel such as pure H_2 is fed to the anode. However, for fuels containing less than 100% H_2 (or less than 100% of fuel that can be electrochemically oxidized after chemical equilibrium, e.g., CO) ε_{FC} is given by

$$\varepsilon_{FC} = \frac{n_i FVU\Gamma_{H_2}}{\Delta H_c} \tag{2-29}$$

where Γ_{H_2} is the mole fraction of H_2 in the fuel. The fuel-cell efficiency is a function of the cell voltage and the fuel utilization. This efficiency is higher than that expected for a total fuel-cell power plant because the efficiency of the fuel processor and power conditioner are not considered. In addition, the efficiency gain expected from the use of reject heat is not included.

Consider the case where the HHV of the fuel is used in calculating ε_{FC} for a fuel cell. For H_2 and CH_4, the voltage equivalent for HHV of these fuels is $\Delta H_c/nF$ (23.06 kcal/equivalent = 1 V), or 1.481 V and 1.143 V, respectively. Based on the HHV of H_2 and CH_4, the theoretical fuel-cell efficiencies calculated by Equation 2-28 are plotted in Figure 2-3 as a function of cell voltage and utilization. The Nernst potential for the reactant gas composition at the fuel-cell outlet limits the maximum potential attainable. For utilizations of ≤90% shown in Figure 2-3, the calculated Nernst potentials for the outlet gas compositions of H_2/O_2 and CH_4/O_2 fuel cells at 25°C are >1.0 V. An actual fuel cell would not operate at 100% utilization because of the Nernst effect discussed above

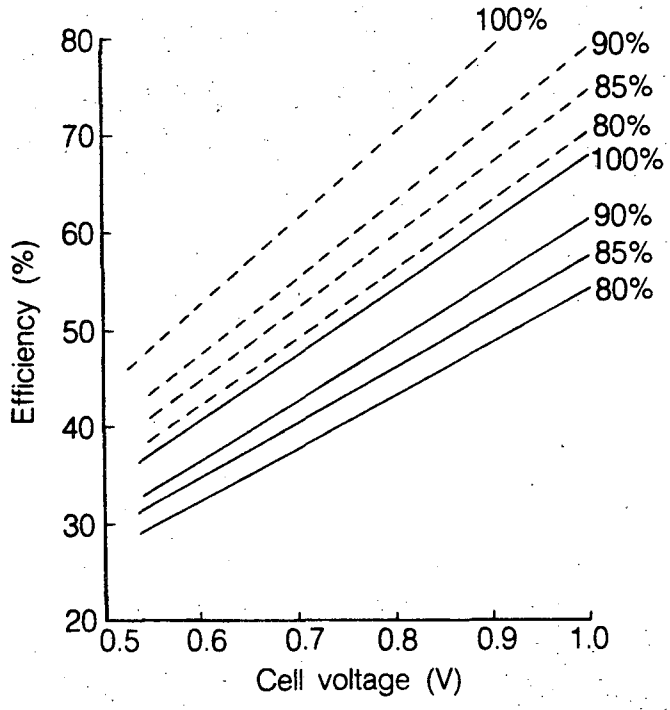

Figure 2-3. Theoretical fuel-cell efficiency as a function of cell voltage. Fuel utilization (%) is parameter.
———————, H_2,
— — — — —, CH_4.

and the inherent polarization. However, curves are presented in Figure 2-3 at 100% utilization to illustrate the theoretical maximum efficiencies attainable (i.e., the Nernst effect and polarization were assumed to be negligible). These plots clearly show the advantage of operating a fuel cell at high utilization and high cell voltage to achieve high efficiency. Unfortunately, the fuel cell voltage decreases because of increased polarization at higher utilization. For a practical fuel utilization of 85% and a cell voltage of 0.7 V, ε_{FC} for a H_2/O_2 fuel cell is about 40%.[g] If a fuel cell utilizes CH_4 by internal steam reforming, an increase in efficiency is obtained. According to the data in Figure 2-3, the efficiency of a CH_4/O_2 fuel cell at 0.7 V is over 10% higher at 85% fuel utilization than a corresponding H_2/O_2 fuel cell. These results suggest there is a large efficiency gain from internal steam reforming of CH_4; this approach is currently under investigation and is described in Chapter 4.

The heat rate (HR in Btu/kWh, HHV) is a term used primarily by the electric utility industry to describe the amount of chemical energy (Btu) of fuel required to produce 1 kWh of electrical energy, and it provides a convenient parameter for comparison with the performance of conventional power plants. If a fuel cell operates at 100% efficiency, then its heat rate would be 3413 Btu/kWh, and this value is the lowest amount of thermal energy that will produce 1 kWh of electrical energy.

[g] Equation 2-27 yields an efficiency of 41% at 0.7 V, in close agreement with the value obtained by Equation 2-28. A more detailed discussion on the calculation of fuel-cell efficiency is presented in Reference 1.

The heat rate is inversely proportional to the fuel-cell efficiency,

$$\varepsilon_{FC} = \frac{3413}{HR} \tag{2-30}$$

and it can be correlated with the cell voltage by Equation 2-28. The relationship of cell voltage to HR and ε_{FC} is presented in Table 2.3 for a H_2/O_2 fuel cell operating at 100% fuel utilization. These data show that an increase in the operating cell voltage of a fuel cell results in a lower heat rate and a higher efficiency. Unfortunately, the power density (kW/unit electrode area) of a single cell usually decreases with an increase in cell voltage, and the net result is an increase in capital cost[h] for the fuel cell.

Table 2.3 Relationship of Cell Voltage to Fuel-Cell Efficiency and Heat Rate for 100% H_2 Utilization at 25°C

Cell Voltage[a] (V)	Fuel Cell Efficiency (%)	Heat Rate (Btu/kWh)
1.229	83[b]	4112
1.185	80	4266
1.037	70	4876
0.889	60	5688
0.741	50	6826
0.592	40	8533
0.444	30	11377

[a] Based on HHV of H_2, which has a voltage equivalent of 1.481 V for 100% efficiency

[b] Maximum efficiency possible, equal to $\frac{\Delta G^o}{\Delta H^o}$

[h] The capital cost of a fuel cell, expressed as dollars per kW of capacity, is inversely proportional to the power density of a single cell. Thus, the power rating of the cell effectively establishes the capital cost of a fuel-cell stack.

References

1. T.G. Benjamin, E.H. Camara and L.G. Marianowski, *Handbook of Fuel Cell Performance,* prepared by the Institute of Gas Technology for the United States Department of Energy under Contract No. EC-77-C-03-1545 (May 1980).
2. S.N. Simons, R.B. King and P.R. Prokopius, in *Symposium Proceedings Fuel Cells Technology Status and Applications,* Edited by E.H. Camara, Institute of Gas Technology, Chicago, IL (1982) p. 45.
3. E.J. Cairns and H.A. Liebhafsky, *Energy Conversion,* **9,** 63 (1969).
4. J.J. Gilvarry and J.I. Slaughter, *Electrochim. Acta,* **8,** 711 (1963).
5. M. Eisenberg, *Electrochim. Acta,* **6,** 93 (1962); in *Advances in Electrochemistry and Electrochemical Engineering,* Volume 2, Edited by C.W. Tobias, Interscience Publishers, New York, NY, (1962), p. 235.
6. A.P. Fickett, *Scientific American,* p. 70 (December 1978).

3. PHOSPHORIC ACID FUEL CELL

The PAFC is the fuel-cell technology that is closest to commercialization, and field tests of 4.8-MW, 40-kW and 12-kW power plants have been completed. The major efforts in the United States (U.S.) are concentrated on the development of PAFCs for stationary dispersed power plants and stationary baseload power plants, and these aspects have been reviewed by Warshay (1) and Appleby (2). The major industrial participants in the U.S. are International Fuel Cells Corporation, Westinghouse Electric Corporation/Energy Research Corporation and Engelhard Corporation. In this chapter, the status of the cell components and performance of PAFC is discussed.

The electrochemical reactions occurring in PAFCs are

$$H_2 \rightarrow 2H^+ + 2e^- \tag{3-1}$$

at the anode, and

$$\tfrac{1}{2}O_2 + 2H^+ + 2e^- \rightarrow H_2O \tag{3-2}$$

at the cathode. The overall cell reaction is

$$\tfrac{1}{2}O_2 + H_2 \rightarrow H_2O \tag{3-3}$$

The electrochemical reactions occur on highly dispersed electrocatalyst particles supported on carbon black. At the cathode, the typical electrocatalyst is Pt, while at the anode, Pt or an alloy containing Pt is commonly used.

3.1 Cell Components

3.1.1 State-of-the-Art Components

The evolution from 1965 to the present day in the development of cell components for PAFCs is summarized in Table 3.1. In the mid 1960s, the conventional porous electrodes were PTFE-bonded Pt black, and the loadings were about 9 mg Pt/cm^2. During the past two decades, Pt supported on carbon black has replaced Pt black in porous PTFE-bonded electrode structures as the electrocatalyst. A dramatic reduction in Pt loading has also occurred; the loadings[a] are currently

[a] Assuming a cell voltage of 700 mV at 200 mA/cm^2 and the current Pt loadings at the anode and cathode, ~5.36 g Pt is required per kilowatt of power generated.

Table 3.1 Evolution of Cell Component Technology for Phosphoric Acid Fuel Cells

Component	ca. 1965	ca. 1975	Current Status
Anode	• PTFE-bonded Pt black	• PTFE-bonded Pt/C	• PTFE-bonded Pt/C
		• Vulcan XC-72[a]	• Vulcan XC-72[a]
	• 9 mg/cm^2	• 0.25 mg Pt/cm^2	• 0.25 mg Pt/cm^2
Cathode	• PTFE-bonded Pt black	• PTFE-bonded Pt/C	• PTFE-bonded Pt/C
		• Vulcan XC-72[a]	• Vulcan XC-72[a]
	• 9 mg/cm^2	• 0.5 mg Pt/cm^2	• 0.5 mg Pt/cm^2
Electrode Support	• Ta mesh screen	• carbon paper	• carbon paper
Electrolyte Support	• glass fiber paper	• PTFE-bonded SiC	• PTFE-bonded SiC
Electrolyte	• 85% H_3PO_4	• 95% H_3PO_4	• 100% H_3PO_4

[a] Conductive oil furnace black, product of Cabot Corp. Typical properties: 002 d-spacing of 3.6 Å by X-ray diffraction, surface area of 220 m^2/g by nitrogen adsorption, and average particle size of 30 μm by electron microscopy.

about 0.25 mg Pt/cm^2 in the anode and about 0.50 mg Pt/cm^2 in the cathode (At both electrodes, Pt may be alloyed with other metals). The operating temperature, and correspondingly the acid concentration, of PAFCs has increased to achieve higher cell performance; temperatures of about 200°C and acid concentrations of 100% H_3PO_4 are commonly used today. In addition, the operating pressure of PAFCs has surpassed 5 atm in many tests, and commercial electric utility systems are planned to operate at 8.2 atm.

One of the major breakthroughs in PAFC technology that occurred in the late 1960s was the development of carbon blacks and graphites for cell-construction materials; these developments are reviewed by Appleby (3) and Kordesch (4). It was shown at that time that carbon black and graphite were sufficiently stable to replace the more expensive gold-plated tantalum cell hardware. The use of high-surface-area carbon blacks to support Pt permitted a dramatic reduction in Pt loading, without sacrificing electrode performance. It has been reported (3) that "without carbon, a reasonably inexpensive acid fuel cell would be impossible, since no other material combines the necessary properties of electronic conductivity, good corrosion resistance, low density, surface properties (especially in high-area form) and above all, low cost." However, carbon corrosion and Pt dissolu-

tion become problematic at cell voltages above ~0.8 V, consequently, low current densities and hot-standby at open-circuit cathode potential are to be avoided.

The porous electrodes used in PAFCs are described extensively in the patent literature (5); see also the review by Kordesch (4). These electrodes contain a mixture of the electrocatalyst supported on carbon black and a polymeric binder, usually PTFE (about 30 to 50 wt%). The PTFE binds the carbon black particles together to form an integral (but porous) structure, which is supported on a porous carbon-paper substrate. The carbon paper serves as a structural support for the electrocatalyst layer, as well as the current collector. A typical carbon paper used in PAFCs has an initial porosity of about 90%, which is reduced to about 60% by impregnation with 40 wt% PTFE. This wet-proof carbon paper contains macropores of 3- to 50-μm diameter (median pore diameter of about 12.5 μm) and micropores with a median pore diameter of about 34 Å for gas permeability. The composite structure consisting of a carbon black/PTFE layer on carbon-paper substrate forms a stable three-phase interface in the fuel cell, with H_3PO_4 electrolyte on one side (electrocatalyst side) and the reactant gas environment on the other side of the carbon paper.

A bipolar plate serves to separate the individual cells and electrically connect them in series in a fuel-cell stack (see Figure 1-2). It also contains the gas channels for introducing the reactant gases to the porous electrodes and removing the products and inerts. Bipolar plates made from graphite-resin mixtures that are carbonized at low temperature (~900°C) are not suitable because of their rapid degradation in PAFC operating environments (6,7). However, the corrosion stability is improved by heat-treatment to 2700°C (7), i.e., the corrosion current is reduced by two orders of magnitude at 0.8 V in 97% H_3PO_4 at 190°C and 4.8 atm. The all-graphite bipolar plates are sufficiently corrosion-resistant for a projected life of 40,000 h in PAFCs, but they are still relatively costly to produce.

Several designs for the bipolar plate and ancillary stack components are being used by fuel cell developers, and these aspects are described in detail elsewhere (8-10). A typical PAFC stack contains cells connected in (electrical) series to obtain the practical voltage level desired for delivery to the load. In such an arrangement, individual cells are stacked with bipolar plates between the cells. The bipolar plates used in early PAFCs consisted of a single piece of graphite with gas channels machined on either side to direct the flow of fuel and oxidant gases in adjacent cells. Currently, both bipolar plates of the previous design and new designs consisting of several components are being considered. In the multi-component bipolar plates, a thin impervious plate serves to separate the reactant gases in adjacent cells in the stack, and separate porous plates with ribbed channels are used for directing gas flow. In a cell stack, the impervious plate is located between the two porous plates. The porous structure, which allows rapid gas permeability, is also used for storing additional acid to replenish the supply lost by evaporation during the cell operating life.

In PAFC stacks, provisions must be included to remove the heat generated during cell operation. Heat is removed by either liquid (two-phase water or a dielectric fluid) or gas (air) coolants which are pumped through cooling channels located (usually about every fifth cell) in the cell stack. Liquid cooling requires complex manifolds and connections, but better heat removal is achieved than with air cooling. The advantage of gas cooling is its simplicity, reliability and relatively low cost.

3.1.2 Alternative Components

Despite the progress in the development of cell components for PAFCs over the past decade, there is still active research underway on alternative components that offer the possibility of lower

cost and/or greater corrosion stability. The search for alternative electrocatalysts and electrocatalyst supports is one such area of R&D.

Transition metal (e.g., iron, cobalt) organic macrocycles[b] from the families of tetramethoxyphenylporphyrins (TMPP), phthalocyanines (PC), tetraazaannulenes (TAA) and tetraphenylporphyrins (TPP) have been evaluated as O_2-reduction electrocatalysts in PAFCs. One major problem with these organic macrocycles is their limited chemical stability in hot concentrated phosphoric acid. However, after heat-treatment of the organic macrocycle (i.e., CoTAA, CoPC, CoTMPP, FePC, FeTMPP) on carbon at about 500 to 800°C, the pyrolyzed residue exhibits electrocatalytic activity, which in some instances is comparable to that of Pt, and has promising stability, at least up to about 100°C (11). Another approach that has been successful for enhancing the electrocatalysis of O_2 reduction is to alloy Pt with transition metals such as Ti (12), Cr (13), V (14), Zr (14) and Ta (14). The enhancement in electrocatalytic activity has been explained by a correlation between the optimum nearest-neighbor distance of the elements in the alloy and the bond length in O_2 (15).

As the operating temperature and pressure of PAFCs increase, the corrosion stability of carbon-containing cell components becomes a greater issue. It appears that the present components are capable of providing cell lifetimes of 40,000 h. However, the PAFCs are designed and operated to minimize degradation of the carbon-containing components. Alternative support materials with improved physicochemical properties are desired to increase the flexibility and to remove the constraints placed on current PAFCs. A review of alternative materials to carbon for PAFCs has been presented by Jalan (16).

TiC is one example of an alternative material that showed good stability and promising performance as an electrocatalyst support for PAFCs (16,17), and it was estimated that this material may improve the heat rate of PAFCs by 500 Btu/kWh to yield an ultimate end-of-life value of 7800 Btu/kWh (18). Unfortunately, reproducible samples were difficult to prepare, and further development of TiC has been curtailed (19). Another carbide, SiC, which is an electrical insulator and used in the electrolyte matrix, was also considered for a cathode support after the SiC particles are coated with a novel carbon material to provide electrical conductivity (20).

3.2 Performance

The sources of polarization in PAFCs (cathode and anode Pt loadings of 0.5 mg Pt/cm^2, 180°C, 1 atm, 100% H_3PO_4) are illustrated in the current density-voltage plots in Figure 3-1. It is clear that the major polarization occurs at the cathode, and furthermore, the polarization is greater with air (560 mV at 300 mA/cm^2) than with pure oxygen (480 mV at 300 mA/cm^2) because of dilution of the reactant. The anode exhibits very low polarization (~4 mV/100 mA/cm^2) on pure H_2, which increases when CO is present in the fuel gas. The ohmic (IR) loss in PAFCs is also relatively small, amounting to about 12 mV/100 mA/cm^2. Based on the polarization values shown in Figure 3-1, an enhancement in cathode performance provides the best opportunity for improving the overall performance of PAFCs.

During the late 1970s, the PAFC operated at 150 to 200°C and 1 to 3 atm. The typical performance at that time was 0.55 to 0.65 V/cell at 100 to 400 mA/cm^2 (21). Figure 3-2 illustrates the improvement in the cell performance of PAFCs from 1967 to the mid 1980s. The data for 1967 and 1977 were taken from the report by Benjamin et al. (21), and originally published by Fickett (22).

[b] See Reference 11 for literature survey.

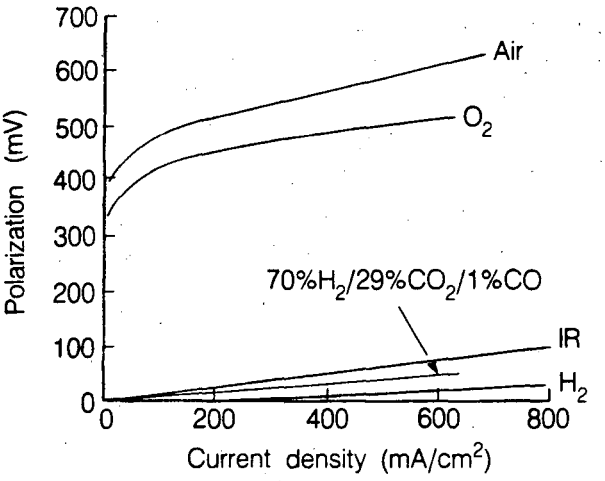

Figure 3-1. Contribution to polarization in PAFCs. Pt loading in anode and cathode is 0.5 mg/cm^2. 100% H_3PO_4, 180°C, 57°C dew point, 1 atm.

Source: (Figure 2-1, page 2-1) J.A.S. Bett, H.R. Kunz, S.W. Smith and L.L. Van Dine, "Investigation of Alloy Catalysts and Redox Catalysts for Phosphoric Acid Electrochemical Systems," FCR-7157F, prepared by International Fuel Cells under Contract No. 9-X13-D6271-1 for Los Alamos National Laboratory (1985).

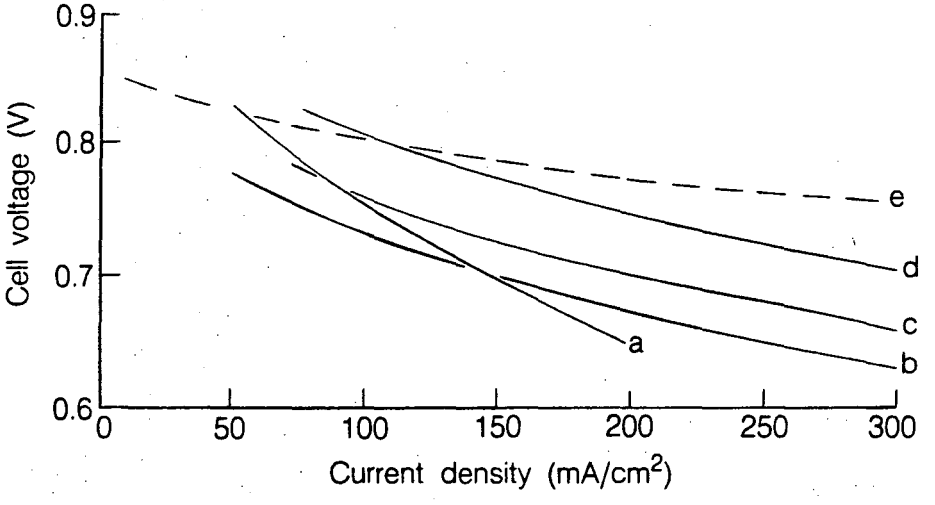

Figure 3-2. Improvement in the performance of H_2/air PAFCs.

(a) 1967—160°C, 1 atm, Pt loading of 20 mg/cm^2 on each electrode (22);
(b) 1977—190°C, 3 atm, Pt loading of 0.75 mg/cm^2 on each electrode (22);
(c) 1981—190°C, 3.4 atm, cathode Pt loading of 0.5 mg/cm^2 (23);
(d) 1981—205°C, 6.3 atm, cathode Pt loading of 0.5 mg/cm^2 (23).
(e) 1984—205°C, 8 atm, electrocatalyst loading was not specified (24).

The data from the 1980s were reported by Appleby (23) and Huff (24). The results show that the cell voltage at 190°C has increased by about 30 mV from 1967 to 1980, and large improvements in cell voltage are evident by increasing both the cell temperature and pressure.

Dramatic improvements in stack performance have been achieved since 1980, and these results (25) are illustrated in Figure 3-3. The relative power density of the short stacks has progressively improved along with an increase in the electrode areas and the number of cells in the stack. The encouraging progress in the performance of typical laboratory cells in 1985 indicates that further improvements in the power density of stacks should be achievable.

3.2.1 Effect of Pressure and Temperature

Pressure: It is well-known that an increase in the cell operating pressure enhances the performance of PAFCs (23,26,27). The change in pressure (P) at 169°C is predicted to produce a voltage gain (ΔV_p) that follows the relationship (26)

$$\Delta V_p = \frac{3(2.3RT)}{2F} \log \frac{P_2}{P_1} \tag{3-4}$$

where $\frac{3(2.3RT)}{2F}$ = 132 mV at 169°C. Benjamin et al. (21) reported that the effect of pressure on cell performance at 190°C and 323 mA/cm^2 is correlated by the equation

$$\Delta V_p \text{ (mV)} = 146 \log \frac{P_2}{P_1} \tag{3-5}$$

where P_1 and P_2 are different cell pressures. The data from Appleby (23) in Figure 3-2 indicate that the voltage gain observed by increasing the pressure from 3.4 atm (190°C) to 6.3 atm (205°C) is about 44 mV. According to Equation 3-5, the voltage gain calculated for this increase in pressure at

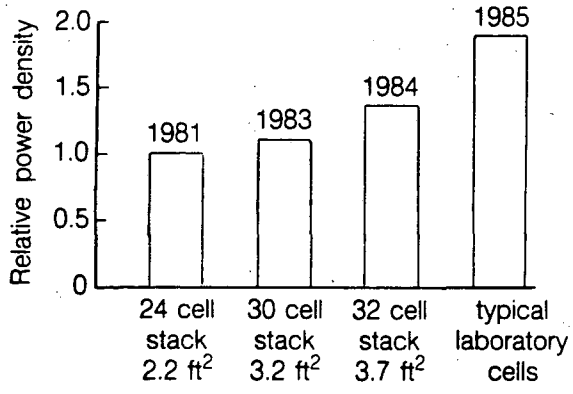

Figure 3-3. Relative performance improvements in short stacks and recent laboratory cells. *Source*: (Figure 1, p. 26) J.M. King and B.R. Will, *Abstracts 1985 Fuel Cell Seminar*, May 19-22, 1985, Tucson, AZ (1985).

190°C is 39 mV,[c] in reasonable agreement with experimental data in Figure 3-2. Measurements (26) of ΔV_p for an increase in pressure from 1 to 6 atm in small 6-cell stacks (350-cm^2 electrode area) show that ΔV_p is a function of current density, increasing from 94 mV at 100 mA/cm^2 to 118 mV at 300 mA/cm^2 (50% O_2 utilization with air oxidant, 70% H_2 utilization with pure H_2 fuel). From Equation 3-4, ΔV_p is 85 mV for an increase in pressure from 1 to 4.4 atm at 169°C, which is close to the experimental value obtained at 100 mA/cm^2. Other measurements (28) at 190°C show somewhat better agreement between the experimental data and Equation 3-4, however the measured values are greater than the predicted values.

The improvement in cell performance at higher pressure and high current density can be attributed to a lower diffusion polarization at the cathode and an increase in the reversible cell potential. In addition, pressurization is also expected to lower the acid concentration, and correspondingly the ionic conductivity will increase, with the net result being a reduction in the ohmic loss in the cell, if the partial pressure of water is allowed to vary. It is reported (26) that an increase in pressure of a cell (100% H_3PO_4, 169°C) from 1 to 4.4 atm produces a reduction in acid concentration to 97%, and a decrease of about 0.001 ohm in the resistance of a small 6-cell stack (350-cm^2 electrode area). An empirical equation has been derived (28) that takes into account the effects of pressure on the reversible cell potential, ohmic resistance, and activation and concentration polarizations at the cathode, i.e.,

$$\Delta V_p\ (mV) = \frac{RT}{4F}(2 + 4\alpha_c)\ \ln P + 1.22 \times 10^{-4} i + 4.8 \times 10^{-3} P - 1.93 \times 10^{-5}\ iP - 1.95 \times 10^{-2} \quad (3\text{-}6)$$

where α_c is the transfer coefficient for O_2 reduction, i is the current density (mA/cm^2) and P is the operating cell pressure (atm). The measured values of ΔV_p at 2.4 to 6.8 atm show excellent agreement (±2%) with the calculated values from Equation 3-6, assuming $\alpha_c = 0.85$.

The rate of oxygen reduction (i_{O_2}) on smooth Pt in concentrated H_3PO_4 follows a first-order dependence (29) on O_2 partial pressure; the reduction current at fixed electrode potential increases linearly with oxygen partial pressure, i.e.,

$$i_{O_2} \propto P_{O_2} \exp\ [-FV/RT] \quad (3\text{-}7)$$

The dependence of oxygen reduction current on electrode potential at different oxygen partial pressures is illustrated in Fig. 3-4 for a Pt electrocatalyst supported on graphitized carbon black in 99% H_3PO_4 at 170°C (30). Below about 50 mA/cm^2, the current ratios are 5:1, as expected for a linear dependence of i_{O_2} on P_{O_2}. However, at higher current densities, the current/pressure ratio becomes less than 5:1, and a minimum value of 2.8:1 is observed in some cases. This so-called "anomalous current ratio" is attributed to the resistance polarization in the porous electrode, and it is discussed in detail by Ross (30).

The influence of elevated oxygen pressures on the kinetics of oxygen reduction on smooth Pt in 89.5% H_3PO_4 at 175 and 205°C is shown in Figure 3-5 from data by McBreen et al. (27). A Tafel

[c] The difference in temperature between 190 and 205°C is disregarded so Equation 3-5 is assumed to be valid at both temperatures.

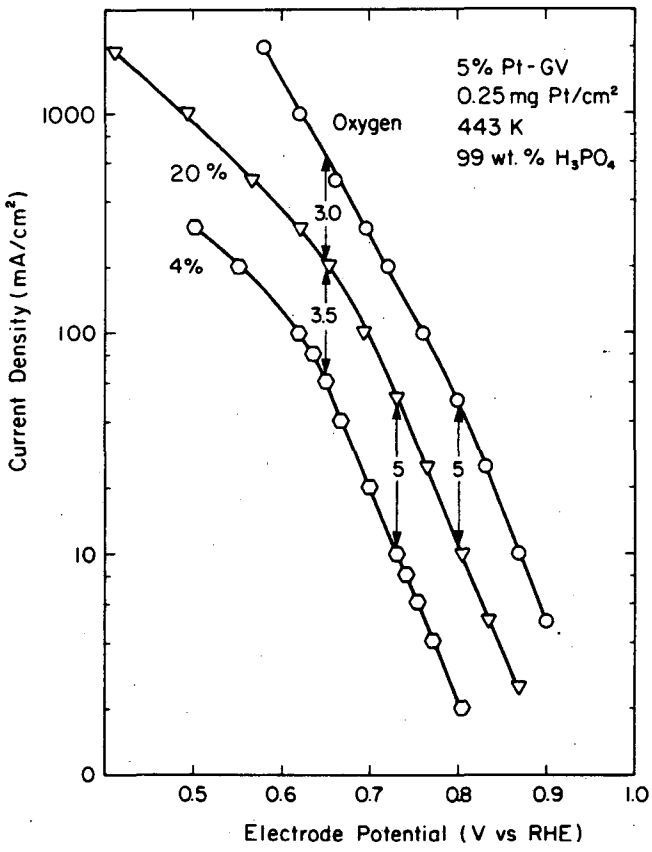

Figure 3-4. Effect of gas composition on O_2 reduction kinetics on Pt (0.5 mg/cm^2 Pt on carbon) in 99% H_3PO_4 at 170°C.

Source: (Figure 2, p. 30) P.N. Ross, "Anomalous Current Ratios in Phosphoric Acid Fuel Cell Cathodes," LBL-13955 (March 1986).

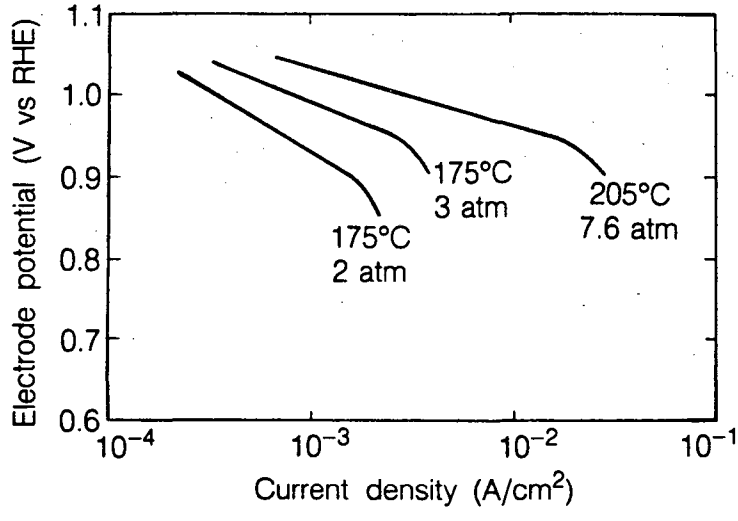

Figure 3-5. Tafel plots for O_2 reduction on Pt in 89.5% H_3PO_4 as a function of temperature and pressure.

Source: (Figure 2, p. 1216) J. McBreen, W.E. O'Grady and R. Richter, *J. Electrochem. Soc.*, **131**, 1215 (1984).

slope of ~RT/F is observed at 175°C and 3-atm pressure, and at higher pressures the current is proportional to pressure. It is apparent that the Tafel slope changes at 175°C when the pressure is increased from 2 to 3 atm, i.e., the higher pressure results in improved performance with a lower Tafel slope.

Although the rate of oxygen reduction at the cathode exhibits a first-order dependence on O_2 partial pressure, the PAFC does not show the same response because of the higher partial pressure of water and its effect on the reversible anode potential (23). The hydrogen electrode operates nearly reversibly, thus pressure has little influence on its performance. However, the partial pressure of water affects the reversible hydrogen potential, and in this manner, can influence the cell potential. It should be mentioned here that the water partial pressure and the resulting equilibrium acid concentration also has an affect on the oxygen reduction kinetics; the exchange current density decreases with an increase in H_3PO_4 concentration from 88 to 105% (31). There is some disagreement on the influence of the acid concentration on the activation energy for O_2 reduction (E_a); Kunz and Gruver (31) report E_a is constant (22 kcal/mol) in 85 to 105% H_3PO_4, whereas McBreen et al. (32) report that E_a is lower at higher acid concentrations.

Temperature: Figure 1-2 shows that the reversible cell potential for PAFCs consuming H_2 and O_2 decreases as the temperature increases by 0.27 mV/°C under standard conditions (product is water vapor). However, as discussed in Chapter 2, an increase in temperature has a beneficial effect on cell performance because activation polarization, mass transfer polarization and ohmic losses are reduced.

The kinetics for the reduction of oxygen on Pt (10% Pt on Vulcan XC-72, 0.5 mg Pt/cm^2 loading) improves[d] as the cell temperature (1-atm operation) increases from 100 to 180°C (see Figure 3-6). At 300 mA/cm^2, the voltage gain (ΔV_T) with increasing temperature of pure O_2 is given by

$$\Delta V_T \text{ (mV)} = 0.55 \ (T_2 - T_{1)} \text{ (°C)} \qquad (3\text{-}8)$$

It is apparent from this equation that each degree increase in cell temperature should produce a performance increase of 0.55 mV at 300 mA/cm^2. According to the analysis by Benjamin et al. (21), the increase in cell performance (at 300 mA/cm^2, 3.4 atm pressure, low H_2 and O_2 utilizations) that is obtained by an increase in cell temperature between 190 and 250°C is 1.15 mV/°C. However, at the operating conditions in practical power plants, increasing the temperature has little effect on performance except to decrease the effect of CO poisoning (33). This behavior arises because in a practical power plant it is not possible to decouple pressure and temperature if the waste heat from the fuel-cell power section is used to raise steam for the fuel processor.[e] Practical operating pressure-temperature combinations are: 3 atm at 190°C, 6 atm at 210°C, and 8 atm at 220°C (33). The initial cell performances of PAFCs operating under these conditions are compared to that at atmospheric pressure and 190°C in Figure 3-7. Comparison of the cell voltage at 190°C and 1- or 3-atm pressure indicate an improvement of about 38 mV at the higher pressure. At 220°C and 8-atm pressure, a substantial improvement is obtained by use of Pt-V electrocatalyst rather than Pt in the cathode.

---

[d] The anode shows no significant performance improvement from 140 to 180°C on pure H_2, but in the presence of CO, increasing the temperature results in a marked improvement in performance (see discussion in 3.2.3).

[e] The fuel-cell temperature must be high enough to produce steam at a pressure sufficient for injection into the fuel processor, which operates at a higher pressure.

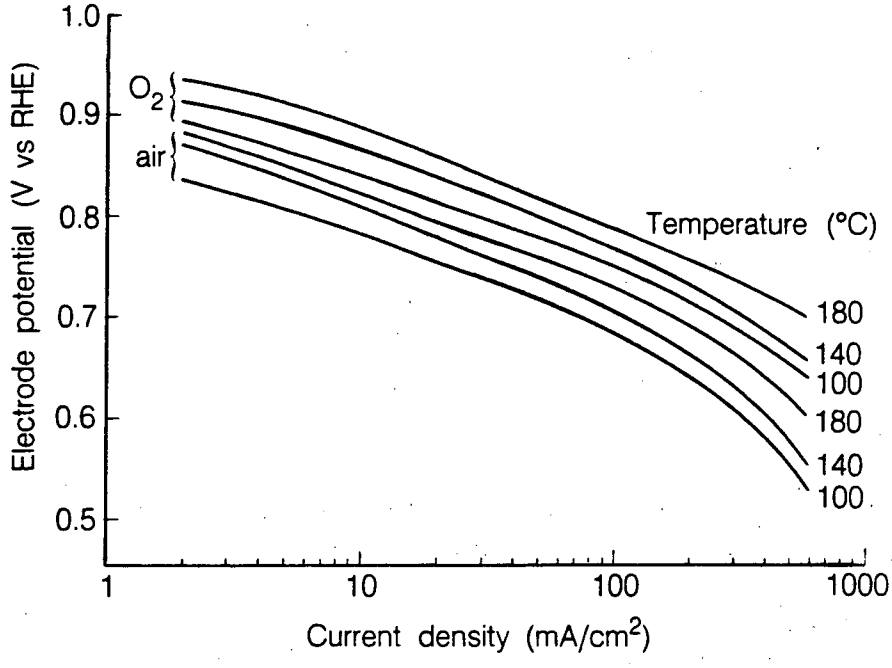

Figure 3-6. Influence of temperature on O_2 reduction in PAFCs. 10% Pt on Vulcan XC-72, 0.5 mg Pt/cm^2. Dew point, 57°C. H_3PO_4 concentration: 84% at 100°C, 94% at 140°C and 100% at 180°C.
Source: (Figure 2-19, p. 2-32) J.A.S. Bett, H.R. Kunz, S.W. Smith and L.L. Van Dine, "Investigation of Alloy Catalysts and Redox Catalysts for Phosphoric Acid Electrochemical Systems," FCR-7157F, prepared by International Fuel Cells under Contract No. 9-X13-D6271-1 for Los Alamos National Laboratory (1985).

3.2.2 Effect of Reactant Gas Composition and Utilization

Hydrogen for PAFC power plants will typically be derived by conversion of a wide variety of primary fuels such as CH_4 (e.g., natural gas), petroleum products (e.g., naphtha), coal liquids (e.g., CH_3OH) or coal gases. Besides H_2, CO and CO_2 are also produced during conversion of these fuels (unreacted hydrocarbons are also present). These reformed fuels contain low levels of CO (after steam-reforming and shift-conversion reactions in the fuel processor) that affect the anode performance in PAFCs. The CO_2 and unreacted hydrocarbons (e.g., CH_4) are electrochemically inert and act as diluents.

The reactant gas composition and utilization are parameters that affect the cathode performance, as evident in Figures 3-1, 3-4 and 3-6. Air, which contains ~20% O_2, is the oxidant of choice for PAFCs. As noted in Figure 3-4, the use of air with ~20% O_2 instead of pure O_2 results in a decrease in the current density of about a factor of 5 at constant electrode potential. The polarization at the cathode increases with an increase in O_2 utilization. Lu and France (34) measured the change of overpotential ($\Delta\eta_c$) at a PTFE-bonded porous electrode in 100% H_3PO_4 (191°C, atmospheric pressure) as a function of O_2 utilization. Their data are plotted in Figure 3-8 with

$$\Delta\eta_c = \eta_c - \eta_{c,\infty} \tag{3-9}$$

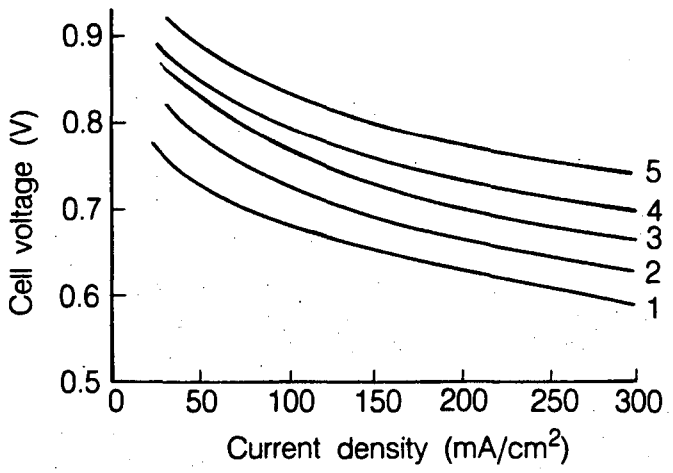

Figure 3-7. Influence of temperature and pressure on the initial performance of PAFCs.
(1) 1 atm, 190°C, 0.5 mg/cm^2 Pt on carbon;
(2) 3 atm, 190°C, 0.5 mg/cm^2 Pt on carbon;
(3) 6 atm, 210°C, 0.5 mg/cm^2 Pt on carbon;
(4) 8 atm, 220°C, 0.5 mg/cm^2 Pt on carbon;
(5) 8 atm, 220°C, 0.5 mg/cm Pt-V intermetallic on carbon.
Source: (Figure 43.7, p. 43-10) A.P. Fickett, in *Handbook of Fuel Cells and Batteries*, Edited by D. Linden, McGraw-Hill Book Co., New York, NY (1984).

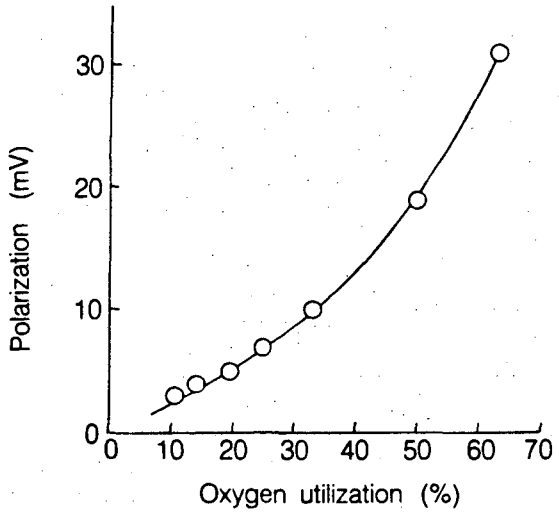

Figure 3-8. Polarization at cathode (0.52 mg Pt/cm^2) as a function of O_2 utilization, which is increased by decreasing the flow rate of the oxidant at atmospheric pressure. 100% H_3PO_4, 191°C, 300 mA/cm^2.
Source: Data taken from Table 5, Reference 34.

where η_c and $\eta_{c,\infty}$ are the cathode polarizations at finite and infinite (i.e., high flow rate, close to 0% utilization) flow rates, respectively. The additional polarization that is attributed to O_2 utilization is reflected in the results, and the magnitude of this loss increases rapidly as the utilization increases. At a nominal O_2 utilization of 50% for prototype PAFC power plants, the additional polarization estimated from the results in Figure 3-8 is 19 mV.

A voltage loss (ΔV_{CO_2}) occurs at the anode when a H_2-rich fuel is diluted with CO_2 (34), and the following relationship is observed,

$$\Delta V_{CO_2}\,(mV) = -10^3 \frac{RT}{2F} \ln P_{H_2} \qquad (3\text{-}10)$$

where P_{H_2} is the partial pressure of H_2 in the system. At 190°C, the presence of 10% CO_2 in H_2 should cause a voltage loss of about 2 mV. Thus, diluents in low concentrations are not expected to have a major effect on electrode performance; however, relative to the total anode polarization (i.e., 3 mV/100 mA/cm^2), the effects are large. Furthermore, because the anode reaction is nearly reversible, the fuel composition and hydrogen utilization do not strongly affect the cell performance. It has been reported (28) that with pure H_2, the cell voltage at 200 mA/cm^2 remains nearly constant at H_2 utilizations up to 90%, and then it decreases sharply at a H_2 utilization of 92%. When the fuel gas contains 74% H_2, 25% CO_2 and 1% CO, the cell voltage decreases gradually with H_2 utilization, ~1 mV for each 10% increase in utilization up to 70%, and decreases more rapidly at >70%.

3.2.3 Effect of Impurities

The concentration level of impurities entering the PAFC is very low relative to that of diluents or reactant gases, but their impact on the performance is large. Some impurities (e.g., sulfur compounds) originate from the fuel gas entering the fuel processor and are carried into the fuel cell with the reformed fuel, whereas others (e.g., CO) are produced in the fuel processor.

Carbon Monoxide: The presence of CO in a H_2-rich fuel has a significant effect on the anode performance because CO poisons the electrocatalytic activity of Pt electrodes. The poisoning of Pt by CO is reported to arise from the dual-site replacement of one H_2 molecule by two CO molecules on the Pt surface (36,37). According to this model, the anodic oxidation current at a fixed overpotential, with (i_{CO}) and without (i_{H_2}) CO present, is given as a function of CO coverage (θ_{CO}) by the equation

$$\frac{i_{CO}}{i_{H_2}} = (1 - \theta_{CO})^2 \qquad (3\text{-}11)$$

For $[CO]/[H_2] = 0.025$, $\theta_{CO} = 0.31$ at 190°C (34), therefore, i_{CO} is about 50% of i_{H_2}.

Both temperature and CO concentration have a major influence on the oxidation of H_2 on Pt in CO-containing fuel gases. The results in Figure 3-9 show the change in the H_2 oxidation current (at a polarization of 50 mV on 10% Pt on Vulcan XC-72, 0.5 mg Pt/cm^2) in the presence of 1% CO at 100 to 180°C. At low temperature (100°C), the current density that can be sustained at 50 mV polarization is low, but it increases dramatically as the temperature is raised to 180°C. Benjamin et al. (21) derived an equation for the voltage loss (at 269 mA/cm^2) resulting from CO poisoning as a

function of temperature,

$$\Delta V_{CO} = k(T)\ ([CO]_2 - [CO]_1) \qquad (3\text{-}12)$$

where k(T) is a constant that is a function of temperature and $[CO]_1$ and $[CO]_2$ are the per cent CO in the fuel gas. The values of k(T) at various temperatures are listed in Table 3.2. Using Equation 3-12 and the data in Table 3.2, it is apparent that for a given change in CO content, ΔV_{CO} is about 8.5 times larger at 163°C than at 218°C. The correlation provided by Equation 3-12 was obtained at 269 mA/cm^2, thus, its use at a different current density may not be appropriate.

The data in Figure 3-10 illustrate the influence of H_2 partial pressure and CO content on the performance of Pt anodes (10% Pt supported on Vulcan XC-72, 0.5 mg Pt/cm^2) in 100% H_3PO_4 at 180°C (10). Diluting the H_2 fuel gas with 30% CO_2 produces an additional polarization of about 11 mV at 300 mA/cm^2. The results show that the anode polarization with fuel gases of composition 70% H_2/(30-x)% CO_2/x% CO (x = 0, 0.3, 1, 3 and 5) increases considerably as the CO content increases to 5%. The voltage loss ($\Delta V_{CO} = V_{(H_2\text{-containing CO})} - V_{H_2}$) obtained at 180°C from Figure 3-10 and published data at 160°C (10) are plotted in Figure 3-11 as a function of $[CO]/[H_2]$ ratio at three current densities—100, 200 and 300 mA/cm^2. A dramatic increase in ΔV_{CO} with an increase in the $[CO]/[H_2]$ ratio is apparent at higher current density and lower temperature. The results of a similar study by Dhar et al. (35) with Pt (0.4 mg/cm^2 Pt supported on Vulcan XC-72) anodes obtained at at 100, 200 and 300 mA/cm^2 in 100% H_3PO_4 at 190°C are shown in Figure 3-12. Their results indicate a linear logarithmic dependence of voltage loss to the $[CO]/[H_2]$ ratio (1% CO with

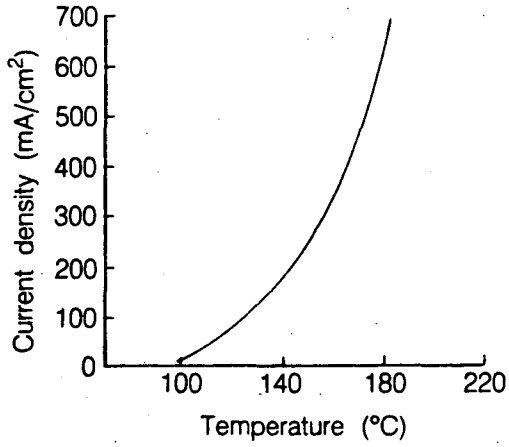

Figure 3-9. Effect of H_3PO_4 temperature on anode performance at a polarization of 50 mV in the presence of 1% CO. 10% Pt supported on Vulcan XC-72, 0.5 mg Pt/cm^2. Dew point, 57°C. Fuel composition, 70% H_2/29% CO_2/1% CO.

Source: (Figure 3-1, p. 3-1) J.A.S. Bett, H.R. Kunz, S.W. Smith and L.L. Van Dine, "Investigation of Alloy Catalysts and Redox Catalysts for Phosphoric Acid Electrochemical Systems," FCR-7157F, prepared by International Fuel Cells under Contract No. 9-X13-D6271-1 for Los Alamos National Laboratory (1985).

Table 3.2 Dependence of k(T) on Temperature

T (°C)	k(T)[a] (mV/%)
163	-11.1
177	-6.14
190	-3.54
204	-2.05
218	-1.30

[a] Based on electrode with 0.35 mg Pt/cm^2, and at 269 mA/cm^2.

Source: T.G. Benjamin, E.H. Camara and L.G. Marianowski, *Handbook of Fuel Cell Performance,* prepared by the Institute of Gas Technology for the United States Department of Energy under Contract No. EC-77-C-03-1545 (May 1980) p. 40.

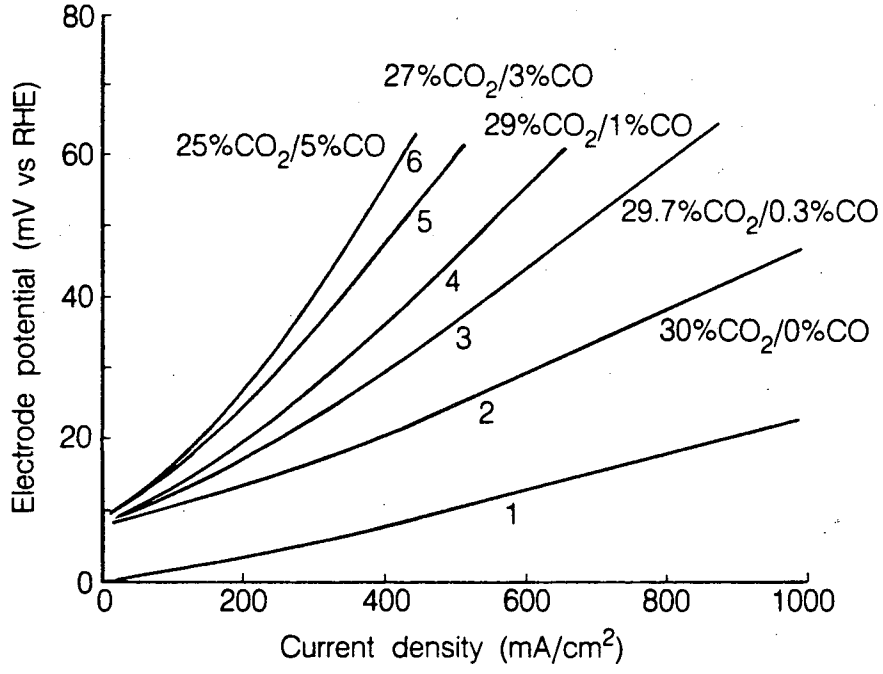

Figure 3-10. Influence of CO and fuel gas composition on the performance of Pt anodes in 100% H_3PO_4 at 180°C. 10% Pt supported on Vulcan XC-72, 0.5 mg Pt/cm^2. Dew point, 57°C. Curve 1, 100% H_2; Curves 2-6, 70% H_2 and CO_2/CO contents (mol%) specified.

Source: (Page A-16) J.A.S. Bett, H.R. Kunz, S.W. Smith and L.L. Van Dine, "Investigation of Alloy Catalysts and Redox Catalysts for Phosphoric Acid Electrochemical Systems," FCR-7157F, prepared by International Fuel Cells under Contract No. 9-X13-D6271-1 for Los Alamos National Laboratory (1985).

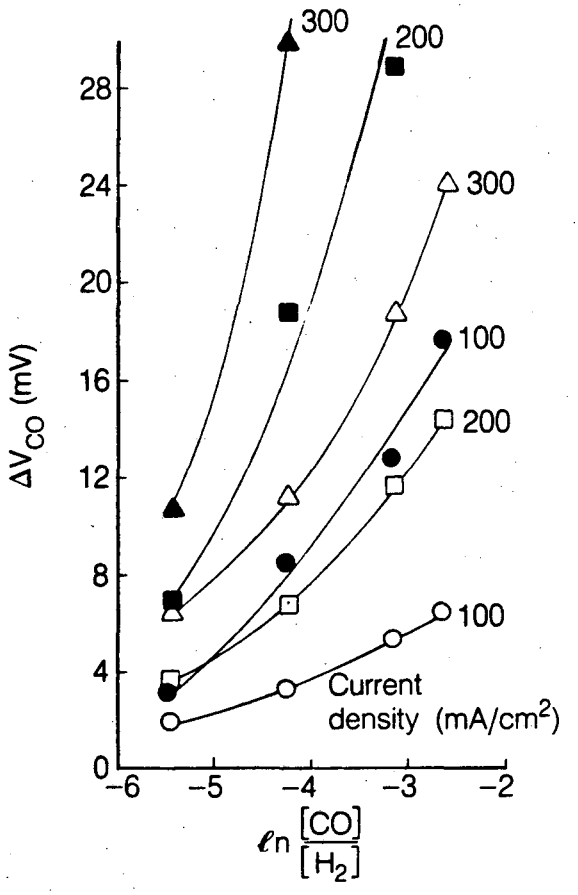

Figure 3-11. The voltage loss (ΔV_{CO}) as a function of $[CO]/[H_2]$ ratio at Pt anodes. 10% Pt supported on Vulcan XC-72, 0.5 mg Pt/cm^2. Dew point, 57°C. Open symbols, 180°C; solid symbols, 160°C.

Source: Data from p. A-15 and p. A-16, J.A.S. Bett, H.R. Kunz, S.W. Smith and L.L. Van Dine, "Investigation of Alloy Catalysts and Redox Catalysts for Phosphoric Acid Electrochemical Systems," FCR-7157F, prepared by International Fuel Cells under Contract No. 9-X13-D6271-1 for Los Alamos National Laboratory (1985).

40-99% H_2 and 0-59% CO_2). These data and results obtained more recently by Dhar et al. (38) can be fitted to the equation

$$\Delta V_{CO}\ (mV) = 2.5 \times 10^7 \exp(-0.0424T) + 7.47 \times 10^6 i \ln\frac{[CO]}{[H_2]} \exp(-0.0436T) \qquad (3\text{-}13)$$

where i is the current density (mA/cm^2). This equation is limited to T = 110-190°C and [CO] = 0-8.7%. According to Equation 3-13, ΔV_{CO} at 190°C and 269 mA/cm^2 is close to 2 mV for CO levels of ~1.0%. The data published by Kunz (39) show that ΔV_{CO} with Pt (0.35 mg/cm^2) anodes at 190°C is about 3 mV at 269 mA/cm^2 for the oxidation of H_2 containing 1.0% CO. Based on current PAFC technology, a CO content of ≤1% in reformed fuels should have minimal affect on anode performance at temperatures above 190°C.

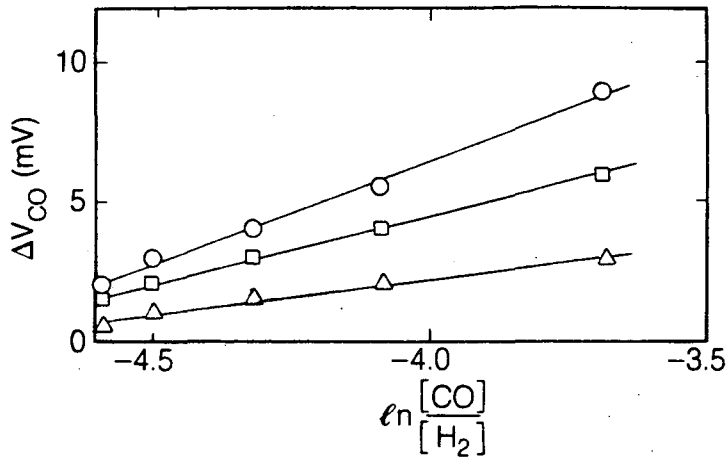

Figure 3-12. Anode polarization by CO poisoning as a function of $[CO]/[H_2]$ ratio at Pt anodes. Pt supported on Vulcan XC-72 carbon black, 0.4 mg Pt/cm^2.
(Δ) 100 mA/cm^2,
(□) 200 mA/cm^2,
(○) 300 mA/cm^2.
Source: (Figure 9, p. 1578) H.P. Dhar, L.G. Christner, A.K. Kush and H.C. Maru, *J. Electrochem. Soc.*, **133**, 1574 (1986).

Sulfur-Containing Compounds: Hydrogen sulfide and carbonyl sulfide (COS) are impurities[f] in fuel gases from fuel processors and coal gasifiers in PAFC power plants. The concentration levels of H_2S in an operating PAFC (190 to 210°C, 120 psig, 80% H_2 utilization at <325 mA/cm^2) that can be tolerated by Pt anodes without suffering a deleterious loss in performance are <50 ppm (H_2S + COS) or <20 ppm (H_2S) (39), and rapid cell failure occurs with fuel gas containing more than 50 ppm H_2S. Sulfur poisoning does not affect the cathode, and poisoned anodes can be re-activated by polarization at high potentials (i.e., operating cathode potentials).

Experimental studies by Chin and Howard (41) indicate that H_2S adsorbs on Pt and blocks the active sites for H_2 oxidation. The following electrochemical reactions involving H_2S are postulated to occur on Pt electrodes

$$Pt + HS^- \rightarrow Pt\text{–}HS_{ads} + e^- \quad (3\text{-}14)$$

$$Pt\text{–}H_2S_{ads} \rightarrow Pt\text{–}HS_{ads} + H^+ + e^- \quad (3\text{-}15)$$

and

$$Pt\text{–}HS_{ads} \rightarrow Pt\text{–}S_{ads} + H^+ + e^- \quad (3\text{-}16)$$

[f] Anode gases from coal gasifiers may contain total sulfur of 100 to 200 ppm.

Elemental sulfur (see Equation 3-16) is only expected on Pt electrodes at high anodic potentials, and at sufficiently high potentials, sulfur is oxidized to SO_2. The extent of poisoning by H_2S increases with increasing H_2S concentration, electrode potential and exposure time. The influence of 1.5% H_2S on the overpotential for H_2 oxidation on Pt in 94% H_3PO_4 at 100 to 170°C is illustrated in Figure 3-13, where i_{H_2S}/i_{H_2} is the ratio of the oxidation current with and without H_2S present in H_2. This ratio increases with increasing temperature, indicating that the extent of H_2S poisoning decreases with increasing cell temperature.

Other Compounds: The effect of other compounds such as those containing nitrogen on PAFC performance has been adequately reviewed by Benjamin et al. (21). Molecular nitrogen acts as a diluent but other nitrogen compounds (e.g., NH_3, HCN, NO_x) may not be as innocuous. For instance, NH_3 in the fuel or oxidant gases reacts with H_3PO_4 to form a phosphate salt

$$H_3PO_4 + NH_3 \rightarrow (NH_4)H_2PO_4 \qquad (3\text{-}17)$$

which results in a decrease in the rate of O_2 reduction. A concentration of less than 0.2 mol% $(NH_4)H_2PO_4$ must be maintained to avoid unacceptable performance losses (42). The effect of HCN and NO_x on fuel-cell performance has not been clearly established.

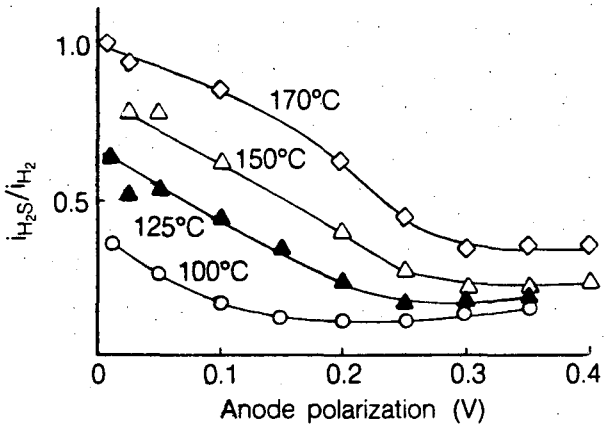

Figure 3-13. Effect of temperature on the poisoning of smooth Pt anodes by H_2S in 94% H_3PO_4. *Source*: (Figure 5, p. 2449) D.T. Chin and P.D. Howard, *J. Electrochem. Soc.*, **133**, 2447 (1986).

References

1. M. Warshay, *Prog. Batteries & Solar Cells,* **5,** 7 (1984).
2. J. Appleby, *Energy,* **11,** 13 (1986).
3. J. Appleby, in *Proceedings of the Workshop on The Electrochemistry of Carbon,* Edited by S. Sarangapani, J.R. Akridge and B. Schumm, The Electrochemical Society, Inc., Pennington, NJ (1984), p. 251.
4. K.V. Kordesch, "Survey of Carbon and Its Role in Phosphoric Acid Fuel Cells," BNL 51418, prepared for Brookhaven National Laboratory (December 1979).
5. K. Kinoshita, *Carbon: Electrochemical and Physicochemical Properties,* Wiley Interscience, New York, NY (1988).
6. L. Christner, J. Ahmad and M. Farooque, in *Proceedings of the Symposium on Corrosion in Batteries and Fuel Cells and Corrosion in Solar Energy Systems,* Edited by C.J. Johnson and S.L. Pohlman, The Electrochemical Society, Inc., Pennington, NJ (1983), p. 140.
7. P.W.T. Lu and L.L. France, in *Extended Abstracts,* Fall Meeting of The Electrochemical Society, Inc., Volume 84-2, Abstract No. 573, The Electrochemical Society, Inc., Pennington, NJ (1984), p. 837.
8. M. Warshay, in *The Science and Technology of Coal and Coal Utilization,* Edited by B.R. Cooper and W.A. Ellingson, Plenum Press, New York, NY (1984), p. 339.
9. P.R. Prokopius, M. Warshay, S.N. Simons and R.B. King, in *Proceedings of the 14th Intersociety Energy Conversion Engineering Conference,* Volume 2, American Chemical Society, Washington, D.C. (1979), p. 538.
10. S.N. Simons, R.B. King and P.R. Prokopius, in *Symposium Proceedings Fuel Cells Technology Status and Applications,* Edited by E.H. Camara, Institute of Gas Technology, Chicago, IL (1982), p. 45.
11. J.A.S. Bett, H.R. Kunz, S.W. Smith and L.L. Van Dine, "Investigation of Alloy Catalysts and Redox Catalysts for Phosphoric Acid Electrochemical Systems," FCR-7157F, prepared by International Fuel Cells for Los Alamos National Laboratory under Contract No. 9-X13-D6271-1 (1985).
12. B.C. Beard and P.N. Ross, *J. Electrochem. Soc.,* **133,** 1839 (1986).
13. J.T. Glass, G.L. Cahen, G.E. Stoner and E.J. Taylor, *J. Electrochem. Soc.,* **134,** 58 (1987)
14. P.N. Ross, "Oxygen Reduction on Supported Pt Alloys and Intermetallic Compounds in Phosphoric Acid," Final Report, EM-1553, prepared under Contract 1200-5 for the Electric Power Research Institute, Palo Alto, CA (September 1980).
15. V. Jalan and J. Giner, in *DECHEMA Monographs,* Volume 102, Edited by J.W. Schultze, VCH Verlagsgesellschaft, Weinheim, West Germany (1986), p. 315.
16. V.M. Jalan, in *Proceedings of the Workshop on The Electrochemistry of Carbon,* Edited by S. Sarangapani, J.R. Akridge and B. Schumm, The Electrochemical Society, Inc., Pennington, NJ (1984), p. 554.
17. V.M. Jalan, in *Extended Abstracts,* Spring Meeting of The Electrochemical Society, Inc., Volume 86-1, Abstract No. 340, The Electrochemical Society, Inc., Pennington, NJ (1986), p. 496.
18. J. Appleby, *EPRI Journal,* p. 55 (September 1983).
19. V.M. Jalan, private communication (February 20, 1987).
20. R. Allen, paper presented at the Twentieth EPRI Workshop on Phosphoric Acid Fuel Cell Technology, February 17, 1987, at Clearwater, FL.

21. T.G. Benjamin, E.H. Camara and L.G. Marianowski, *Handbook of Fuel Cell Performance,* prepared by the Institute of Gas Technology for the United States Department of Energy under Contract No. EC-77-C-03-1545 (May 1980).
22. A.P. Fickett, in *Proceedings of the Symposium on Electrode Materials and Processes for Energy Conversion and Storage,* Edited by J.D.E. McIntyre, S. Srinivasan and F.G. Will, The Electrochemical Society, Inc., Pennington, NJ (1977), p. 546.
23. A.J. Appleby, *J. Electroanal. Chem.,* **118,** 31 (1981).
24. J. Huff, paper presented at the 1986 National Fuel Cell Seminar, October 26-29, 1986, Tucson, AZ.
25. J.M. King and B.R. Will, in *Abstracts 1985 Fuel Cell Seminar,* May 19-22, 1985, Tucson, AZ (1985), p. 25.
26. M. Farooque, "Evaluation of Gas-Cooled Pressurized Phosphoric Acid Fuel Cells for Electric Utility Power Generation," Final Technical Report, NASA CR-168298 prepared by Energy Research Corp. under Contract No. DEN 3-201 for NASA Lewis Research Center (September 1983).
27. J. McBreen, W.E. O'Grady and R. Richter, *J. Electrochem. Soc.,* **131,** 1215 (1984).
28. J.M. Feret, "Gas Cooled Fuel Cell Systems Technology Development," Final Report, NASA CR-175047, prepared by Westinghouse Electric Corp. under Contract No. DEN 3-290 for NASA Lewis Research Center (August 1985).
29. A.J. Appleby, *J. Electrochem. Soc.,* **117,** 641 (1970).
30. P.N Ross, "Anomalous Current Ratios in Phosphoric Acid Fuel Cell Cathodes," LBL-13955 (March 1986); submitted to *J. Electrochem. Soc.,*
31. H.R. Kunz and G.A. Gruver, *Electrochim. Acta,* **23,** 219 (1978).
32. J. McBreen, W.E. O'Grady and S. Srinivasan, in *Proceedings of the Symposium on Electrocatalysis,* Edited by W.E. O'Grady, P.N. Ross and F.G. Will, The Electrochemical Society, Inc., Pennington, NJ (1982), p. 120.
33. A.P. Fickett, in *Handbook of Fuel Cells and Batteries,* Edited by D. Linden, McGraw-Hill Book Co., New York, NY (1984), p. 43-3.
34. P.W.T. Lu and L.L. France, in *Proceedings of the Symposium on Transport Processes in Electrochemical Systems,* R.S. Yeo, K. Katan and D.T. Chin, The Electrochemical Society, Inc., Pennington, NJ (1982), p. 77.
35. H.P. Dhar, L.G. Christner, A.K. Kush and H.C. Maru, *J. Electrochem. Soc.,* **133,** 1574 (1986).
36. P. Ross and P. Stonehart, *Electrochim. Acta,* **21,** 441 (1976).
37. W. Vogel, J. Lundquist, P. Ross and P. Stonehart, *Electrochim. Acta,* **20,** 79 (1975).
38. H.P. Dhar, L.G. Christner and A.K. Kush, *J. Electrochem. Soc.,* **134,** 3021 (1987).
39. H.R. Kunz, in *Proceedings of the Symposium on Electrode Materials and Processes for Energy Conversion and Storage,* Edited by J.D.E. McIntyre, S. Srinivasan and F.G. Will, The Electrochemical Society, Inc., Pennington, NJ (1977), p. 607.
40. P.N. Ross, "The Effect of H_2S and COS in the Fuel Gas on the Performance of Ambient Pressure Phosphoric Acid Fuel Cells," Interim Report LBL-18001, prepared by Lawrence Berkeley Laboratory under Contract RP-1676-2 for the Electric Power Research Institute, Palo Alto, CA (April 1985).
41. D.T. Chin and P.D. Howard, *J. Electrochem. Soc.,* **133,** 2447 (1986).
42. S.T. Szymanski, G.A. Gruver, M. Katz and H.R. Kunz, *J. Electrochem. Soc.,* **127,** 1440 (1980).

4. MOLTEN CARBONATE FUEL CELL

The MCFC is often referred to as a second-generation fuel cell because it is expected to reach commercialization after PAFCs are available in the marketplace. Currently, three industrial corporations are actively pursuing the commercialization of MCFCs in the United States, these are International Fuel Cells Corporation, Energy Research Corporation and M-C Power, which was formed by GDC, Inc., a wholly owned subsidiary of the Institute of Gas Technology.

The electrochemical reactions occurring in MCFCs are

$$H_2 + CO_3^{=} \rightarrow H_2O + CO_2 + 2e^- \tag{4-1}$$

at the anode, and

$$\tfrac{1}{2}O_2 + CO_2 + 2e^- \rightarrow CO_3^{=} \tag{4-2}$$

at the cathode. The overall cell reaction[a] is

$$H_2 + \tfrac{1}{2}O_2 + CO_2\ (\text{cathode}) \rightarrow H_2O + CO_2\ (\text{anode}) \tag{4-3}$$

Besides the reaction involving H_2 and O_2 to produce H_2O, there occurs a transfer of CO_2 from the cathode compartment to the anode compartment, with 1 mole CO_2 transferred along with 2 Faradays of charge. The reversible potential for a MCFC, taking into account the transfer of CO_2, is given by the equation

$$E = E^o + \frac{RT}{2F} \ln \frac{P_{H_2} P_{O_2}^{1/2}}{P_{H_2O}} + \frac{RT}{2F} \ln \frac{P_{CO_{2,c}}}{P_{CO_{2,a}}} \tag{4-4}$$

where the subscripts a and c refer to the anode and cathode compartments, respectively. When the partial pressures of CO_2 are identical at the anode and cathode, and the electrolyte is invariant, the cell potential depends only on the partial pressures of H_2, O_2 and H_2O. Typically, the CO_2 partial pressures are different in the two electrode compartments, and the cell potential is affected

[a] CO is not directly utilized by electrochemical oxidation, but it is a source of H_2 from the water-gas shift reaction.

accordingly, as shown in Equation 4-4.

In a practical MCFC, the CO_2 generated at the anode will be recycled to the cathode where it is consumed. Some type of device that allows (i) CO_2 to be transferred from the anode exit gas to the cathode inlet gas ("CO_2 transfer device"), or (ii) a combustion reactor that produces CO_2 by combustion of the anode exhaust gas, which is mixed with the cathode inlet gas, will be required.

MCFCs differ in many respects from PAFCs because of their higher operating temperature (650 vs 200°C) and the nature of the electrolyte. The higher operating temperature of MCFCs provides the opportunity for achieving higher overall system efficiencies (potential for heat rates below 7500 Btu/kWh) and greater flexibility in the use of available fuels.[b] On the other hand, the higher operating temperature places severe demands on the corrosion stability and life of cell components, particularly in the aggressive environment of the molten carbonate electrolyte. Another difference between PAFCs and MCFCs lies in the method used for electrolyte management in the respective cells. In a PAFC, PTFE serves as a binder and wet-proofing agent to maintain the integrity of the electrode structure and to establish a stable electrolyte/gas interface in the porous electrode. The phosphoric acid is retained in a matrix of PTFE and SiC between the anode and cathode. There are no materials available for use in MCFCs that are comparable to PTFE. Thus, a different approach is required to establish a stable electrolyte/gas interface in MCFC porous electrodes, and this is illustrated schematically in Figure 4-1. The MCFC relies on a balance in capillary pressures to establish the electrolyte interfacial boundaries in the porous electrodes (1-3). At thermodynamic equilibrium, the diameters of the largest flooded pores in the porous components are related by the equation

$$\frac{\gamma_c \cos\theta_c}{D_c} = \frac{\gamma_e \cos\theta_e}{D_e} = \frac{\gamma_a \cos\theta_a}{D_a} \qquad (4\text{-}5)$$

where γ is the interfacial surface tension, θ is the contact angle of the electrolyte, D is the pore diameter, and the subscripts a, c and e refer to the anode, cathode and electrolyte matrix, respectively. By properly coordinating the pore diameters in the electrodes with those of the electrolyte matrix, which contains the smallest pores, the electrolyte distribution depicted in Figure 4-1 is established. This arrangement permits the electrolyte matrix to remain completely filled with molten carbonate, while the porous electrodes are partially filled, depending on their pore-size distributions. According to the model illustrated in Figure 4-1 and described by Equation 4-5, the electrolyte content in each of the porous components will be determined by the equilibrium pore size (<D>) in that component; pores smaller than <D> will be filled with electrolyte, and pores larger than <D> will remain empty. A reasonable estimate of the volume distribution of electrolyte in the various cell components is obtained from the measured pore-volume-distribution curves and the above relationship for D (1,2).

Electrolyte management, that is, the control over the optimum distribution of molten carbonate electrolyte in the different cell components, is critical for achieving high performance and endurance with MCFCs. Various processes (i.e., consumption by corrosion reactions, potential-driven migration, creepage of salt and salt vaporization) occur, all of which contribute to the redistribution of molten carbonate in MCFCs; these aspects are discussed by Maru et al. (4) and Kunz (5).

[b] *In situ* reforming of fuels in MCFCs is possible, and this is discussed later in the chapter.

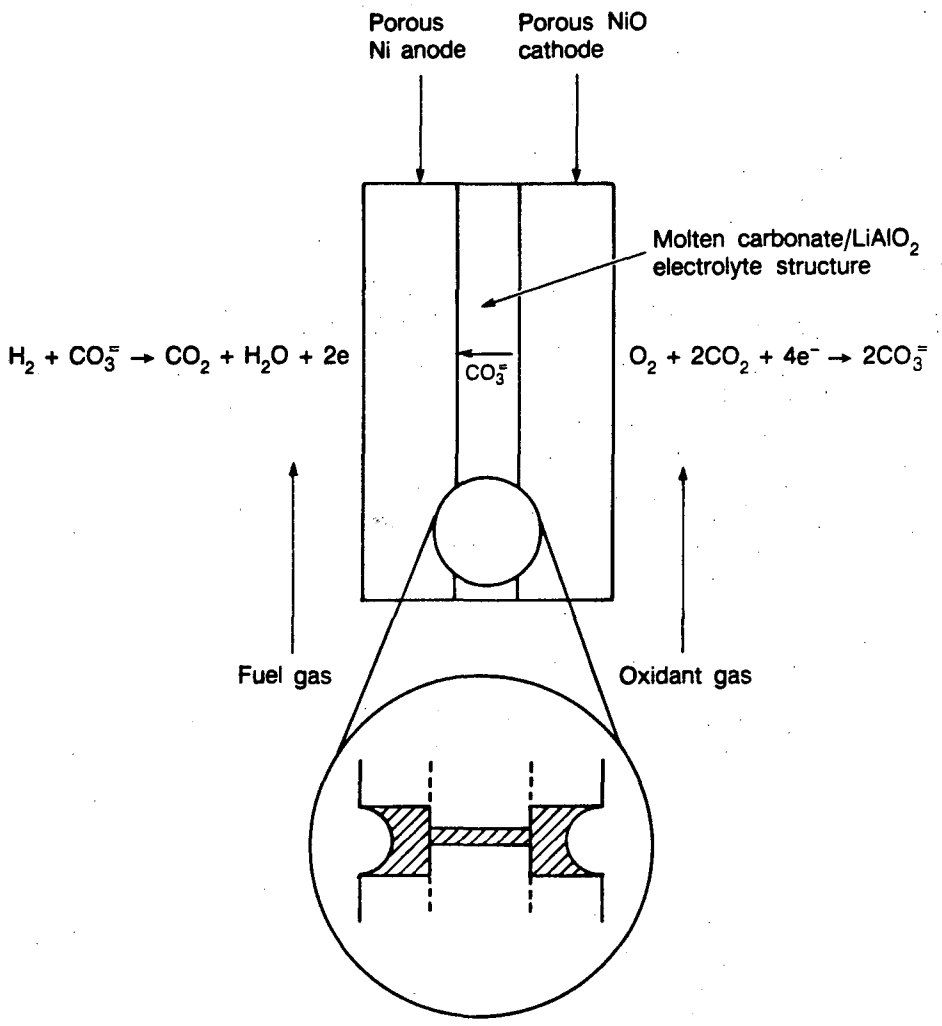

Figure 4-1. Schematic representation of a MCFC showing the dynamic equilibrium of molten carbonate in the porous cell components. The porous electrodes are depicted with pores covered by a thin film of electrolyte.

4.1 Cell Components

4.1.1 State-of-the-Art

The data in Table 4.1 provide a chronology of the recent evolution in cell-component technology for MCFCs. In the mid 1960s, the electrode materials were, in many cases, precious metals, but the technology soon evolved to the use of Ni-based alloys at the anode and oxides at the cathode. Since the mid 1970s, the materials for the electrodes and electrolyte structure (molten carbonate/$LiAlO_2$) have remained essentially unchanged. A major development in the last 10 years has been the evolution in the technology for fabrication of electrolyte structures. Recent developments in cell components for MCFCs have been reviewed by Maru and co-workers (6, 7), Petri and Benjamin (8) and Selman (9).

Table 4.1 Evolution of Cell Component Technology for Molten Carbonate Fuel Cells

Component	ca. 1965	ca. 1975	Current Status
Anode	• Pt, Pd, or Ni	• Ni-10 wt% Cr	• Ni-10 wt% Cr • 3-6 μm pore size • 50-70% porosity • 0.5-1.5 mm thickness • 0.1-1 m^2/g
Cathode	• Ag_2O or lithiated NiO	• lithiated NiO	• lithiated NiO • 7-15 μm pore size • 70-80% porosity • 0.5-0.75 mm thickness • 0.5 m^2/g
Electrolyte Support	• MgO	• mixt. of α-, β- and γ-$LiAlO_2$ • 10-20 m^2/g	• γ-$LiAlO_2$ • 0.1-12 m^2/g
Electrolyte[a]	• 52 Li-48 Na • 43.5 Li-31.5 Na-25 K	• 62 Li-38 K • ~60-65 wt%	• 62 Li-38 K • 50 Li-50 Na • 50 Li-50 K • ~50 wt%
Fabrication Process	• "paste"	• hot-press "tile" • 1.8-mm thickness	• tape-cast • 0.5-mm thickness

[a] Mole percent of alkali carbonate salt

Specifications (current status) for the anode and cathode were obtained from: A. Pigeaud, H.C. Maru, L. Paetsch, J. Doyon and R. Bernard, in *Proceedings of the Symposium on Porous Electrodes: Theory and Practice,* Edited by H.C. Maru, T. Katan and M.G. Klein, The Electrochemical Society, Inc., Pennington, NJ (1984) p. 234.

The conventional process used to fabricate electrolyte structures until about 1980 involved hot-pressing (about 5000 psi) mixtures of $LiAlO_2$ and alkali carbonates (typically >50 vol% in liquid state) at temperatures slightly below the melting point of the carbonate salts (e.g., 490°C for electrolyte containing 62 mol% Li_2CO_3-38 mol% K_2CO_3). These electrolyte structures (also called "electrolyte tiles") were relatively thick (1-2 mm) and difficult to produce in large sizes[c] because large

[c] The largest electrolyte tile produced by hot-pressing was about 1.5 m^2 in area (7).

tooling and presses were required. The electrolyte structures produced by hot-pressing are often characterized by: (i) void spaces (<5% porosity), (ii) poor uniformity of microstructure, (iii) generally poor mechanical strength, and (iv) high IR drop. To overcome these shortcomings of hot-pressed electrolyte structures, alternative processes such as tape-casting (7) and electrophoretic deposition (10) for fabricating thin electrolyte structures were developed. The greatest success to date with an alternative process has been reported with tape-casting, which is a common processing technique used by the ceramics industry. This process involves dispersing the ceramic powder in a solvent,[d] which contains dissolved binders (usually an organic compound), plasticizers, and additives to yield the proper slip rheology. The slip is cast over a smooth substrate, and the desired thickness is established with a doctor-blade device. After drying the slip, the "green" structure is assembled into the fuel cell where the organic binder is removed by thermal decomposition and the absorption of alkali carbonate into the ceramic structure occurs during cell start up.

The tape-casting and electrophoretic-deposition processes are amenable to scale up, and thin electrolyte structures (0.25-0.5 mm) can be produced. The ohmic resistance of an electrolyte structure,[e] and the resulting ohmic polarization, have a large influence on the operating voltage of MCFCs. At a current density of 160 mA/cm^2, the voltage drop (ΔV_{ohm}) of a 0.18-cm thick electrolyte structure, with a specific conductivity of ~0.3 ohm^{-1}cm^{-1} at 650°C, was found to obey the relationship (10)

$$\Delta V_{ohm}\,(V) = 0.533t \qquad (4\text{-}6)$$

where t is the thickness. Given this equation, it is apparent that a fuel cell with an electrolyte structure of 0.025-cm thickness would operate at a cell voltage that is 82 mV higher than that of an identical cell with an electrolyte structure of 0.18-cm thickness because of the lower ohmic loss. Thus, there is a strong incentive for making thinner electrolyte structures to obtain better cell performance.

An additional feature that has been recently added to MCFC technology is the so-called "bubble pressure barrier" (bpb), which consists of a dense, fine-pore-size metal ($LiAlO_2$ and other metal oxides have also been used) structure that is usually located between the anode and electrolyte structure, and filled with molten carbonate electrolyte (12). The purpose of this additional layer is to prevent gas crossover from one electrode to the other and to reinforce the electrolyte matrix. The bpb can be fabricated as an integral part of the anode structure; a schematic representation of such a structure and the pore size distributions of the components are shown in Figure 4-2. To design an effective bpb requires carefully matching its pore-size distribution with those of the anode and electrolyte matrix. If the median pore size of the anode is 4 to 8 μm, and that of the electrolyte matrix is 0.5 to 0.8 μm, then an appropriate pore-size distribution for the bpb is 1.0 to 1.5 μm. This combination of pore sizes for the bpb and other cell components should minimize the drainage of molten electrolyte from the electrolyte matrix by capillary pressure. If the electrolyte matrix develops a crack, the bpb provides an electrolyte-filled barrier to minimize the crossover of gases from one electrode to the other. The bpb must be completely filled with molten carbonate to act as a barrier for gas diffusion, and also to transport carbonate ions through the cell.

---

[d] An organic solvent is used because $LiAlO_2$ in the slip reacts with H_2O.

[e] Electrolyte structures containing 45 wt% $LiAlO_2$ and 55 wt% molten carbonate (62 mol% Li_2CO_3-38 mol% K_2CO_3) have a specific conductivity at 650°C of about 1/3 that of the pure carbonate phase (11).

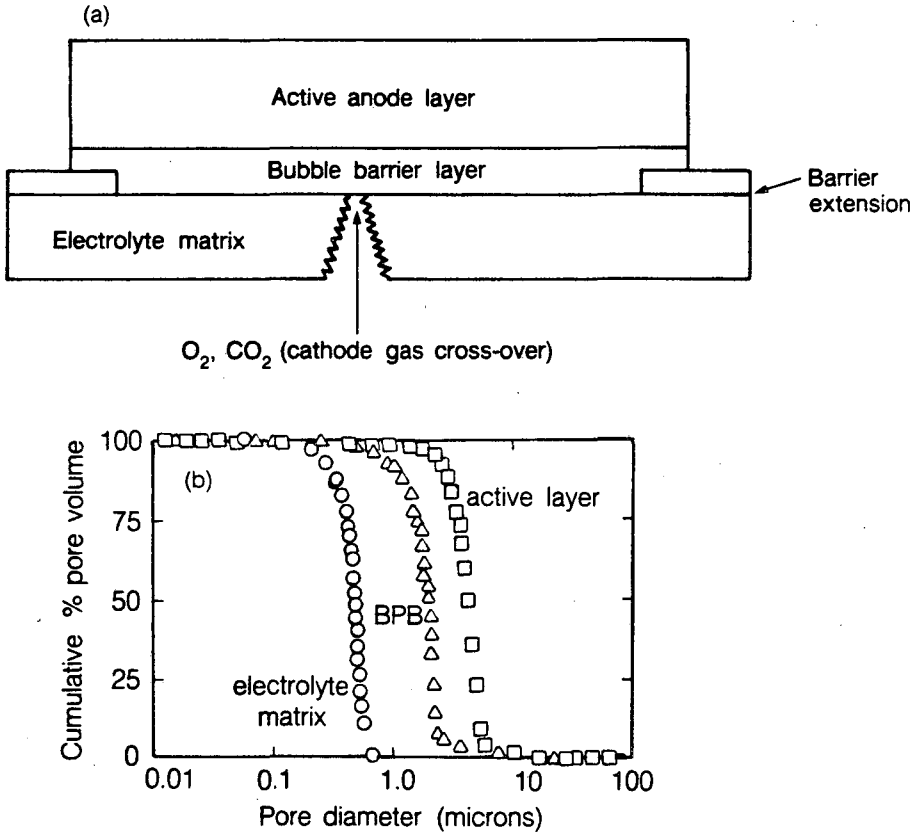

Figure 4-2. Schematic representation of the bubble pressure barrier (BPB) in MCFCs (a) and the pore-size distribution of the components (b).
Source: (Figure 1, p. 1595) C.D. Iacovangelo and B.R. Karas, *J. Electrochem. Soc.*, **133**, 1595 (1986).

The electrolyte composition affects the performance and endurance of MCFCs in several ways. Higher ionic conductivities, and hence lower ohmic polarization, are achieved with Li-rich electrolytes because of the relative high ionic conductivity of Li_2CO_3 compared to that of Na_2CO_3 and K_2CO_3. However, gas solubility and diffusivity are lower, and corrosion is more rapid, in Li_2CO_3.

The major problems with Ni-based anodes and NiO cathodes are structural stability and NiO dissolution, respectively (9). Sintering and mechanical deformation of the porous Ni-based anode under compressive load leads to severe performance decay by redistribution of electrolyte in a MCFC stack. The dissolution of NiO in molten carbonate electrolyte became evident when thin electrolyte structures were used. Despite the low solubility of NiO in carbonate electrolytes (~10 ppm), Ni ions diffuse in the electrolyte towards the anode and metallic Ni can precipitate in regions where a H_2 reducing environment is encountered. The precipitation of Ni provides a sink for Ni ions, and thus promotes the diffusion of dissolved Ni from the cathode. This phenomenon becomes worse at high CO_2 partial pressures (13, 14) because dissolution may involve the following mechanism,

$$NiO + CO_2 \rightarrow Ni^{2+} + CO_3^{2-} \qquad (4\text{-}7)$$

The dissolution of NiO has been correlated to the acid-base properties of the molten carbonate. The basicity of the molten carbonate is defined as equal to -log (activity of O^{2-}) or -log a_{M_2O}, where a is the activity of the alkali metal oxide M_2O. Based on this definition, acidic oxides are associated with carbonates (e.g., K_2CO_3) that do not dissociate to M_2O, and basic oxides are formed with highly dissociated carbonate salts (e.g., Li_2CO_3). The solubility of NiO in binary carbonate melts shows a clear dependence on the acidity/basicity of the melt (15, 16). In relatively acidic melts NiO dissolution can be expressed by:

$$NiO \rightarrow Ni^{2+} + O^{2-} \tag{4-8}$$

In basic melts NiO reacts with O^{2-} to produce one of two forms of nickelate ions:

$$NiO + O^{2-} \rightarrow NiO_2^{2-} \tag{4-9}$$

or

$$2NiO + O^{2-} + \tfrac{1}{2}O_2 \rightarrow 2NiO_2^{-} \tag{4-10}$$

A distinct minimum in NiO solubility is observed in plots of log (NiO solubility) versus basicity (-log a_{M_2O}), which can be demarcated into two branches corresponding to acidic and basic dissolution. Acidic dissolution is represented by a straight line with a slope of +1, and a NiO solubility that decreases with an increase in a_{M_2O}. Basic dissolution is represented by a straight line with a slope corresponding to either -1 or -½, corresponding to Reactions 4-9 and 4-10, respectively. The CO_2 partial pressure is an important parameter in the dissolution of NiO in carbonate melts because the basicity is directly proportional to log P_{CO_2}. A MCFC usually operates with a molten carbonate electrolyte that is acidic.

The goal of 40,000 h for the lifetime of MCFCs appears achievable with cell operation at atmospheric pressure, but at 10-atm cell pressure only about 5,000 to 10,000 h may be possible with currently available NiO cathodes (17). The solubility of NiO in molten carbonates is complicated by its dependence on several parameters: carbonate composition, H_2O partial pressure, CO_2 partial pressure, and temperature. For example, measurements of NiO dissolution by Kaun (18) indicate that the solubility is affected by changing the electrolyte composition; a lower solubility is obtained in a Li_2CO_3–K_2CO_3 electrolyte that contains less Li_2CO_3 (i.e, lower solubility in 38 mol% Li_2CO_3-62 mol% K_2CO_3 than in 62 mol% Li_2CO_3-38 mol% K_2CO_3 at 650°C). However, the solubility of Ni increases in the electrolyte with 38 mol% Li_2CO_3 when the temperature decreases, whereas the opposite trend is observed in the electrolyte with 62 mol% Li_2CO_3. Another study reported by Appleby (19) indicates that the solubility of Ni decreases from 9 to 2 ppm by increasing the Li concentration in Li_2CO_3–K_2CO_3 from 62 to 75 at%, and a lower solubility is obtained in 60 mol% Li_2CO_3-40 mol% Na_2CO_3 at 650°C. The total loss of Ni from the cathode by dissolution in 40,000 h is expected to correspond to only about 10% of the total cathode thickness. Thus loss of NiO from the cathode can be a critical problem if the possibility of a short circuit exists in the cell and facilitates compaction of the cathode. The compaction of cathodes became evident in MCFC stacks which contained strengthened anodes (i.e., oxide-dispersion-strengthened anode).

The bipolar plates used in MCFC stacks are usually fabricated from thin (~15 mil) sheets of an alloy (e.g., Incoloy 825, 310S or 316L stainless steel) that is coated on one side (i.e., the side exposed to fuel gases in the anode compartment) with a Ni layer. The Ni layer is stable in the reducing gas environment of the anode compartment, and it provides a conductive surface coating

with low contact resistance. Approaches to circumvent the problems associated with gas leaks and corrosion of bipolar plates are described by Pigeaud et al. (20). Corrosion is largely overcome by application of a coating (about 50-μm thickness) at the vulnerable locations on the bipolar plate. For example, the wet-seal[f] area on the anode side is subject to a high chemical potential gradient because of the fuel gas inside the cell and the ambient environment (usually air) on the outside of the cell, which promotes corrosion (about two orders of magnitude greater than in the cathode wet-seal area (21)). A general discussion on corrosion in the wet-seal area of MCFCs is presented by Donado et al. (22). A thin Al coating in the wet-seal area of a bipolar plate provides corrosion protection by forming a protective layer of $LiAlO_2$ after reaction of Al with Li_2CO_3 (23). Such a protective layer would not be useful in areas of the bipolar plate that must permit electronic conduction because $LiAlO_2$ is an insulating material.

A dense and electronically insulating layer of $LiAlO_2$ is not suitable for providing corrosion resistance to the cell current collectors because these components must remain electrically conductive. The typical materials used for this application are 316 stainless steel and chromium-plated stainless steels. However, materials with better corrosion resistance are required for long-term operation of MCFCs. Research is underway to understand the corrosion processes of chromium in molten carbonate salts under both fuel gas and oxidizing gas environments (24) and to identify improved alloys (25) for MCFCs. Stainless steels such as Type 310 and 446 have demonstrated better corrosion resistance than Type 316 in corrosion tests (25).

4.1.2 Alternative Components

Research is underway to develop alternative materials to overcome the problems mentioned above with the state-of-the art components for MCFCs. Of the three major cell components (i.e., anode, cathode and electrolyte structure), the development of an alternative to $LiAlO_2$ for electrolyte structures appears to have the lowest priority (8). A review of materials used in electrodes and their performance in MCFCs is presented by Kinoshita (26). A literature survey (27) and extensive experiments (28) have been conducted on the corrosion of materials in MCFCs, and these studies provide further information on useful materials for electrodes, bipolar separators and current collectors for MCFCs.

Anode: Several metal and alloy materials have been proposed as alternative anodes. The Ni-Cr (1-10 wt% Cr) anodes currently in use yield acceptable performance in MCFCs, but they are relatively high-cost components, and they are susceptible to mechanical deformation. The Cr in the Ni-Cr alloys reacts to form $LiCrO_2$ which aids in stabilizing the porous anode structure from sintering (29). However, the high compressive loads encountered in fuel-cell stacks cause the anodes to undergo mechanical creep. An anode of Ni-10Cr alloy in a MCFC (8) exhibited a creep of about 4% after a 10,000-h test, which is 4 times higher than the goal of 1% creep. Oxide-dispersion-strengthened (ODS) anodes demonstrated encouraging results towards minimizing creep. These anodes rely on the ability of small metal oxide particles in the metal to inhibit sintering and creep. Metal oxides, such as Al_2O_3, $LiAlO_2$ and ZrO_2, and metals, such as Ti, Co and Al, have been incorporated in anode structures (6, 8, 29-31). Copper-based materials have also been evaluated as low-cost alternative anodes to Ni-based materials (29, 32, 33). The kinetics of fuel oxidation on Cu

[f] The area of contact between the outer edge of the bipolar plate and the electrolyte structure prevents gas from leaking out of the anode and cathode compartments. The gas seal is formed by compressing the contact area between the electrolyte structure and the bipolar plate so that the liquid film of molten carbonate at operating temperature does not allow gas to permeate through.

appears to be acceptable in MCFCs, but sintering and mechanical deformation are more severe than with Ni. Consequently, ODS Cu and/or Cu alloys are necessary if Cu-based materials are used in MCFC anodes. Currently, porous Ni containing 2-5% Al is showing encouraging results as anodes in MCFCs.

Cathode: An acceptable candidate material for cathodes must have adequate electrical conductivity and good structural strength, and a low dissolution rate in molten alkali carbonates to avoid precipitation of metal in the electrolyte structure. An extensive search of over 50 materials has been conducted to identify alternative materials to NiO for cathodes in MCFCs (34-36). Perovskite-type compounds, $Ln_{1-x}M_xM'O_3$ (Ln = lanthanide element, M = alkaline earth metal or transition metal, M′ = transition metal), and mixed metal oxides have been evaluated as cathodes. Two metal oxides, Mn-doped $LiFeO_2$ and Mg-doped Li_2MnO_3 with bulk resistivities of 5-30 ohm-cm at 650°C, have emerged from these studies as leading candidates for alternative cathode materials (35). The study by Hsu et al. (37) concluded that $LiFeO_2$ is a viable candidate for cathodes in MCFCs despite its solubility (78 ppm Fe) in Li_2CO_3/K_2CO_3 at 650°C. In addition, the solubility of $LiFeO_2$ is independent of the partial pressure of CO_2 and O_2, in contrast to NiO.

Electrolyte Structure: Since the adoption of $LiAlO_2$ as the support material in electrolyte structures, there has been little effort devoted to identifying an alternative material. One material that has been identified (38, 39) is $SrTiO_3$, but it reacts with Li_2CO_3 to form Li_2TiO_3 and $SrCO_3$ (28). The reaction of $SrTiO_3$ with Li_2CO_3 is inhibited by adding 10 mol% $SrCO_3$ to the carbonate melt. Unfortunately the melting point of the carbonate eutectic with $SrCO_3$ is lowered and melting occurs over a broader temperature range, which presents difficulties in fabricating electrolyte structures. To date, the suitability of this alternative support material in MCFCs has not been demonstrated.

4.2 Performance

Over the past 20 years, the performance of single cells has improved from about 10 mW/cm^2 to >150 mW/cm^2. Since the early 1980s both the performance and endurance of MCFC stacks have shown dramatic improvements. The data in Figure 4-3 and 4-4, respectively, illustrate the dramatic progress that has been made in the performance of single cells, and in the cell voltage at 160 A/ft^2 (172 mA/cm^2) of small stacks at 650°C, with low-Btu fuel [17% (H_2 + CO)] at 65 psia. In Figure 4-4, the rectangular boxes represent the range of cell voltages of cells in stacks, with the intermediate line in the box being the average cell voltage. The stack tested in early 1980 was the last to be built with hot-pressed electrolyte structures, and this stack shows a wide spread in individual cell voltages. All subsequent results in Figure 4-4 were obtained with stacks containing tape-cast electrolyte structures. From mid 1981 to mid 1982, the cell stacks showed only a small spread in the voltage of individual cells. The improved results obtained with the 20-cell stack in late 1983 is attributed to a slight change in the electrolyte composition, from 62 mol% Li_2CO_3-38 mol% K_2CO_3 to about 70 mol% Li_2CO_3-30 mol% K_2CO_3. Overall, the development of improved cell components, and cell operation at higher pressures, has led to a progressive increase in cell performance. The improvements leading to the performance of 20-cell stacks in 1984 and 1985 are attributed to the enhanced ionic conductivity of the electrolyte and to improved electrolyte management provided by modifications to the cell and stack design (40).

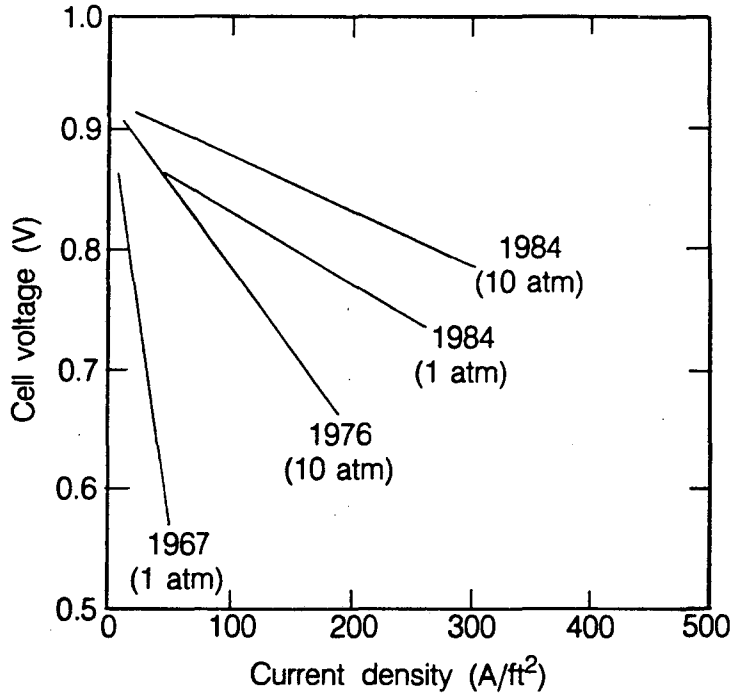

Figure 4-3. Progress in the generic performance of MCFCs on reformate gas and air.
Source: J.R. Huff, paper presented at the 1986 Fuel Cell Seminar, October 26-29, 1986, Tucson, AZ.

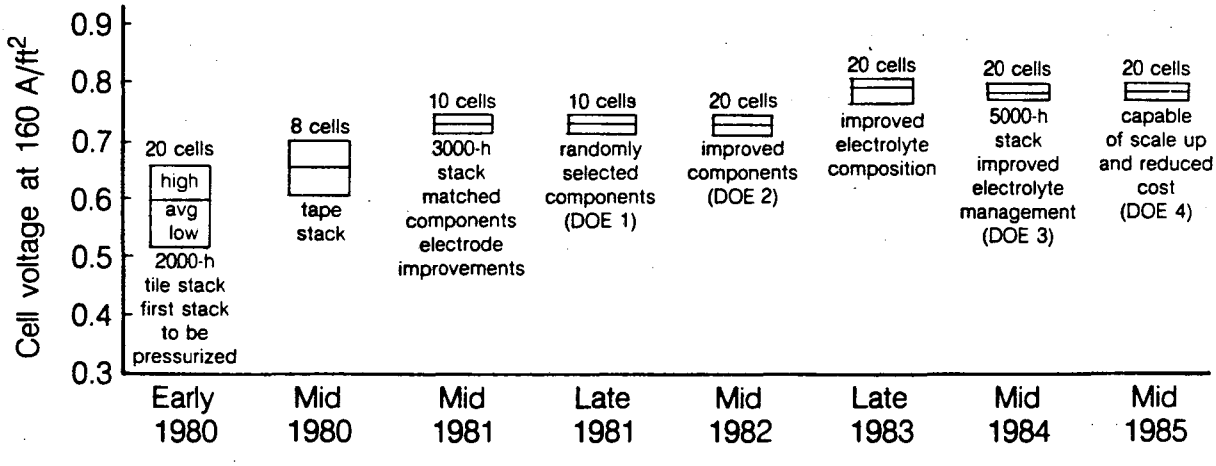

Figure 4-4. Improvements in the cell voltage at 172 mA/cm^2 of MCFC stacks on low-BTU fuel [17% (H_2 + CO)] at 65 psia and 650°C. Brief descriptions of the technology and program sponsors are noted in the figure.
Source: (Figure 3, p. 1129) F. Gmeindl, in *Proceedings of the 21st Intersociety Energy Conversion Engineering Conference*, Volume 2, American Chemical Society, Washington, D.C. (1986).

Typical cathode performance curves obtained at 650°C with an oxidant composition (12.6% O_2/18.4% CO_2/69% N_2), which is anticipated for use in MCFCs, and a common baseline composition (33% O_2/67% CO_2) are presented in Figure 4-5 (17, 41). The baseline composition contains the reactants, O_2 and CO_2, in the stoichiometric ratio that is needed in the electrochemical reaction at the cathode (Equation 4-2). With this gas composition, little or no diffusion limitations occur in the cathode because the reactants are provided primarily by bulk flow. The other gas composition, which contains a substantial fraction of N_2, yields a cathode performance that is limited by gas-phase diffusion from dilution by an inert gas.

In the last decade the performance of MCFC stacks has increased dramatically, and cells as large as 0.74 m^2 (8 ft^2) are currently being tested in stacks. Cells with an electrode area of 0.3 m^2 (1 ft^2) are routinely tested at ambient and above-ambient pressures with improved electrolyte structures made by tape-casting processes (17). The average voltage[g] as a function of current (after 167 h) for a 0.3-m^2 stack consisting of 10 cells is shown in Figure 4-6, and data on the initial performance of individual cells is shown in Figure 4-7. The data were obtained with the cell stack at 650°C and fuel gas (14.2% H_2/3% CO/20.4% CO_2/17% N_2/45.4% H_2O) and oxidant gas (14.9% CO_2/7.5% O_2/69.1% N_2/8.5% H_2O) both at 65 psia. The voltages of individual cells at 172 mA/cm^2 (160 A/ft^2) were uniform to within 30 mV (average 0.736 V at 172 mA/cm^2 at 167 h). The average ohmic loss of the cells was about 38 mV at 172 mA/cm^2, and varied by less than 3 mV between cells, as shown in Figure 4-7. It should be noted that the IR loss in this stack is comparable to that reported (40 mV at 160 mA/cm^2) for tape-cast electrolyte structures of 0.5-mm thickness and containing 40 wt% molten carbonate (Figure 5.5C-1, Reference 8).

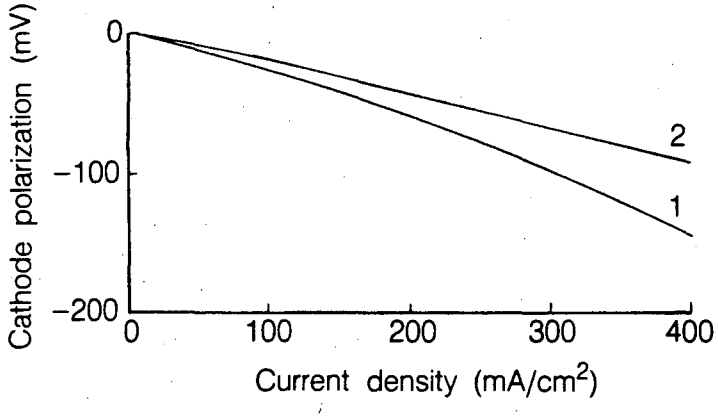

Figure 4-5. The effect of oxidant gas composition on cathode performance in MCFCs at 650°C. Curve 1, 12.6% O_2/18.4% CO_2/69.0% N_2; Curve 2, 33% O_2/67% CO_2.

Source: (Figure 3, p. 2712) L.J. Bregoli and H.R. Kunz, *J. Electrochem. Soc.*, **129**, 2711 (1982).

[g] The average cell voltage in the 10-cell stack is in good agreement with the cell-voltage projection based on 10-cm x 10-cm single cells operating at ambient pressure.

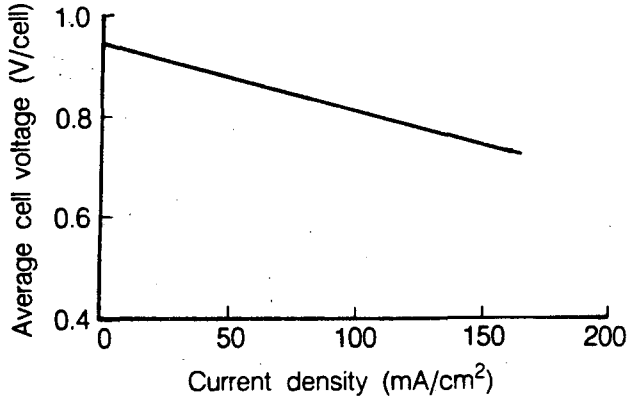

Figure 4-6. Average cell voltage of 0.3-m^2 MCFC stack after 167 h at 650°C and 65 psia. Fuel gas, 14.2% H_2/3% CO/20.4% CO_2/17% N_2/45.4% H_2O; oxidant gas, 14.9% CO_2/7.5% O_2/69.1% N_2/8.5% H_2O.

Source: (Figure 4-15, p. 4-20) J.M. King, A.P. Meyer, C.A. Reiser and C.R. Schroll, "Molten Carbonate Fuel Cell System Verification and Scale-up," EM-4129, final report prepared by United Technologies Corp. for the Electric Power Research Institute, Research Project 1273-1 (July 1985).

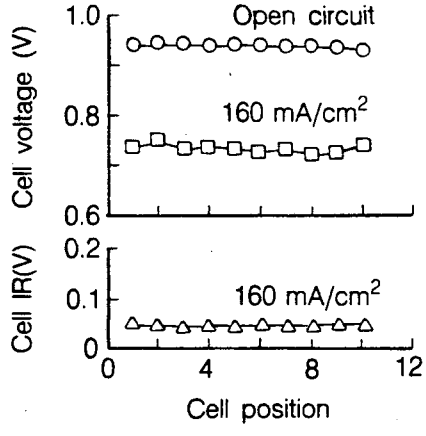

Figure 4-7. Performance data at 167-h operation of 0.3-m^2 MCFC stack at 650°C and 65 psia. Fuel gas—14.2% H_2/3% CO/20.4% CO_2/17% N_2/45.4% H_2O; oxidant gas—14.9% CO_2/7.5% O_2/69.1% N_2/8.5% H_2O.

Source: (Figure 4-16, p. 4-20) J.M. King, A.P. Meyer, C.A. Reiser and C.R. Schroll, "Molten Carbonate Fuel Cell System Verification and Scale-up," EM-4129, final report prepared by United Technologies Corp. for the Electric Power Research Institute, Research Project 1273-1 (July 1985).

4.2.1 Effect of Pressure and Temperature

Pressure: The dependence of the reversible cell potential of MCFCs on pressure is evident from the Nernst equation. For a change in pressure from P_1 to P_2, the change in reversible potential (ΔV_P) is given by

$$\Delta V_P = \frac{RT}{2F} \ln \frac{P_{1,a}}{P_{2,a}} + \frac{RT}{2F} \ln \frac{P_{2,c}^{3/2}}{P_{1,c}^{3/2}} \tag{4-11}$$

where the subscripts a and c refer to the anode and cathode, respectively. In a MCFC with the anode and cathode compartments at the same pressure (i.e., $P_1 = P_{1,a} = P_{1,c}$ and $P_2 = P_{2,a} = P_{2,c}$)

$$\Delta V_P = \frac{RT}{2F} \ln \frac{P_1}{P_2} + \frac{RT}{2F} \ln \frac{P_2}{P_1^{3/2}} = \frac{RT}{4F} \ln \frac{P_2}{P_1} \tag{4-12}$$

At 650°C,

$$\Delta V_P \text{ (mV)} = 20 \ln \frac{P_2}{P_1} \tag{4-13}$$

Thus, a 10-fold increase in cell pressure corresponds to an increase of 46 mV in the reversible cell potential at 650°C.

Increasing the operating pressure of MCFCs results in enhanced cell voltages because of the increase in the partial pressure of the reactants, and the concomitant increase in gas solubilities. Opposing the benefits of increased pressure are the effects of pressure on undesirable side reactions such as carbon deposition (Boudouard reaction)

$$2CO \rightarrow C + CO_2 \tag{4-14}$$

and methane formation (methanation)

$$CO + 3H_2 \rightarrow CH_4 + H_2O \tag{4-15}$$

In addition, decomposition of CH_4 to carbon and H_2 is possible,

$$CH_4 \rightarrow C + 2H_2 \tag{4-16}$$

but this reaction is suppressed at higher pressure. According to the Le Chatelier principle, an increase in pressure will favor carbon deposition[h] and methane formation. The water-gas shift reaction[i]

$$CO_2 + H_2 = CO + H_2O \tag{4-17}$$

[h] Data from translation of Russian literature (42) indicate the equilibrium constant is almost independent of pressure.

[i] Data from translation of Russian literature (43) indicate the equilibrium constant K is a function of pressure. In relative terms, if K (627°C) = 1 at 1 atm, it decreases to 0.74K at 500 atm and 0.60K at 1000 atm. At the operating pressures of the MCFC, the equilibrium constant can be considered invariant with pressure.

is not expected to be affected significantly by an increase in pressure because the number of moles of gaseous reactants and products in the reaction is identical. Carbon deposition in a MCFC is to be avoided because it can lead to plugging of the gas passages in the anode side. Methane is detrimental to cell performance because the formation of each mole consumes 3 moles of H_2, which represents a considerable loss of reactant and would reduce the power plant efficiency.

The addition of H_2O and CO_2 to the fuel gas modifies the equilibrium gas composition so that the formation of CH_4 is minimized. Carbon deposition can be avoided by increasing the partial pressure of H_2O in the gas stream. The measurements (17) on 10-cm x 10-cm cells at 650°C using simulated gasified coal GF-1 (38% H_2/56% CO/6% CO_2) at 150 psia showed that only a small amount of CH_4 is formed. At open circuit, 1.4 vol% CH_4 (dry-gas basis) was detected, and at fuel utilizations of 50 to 85%, 1.2 to 0.5% CH_4 was measured. The experiments with a high-CO fuel gas (GF-1) at 150 psia, and humidified at 163°C, showed no indication of carbon deposition in a subscale MCFC. These studies indicate that CH_4 formation and carbon deposition at anodes in MCFC operating on coal-derived fuels can be controlled, and under these conditions the side reactions would have little influence on power plant efficiency.

The effect of changes in pressure from 1 to 10 atm on the performance of MCFCs is illustrated in Figures 4-8a and 4-8b. The performance of a MCFC (300-cm^2 cell at 650°C) with an anode gas (28% H_2/28% CO_2/44% N_2) at 80% utilization and a cathode gas (15% O_2/30% CO_2/55% N_2) at 50% utilization is presented in Figure 4-8a (44). Operating the cell at higher pressure (10 atm vs 1 atm) enhances its performance by about 100 mV at 160 mA/cm^2. This enhancement is attributed to the lower polarization and higher gas solubilities at elevated pressure. The dependence of cell voltage on pressure at a fixed current density is plotted in Figure 4-9, using data at 160 mA/cm^2 from Figure 4-8a. The enhancement in cell voltage (ΔV_p) with pressure can be expressed by the equation

$$\Delta V_p \text{ (mV)} = 104 \log \frac{P_2}{P_1} \qquad (4\text{-}18)$$

It should be noted that improvements in cell performance will lead to a change in the coefficient for the logarithmic term, and recent results (45) indicate that the coefficient is less than 104 mV. An earlier analysis by Benjamin et al. (46) concluded that ΔV_p at 160 mA/cm^2 for a wide range of fuel gas compositions at 650°C followed the relationship

$$\Delta V_p \text{ (mV)} = 76.5 \log \frac{P_2}{P_1} \qquad (4\text{-}19)$$

The ΔV_P (104 mV) observed at 160 mA/cm^2 (see Figure 4-9) is considerably greater that that predicted thermodynamically; the enhancement in cell voltage at 650°C for a pressure increase from 1 to 10 atm is greater by a factor of 2.3 than that predicted by Equation 4-13 for the reversible cell potential. This result indicates that the polarization is reduced at higher operating pressures.

Figure 4-8b shows the effect of pressure (3, 5 and 10 atm) and oxidant composition (3.2% CO_2/23.2% O_2/66.3% N_2/7.3% H_2O and 18.2% CO_2/9.2% O_2/65.3% N_2/7.3% H_2O) on the performance of 70.5-cm^2 MCFCs at 650°C (47). The major difference in the results that occurs as the CO_2 pressure changes is the change in the open-circuit potential, which increases with an increase in cell pressure and CO_2 content (see Equation 4-11). At 160 mA/cm^2, ΔV_P is ~44 mV for a pressure change from 3 to 10 atm for both oxidant compositions, and it is comparable to that indicated in

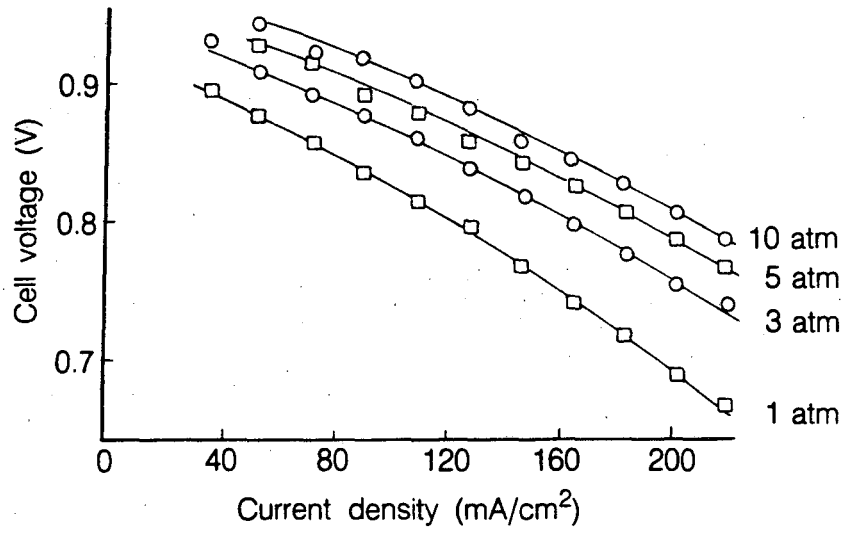

Figure 4-8a. The influence of cell pressure on the performance of a 300-cm^2 MCFC at 650°C. Anode gas, 28% H_2/28% CO_2/44% N_2, 80% utilization; cathode gas, 15% O_2/30% CO_2/55% N_2, 50% utilization.

Source: (Figure 5, p. 15) B.S. Baker, in *Proceedings of the Symposium on Molten Carbonate Fuel Cell Technology*, Edited by J.R. Selman and T.D. Claar, The Electrochemical Society, Inc., Pennington, NJ (1984).

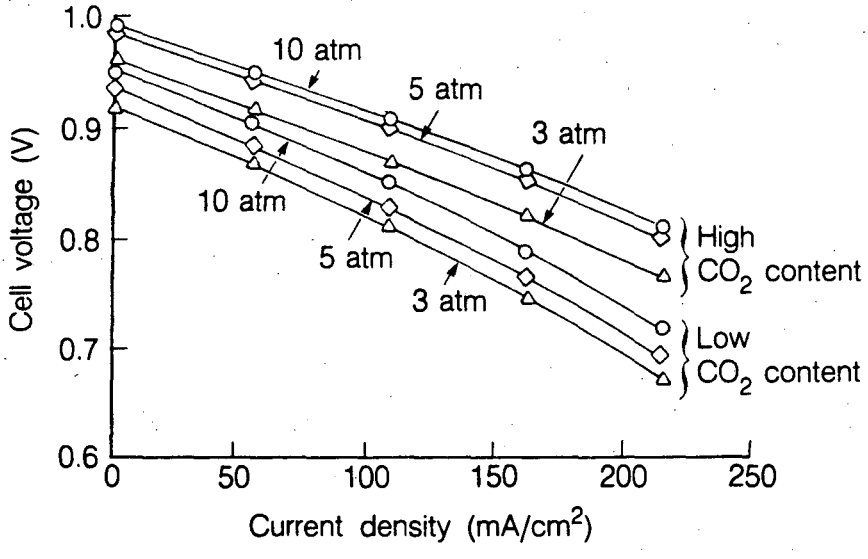

Figure 4-8b. The influence of cell pressure on the performance of a 70.5-cm^2 MCFC at 650°C. Anode gas, not specified; cathode gases, 23.2% O_2/3.2% CO_2/66.3% N_2/7.3% H_2O and 9.2% O_2/18.2% CO_2/65.3% N_2/7.3% H_2O; 50% CO_2 utilization at 215 mA/cm^2.

Source: (Figure 4, p. 395) H.R. Kunz and L.A. Murphy, in *Proceedings of the Symposium on Electrochemical Modeling of Battery, Fuel Cell, and Photoenergy Conversion Systems*, Edited by J.R. Selman and H.C. Maru, The Electrochemical Society, Inc., Pennington, NJ (1986).

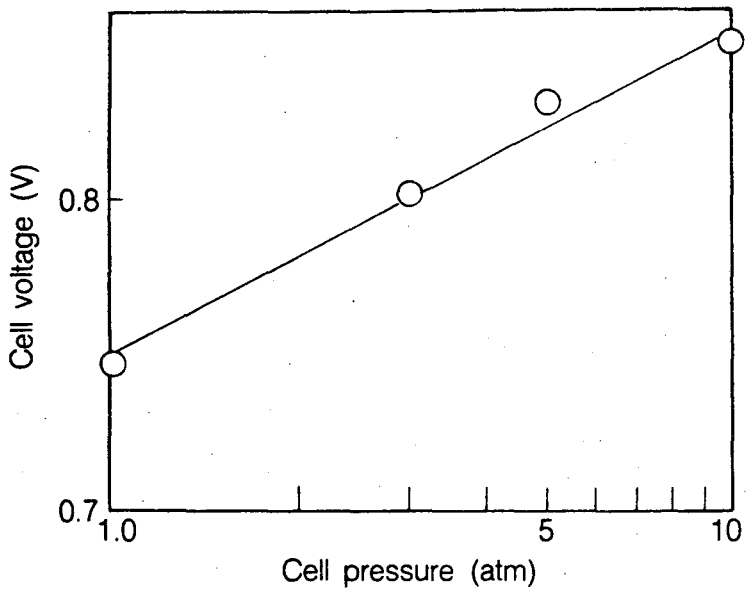

Figure 4-9. The dependence of cell voltage on pressure at 160 mA/cm^2. Data taken from Figure 4-8a.

Figure 4-8a. Because ΔV_P is a function of the total gas pressure, the gas compositions in Figures 4-8a and 4-8b have little influence on ΔV_P.

Temperature: The influence of temperature on the reversible potential of MCFCs depends on several factors, one of which involves the equilibrium composition of the fuel gas.[j] The water-gas shift reaction achieves rapid equilibrium[k] at the anode in MCFCs, and consequently CO serves as an indirect source of H_2. The equilibrium constant (K)

$$K = \frac{P_{CO}\, P_{H_2O}}{P_{H_2} P_{CO_2}} \tag{4-20}$$

increases with temperature (see Table 4.2 and Appendix 9.3), and the equilibrium composition changes with temperature and utilization to affect the cell voltage.

The influence of temperature on the voltage of MCFCs is illustrated by the following example. Consider a cell with an oxidant gas mixture of 30% O_2/60% CO_2/10% N_2, and a fuel gas mixture of 80% H_2/20% CO_2. When the fuel gas is saturated with H_2O vapor at 25°C, its composition becomes 77.5% H_2/19.4% CO_2/3.1% H_2O. After considering the equilibrium established by the water-gas shift reaction (Equation 4-17), the equilibrium concentrations can be calculated (see also Appendix 9.2) using Equation 4-20 and the equilibrium constant; see for instance, Broers and Treijtel (51). The equilibrium concentrations are substituted into Equation 4-4 to determine E as a function of T.

[j] For a fixed gas composition of H_2, H_2O, CO, CO_2 and CH_4 there is a temperature, T_b, below which the exothermic Boudouard reaction is thermodynamically favored, and a temperature, T_m, above which carbon formation by the endothermic decomposition of CH_4 is thermodynamically favored; more extensive details on carbon deposition are found elsewhere (17, 48-50).

[k] The dependence of equilibrium constant on temperature for carbon deposition, methanation and water-gas shift reactions is presented in Appendix 9.3.

Table 4.2 Equilibrium Composition of Fuel Gas and Reversible Cell Potential as a Function of Temperature

Parameter[a]	Temperature (°K)		
	800	900	1000
P_{H_2}	0.669	0.649	0.643
P_{CO_2}	0.088	0.068	0.053
P_{CO}	0.106	0.126	0.141
P_{H_2O}	0.137	0.157	0.172
E^b (V)	1.155	1.143	1.133
K^c	0.2474	0.4538	0.7273

[a] P is the partial pressure computed from the water-gas shift equilibrium of inlet gas with composition 77.5% H_2/19.4% CO_2/3.1% H_2O at 1 atm

[b] Cell potential calculated using Nernst equation and cathode gas composition of 30% O_2/60% CO_2/10% N_2

[c] Equilibrium constant for water-gas shift reaction from Reference 48.

The results of these calculations are presented in Table 4.2. Inspection of the results shows a change in the equilibrium gas composition with temperature. The partial pressures of CO and H_2O increase at higher T because of the dependence of K on T. The result of the change in gas composition, and the decrease in E^o with increasing T, is that E decreases with an increase in T. In an operating cell, the polarization is lower at higher temperatures, and the net result is that a higher cell voltage is obtained at elevated temperatures. The electrode potential measurements (9) in a 3-cm^2 cell[l] show that the polarization at the cathode is greater than at the anode, and that the polarization is reduced more significantly at the cathode with an increase in temperature. At a current density of 160 mA/cm^2, cathode polarization is reduced by about 160 mV when the temperature increases from 550 to 650°C, whereas the corresponding reduction in anode polarization is only about 9 mV (between 600 and 650°C, no significant difference in polarization is observed at the anode).

Baker et al. (52) investigated the effect of temperature (575 to 650°C) on the initial performance of small cells (8.5 cm^2). With steam-reformed natural gas as the fuel and 30% CO_2/70% air as the oxidant, the cell voltage[m] at 200 mA/cm^2 decreased by ~1.4 mV/°C for a reduction in temperature from 650 to 600°C, and 2.2 mV/°C for a decrease from 600 to 575°C. The two major con-

[l] Electrolyte is 55 wt% carbonate eutectic (57 wt% Li_2CO_3, 31 wt% Na_2CO_3, 12 wt% K_2CO_3) and 45 wt% $LiAlO_2$, anode is Co + 10% Cr, cathode is NiO, fuel is 80% H_2/20% CO_2 and oxidant is 30% CO_2/70% air.

[m] Cell was operated at constant flow rate, thus the utilization changes with current density.

tributors responsible for the change in cell voltage with temperature are the ohmic polarization and electrode polarization. It appears that in the temperature range of 575 to 650°C about 1/3 of the total change in cell voltage with decreasing temperature is due to an increase in ohmic polarization, and the remainder from electrode polarization at the anode and cathode.

4.2.2 Effect of Reactant Gas Composition and Utilization

The voltage of MCFCs varies with the composition of the reactant gases. The data in Table 4.3 from Lu and Selman (32) illustrate the dependence of the anode potential on the composition of five typical fuel gases and two chemical equilibria occurring in the anode compartment.[n] The calculations show the gas compositions and open-circuit anode potentials obtained after equilibria by the water-gas shift and CH_4 steam-reforming reactions are considered. The open-circuit anode potential calculated for the gas compositions after equilibration, and experimentally measured, are presented in Table 4.3. The equilibrium gas compositions obtained by the shift and steam-reforming reactions clearly show that, in general, the H_2 and CO_2 contents in the dry gas decrease, and CH_4 and CO are present in the equilibrated gases. The anode potential varies as a function of the $[H_2]/[H_2O][CO_2]$ ratio; a higher potential is obtained when this ratio is higher. The results show that the measured potentials are in good agreement with the values calculated assuming simultaneous equilibria of the shift and the steam-reforming reactions. This agreement is further evidence that both the shift and steam-reforming reactions reach equilibrium rapidly in the anode compartments of MCFCs.

Considering the Nernst equation further, an analysis shows that the maximum cell potential, for a given fuel gas composition, is obtained when $[CO_2]/[O_2] = 2$. Furthermore, the addition of inert gases to the cathode, for a given $[CO_2]/[O_2]$ ratio, causes a decrease in the reversible potential. On the other hand, the addition of inert gases to the anode increases the reversible potential, for a given $[H_2]/[H_2O][CO_2]$ ratio and oxidant composition. This latter result occurs because two moles of products are diluted for every mole of H_2 reactant. However, the addition of inert gases to either gas stream in an operating cell can lead to an increase in concentration polarization.

The electrochemical reaction at the cathode involves the consumption of 2 moles CO_2 per mole O_2 (see Equation 4-2), and this ratio provides the optimum cathode performance. The influence of the $[CO_2]/[O_2]$ ratio on cathode performance is illustrated in Figure 4-10 (41). As this ratio decreases, the cathode performance decreases, and a limiting current is discernible. In the limit where no CO_2 is present in the oxidant feed, the equilibrium

$$CO_3^{2-} = CO_2 + O^{2-} \qquad (4\text{-}21)$$

involving the dissociation of carbonate ions becomes important. Under these conditions the cathode performance shows the greatest polarization because of the composition changes that occur in the electrolyte.

As reactant gases are consumed in an operating cell, the cell voltage decreases in response to the polarization (i.e., activation, concentration) and to the changing gas composition (see discussion in Chapter 2). In cells operating at high utilization, the current density distribution over the electrode surface can become extremely nonuniform because of changes in the gas composition; this topic is addressed by Wolf and Wilemski (53). The change in the average cell voltage of a 10-cell

[n] No gas-phase equilibrium exists between O_2 and CO_2 in the oxidant gas which could alter the composition or cathode potential.

Table 4.3 Influence of Fuel Gas Composition on Reversible Anode Potential at 650°C

Typical Fuel Gas[a]	Gas Composition (mole fraction) H_2	H_2O	CO	CO_2	CH_4	N_2	-E[b] (mV)
Dry gas							
High Btu (53°C)	0.80	-	-	0.20	-	-	1116 ± 3[c]
Intermed. Btu (71°C)	0.74	-	-	0.26	-	-	1071 ± 2[c]
Low Btu 1 (71°C)	0.213	-	0.193	0.104	0.011	0.479	1062 ± 3[c]
Low Btu 2 (60°C)	0.402	-	-	0.399	-	0.199	1030 ± 2[c]
Very low Btu (60°C)	0.202	-	-	0.196	-	0.602	1040 ± 3[c]
Shift equilbrium							
High Btu (53°C)	0.591	0.237	0.096	0.076	-	-	1122[d]
Intermed. Btu (71°C)	0.439	0.385	0.065	0.112	-	-	1075[d]
Low Btu 1 (71°C)	0.215	0.250	0.062	0.141	0.008	0.326	1054[d]
Low Btu 2 (60°C)	0.231	0.288	0.093	0.228	-	0.160	1032[d]
Very low Btu (60°C)	0.128	0.230	0.035	0.123	-	0.484	1042[d]
Shift and Steam-reforming							
High Btu (53°C)	0.555	0.267	0.082	0.077	0.020	-	1113[d]
Intermed. Btu (71°C)	0.428	0.394	0.062	0.112	0.005	-	1073[d]
Low Btu 1 (71°C)	0.230	0.241	0.067	0.138	0.001	0.322	1059[d]
Low Btu 2 (60°C)	0.227	0.290	0.092	0.229	0.001	0.161	1031[d]
Very low Btu (60°C)	0.127	0.230	0.035	0.123	0.0001	0.485	1042[d]

[a] Temperature in parenthesis is the humidification temperature

[b] Anode potential with respect to 33% O_2/67% CO_2 reference electrode

[c] Measured anode potential

[d] Calculated anode potential, taking into account the equilibrated gas composition

Source: (Table 1, p. 385) S.H. Lu and J.R. Selman, in *Proceedings of the Symposium on Molten Carbonate Fuel Cell Technology,* Edited by J.R. Selman and T.D. Claar, The Electrochemical Society, Inc., Pennington, NJ (1984).

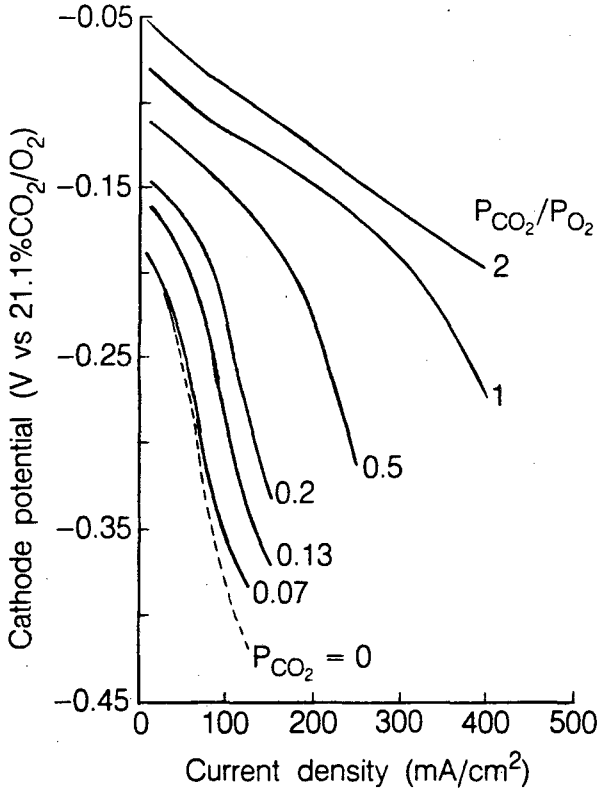

Figure 4-10. The effect of CO_2/O_2 ratio on cathode performance in a MCFC. Oxygen pressure is 0.15 atm.
Source: (Figure 5-10, p. 5-20) "Development of Improved Molten Carbonate Fuel Cell Technology," final report prepared by United Technologies Corp. for the Electric Power Research Institute under Contract #RP1085-4 (July 1983).

stack (see Figures 4-6 and 4-7 for additional performance data) as a function of utilization is illustrated in Figure 4-11. In this stack, the average cell voltage at 172 mA/cm^2 decreases by about 30 mV for a 30% increase in fuel (30 to 60%) or oxidant (20 to 50%) utilization. The relationship between utilization and cell voltage varies with the MCFC operating parameters such as gas composition, current density, flow geometry, temperature and pressure. Consequently, no unique relationship between utilization and voltage of operating cells is available.

4.2.3 Effect of Impurities

Gasified coal is expected to be the major source of fuel gas for MCFCs, but because coal contains many contaminants in a wide range of concentrations, fuel derived from this source also contains a considerable amount of contaminants.[o] A critical concern with these contaminants is the concentration levels that can be tolerated by MCFCs without suffering significant degradation in performance or reduction in cell life. A list of some possible effects of contaminants from coal-derived fuel gases on MCFCs is summarized in Table 4.4 (54).

[o] See Table 9.2 for contaminant levels found in fuel gases from various coal-gasification processes.

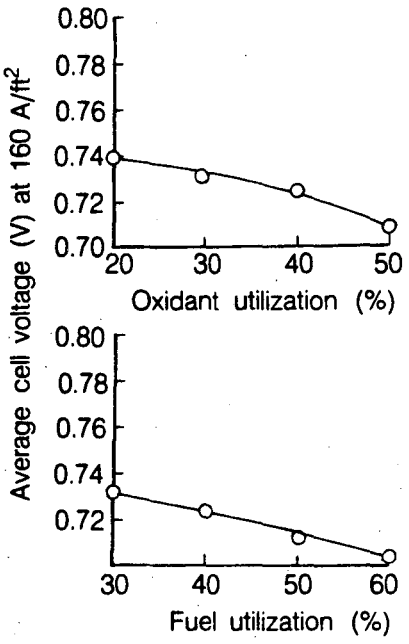

Figure 4-11. Influence of reactant gas utilization on the average cell voltage of a MCFC stack. See Figure 4-7 for additional details.
Source: (Figure 4-21, p. 4-24) J.M. King, A.P. Meyer, C.A. Reiser and C.R. Schroll, "Molten Carbonate Fuel Cell System Verification and Scale-up," EM-4129, final report prepared by United Technologies Corp. for the Electric Power Research Institute, Research Project 1273-1 (July 1985).

The typical fuel gas composition and contaminants from an air-blown gasifier, which enter the MCFC at 650°C after hot-gas cleanup, and the tolerance level of MCFCs to these contaminants are listed in Table 4.5 (55, 56). It is apparent from this example that a wide spectrum of contaminants is present in coal-derived fuel gas. The removal of these contaminants can add considerably to the cost of a fuel-cell power plant integrated with a coal gasifier, and can also decrease the plant efficiency. A review of various options for gas cleanup is presented by Anderson and Garrigan (54) and Jalan et al. (57).

Sulfur: It is now well-established that sulfur compounds in low-ppm (parts-per-million) concentrations in fuel gas are detrimental to MCFCs (58-62). The tolerance of MCFCs to sulfur compounds (60) is strongly dependent on temperature, pressure, gas composition, cell components and system operation (i.e., recycle, venting, gas cleanup). The principal sulfur compound that has an adverse affect on cell performance is H_2S. At atmospheric pressure and high gas utilization (~75%), <10 ppm H_2S (tolerance level depends on anode gas composition and partial pressure of H_2) in the fuel can be tolerated at the anode, and <1 ppm SO_2 is acceptable in the oxidant (60). These concentration limits increase when the temperature increases, but they decrease at increasing pressures.

The mechanisms by which H_2S affects cell performance has been investigated extensively (58, 59, 61, 62). The adverse affects of H_2S occur because of:

- Chemisorption on Ni surfaces to block active electrochemical sites
- Poisoning of catalytic reaction sites for the water-gas shift reaction

Table 4.4 Contaminants from Coal-Derived Fuel Gas and Their Potential Effect on MCFCs

Class	Contaminant	Potential Effect
Particulates	Coal fines, ash	• Plugging of gas passages
Sulfur-containing compounds	H_2S, COS, CS_2, C_4H_4S	• Voltage losses • Reaction with electrolyte via SO_2
Halogen-containing compounds	HCl, HF, HBr, $SnCl_2$	• Corrosion • Reaction with electrolyte
Nitrogen-containing compounds	NH_3, HCN, N_2	• Reaction with electrolyte via NO_x
Trace metals	As, Pb, Hg, Cd, Sn Zn, H_2Se, H_2Te, AsH_3	• Deposits on electrode • Reaction with electrolyte
Hydrocarbons	C_6H_6, $C_{10}H_8$, $C_{14}H_{10}$	• Carbon deposition

Source: (Table 1, p. 299) G.L. Anderson and P.C. Garrigan, in *Proceedings of the Symposium on Molten Carbonate Fuel Cell Technology,* Edited by R.J. Selman and T.D. Claar, The Electrochemical Society, Inc., Pennington, NJ (1984).

- Oxidation to SO_2 in a combustion reaction, and subsequent reaction with carbonate ions in the electrolyte.

The adverse effect of H_2S on the performance of MCFCs is illustrated in Figure 4-12. The cell voltage of a 10-cm x 10-cm cell at 650°C decreases when 5-ppm H_2S is added to the fuel gas (10% H_2/5% CO_2/10% H_2O/75% He), and current is drawn from the cell. The measurements indicate that low concentrations of H_2S do not affect the open-circuit potential, but they have a major impact on the cell voltage as the current density is progressively increased. The decrease in cell voltage is not permanent;[p] when fuel gas without H_2S is introduced into the cell, the cell voltage returns to the level for a cell with clean fuel. These results can be explained by the chemical and electrochemical reactions that occur involving H_2S and $S^=$. A nickel anode at anodic potentials reacts with H_2S to form nickel sulfide:

$$H_2S + CO_3^= \rightarrow H_2O + CO_2 + S^= \quad (4\text{-}22)$$

followed by

$$Ni + xS^= \rightarrow NiS_x + 2xe^- \quad (4\text{-}23)$$

[p] The effects of H_2S on cell voltage is reversible if H_2S concentrations are present at levels below that required to form nickel sulfide.

Table 4.5 Typical Fuel Gas Composition and Contaminants from Air-Blown Coal Gasifier After Hot-Gas Cleanup, and Tolerance Limit of MCFCs to Contaminants

Fuel Gas[a] (mol%)	Contaminants[b]	Content[b]	Remarks[b]	Tolerance[c] Limit
19.2 CO	Particulates	<0.5 mg/l	Also includes ZnO from H_2S cleanup stage	<0.1 g/l for large particulates >0.3 μm
13.3 H_2	NH_3	2600 ppm		<5000 ppm
2.6 CH_4	As	<5 ppm		<1 ppm
6.1 CO_2	H_2S	<10 ppm	After first-stage cleanup	~1
12.9 H_2O	HCl	500 ppm	Also includes other halides	<10 ppm
45.8 N_2	Trace metals	<2 ppm	Pb, Hg, Sn, etc.	<1 ppm
	Zn	<50 ppm	From H_2S hot cleanup	<20 ppm
	Tar	4000 ppm	Formed during desulfurization cleanup stage	<2000 ppm[d]

[a] Humidified fuel gas enters MCFC at 650°C

[b] (Table 1, p. 177) A. Pigeaud, in *Proceedings of the Sixth Annual Contractors Meeting on Contaminant Control in Coal-Derived Gas Streams,* DOE/METC-86/6042, Edited by K.E. Markel and D.C. Cicero, U.S. Department of Energy, Morgantown, WV (July 1986).

[c] A. Pigeaud, Progress Report prepared by Energy Research Corporation for the U.S. Department of Energy, Morgantown, WV under Contract No. DE-AC21-84MC21154 (June 1987).

[d] Benzene

When the sulfided anode returns to open circuit, the NiS_x is reduced by H_2:

$$NiS_x + xH_2 \rightarrow Ni + xH_2S \qquad (4\text{-}24)$$

Similarly when a fuel gas without H_2S is introduced to a sulfided anode, reduction of NiS_x to Ni can also occur. Detailed discussions on the effect of H_2S on cell performance is presented by Vogel and co-workers (58, 59) and Remick (61, 62).

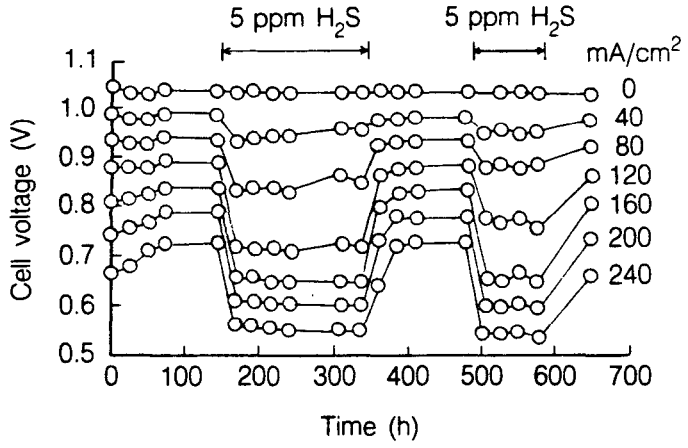

Figure 4-12. Influence of 5 ppm H_2S on the performance of a bench-scale MCFC (10 cm x 10 cm) at 650°C. Fuel gas (10% H_2/5% CO_2/10% H_2O/75% He) at 25% H_2 utilization. *Source*: (Figure 4, p. 443) R.J. Remick, in *Proceedings of the Fourth Annual Contractors Meeting on Contaminant Control in Hot Coal-Derived Gas Streams*, DOE/METC-85/3, Edited by K.E. Markel, U.S. Department of Energy, Morgantown, WV (May 1984).

The rapid equilibration of the water-gas shift reaction in the anode compartment provides an indirect source of H_2 by the reaction of CO and H_2O. If H_2S poisons the active sites for the shift reaction, this equilibrium might not be established in the cell, and a lower H_2 content and a higher CO content than predicted would be expected. Fortunately, the evidence (61, 62) indicates that the shift reaction is not significantly poisoned by H_2S. In fact, Cr used in stabilized-Ni anodes appears to act as a sulfur-tolerant catalyst for the water-gas shift reaction (62).

The CO_2 required for the cathode reaction is expected to be supplied by recycling the anode gas exhaust (after combustion of the residual H_2) to the cathode. Therefore, any sulfur in the anode effluent will be present at the cathode inlet unless provisions are made for sulfur removal. In the absence of a sulfur-removal scheme, sulfur enters the cathode inlet as SO_2, which reacts quantitatively (equilibrium constant is 10^{15} to 10^{17}) with carbonate ions to produce alkali sulfates. These sulfate ions are transported through the electrolyte structure to the anode during cell operation. At the anode, $SO_4^=$ is reduced to $S^=$, thus increasing the concentration of $S^=$ there.

Based on the current understanding of the effect of sulfur on MCFCs, and with the available cell components, it is projected that long-term operation (40,000 h) of MCFCs will require fuel gases with sulfur[q] levels of the order 0.01 ppm or less, unless the system is purged of sulfur at periodic intervals or sulfur is scrubbed from the cell-burner loop (59). Considerable effort has been devoted to develop low-cost techniques for sulfur removal, and R&D is still continuing (63, 64).

Halogen Compounds: Halogen-containing compounds are deleterious to MCFCs because they can lead to severe corrosion of cathode hardware. Thermodynamic calculations (65) show that HCl and HF react with molten carbonates (Li_2CO_3 and K_2CO_3) to form CO_2, H_2O and the respective alkali

[q] Both COS and CS_2 appear to be equivalent to H_2S in their effect on MCFCs (59).

halides. Furthermore the rate of electrolyte loss in the cell is expected to increase because of the high vapor pressure of LiCl and KCl. The concentration of Cl^- species in coal-derived fuels is typically in the range 1 to 500 ppm. It has been suggested (66) that the level of HCl should be kept below 1 ppm in the fuel gas, but the tolerable level for long-term operation has not been established.

Nitrogen Compounds: Compounds such as NH_3 and HCN do not appear to to be harmful to MCFCs (54). However, if NO_x is produced by combustion of the anode effluent in the cell-burner loop, it could react irreversibly with the electrolyte in the cathode compartment to form nitrate salts. The projection by Gillis (67) for the NH_3 tolerance level of MCFCs was 0.1 ppm (see Table 1.4), but this level has not been experimently verified. Preliminary studies (56) indicate that the tolerance limit of MCFCs to NH_3 is <0.5 vol%.

Solid Particulates: These contaminants can originate from a variety of sources, and their presence is a major concern because they can block gas passage ways and/or the anode surface. Carbon deposition, and conditions which can be used to control its formation, has been discussed earlier in this chapter. Solid particles such as ZnO, which is used for sulfur removal, can be entrained in the fuel gas leaving the desulfurizer. The results by Pigeaud (56) indicate that the tolerance limit of MCFCs to particulates larger than 3-μm diameter is <0.1 g/l.

Other Compounds: Experimental studies indicate that 1-ppm As from gaseous AsH_3 in fuel gas does not affect cell performance, but when the level is increased to 9-ppm As, the cell voltage drops rapidly by about 120 mV at 160 mA/cm^2 (55). Trace metals, such as Hg, Sn and Pb in the fuel gas, are of concern because they can deposit on the electrode surface or react with the electrolyte. Research is currently underway to define the tolerance level of MCFCs to these metals (56).

4.3 Internal Reforming

In a conventional fuel-cell system, a carbonaceous fuel is fed to a fuel processor where it is steam-reformed to produce H_2 (as well as other products—CO and CO_2, for example), which is then introduced into the fuel cell and electrochemically oxidized. Efforts are underway to develop a fuel-cell system that eliminates the need for a separate fuel processor by providing for the reforming of carbonaceous fuels in the fuel cell (i.e., internal reforming), and near the electrochemically active sites. This concept appears practical in high-temperature fuel cells where the stream-reforming reaction[r] can be sustained with catalysts. By integrating the reforming reaction and the electrochemical oxidation reaction in the fuel cell, the concept of the internal-reforming MCFC (IRMCFC) is realized. The IRMCFC eliminates the need for the external fuel processor with its ancillary equipment, and it is believed to provide a highly efficient, simple, reliable and cost-effective alternative to the conventional MCFC system (68).

Methane is a common fuel utilized in IRMCFCs, where the steam-reforming reaction

$$CH_4 + H_2O \rightarrow CO + 3H_2 \qquad (4\text{-}25)$$

occurs simultaneously with the electrochemical oxidation of hydrogen (see Reaction 4-1) in the

[r] Steam reforming of CH_4 is typically performed at 750 to 900°C, thus at the lower operating temperature of MCFCs a high-activity catalyst is required. Methanol is also a suitable fuel for internal reforming, and it does not require an additional catalyst because the Ni-based anode is sufficiently active.

anode compartment. The steam-reforming reaction is endothermic, with $\Delta H_{650°C}$ = 53.87 kcal/mol (68), whereas the overall fuel-cell reaction is exothermic. In an IRMCFC, the heat required for Reaction 4-25 is supplied by the waste heat from the fuel-cell reaction, thus eliminating the need for external heat exchange which is required by a conventional fuel processor. In addition, the product steam from Reaction 4-1 can be used to enhance the reforming reaction and the water-gas shift reaction (Reaction 4-17) to produce additional H_2. The forward direction of Reaction 4-25 is favored by high temperature and low pressure, and thus an IRMCFC is best suited to operate near atmospheric cell pressure.

A supported Ni catalyst (e.g., Ni supported on MgO or $LiAlO_2$) provides sufficient catalytic activity to sustain the steam-reforming reaction at 650°C to produce sufficient H_2 to meet the needs of the fuel cell. The interrelationship between the conversion of CH_4 to H_2 and its utilization in an IRMCFC at 650°C is illustrated in Figure 4-13. At open circuit, about 83% of the CH_4 was converted to H_2, which corresponds closely to the equilibrium concentration at 650°C. When current is drawn from the cell, H_2 is consumed and H_2O is produced, and the conversion of CH_4 increases and approaches 100% at fuel utilizations greater than about 50%. Thus, by appropriate thermal management and adjustment of H_2 utilization with the rate of CH_4 reforming, a similar performance can be obtained in IRMCFC stacks with natural gas and with synthesized-reformate gas containing H_2 and CO_2. Currently, the concept of internal reforming has been successfully demonstrated for over 7000 h in small cells, and also in small (0.09 m^2), 10-cell stacks. A recent study (69) suggested that a 1.8-MW IRMCFC using natural gas should be capable of achieving a heat rate of 6450 Btu/kWh (52.9% efficiency).

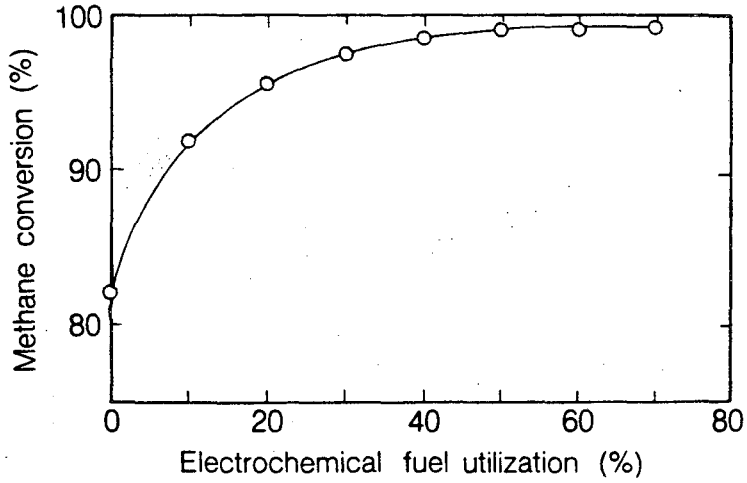

Figure 4-13. Relationship between CH_4 conversion and fuel utilization in an IRMCFC at 650°C and 1 atm. Steam/carbon ratio = 2.5, hydrogen/carbon ratio = 0.1.
Source: (Figure 3, p. 269) H.C. Maru and B.S. Baker, *Prog. Batteries & Solar Cells*, **5**, 264 (1984).

References

1. H.C. Maru and L.G. Marianowski, *Extended Abstracts,* Abstract #31, Fall Meeting of the Electrochemical Society, October 17-22, 1976, Las Vegas, NV (1976) p. 82.
2. J. Mitteldorf and G. Wilemski, *J. Electrochem. Soc.,* **131,** 1784 (1984).
3. R.H. Arendt, *J. Electrochem. Soc.,* **129,** 942 (1982).
4. H.C. Maru, A. Pigeaud, R. Chamberlin and G. Wilemski, in *Proceedings of the Symposium on Electrochemical Modeling of Battery, Fuel Cell, and Photoenergy Conversion Systems,* Edited by J.R. Selman and H.C. Maru, The Electrochemical Society, Inc., Pennington, NJ (1986) p. 398.
5. H.R. Kunz, *J. Electrochem. Soc.,* **134,** 105 (1987).
6. A. Pigeaud, H.C. Maru, L. Paetsch, J. Doyon and R. Bernard, in *Proceedings of the Symposium on Porous Electrodes: Theory and Practices,* Edited by H.C. Maru, T. Katan and M.G. Klein, The Electrochemical Society, Inc., Pennington, NJ (1984) p. 234.
7. H.C. Maru, L. Paetsch and A. Pigeaud, in *Proceedings of the Symposium on Molten Carbonate Fuel Cell Technology,* Edited by R.J. Selman and T.D. Claar, The Electrochemical Society, Inc., Pennington, NJ (1984) p. 20.
8. R.J. Petri and T.G. Benjamin, in *Proceedings of the 21st Intersociety Energy Conversion Engineering Conference,* Volume 2, American Chemical Society, Washington, DC (1986) p. 1156.
9. R.J. Selman, *Energy,* **11,** 153 (1986).
10. C.E. Baumgartner, V.J. DeCarlo, P.G. Glugla and J.J. Grimaldi, *J. Electrochem. Soc.,* **132,** 57 (1985).
11. P.G. Glugla and V.J. DeCarlo, *J. Electrochem. Soc.,* **129,** 1745 (1982).
12. C.D. Iacovangelo and B.R. Karas, *J. Electrochem. Soc.,* **133,** 1595 (1986).
13. C. Baumgartner, *J. Electrochem. Soc.,* **131,** 1850 (1984).
14. W.M. Vogel, L.J. Bregoli, H.R. Kunz and S.W. Smith, in *Proceedings of the Symposium on Molten Carbonate Fuel Cell Technology,* Edited by R.J. Selman and T.D. Claar, The Electrochemical Society, Inc., Pennington, NJ (1984) p. 443.
15. M.L. Orfield and D.A. Shores, in *Corrosion 86,* Paper No. 88, National Association of Corrosion Engineers, Houston, TX (1986).
16. D.A. Shores, in *Proceedings of the 22nd Intersociety Energy Conversion Engineering Conference,* Volume 2, American Institute of Aeronautics & Astronautics, New York, NY (1987) p. 1023.
17. "Development of Improved Molten Carbonate Fuel Cell Technology," Final Report prepared by United Technologies Corp. for the Electric Power Research Institute, Palo Alto, CA, under Contract #RP1085-4 (July 1983).
18. T.D. Kaun, in *Proceedings of the Fourth International Symposium on Molten Salts,* Edited by M. Blander, D.S. Newman, M.L. Saboungi, G. Mamantov and K. Johnson, The Electrochemical Society, Inc., Pennington, NJ (1984) p. 489.
19. A.J. Appleby, "Advanced Fuel Cells and Their Future Market," to be published in *Energy Conservation Strategies,* Progress Series, Edited by W.E. Murphy and L.H. Fletcher, American Society of Aeronautics and Astronautics, New York, NY.
20. A. Pigeaud, A.J. Skok, P.S. Patel and H.C. Maru, *Thin Solid Films,* **83,** 1449 (1981).
21. R.A. Donado, L.G. Marianowski, H.C. Maru and J.R. Selman, *J. Electrochem. Soc.,* **131,** 2541 (1984).

22. R.A. Donado, L.G. Marianowski, H.C. Maru and J.R. Selman, *J. Electrochem. Soc.,* **131,** 2535 (1984).
23. R.B. Swaroop, J.W. Sim and K. Kinoshita, *J. Electrochem. Soc.,* **125,** 1799 (1978).
24. H.S. Hsu and J.H. DeVan, *J. Electrochem. Soc.,* **133,** 2077 (1986).
25. D.A. Shores and P. Singh, in *Proceedings of the Symposium on Molten Carbonate Fuel Cell Technology,* Edited by R.J. Selman and T.D. Claar, The Electrochemical Society, Inc., Pennington, NJ (1984) p. 271.
26. K. Kinoshita, "Critical Survey on Electrode Aging in Molten Carbonate Fuel Cells," ANL-79-55, Argonne National Laboratory, Argonne, IL (1979).
27. "Corrosion of Materials in Molten Carbonate Fuel Cells (MCFC)," prepared by the IIT Research Institute for the U.S. Department of Energy, Morgantown, WV under Contract No. DE-AC21-86MC23265 (January 29, 1987).
28. "Development of Molten Carbonate Fuel Cell Power Plant," Final Report, DOE/ET/17019-20, Volume 1, prepared by General Electric Co. for the U.S. Department of Energy, Morgantown, WV, under Contract No. DE-AC02-80ET17019 (March 1985) p. 4-177.
29. C.D. Iacovangelo, in *Proceedings of the Symposium on Molten Carbonate Fuel Cell Technology,* Edited by R.J. Selman and T.D. Claar, The Electrochemical Society, Inc., Pennington, NJ (1984) p. 397.
30. D.S. Erickson, E.T. Ong and R. Donado, in *Abstracts 1986 Fuel Cell Seminar,* October 26-29, 1986, Tucson, AZ (1986) p. 168.
31. C.D. Iacovangelo, *J. Electrochem. Soc.,* **133,** 2410 (1986).
32. S.H. Lu and J.R. Selman, in *Proceedings of the Symposium on Molten Carbonate Fuel Cell Technology,* Edited by R.J. Selman and T.D. Claar, The Electrochemical Society, Inc., Pennington, NJ (1984) p. 372.
33. S.H. Lu and J.R. Selman, *J. Electrochem. Soc.,* **131,** 2827 (1984).
34. C.E. Baumgartner, R.H. Arendt, C.D. Iacovangelo and B.R. Karas, *J. Electrochem. Soc.,* **131,** 2217 (1984).
35. R.D. Pierce, J.L. Smith and G.H. Kucera, *Prog. Batteries & Solar Cells,* **6,** 159 (1987).
36. K. Scott, M.P. Kang and J. Winnick, *J. Electrochem. Soc.,* **130,** 527 (1983).
37. H.S. Hsu, J.H. DeVan and M. Howell, *J. Electrochem. Soc.,* **134,** 2146 (1987).
38. R.H. Arendt, *J. Electrochem. Soc.,* **129,** 979 (1982).
39. R.H. Arendt and W.D. Pasco, *J. Electrochem. Soc.,* **134,** 733 (1987).
40. J.M. King, A.P. Meyer, C.A. Reiser and C.R. Schroll, "Molten Carbonate Fuel Cell System Verification and Scale-up," EM-4129, Final Report prepared by United Technologies Corp. for the Electric Power Research Institute, Palo Alto, CA, Research Project 1273-1 (July 1985).
41. L.J. Bregoli and H.R. Kunz, *J. Electrochem. Soc.,* **129,** 2711 (1982).
42. M.G. Gonikberg, *Chemical Equilibria and Reaction Rates at High Pressures,* Translated from Russian by M. Artman, Edited by S. Monson, published for the National Science Foundation, Washington, DC, by the Israel Program for Scientific Translations, Jerusalem, Israel (1963) p. 58.
43. M.G. Gonikberg, *Chemical Equilibria and Reaction Rates at High Pressures,* Translated from Russian by M. Artman, Edited by S. Monson, published for the National Science Foundation, Washington, DC, by the Israel Program for Scientific Translations, Jerusalem, Israel (1963) p. 133.

44. B.S. Baker, in *Proceedings of the Symposium on Molten Carbonate Fuel Cell Technology,* Edited by R.J. Selman and T.D. Claar, The Electrochemical Society, Inc., Pennington, NJ (1984) p. 2.
45. H. Maru, private communication, March 6, 1987.
46. T.G. Benjamin, E.H. Camara and L.G. Marianowski, *Handbook of Fuel Cell Performance,* prepared by the Institute of Gas Technology for the United States Department of Energy under Contract No. EC-77-C-03-1545 (May 1980).
47. H.R. Kunz and L.A. Murphy, in *Proceedings of the Symposium on Electrochemical Modeling of Battery, Fuel Cell, and Photoenergy Conversion Systems,* Edited by J.R. Selman and H.C. Maru, The Electrochemical Society, Inc., Pennington, NJ (1986) p. 379.
48. J.R. Rostrup-Nielsen, in *Catalysis Science and Technology,* Edited by J.R. Anderson and M. Boudart, Springer-Verlag, Berlin, German Democratic Republic (1984) p. 1.
49. H.A. Liebhafsky and E.J. Cairns, *Fuel Cells and Fuel Batteries,* John Wiley and Sons, Inc., New York, NY (1968) p. 654.
50. T.D. Tawari, E. Pigeaud and H.C. Maru, in *Proceedings of the Fifth Annual Contractors Meeting on Contaminant Control in Coal-Derived Gas Streams,* DOE/METC-85/6025, Edited by D.C. Cicero and K.E. Markel, U.S. Department of Energy, Morgantown, WV (January 1986) p. 425.
51. G.H.J. Broers and B.W. Treijtel, *Advanced Energy Conversion,* **5,** 365 (1965).
52. B. Baker, S. Gionfriddo, A. Leonida, H. Maru and P. Patel, "Internal Reforming Natural Gas Fueled Carbonate Fuel Cell Stack," Final Report prepared by Energy Research Corporation for the Gas Research Institute, Chicago, IL under Contract No. 5081-244-0545 (March 1984).
53. T.L. Wolf and G. Wilemski, *J. Electrochem. Soc.,* **130,** 48 (1983).
54. G.L. Anderson and P.C. Garrigan, in *Proceedings of the Symposium on Molten Carbonate Fuel Cell Technology,* Edited by R.J. Selman and T.D. Claar, The Electrochemical Society, Inc., Pennington, NJ (1984) p. 297.
55. A. Pigeaud, in *Proceedings of the Sixth Annual Contractors Meeting on Contaminant Control in Coal-Derived Gas Streams,* DOE/METC-86/6042, Edited by K.E. Markel and D.C. Cicero, U.S. Department of Energy, Morgantown, WV (July 1986) p. 176.
56. A. Pigeaud, "Study of the Effects of Soot, Particulate and Other Contaminants on Molten Carbonate Fuel Cells Fueled by Coal Gas," Progress Report prepared by Energy Research Corporation for U.S. Department of Energy, Morgantown, WV under Contract No. DE-AC21-84MC21154 (June 1987).
57. V. Jalan, M. Desai and C. Brooks, in *Proceedings of the Symposium on Molten Carbonate Fuel Cell Technology,* Edited by R.J. Selman and T.D. Claar, The Electrochemical Society, Inc., Pennington, NJ (1984) p. 506.
58. W.V. Vogel and S.W. Smith, *J. Electrochem. Soc.,* **129,** 1441 (1982).
59. S.W. Smith, H.R. Kunz, W.M. Vogel and S.J. Szymanski, in *Proceedings of the Symposium on Molten Carbonate Fuel Cell Technology,* Edited by R.J. Selman and T.D. Claar, The Electrochemical Society, Inc., Pennington, NJ (1984) p. 246.
60. L.G. Marianowski, *Prog. Batteries & Solar Cells,* **5,** 283 (1984).
61. R.J. Remick and E.H. Camara, paper presented at the Fall Meeting of The Electrochemical Society, Inc., October 7-12, 1984, New Orleans, LA.
62. R.J. Remick, in *Proceedings of the Fourth Annual Contractors Meeting on Contaminant Control in Hot Coal-Derived Gas Streams,* DOE/METC-85/3, Edited by K.E. Markel, U.S. Department of Energy, Morgantown, WV (May 1984) p. 440.

63. P.S. Patel, S.M. Rich and H.C. Maru, in *Proceedings of the Fourth Annual Contractors Meeting on Contaminant Control in Hot Coal-Derived Gas Streams,* DOE/METC-85/3, Edited by K.E. Markel, U.S. Department of Energy, Morgantown, WV (May 1984) p. 425.
64. G.L. Anderson, F.O. Berry, B.D. Harmon, R.M. Laurens and R. Biljetina, in *Proceedings of the Fifth Annual Contractors Meeting on Contaminant Control in Coal-Derived Gas Streams,* DOE/METC-85/6025, Edited by D.C. Cicero and K.E. Markel, U.S. Department of Energy, Morgantown, WV (January 1986) p. 87.
65. T.P. Magee, H.R. Kunz, M. Krasij and H.A. Cole, "The Effects of Halides on the Performance of Coal Gas-Fueled Molten Carbonate Fuel Cell," Semi-Annual Report, October 1986 - March 1987, prepared by International Fuel Cells for the U.S. Department of Energy, Morgantown, WV under Contract No. DE-AC21-86MC23136 (May 1987).
66. G.N. Krishnan, B.J. Wood, G.T. Tong and M.A. Quinlan, in *Proceedings of the Fifth Annual Contractors Meeting on Contaminant Control in Coal-Derived Gas Streams,* DOE/METC-85/6025, Edited by D.C. Cicero and K.E. Markel, U.S. Department of Energy, Morgantown, WV (January 1986) p. 448.
67. E.A. Gillis, *Chem. Eng. Prog.*, **88,** (October 1980).
68. H.C. Maru and B.S. Baker, *Prog. Batteries & Solar Cells,* **5,** 264 (1984).
69. P.S. Patel, "Assessment of a 6500-Btu/kWh Heat Rate Dispersed Generator," EM-3307, Final Report prepared by Energy Research Corp. for the Electric Power Research Institute, Palo Alto, CA, under Contract #1041-12 (November 1983).

5. SOLID OXIDE FUEL CELL

The SOFC technology has emerged in the 1980s from scale up of single cells to prototype multi-cell arrays. The SOFC, besides its high temperature (~1000°C) of operation, differs from other fuel cells (AFC, PAFC, MCFC) in that a liquid electrolyte is not used. Instead, the electrolyte is a solid, and thus, electrolyte-management problems that are common to the other conventional fuel cells are not a concern for SOFCs. In addition, SOFCs do not require CO_2 recycle from the anode to the cathode, such as in MCFCs. Westinghouse Electric Corporation is the principal industrial company in the United States which is involved in the development of SOFCs for utility applications. Other groups at Argonne National Laboratory, BP America, Ceramatec, Inc., Combustion Engineering, Garrett/AiResearch, International Fuel Cells Corp., and Ztek Corporation have more recently initiated programs on alternative cell designs and electrolyte structures for SOFCs.

The electrochemical reactions occurring in SOFCs utilizing H_2 and O_2 are

$$H_2 + O^{=} \rightarrow H_2O + 2e^{-} \tag{5-1}$$

at the anode, and

$$\tfrac{1}{2}O_2 + 2e^{-} \rightarrow O^{=} \tag{5-2}$$

at the cathode. The overall cell reaction is

$$H_2 + \tfrac{1}{2}O_2 \rightarrow H_2O \tag{5-3}$$

The corresponding Nernst equation for Reaction 5-3 is

$$E = E^{o} + \frac{RT}{2F} \ln \frac{P_{H_2} P_{O_2}^{1/2}}{P_{H_2O}} \tag{5-4}$$

If dissociation of H_2O (reverse of Reaction 5-3) occurs at 1000°C, the relationship for the equilibrium reaction is expressed by

$$\frac{P_{H_2O}}{P_{H_2}} = K_p P_{O_2}^{1/2} \tag{5-5}$$

The equilibrium constant (K_p) can be expressed as a function of ΔG° and E° by the relationship:

$$\Delta G^\circ = -RT \ln K_p = -2FE^\circ \tag{5-6}$$

Upon substituting Equations 5-5 and 5-6 into Equation 5-4, the open-circuit potential can be expressed in terms of the partial pressures of O_2 in the anode (subscript a) and cathode (subscript c) compartments,

$$E = \frac{RT}{4F} \ln \frac{P_{O_{2,c}}}{P_{O_{2,a}}} \tag{5-7}$$

This equation expresses the relationship between the potential and partial pressure of O_2 in a concentration cell; the SOFC is not a concentration cell because the electrochemical reaction that occurs is given by Reaction 5-3. However, the possibility of a SOFC operating with different O_2 partial pressures in the anode and cathode compartments was considered for space applications (1). If $P_{O_{2,c}}$ = 1 atm and $P_{O_{2,a}} = 10^{-17}$ atm (anode compartment exposed to an environment comparable to that of reformed natural gas), then according to Equation 5-7, E is about 1 V at 1000°C.

The water-gas shift equilibrium involving CO and the CH_4 steam-reforming reaction occur at the high operating temperature in SOFCs to produce H_2 that is easily oxidized at the anode. The direct oxidation (2, 3) of CO and CH_4, which are commonly present in fuel gases, are possible but they have not been thoroughly investigated in SOFCs.

5.1 Cell Components

5.1.1 State-of-the-Art

In the early 1960s, experimental SOFCs with a planar geometry were evaluated, but this geometry presents a problem for building cell stacks because of difficulties with obtaining adequate gas seals. A tubular configuration[a] (i.e., cylindrical design) was adopted for SOFCs which appeared to alleviate the problems with gas seals. An early tubular design is illustrated in the schematic representation of the cross section of a SOFC stack in Figure 5-1a. Overlapping components (i.e., electrodes, electrolyte, cell interconnection) in thin layers (10-50 μm) are deposited on a porous support tube of calcia-stabilized zirconia; fabrication of the fuel-cell stack is described by Isenberg (3) and Sverdrup et al. (4). In this tubular design, individual fuel cells are arranged in bands along the support tube and are connected in series by a ceramic interconnect material. Another variation of an early tubular design is referred to as a "bell and spigot" configuration (see Figure 5.1b), which consists of short, cylindrical electrolyte segments shaped so that they can be fitted one into the other and connected to form a long tube by bell-and-spigot joints (5, 6). A schematic representation of

[a] Recently, the monolith and the planar structures using bipolar current collection have received more consideration for SOFCs (see discussion later in this chapter).

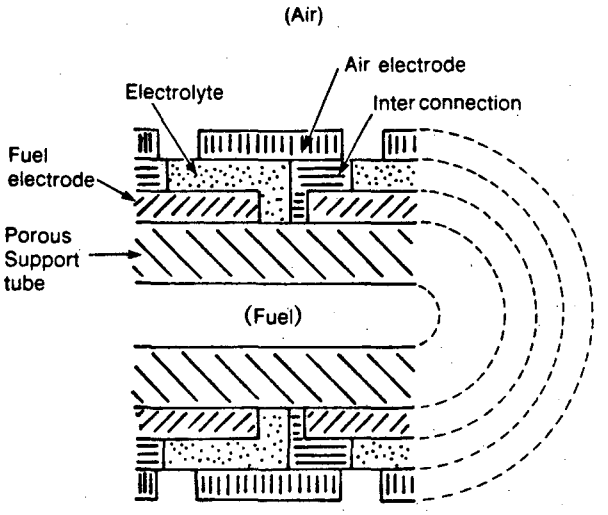

Figure 5-1a. Schematic representation of the cross section (in the axial direction of the support tube) of an early tubular configuration for SOFCs.
Source: (Figure 2, p. 256) E.F. Sverdrup, C.J. Warde and A.D. Glasser, in *From Electrocatalysis to Fuel Cells*, Edited by G. Sandstede, University of Washington Press, Seattle, WA (1972).

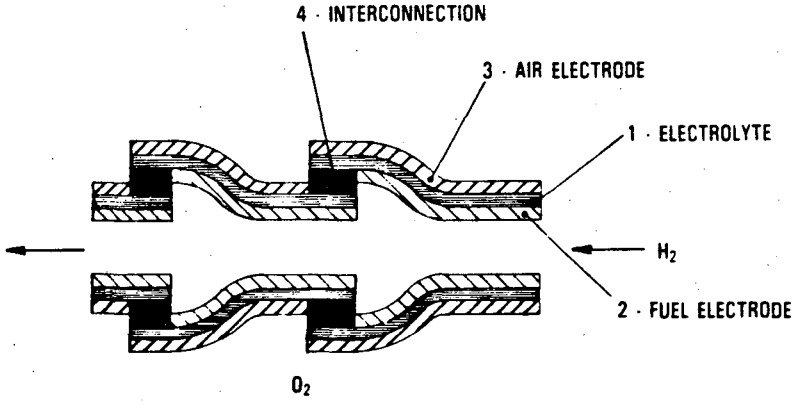

Figure 5-1b. Schematic representation of the cross section (in the axial direction of the series-connected cells) of an early "bell and spigot" configuration for SOFCs.
Source: (Figure 24, p. 332) *Fuel Cells*, DOE/METC-86/0241, Technology Status Report, Morgantown Energy Technology Center, Morgantown, WV (1986).

the cross section of the present tubular design[b] for a SOFC and its gas manifold are presented in Figures 5-2a and 5-2b, respectively . In this design, the cathode, cell interconnection, electrolyte and anode are sequentially deposited on a closed-end porous tubular support material which provides a mechanically strong structure for the thin cell components. A major advantage of this design over earlier designs is that relatively large single tubular cells can be constructed in which the successive active layers can be deposited without chemical or materials interference with previously deposited layers. The manifolding of the oxidant and fuel gases for this tubular cell is illustrated in Figure 5-2b. The oxidant gas is introduced via a central Al_2O_3 tube, and the fuel gas is supplied to the exterior of the closed-end tube. In this arrangement, the Al_2O_3 tube extends to the proximity of the closed end of the support tube, and the oxidant flows back past the cathode surface to the open end. The fuel gas flows past the anode on the exterior of the cell, and in a parallel direction (co-flow) to the oxidant gas. The spent gases are exhausted into a common plenum where the remaining active gases react, and the generated heat serves to preheat the incoming oxidant stream. One attractive feature of this arrangement is that it eliminates the need for leak-free gas manifolding of the fuel and oxidant streams.

Table 5.1 provides a brief description of the materials currently used in the various cell components, and those that were considered earlier. Because of the high operating temperatures of SOFCs, the materials used in the cell components are limited by: (i) chemical stability in oxidizing and/or reducing environments, (ii) chemical stability of contacting materials, (iii) conductivity and (iv) thermomechanical compatibility. A discussion on the current status of the cell components listed in Table 5.1 is presented by Brown (7) and Appleby (8), and many aspects of SOFC technology were discussed at a workshop in 1983 (9).

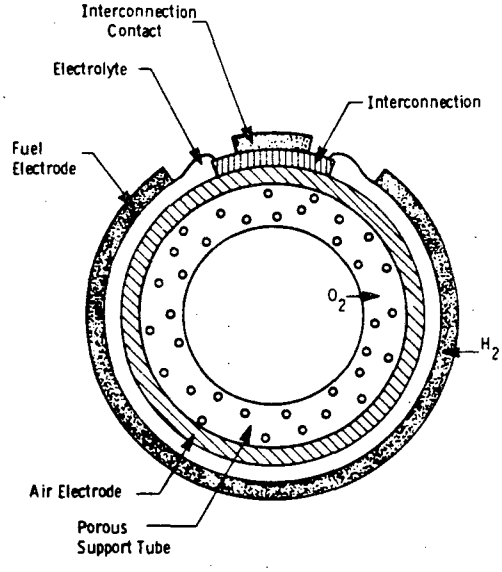

Figure 5-2a. Schematic representation of the cross section of present tubular configuration for SOFCs.

Source: (Figure 23, p. 32) *Fuel Cells*, DOE/METC-86/0241, Technology Status Report, Morgantown Energy Technology Center, Morgantown, WV (1986).

[b] The present tubular design uses a porous support tube of about 30-cm length and 1.27-cm diameter, with an active area of about 110 cm^2. These cells produce about 18 W each, thus about 55 cells are required to generate 1 kW.

An "electrochemical vapor deposition" (EVD) technique has been developed which produces thin layers of refractory oxides that are suitable for the electrolyte and cell interconnection in SOFCs (10). In this technique, the appropriate metal chloride vapor is introduced on one side of a porous support tube, and H_2/H_2O is introduced on the other side. The gas environments on both sides of the support tube act to form two galvanic couples, i.e.,

$$MeCl_x + yO^{=} \rightarrow MeO_y + \tfrac{1}{2}xCl_2 + 2ye^{-} \tag{5-8}$$

and

$$H_2O + 2e^{-} \rightarrow H_2 + O^{=} \tag{5-9}$$

The net result is the formation of a dense and uniform metal oxide layer in which the deposition rate is controlled by the diffusion rate of ionic species and the concentration of electronic charge carriers.

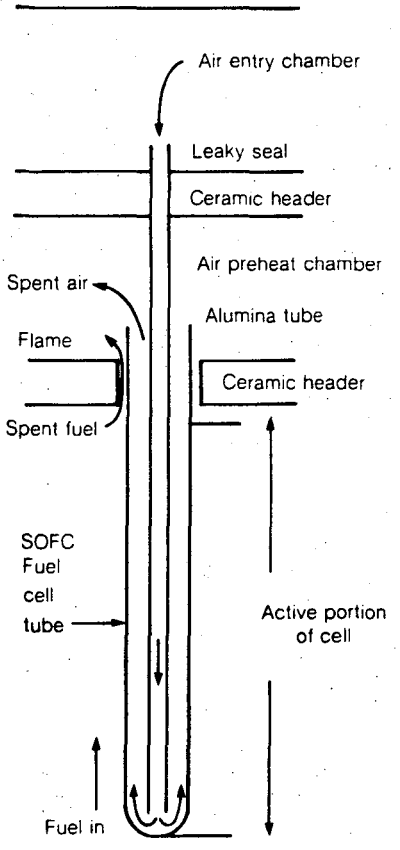

Figure 5-2b. Schematic representation of the gas-manifold design for a tubular SOFC.
Source: A.J. Appleby, "Advanced Fuel Cells and Their Future Market," to be published in *Energy Conservation Strategies*, Progress Series, Edited by W.E. Murphy and L.H. Fletcher, American Society of Aeronautics and Astronautics, New York, NY.

Table 5.1 Evolution of Cell Component Technology for Tubular Solid Oxide Fuel Cells

Component	ca. 1965	ca. 1975	Current Status[a]
Anode	• porous Pt	• Ni-ZrO_2 cermet[b]	• Ni-ZrO_2 cermet[b] • deposit slurry • ~150-μm thickness • 20-40% porosity
Cathode	• porous Pt	• stabilized ZrO_2 impregnated with praesodymium oxide	• Sr-doped lanthanum manganite • deposit slurry, sinter • ~1-mm thickness • 20-40% porosity
Electrolyte	• yttria-stabilized ZrO_2 • 0.5-mm thickness	• yttria-stabilized ZrO_2 • EVD	• yttria-stabilized ZrO_2 • EVD • ~40-μm thickness
Cell Interconnect	• Pt	• Mn-doped cobalt chromite	• Mg-doped lanthanum chromite • EVD • ~40-μm thickness
Support Tube	• yttria-stabilized ZrO_2	• yttria-stabilized ZrO_2	• calcia-stabilized ZrO_2 • 34-35% porosity • 12.8-mm diameter • 1-2-mm wall thickness • 457-mm length

[a] Specifications for Westinghouse 5-kW fuel cell

[b] Y_2O_3-stabilized ZrO_2

EVD = electrochemical vapor deposition

This procedure is used to fabricate the solid electrolyte (yttria-stabilized zirconia) and the interconnection (Mg-doped lanthanum chromite).

The anode consists of metallic Ni and Y_2O_3-stabilized ZrO_2 skeleton, which serves to inhibit sintering of the metal particles and to provide a thermal expansion coefficient comparable to those of the other cell materials. The anode structure is fabricated with a porosity of 20 to 40% to facilitate mass transport of reactant and product gases. The Sr-doped lanthanum manganite ($La_{1-x}Sr_xMnO_3$, x = 0.10-0.15) that is most commonly used for the cathode material is a p-type conductor. Similar to the anode, the cathode is a porous structure that must permit rapid mass transport of reactant and product gases. The cell interconnection material (Mg-doped lanthanum chromite, $LaCr_{1-x}Mg_xO_3$, x = 0.02-0.10), on the other hand, must be impervious to fuel and oxidant gases and must possess good electronic conductivity. In addition, the cell interconnection is exposed to both the cathode and anode environments, thus it must be chemically stable under O_2 partial pressures of about ~1 to 10^{-18} atm at 1000°C.

The solid oxide electrolyte must be free of porosity that permits gas to permeate from one side of the electrolyte layer to the other, and it should be thin to minimize ohmic loss. In addition, the electrolyte must have a transport number for $O^=$ of close to unity as possible, and a transport number for electronic conduction of close to zero as possible. Zirconia-based electrolytes are suitable for SOFCs because they exhibit pure anionic conductivity over a wide range of O_2 partial pressures (1 to 10^{-20} atm). The other cell components should permit only electronic conduction,[c] and interdiffusion of ionic species in these components at 1000°C should not have a major effect on their electronic conductivity. Other severe restrictions placed on the cell components are that they must be stable to the gaseous environments in the cell, and they must be capable of withstanding thermal cycling. The materials listed in Table 5.1 appear to have the optimum properties for meeting these requirements.

The resistivities of typical cell components at 1000°C are (11): 10 ohm-cm (ionic) for the electrolyte (8-10 mol% Y_2O_3-doped ZrO_2), 0.5 ohm-cm (electronic) for the cell interconnection (Mg-doped $LaCrO_3$), 0.013 ohm-cm (electronic) for the cathode (Sr-doped $LaMnO_3$) and 0.001 ohm-cm (electronic) for the anode (Ni-ZrO_2 cermet[d]). It is apparent that the solid oxide electrolyte is the least-conductive of the cell components, followed by the cell interconnection. Furthermore, an operating temperature of about 1000°C is necessary if the ionic conductivity of the solid electrolyte (i.e., 0.02 $ohm^{-1}cm^{-1}$ at 800°C and 0.1 $ohm^{-1}cm^{-1}$ at 1000°C) is to be within even an order of magnitude of that of aqueous electrolytes. The solid electrolyte in SOFCs must be only about 25-50 μm thick if its ohmic loss at 1000°C is to be comparable to that of the electrolyte in PAFCs (8). Fortunately, thin electrolyte structures of about 40-μm thickness can be fabricated by EVD, as well as by tape casting and other ceramic processing techniques.

The successful operation of SOFCs requires individual cell components that are thermally compatible so stable interfaces are established at 1000°C, i.e., thermal expansion coefficients for cell components must be closely matched to minimize or reduce stresses arising from differential thermal expansion between components. Fortunately, the components that are listed in Table 5.1 have reasonably close thermal expansion coefficients (i.e., ~10^{-5}/°C from room temperature to 1000°C), but there is room for improvement in matching these values.

---

[c] Mixed conducting (i.e., electronic and ionic) materials for anodes may be advantageous if H_2 oxidation can occur over the entire surface of the electrode to enhance current production, instead of only in the region of the three-phase interface (gas/solid electrolyte/electrode).

[d] The cermet becomes an electronic conductor at Ni contents of >30 vol% (12).

A configuration for electrically connecting cells to form a stack is illustrated in Figure 5-3. The cells are connected in a series-parallel array by nickel felt strips which are exposed to the reducing fuel gas. In this arrangement the nickel felt strips and cell interconnections extend the length of the support tube. Because the current flows in the peripheral direction of the thin electrodes, a relatively large ohmic loss exists which places a upper limit on the tube diameter.

5.1.2 Alternative Components

Alternative cell configurations to the tubular geometry for SOFCs are currently under evaluation (see discussion in Sections 5.3 and 5.4). Effort is also currently underway to develop improved cell components to those described in the preceding section.

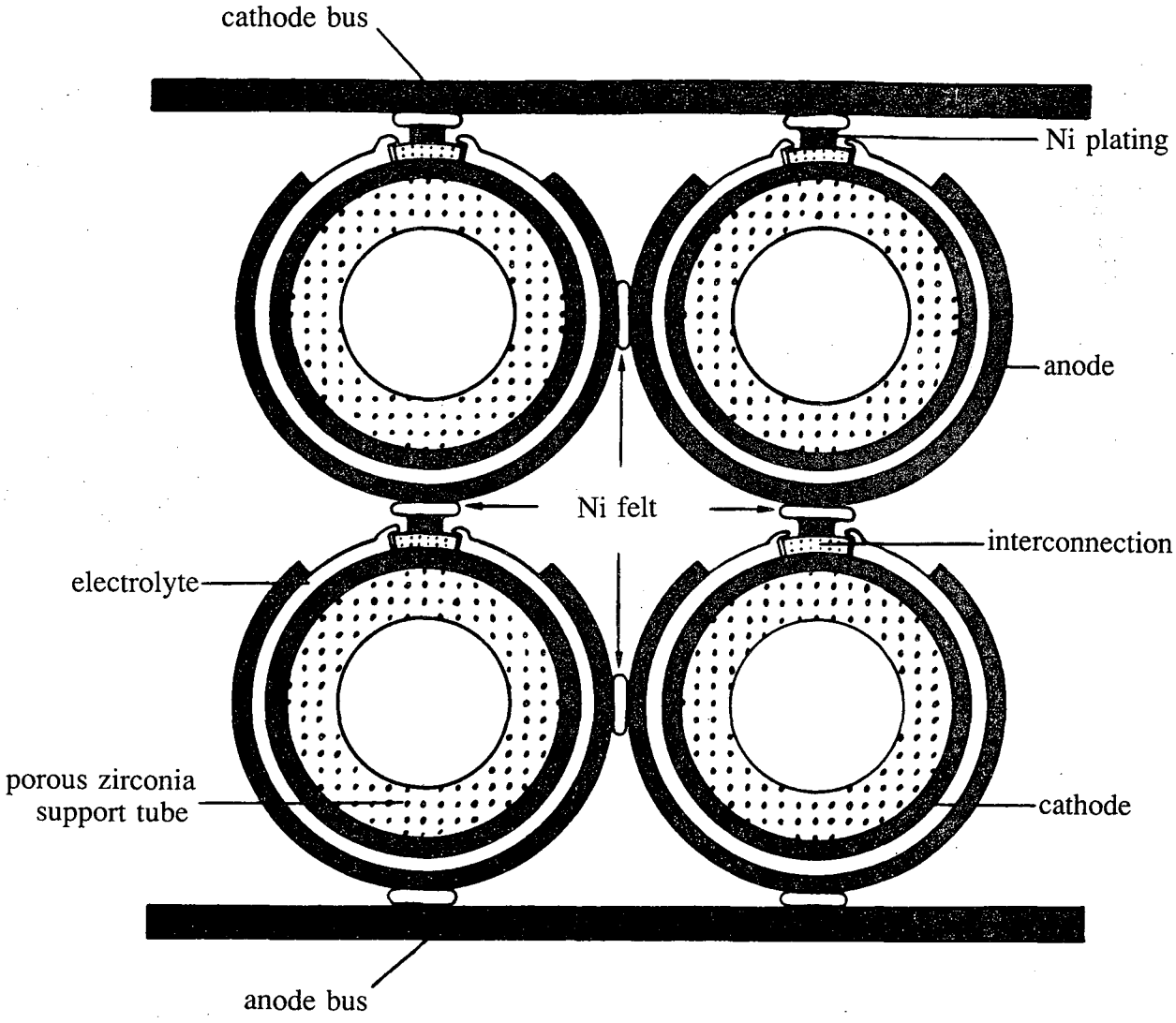

Figure 5-3. Cell-to-cell connections between SOFCs.
Source: (Figure 25, p. 34) *Fuel Cells*, DOE/METC-86/0241, Technology Status Report, Morgantown Energy Technology Center, Morgantown, WV (1986).

Anodes with mixed conduction (ionic and electronic) may permit a larger effective reaction zone and lower polarization for fuel oxidation than anodes that are pure electronic conductors. A larger reaction zone is obtained if ionic transport of $O^=$ occurs through the electrode so that the fuel gas can react with $O^=$ at the electrode/gas interface, as well as at the electrode/solid electrolyte/gas interface. Worrell (13) has recently started to investigate ZrO_2-TiO_2-Y_2O_3 solid solutions for mixed conduction. The major challenges are to develop a solid oxide electrolyte with mixed conduction that is not affected by P_{O_2} and which is chemically stable in the operating temperature range of SOFCs.

High-temperature oxides based on In_2O_3–ZrO_2 (or HfO_2) stabilized by a rare-earth oxide (PrO_2) have been developed as cathodes and possibly cell interconnects for SOFCs (14). Preliminary results at 1000°C are encouraging but long-term tests have not been completed.

The Mg-doped lanthanum chromite in the cell interconnection appears to be adequate for current SOFCs, but it is susceptible to a decrease in electronic conductivity with a decrease in O_2 partial pressure. Furthermore its thermal expansion is about 12 to 14% lower than that of the calcia-stabilized zirconia in the support tube. Thus efforts have been underway (15) to improve the properties of the cell interconnection by increasing the Mg content in the lanthanum chromite, and also to increase its thermal expansion coefficient by chemical modification. In addition, the development of alternative materials for cell interconnections is being pursued.

Electrochemical vapor deposition (EVD) presents several limitations in the fabrication of cell interconnections: (a) limited choice of dopants (only Mg has been successfully utilized in Mg-doped lanthanum chromite); (b) non-uniform film thicknesses are deposited; (c) non-uniform dopant concentrations are obtained; and (d) impurities from the gas phase are deposited which may affect the conductivity of the film. Singhal (16) is investigating alternative materials for cell interconnections. One such material that looks promising is Sr-doped lanthanum chromite, which has a higher electronic conductivity than the state-of-the art material, Mg-doped lanthanum chromite. Preparation of Sr-doped lanthanum chromite by electrochemical vapor deposition does not appear to be feasible, so alternative techniques are currently being explored for its fabrication.

The development of alternative solid electrolytes that are not based on zirconia is hampered by the chemical instability of most materials in the extreme oxidizing and reducing environments encountered in SOFCs. Several metal oxide-doped CeO_2 (17, 18) and MoO_3-doped Bi_2O_3 (19) have specific ionic conductivities that are comparable or higher than that of the calcia- or yttria-doped zirconia electrolytes. However, a major problem with these alternative materials is that they are reduced in low O_2 partial pressures, such as at the anodes in SOFCs, and they are susceptible to significant electronic conduction. At present an alternative solid oxide is not available that offers an improvement over the current zirconia-based solid electrolyte for SOFCs.

5.2 Performance

The thermodynamic efficiency of SOFCs is lower than that of MCFCs and PAFCs which utilize H_2 and O_2 because of the lower ΔG^e at higher temperatures (see discussion in Chapter 2). However, as mentioned in Chapter 2, the higher operating temperature of SOFCs is beneficial in reducing polarization.

[e] ΔG decreases from 54.617 kcal/mole at 27°C to 43.3 kcal/mole at 927°C, whereas ΔH is nearly constant over this temperature range (7).

The polarization in SOFCs is dominated by ohmic losses in the cell components. The contribution to ohmic polarization (IR) in a tubular cell[f] is reported (11) to originate 65% from the cathode, 25% from the anode, 9% from the electrolyte, and 1% from the interconnect, when these components have thicknesses (mm) of 0.7, 0.1, 0.04 and 0.04, respectively, and specific resistivities (ohm-cm) at 1000°C of 0.013, 0.001, 10, and 0.5, respectively. The cathode IR dominates the total ohmic loss despite the higher specific resistivities of the electrolyte and cell interconnection because of the short conduction path through these components and the long current path (i.e., 1.1 cm) in the plane of the cathode. The current path in the anode is about 0.8 cm and its resistivity is about an order of magnitude lower than that of the cathode, so for typical thickness of these electrodes (see above) the IR loss in the cathode is about 2.5 times greater than that in the anode.

The typical cell performance of SOFCs during the period from about 1965 to the mid 1980s is illustrated by the cell voltage-current density curves in Figure 5-4 (3, 6, 20, 21). These results were obtained with two types of SOFCs at 1000°C and with various fuel gases and air for the oxidant. The results reported in 1965 (6) were obtained from a single cell consisting of a flat-plate geometry (i.e., zirconia electrolyte was sandwiched between thin Pt foils for the anode and cathode), and the more recent data (20, 21) are the average cell voltage from a three-cell stack of the present tubular design illustrated in Figure 5-2.

5.2.1 Effect of Pressure and Temperature

Operating SOFCs at gas pressures above one atm has been largely unexplored. It is expected that the SOFC, like the PAFC and MCFC, would show an enhanced performance with an increase in cell pressure. However, data are not available to assess whether the tubular design for SOFCs can be made in large units or can be operated under pressurized conditions.

The dependence of SOFC performance on temperature is illustrated in Figure 5-5 (22) for oxygen (25% utilization) and a fuel of 67% H_2/22% CO/11% H_2O (85% fuel utilization). The sharp decrease in cell voltage as a function of current density at 700°C is a manifestation of the high ohmic polarization (i.e., low ionic conductivity) of the solid electrolyte at this temperature. The ohmic polarization decreases as the operating temperature increases to 1000°C, and correspondingly, the current density at a given cell voltage increases dramatically. The data in Figure 5-5 show a larger decrease in cell voltage with decreasing temperature between 800 and 900°C than that between 900 and 1000°C, at constant fuel utilization and current density. The Nernst potential decreases with an increase in temperature (i.e., theoretical potential of SOFC is about 0.1 V lower than that of the MCFC), and thus it counters the performance improvement that is observed as the temperature increases.

5.2.2 Effect of Reactant Gas Composition and Utilization

Since SOFCs operate at high temperature, they are capable of internally reforming fuel gases (i.e., CH_4 and other light hydrocarbons) without the use of a specific reforming catalyst (i.e., anode itself is sufficient), and this attractive feature of high-temperature operation of SOFCs has recently been experimentally verified. Another important aspect of SOFCs is that recycle of CO_2 from the spent fuel stream to the inlet oxidant, as required by MCFCs, is not necessary because SOFCs utilize only O_2 at the cathode.

[f] A uniform current distribution through the electrolyte is assumed.

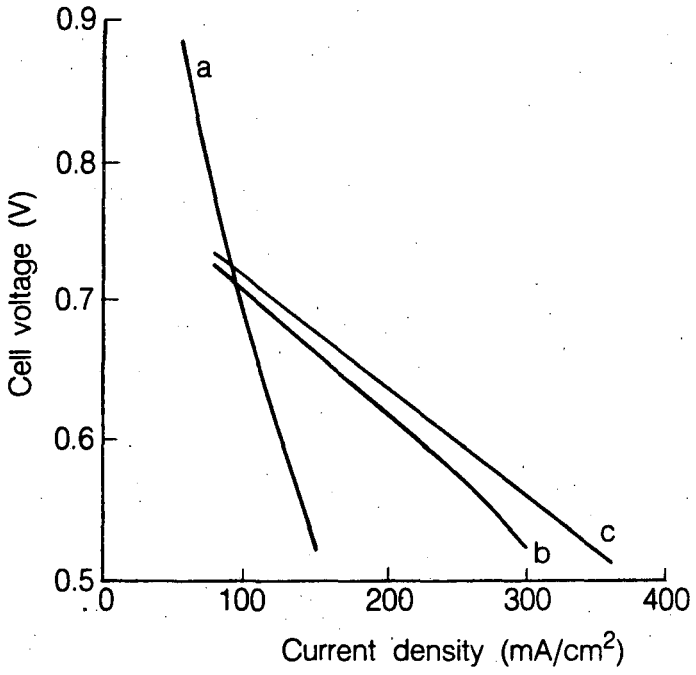

Figure 5-4. Performance of SOFCs at 1000°C with air and various reformate fuel compositions. (a) Single cell of flat-plate geometry from 1965 (6), H_2 fuel; (b) average cell voltage of three-cell stack of tubular geometry (see Fig. 5-2) from 1985 (20), 67% H_2/22% CO/11% H_2O fuel at 80% fuel utilization, 25% oxidant utilization; (c) average cell voltage of three-cell stack of tubular geometry (see Fig. 5-2) from 1986 (21), 67% H_2/22% CO/11% H_2O fuel at 85% fuel utilization; 25% oxidant utilization.

The performance of SOFCs, like that of other fuel cells, improves with pure O_2 rather than air as the oxidant. With a fuel of 67% H_2/22% CO/11% H_2O at 85% utilization, the cell voltage at 1000°C shows an improvement with pure O_2 over that obtained with air (see Figure 5-6). In the figure, the experimental data are extrapolated by a dashed line to the theoretical Nernst potential for the inlet gas compositions. At a target current density of 160 mA/cm^2 for the tubular SOFC operating on the abovementioned fuel gas, a difference in cell voltage of about 55 mV is obtained. The difference in cell voltage with pure O_2 and air increases as the current density increases, which suggests that concentration polarization plays a role during O_2 reduction in air.

The influence of fuel gas composition on the theoretical open-circuit potential of SOFCs is illustrated in Figure 5-7, following the discussion by Sverdrup, et al. (4). The oxygen/carbon (O/C) atom ratio and hydrogen/carbon (H/C) atom ratio, which define the fuel composition, are plotted as a function of the theoretical open-circuit potential at 1000°C. If hydrogen is absent from the fuel gas, H/C = 0. For pure CO, O/C = 1, and for pure CO_2, O/C = 2. The data in the figure show that the theoretical potential decreases from above 1 V to about 0.6 V as the amount of O_2 increases and the fuel gas composition changes from CO to CO_2. The presence of hydrogen in the fuel produces two results: (a) the potential is higher, and (b) the O/C ratio corresponding to complete oxidation extends to higher values. These effects occur because the equilibrium composition obtained by the water-gas shift reaction in gases containing hydrogen (H_2O) and carbon (CO) produces H_2, but this

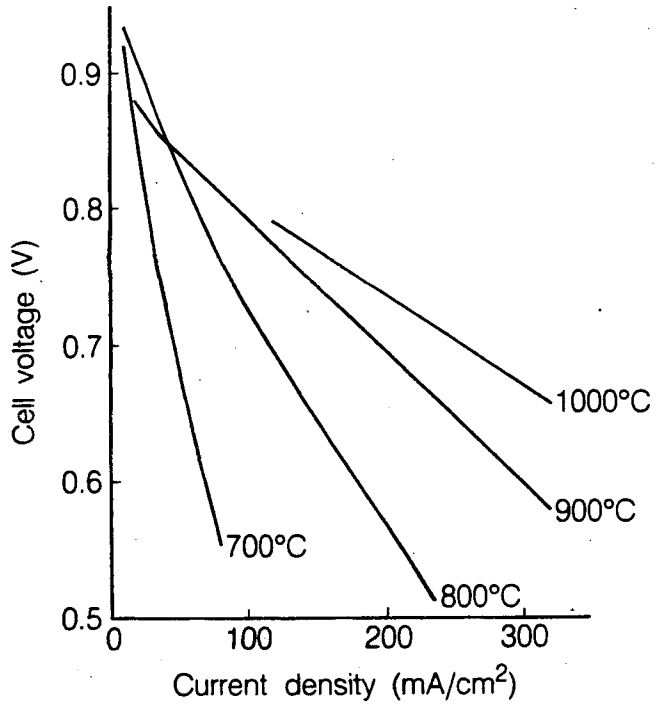

Figure 5-5. Dependence of cell performance on temperature. Fuel (67% H_2/22% CO/11% H_2O) utilization is 85% and oxidant (pure O_2) utilization is 25%.
Source: C. Zeh, private communication (April 29, 1987).

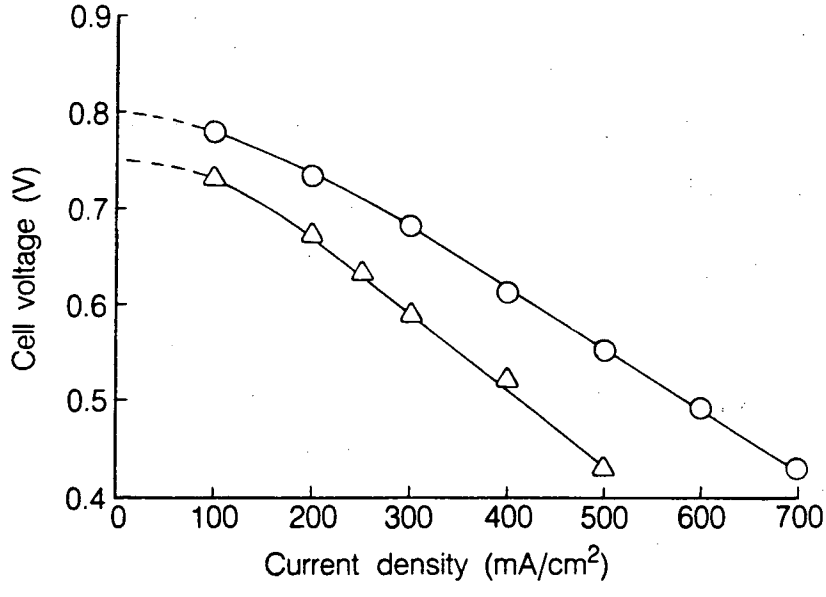

Figure 5-6. Cell performance at 1000°C with pure oxygen (O) and air (Δ), both at 25% utilization. Fuel (67% H_2/22% CO/11% H_2O) utilization is 85%.
Source: C. Zeh, private communication (April 29, 1987).

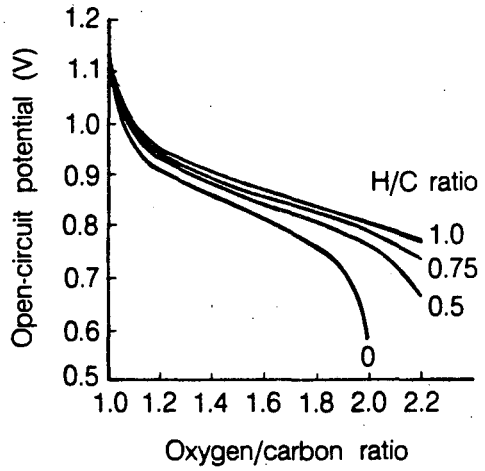

Figure 5-7. Influence of gas composition on the theoretical open-circuit potential of SOFC at 1000°C.

Source: (Figure 3, p. 258) E.F. Sverdrup, C.J. Warde and A.D. Glasser, in *From Electrocatalysis to Fuel Cells*, Edited by G. Sandstede, University of Washington Press, Seattle, WA (1972).

reaction is not favored at higher temperatures (see Appendix 9.3). In addition, the theoretical potential for the H_2/O_2 reaction exceeds that for the CO/O_2 reaction (see Figure 1-2) at temperatures above about 800°C, consequently, the addition of hydrogen to the fuel gas will yield a higher open-circuit potential in SOFCs.

The fuel gas composition also has a major effect on the cell voltage of SOFCs. The performance data (23) obtained from a 15-cell stack (1.7-cm^2 active electrode area per cell) of the tubular configuration (see Figure 5-1a) at 1000°C illustrate the effect of fuel gas composition. With air as the oxidant and fuels of composition 97% H_2/3% H_2O, 97% CO/3% H_2O, and 1.5% H_2/3% CO/75.5% CO_2/20% H_2O, the current densities achieved at 80% voltage efficiency were ~220, ~170 and ~100 mA/cm^2, respectively. The reasonably close agreement in the current densities obtained with fuels of composition 97% H_2/3% H_2O and 97% CO/3% H_2O indicates that CO is a useful fuel for SOFCs. However, with fuel gases that have only a low concentration of H_2 and CO (i.e., 1.5% H_2/3% CO/75.5% CO_2/20% H_2O), concentration polarization becomes significant and the performance is lower.

The reference fuel gas that is currently utilized in experimental SOFCs has a composition 67% H_2/22% CO/11% H_2O. With this fuel (85% utilization) and air as the oxidant (25% utilization), individual cells (~1.5-cm diameter, 30-cm length and ~110-cm^2 active surface area) have delivered a peak power of 22 W (24). The change in the cell voltage with fuel utilization for a SOFC that operates on this reference fuel and pure O_2 or air as oxidant (25% utilization) is shown in Figure 5-8 (22). The cell voltage decreases with an increase in the fuel utilization at constant current density. Insufficient data are available in the figure to determine whether the temperature has a significant effect on the change in cell voltage with utilization. However, the data does suggest that a larger voltage decrease occurs at 1000°C than at 800 or 900°C.

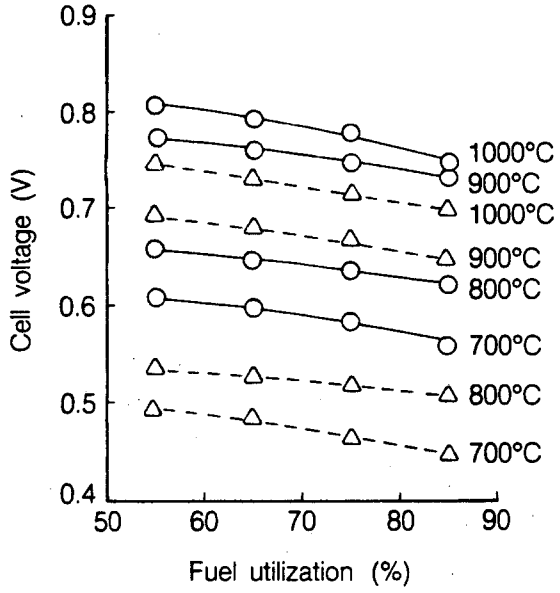

Figure 5-8. Variation in cell voltage as a function of fuel utilization and temperature. Oxidant (O - pure O_2; Δ - air) utilization is 25%. Current density is 160 mA/cm^2 at 800, 900 and 1000°C and 79 mA/cm^2 at 700°C.
Source: C. Zeh, private communication (April 29, 1987).

5.2.3 Effect of Impurities

Sulfur-containing compounds are impurities in fuel gases which are potentially harmful to the operation of SOFCs. The sulfur tolerance of Ni-containing anodes in SOFCs has been predicted theoretically from thermodynamic data and observed experimentally. The thermodynamic data predicts that sulfidation of Ni at 1000°C occurs under equilibrium conditions at 1 atm in a fuel gas [(H_2 + H_2O) = 25% and (CO + CO_2) = 75%] containing about 90 ppm total sulfur species (25). Furthermore, the sulfur tolerance of SOFCs decreases with a decrease in temperature (i.e., 5 ppm at 700°C) and a decrease in the relative amount of H_2 + H_2O. Nevertheless it appears that SOFCs can tolerate one to two orders of magnitude more sulfur than other fuel-cell systems. Experimental measurements have verified the predicted sulfur tolerance of SOFCs (22). A 7-cell stack operating at 1000°C with 15% (H_2 + CO) and the balance CO_2, which simulates a typical fuel composition after 85-88% utilization, was injected with 50 ppm H_2S. The stack voltage at 150 mA/cm^2 decreased to about 95% of the value (4.5 V) obtained with the fuel gas that does not contain H_2S. When H_2S was removed from the fuel gas, the stack voltage nearly returned to its original level. This result demonstrates the reversibility of sulfur chemisorption in SOFCs at 1000°C and a sulfur concentration of 50 ppm.

5.3 Bipolar Structure

A bipolar structure, which is the common configuration for cell stacks in PAFCs and MCFCs, permits a simple series electrical connection between cells and without the need for external cell interconnections such as those used with the tubular configuration shown in Figure 5-3. Perpendicu-

lar current collection in a cell stack with a bipolar design should have a lower ohmic polarization than the tubular configuration, and overall stack performance should be improved. However, gas leaks in a SOFC of bipolar configuration with compressive seals are difficult to prevent, and thermal stresses at interfaces between dissimilar materials must be accommodated to prevent mechanical degradation of cell components. Planar electrodes and solid electrolyte structures were proposed for use in high-temperature fuel cells and electrolysis cells by Hsu and co-workers (26, 27) in the mid 1970s. More recently, Hsu (28, 29) developed bipolar structures for SOFCs which are reported to have the following attractive features: (a) high power density, (b) structural ruggedness, (c) concealed electrodes, (d) ease of heat removal, and (e) low-stress assembly.

Solid electrolyte structures of yttria-stabilized ZrO_2 of up to 10-cm diameter and 0.25-mm thickness with better than 0.025-mm flatness have been fabricated (29). Tests of single and two-cell stacks of SOFCs with a planar configuration (5-cm diameter) have demonstrated power densities up to 0.12 W/cm^2. One major technical difficulty with these structures is their brittleness in tension; the tensile strength is only about 20% of their compressive strength. However, the two-cell stack was able to withstand five thermal cycles without suffering detectable physical damage, and adequate gas sealing between cells was reported. The successful demonstration of larger multicell stacks has yet to be performed.

5.4 Monolith Structure

The so-called monolith structure is a more complex design of bipolar configuration for SOFCs. A schematic representation of a cross section of the monolith structure proposed for SOFCs is presented in Figure 5-9, and details of its fabrication are described by Fee and co-workers (30, 31). The structure resembles the corrugated assembly used in cardboard boxes. The small channels are formed from thin (25 to 100 μm) layers of the active cell components, and these channels serve for passage of the fuel and oxidant streams. In this design the anode, cathode and solid electrolyte, which have the compositions listed in Table 5.1, are tape-cast into thin-layer structures, and then the complete assembly is heat treated in air to produce the SOFC monolith. The principal challenge of this technology is to match the thermal properties (i.e., thermal expansion, shrinkage rates) of the individual materials so that they can be heat treated (i.e., controlled heating to ~400°C to burn out the organic binder, plasticizer and dispersant, and further heating to between 1200 and 1600°C to sinter the ceramic materials, followed by cool down to room temperature) together to form the appropriate monolith structure. The residual thermal stresses that develop because of the differences in thermal expansion of the individual layer components can lead to mechanical failure of the monolith structure, and this problem has been analyzed by Majumdar et al. (32). Another challenge is to manifold the fuel and oxidant gases. A cross-flow pattern for the gases requires only a simple manifold, but the monolith structure for this manifold is more complex than the representation shown in Figure 5-9. A co-flow or counter-flow pattern for the gases could be adapted to the monolith structure in Figure 5-9, but a complex manifold design is required.

The bipolar configuration for the monolith SOFC uses perpendicular current collection and would minimize the IR losses inherent in the arrangement of tubular SOFCs shown in Figure 5-3. In addition, the honeycomb configuration provides a strong self-supporting structure which eliminates the need for a porous support such as the one used in the tubular design. If scale up of the monolith structure from single cells to bipolar SOFC stacks is achieved, a significant improvement in specific energy and specific power over the tubular SOFC structure would result.

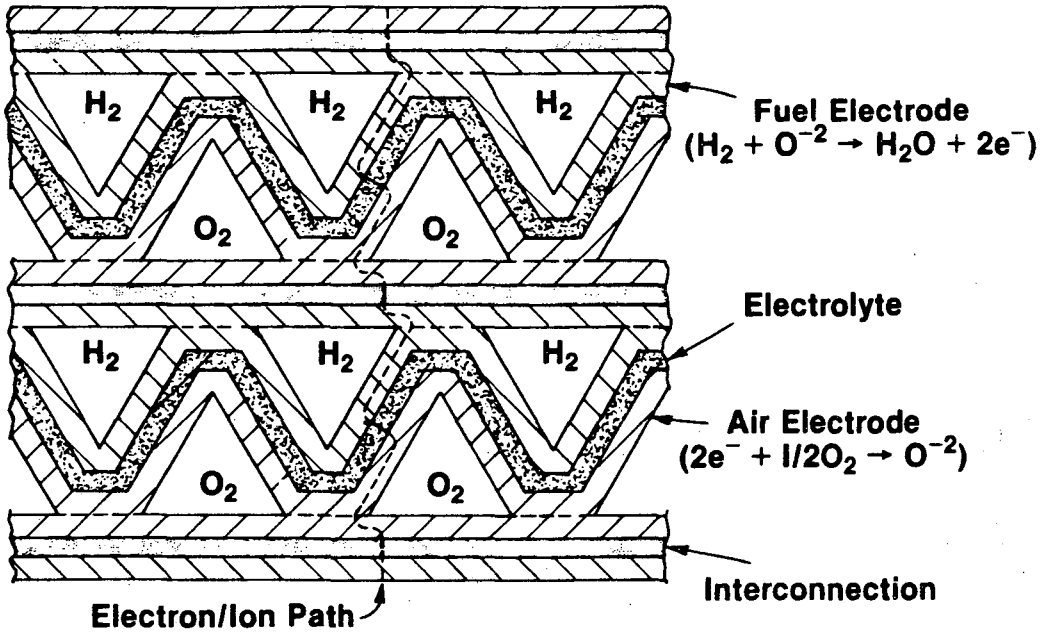

Figure 5-9. Schematic representation of cross section of monolith structure for SOFC. *Source*: D. Fee, Argonne National Laboratory.

Small SOFCs with the monolith structure (9-cm^2 active area) have been fabricated and tested at 1000°C (30). Current densities as high as 2.2 A/cm^2 have been achieved on hydrogen and air, and an array consisting of two cells in series has operated for more than 650 h at 50 mA/cm^2 and ~0.6 V. These cells were also operated with hydrocarbon fuels (e.g., natural gas, CH_4, C_3H_8, C_8H_{18}, C_2H_5OH) that were mixed with H_2O, and the performance was similar to that obtained with hydrogen. Furthermore, the presence of about 5 ppm sulfur in the natural gas had no detrimental effect on cell performance.

The cell performance obtained to date indicates that the ohmic resistance is the limiting factor. In particular the interfacial resistance at the fuel electrode/electrolyte interface needs to be reduced further by optimizing the distribution of Ni. The successful scale up of the small arrays into larger size stacks (i.e., larger area and greater number of cells in series connection) that have a long life has not been demonstrated.

References

1. L.G. Austin, *Fuel Cells,* NASA SP-120, National Aeronautics and Space Administration, Washington, DC (1967) p. 127.
2. T.H. Edsell and S.N. Flengas, *J. Electrochem. Soc.*, **118,** 1890 (1971).
3. A.O. Isenberg, in *Proceedings of the Symposium on Electrode Materials and Processes for Energy Conversion and Storage,* Edited by J.D.E. McIntyre, S. Srinivasan and F.G. Will, The Electrochemical Society, Inc., Pennington, NJ (1977) p. 682.
4. E.F. Sverdrup, C.J. Warde and A.D. Glasser, in *From Electrocatalysis to Fuel Cells,* Edited by G. Sandstede, University of Washington Press, Seattle, WA (1972) p. 255.

5. D.H. Archer, L. Elikan, and R.L. Zahradnik, in *Hydrocarbon Fuel Cell Technology,* Edited by B.S. Baker, Academic Press, New York, NY (1965) p. 51.
6. D.H. Archer, J.J. Alles, W.A. English, L. Elikan, E.F. Sverdrup, and R.L. Zahradnik, in *Fuel Cell Systems, Advances in Chemistry Series 47,* Edited by R.F. Gould, American Chemical Society, Washington, DC, (1965) p. 332.
7. J.T. Brown, *Energy,* **11,** 209 (1986).
8. A.J. Appleby, "Advanced Fuel Cells and Their Future Market," to be published in *Energy Conservation Strategies,* Progress Series, Edited by W.E. Murphy and L.H. Fletcher, American Society of Aeronautics and Astronautics, New York, NY.
9. *Proceedings of the Conference on High Temperature Solid Oxide Electrolytes,* held at Brookhaven National Laboratory, August 16-17, 1983, BNL 51728, compiled by F.J. Salzano (October 1983).
10. A.O. Isenberg, in *Proceedings of the Symposium on Electrode Materials and Processes for Energy Conversion and Storage,* Edited by J.D.E. McIntyre, S. Srinivasan and F.G. Will, The Electrochemical Society, Inc., Pennington, NJ (1977) p. 572.
11. D.C. Fee, S.A. Zwick and J.P. Ackerman, in *Proceedings of the Conference on High Temperature Solid Oxide Electrolytes,* held at Brookhaven National Laboratory, August 16-17, 1983, BNL 51728, compiled by F.J. Salzano (October 1983) p. 29.
12. D.W. Dees, T.D. Claar, T.E. Easler, D.C. Fee and F.C. Mrazek, *J. Electrochem. Soc.,* **134,** 2141 (1987).
13. W.L. Worrell, paper presented at the Third EPRI Solid Oxide Fuel Cell Technology Workshop, February 17, 1987, at Clearwater, FL.
14. J.L. Bates and C.W. Griffin, paper presented at 1986 Fuel Cell Seminar, October 26-29, 1986, Tucson, AZ.
15. S.C. Singhal, R.J. Ruka, and S. Sinharoy, "Interconnection Materials Development for Solid Oxide Fuel Cells," DOE/MC/21184-1985, Report prepared by Westinghouse Electric Corp., for the U.S. Department of Energy; *Energy Res. Abstr.,* **11,** Abstr. No. 9054 (1986).
16. S.C. Singhal, paper presented at the Third EPRI Solid Oxide Fuel Cell Technology Workshop, February 17, 1987, at Clearwater, FL.
17. T. Kudo and H. Obayashi, *J. Electrochem. Soc.,* **122,** 142 (1975).
18. T. Kudo and H. Obayashi, *J. Electrochem. Soc.,* **123,** 415 (1976).
19. T. Takahashi, T. Esaka and H. Iwahara, *J. Appl. Electrochem.,* **7,** 31 (1977).
20. A.O. Isenberg, paper presented at 1985 Fuel Cell Seminar, May 19-22, 1985, Tucson, AZ.
21. P. Reichner and J.M. Makiel, paper presented at 1986 Fuel Cell Seminar, October 26-29, 1986, Tucson, AZ.
22. C. Zeh, private communication (April 29, 1987).
23. A.O. Isenberg, paper presented at ERDA/EPRI Fuel Cell Seminar, June 29-30 to July 1, 1976, Palo Alto, CA.
24. W.J. Dollard and J.T. Brown, paper presented at 1986 Fuel Cell Seminar, October 26-29, 1986, Tucson, AZ.
25. R.J. Ruka, paper presented at National Fuel Cell Seminar, July 14-16, 1980, San Diego, CA.
26. M.S.S. Hsu, W.E. Morrow and J.B. Goodenough, in *Proceedings of the 10th Intersociety Energy Conversion Engineering Conference,* The Institute of Electrical and Electronics Engineering, Inc., New York, NY (1975) p. 555.

27. M.S.S. Hsu and T.B. Reed, in *Proceedings of the 11th Intersociety Energy Conversion Engineering Conference,* American Institute of Chemical Engineers, New York, NY (1976) p. 1.
28. M. Hsu, paper presented at 1985 Fuel Cell Seminar, May 19-22, 1985, Tucson, AZ.
29. M. Hsu, paper presented at 1986 Fuel Cell Seminar, October 26-29, 1986, Tucson, AZ.
30. D.C. Fee, paper presented at 1986 Fuel Cell Seminar, October 26-29, 1986, Tucson, AZ.
31. D.C. Fee, in *Proceedings of the 21th Intersociety Energy Conversion Engineering Conference,* American Chemical Society, Washington, D.C. (1986) p. 1634.
32. S. Majumdar, T. Claar and B. Flandermeyer, *J. Amer. Ceram. Soc.,* **69,** 628 (1986).

6. ALTERNATIVE FUEL CELL TECHNOLOGIES

The discussion in Chapters 3, 4 and 5 focused on the three major fuel-cell systems (i.e., PAFC, MCFC, SOFC) currently under development for utility applications. The other fuel-cell systems, AFC and PEFC, have been demonstrated in space applications, and excellent overviews of the AFC (1,2) and PEFC (3) technologies are available. In this chapter, the status of AFCs and PEFCs will be reviewed. In addition, the research status of alternative electrolytes to those presently used in conventional fuel-cell technology are briefly discussed.

6.1 Alkaline Fuel Cell

Oxygen reduction kinetics are more rapid in alkaline electrolytes than in acid electrolytes, and the use of non-noble metal electrocatalysts in AFCs is feasible. However, a major disadvantage of AFCs is that alkaline electrolytes (i.e., NaOH, KOH) do not reject CO_2. The consequence of this property is that AFCs are currently restricted to specialized applications where pure H_2 and O_2 are utilized.

The AFC used in the U.S. Apollo Space Program was based, in large part, on the technology originally developed by F.T. Bacon (4) in the 1930s. The fuel cell developed by Bacon operated at 200 to 240°C with 45% KOH, and the pressure was maintained at 40 to 55 atm to prevent the electrolyte from boiling. The anode consisted of a dual-porosity Ni electrode (two-layer structure with porous Ni of 16-μm maximum pore diameter on the electrolyte side and 30-μm pore diameter on the gas side), and the cathode consisted of a porous structure of lithiated NiO. The three-phase boundary in the porous electrodes was maintained by a differential gas pressure across the electrode since a wetproofing agent was not available at that time, i.e., PTFE as a wetproofing material did not exist, and it would not be stable in the high-temperature alkaline solution (1).

The AFCs for the U.S. Apollo Space Program (fuel-cell module: 57-cm diameter, 112-cm high, ~110 kg, 1.42 kW at 27-31 V, 0.6-kW average power) utilized pure H_2 and O_2 and concentrated electrolyte (85% KOH) to permit cell operation at lower pressure (~60 psia reactant gas pressure) without electrolyte boiling. With this concentrated electrolyte, the cell performance is not as high as in the less-concentrated electrolyte, consequently the operating temperature was increased to 260°C. The typical performance of this AFC was 0.85 V at 150 mA/cm^2, which compared favorably to the performance of the Bacon cell operating at about 10 times higher pressure. The alkaline fuel cells in the Space Shuttle Orbiter (fuel-cell module: 35-cm high, 38-cm wide, 101-cm long, 91 kg, 12 kW at 27.5 V, 7-kW average power) operate in the same pressure range as for the Apollo program but at a lower temperature (80 to 90°C) and a higher current density (470 mA/cm^2 at 0.86

V). The electrodes contain high loadings of noble metals (anode: 10 mg (80% Pt-20% Pd)/cm^2 on a Ag-plated Ni screen, cathode: 20 mg (90% Au-10% Pt)/cm^2 on a Ag-plated Ni screen) that are bonded with PTFE to achieve high performance at the lower temperature of 80 to 90°C. A wide variety of materials (e.g., potassium titanate, ceria, asbestos, zirconium phosphate gel) have been used in the microporous separators for AFCs. A brief survey of the advanced-technology components in AFCs for space applications is given by Sheibley and Martin (5).

The AFCs for remote applications (i.e., space, undersea, military) are not strongly constrained by cost. On the other hand, the consumer and industrial markets require the development of low-cost components if the AFC is to successfully compete with alternative technologies. Much of the recent interest in AFCs for mobile and stationary terrestrial applications has addressed the development of low-cost cell components. In this regard, carbon-based porous electrodes play a prominent role, and the following discussion focuses on their application in AFCs.

The performance of AFCs since 1960 has undergone many changes, as evident in the performance data in Figure 6-1 (6). The early AFCs were operated at relatively high temperatures and pressures to meet the requirements for space applications, as discussed above. More recently, a major focus of the technology is for terrestrial applications where low-cost components operating at near ambient temperature and pressure with air as the oxidant are desirable. This shift in the fuel-cell operating parameters has resulted in the lower performance shown in Figure 6-1.

The kinetics of O_2 reduction in alkaline electrolytes are more favorable than in H_3PO_4. Consider a Pt cathode (0.25 mg/cm^2) in 30% KOH at 70°C and in 96% H_3PO_4 at 165°C. The cathode potentials (vs RHE) at 100 mA/cm^2 in these two electrolytes are 0.868 and 0.730 mV, respectively, according to data reported by Appleby (Figure 2.15-1 in Reference 7). Various explanations have been advanced for the higher O_2 reduction rates in alkaline electrolytes (8); these explanations are

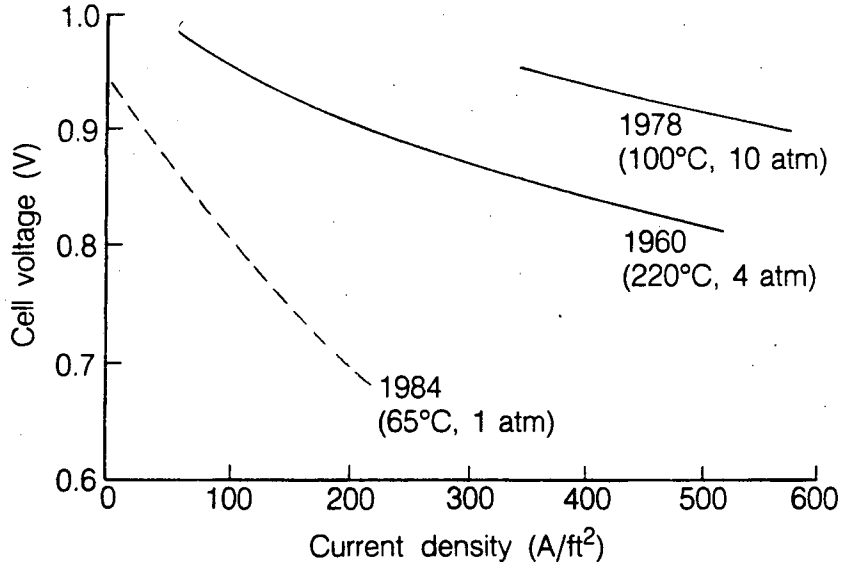

Figure 6-1. Evolutionary changes in the performance of AFCs. Solid line is H_2/O_2 and dashed line is H_2/air.

Source: J.R. Huff, paper presented at the 1986 Fuel Cell Seminar, October 26-29, 1986, Tucson, AZ.

outside the scope of the present discussions. The practical consequence of the higher performance of Pt cathodes in alkaline electrolytes is that AFCs are capable of higher efficiencies than PAFCs at a given current density, or higher power densities at the same efficiency. It is estimated (1) that the efficiency of AFCs on pure H_2 is about 60% and that of PAFCs is about 50%, based on the HHV of H_2.

The performance of catalyzed (0.5-2.0 mg noble metal/cm^2) carbon-based[a] porous electrodes for H_2 oxidation and O_2 reduction in 9 N KOH at 55-60°C is presented in Figure 6-2. These results were obtained in the 1960s (9) using technology that is similar to that employed in fabricating electrodes for PAFCs. The performance of the electrodes shows a dependence on the reactant gas concentration, with a higher polarization evident at lower concentrations. The performance of AFCs with carbon-based electrodes has not changed dramatically since these early results were obtained. The performance of a single cell with supported noble metal electrocatalysts (0.5 mg Pt-Rh/cm^2 anode, 0.5 mg Pt/cm^2 cathode) in 12 N KOH at 65°C is shown in Figure 6-3 (10). These results reported in 1986 are comparable to those obtained in 1965. The IR-free electrode potentials (vs RHE) at 100 mA/cm^2 in Figure 6-3 are 0.9 V with O_2 and 0.85 V with air. One major difference between the early cathodes and the cathodes in current use is the limiting current for O_2 reduction from air has been improved (i.e., 100-200 mA/cm^2 vs >250 mA/cm^2).

The improvement in the air performance of catalyzed carbon-based cathodes with an increase in cell temperature is illustrated in Figure 6-4. As expected, the electrode potential at a given current

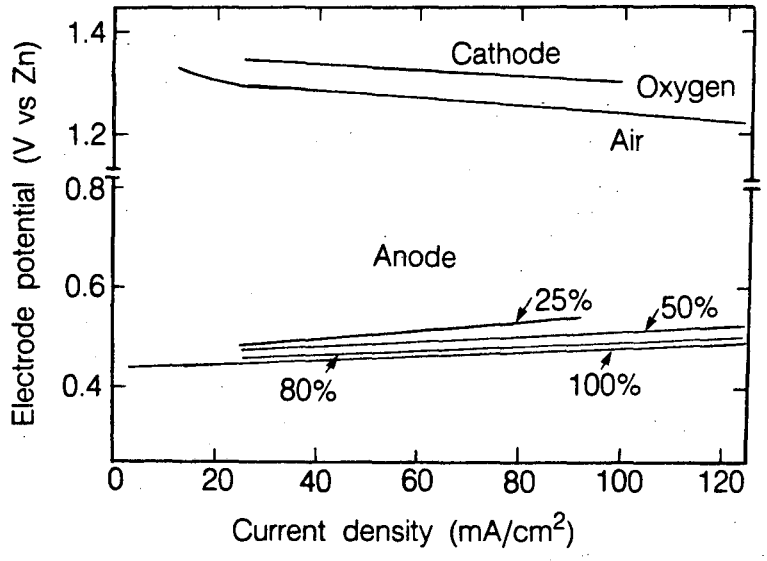

Figure 6-2. IR-free electrode performance with oxygen, air, and various H_2-containing gases in 9 N KOH at 55 to 60°C. Catalyzed (noble metal loading of 0.5 to 2.0 mg/cm^2) carbon-based porous electrode.

Source: (Figure 9, p. 170) M.B. Clark, W.G. Darland and K.V. Kordesch, *Electrochem. Tech.*, **3**, 166 (1965).

[a] Vulcan XC-72 (furnace black) or acetylene black (thermal black) is commonly used.

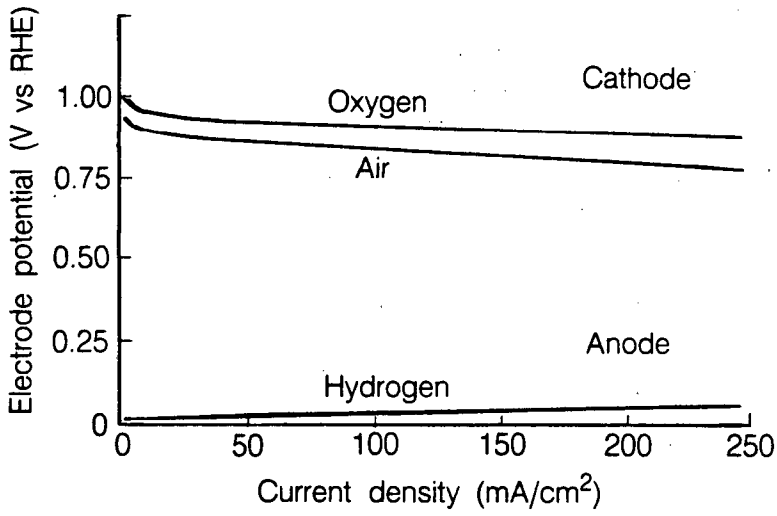

Figure 6-3. IR-free electrode performance in 12 N KOH at 65°C. Catalyzed (0.5 mg Pt/cm^2-cathode, 0.5 mg Pt-Rh/cm^2-anode) carbon-based porous electrodes.
Source: (Figure 22, p. 322) K. Tomantschger, F. McClusky, L. Oporto, A. Reid, and K. Kordesch, *J. Power Sources*, **18**, 317 (1986).

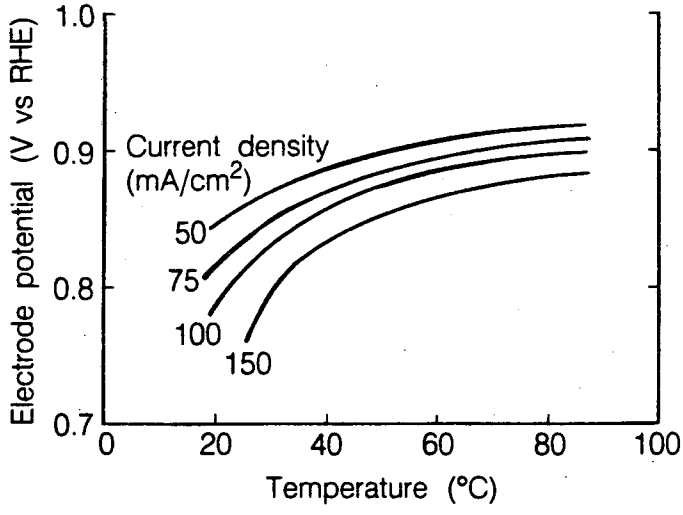

Figure 6-4. Influence of temperature on O_2 (air) reduction in 12 N KOH. Catalyzed (0.5 mg Pt/cm^2 cathode) carbon-based porous electrodes.
Source: (Figure 10, p. 324), K. Tomantschger, F. McClusky, L. Oporto, A. Reid, and K. Kordesch, *J. Power Sources*, **18**, 317 (1986).

density decreases at lower temperatures, and the decrease is more significant at higher current densities. In the temperature range of 60 to 90°C, the cathode performance increases by about 0.5 mV/°C at 50 to 150 mA/cm^2. Early data by Clark et al. (9) indicated a temperature coefficient for AFCs at 50-70°C of about 3 mV/°C at 50 mA/cm^2, and cells with higher polarization had higher temperature coefficients under load. The recent measurements by McBreen et al. (11) on H_2/air single cells (289-cm^2 active area, carbon-based Pd anode and Pt cathode) with 50% KOH showed that the temperature coefficient above 60°C was considerably lower than that obtained at lower temperatures (see Figure 6-5). At 100 mA/cm^2, the temperature coefficient is about 0.7 mV/°C above 63°C and about 4 mV/°C below 63°C.

AFCs suffer a drastic performance loss with fuels containing CO_2 from reformed fuels, and from the presence of CO_2 in air (approximately 350-ppm CO_2 in ambient air). The negative impact of CO_2 arises from its reaction with OH^-

$$CO_2 + 2OH^- \rightarrow CO_3^= + H_2O \qquad (6\text{-}1)$$

which produces the following effects: (i) reduces the OH^- concentration and interferes with kinetics, (ii) causes an increase in the electrolyte viscosity resulting in lower diffusion coefficients and lower limiting currents, (iii) causes the eventual precipitation of carbonate salts in the pores of the porous electrode, (iv) reduces the oxygen solubility, and (v) reduces the electrolyte conductivity. The influence of CO_2 on air cathodes (0.2 mg Pt/cm^2 supported on carbon black) in 6 N KOH at 50°C can be ascertained by analysis of the performance data presented in Figure 6-6 (12). The air electrodes were operated continuously at 32 mA/cm^2, and periodically current-voltage performance

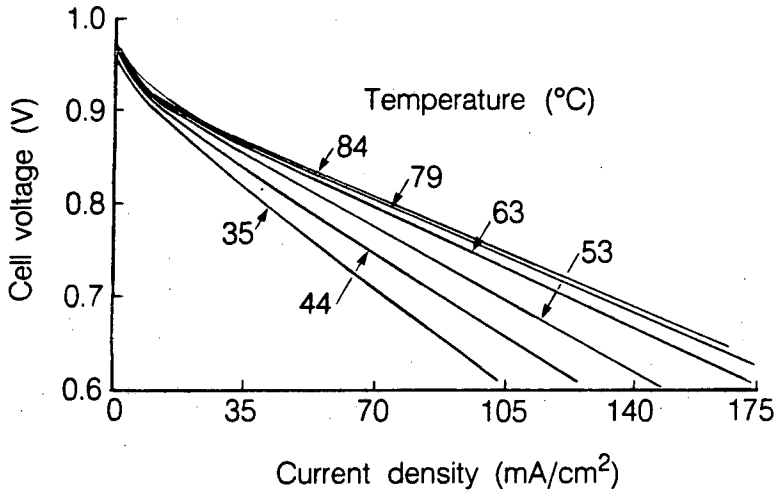

Figure 6-5. Influence of temperature on the cell voltage of an AFC (289 cm^2 active area, carbon-based Pd anode and Pt cathode) with 50% KOH.

Source: (Figure 6, p. 889) J. McBreen, G. Kissel, K.V. Kordesch, F. Kulesa, E.J. Taylor, E. Gannon and S. Srinivasan, in *Proceedings of the 15th Intersociety Energy Conversion Engineering Conference*, Volume 2, American Institute of Aeronautics and Astronautics, New York, NY (1980).

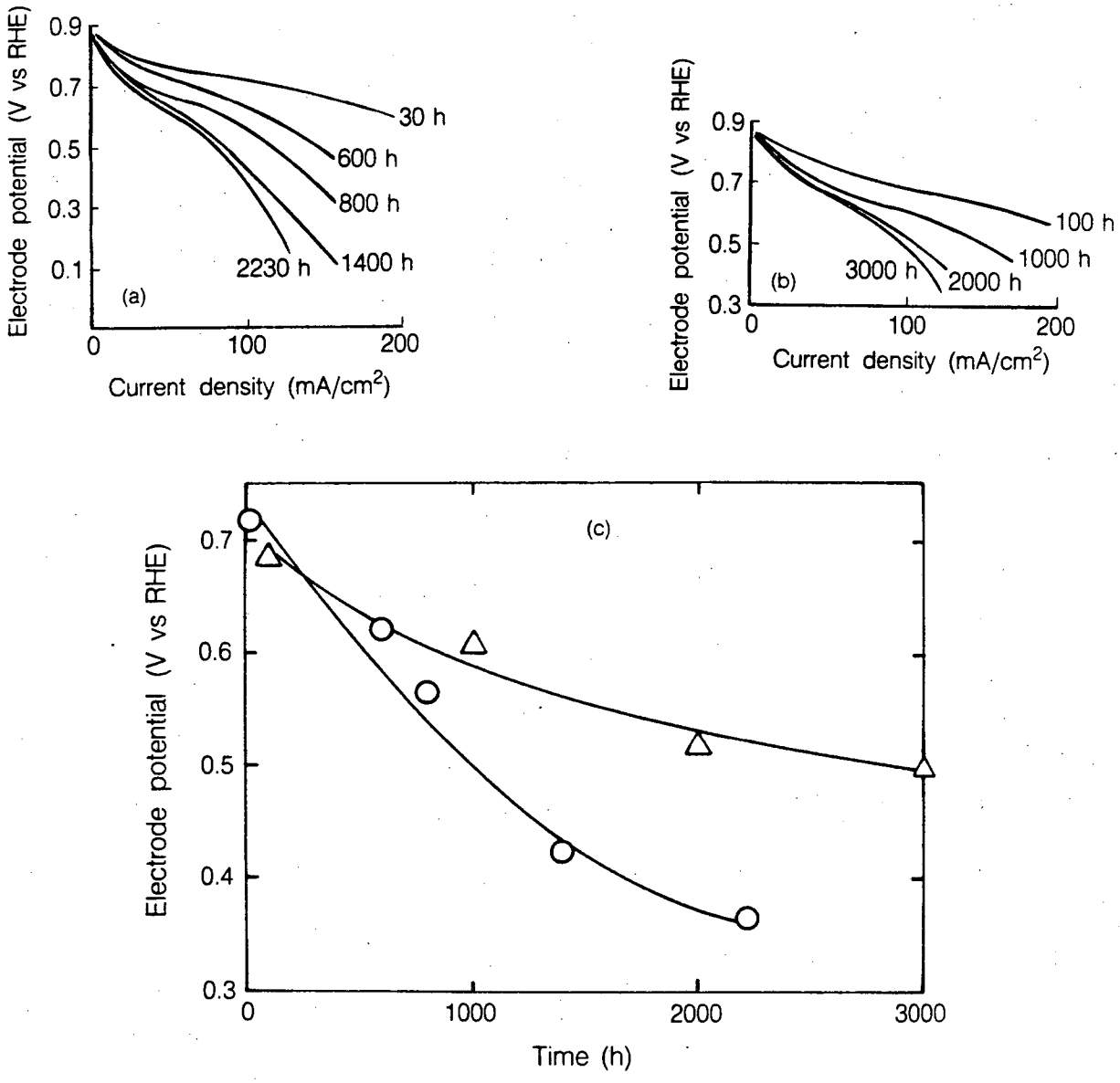

Figure 6-6. Influence of CO_2 on the air performance of supported Pt cathodes (0.2 mg/cm^2 supported on carbon black) in 6 N KOH at 50°C. (a) CO_2-containing air, (b) CO_2-free air. Current-voltage curves were measured periodically for electrodes continuously operated at 32 mA/cm^2. (c) Variation in electrode potential as a function of time at 100 mA/cm^2 with (O) CO_2-containing air and (Δ) CO_2-free air.

Source: (Figures 1 and 2, p. 381) K. Kordesch, J. Gsellmann and B. Kraetschmer, in *Power Sources 9*, Edited by J. Thompson, Academic Press, New York, NY (1983).

curves were measured. The air performance in both CO_2-free air and CO_2-containing air show evidence of degradation with time. However, with CO_2-free air the performance remains nearly constant from 2000 to 3000-h operation. Another method to illustrate the influence of CO_2 on air performance is obtained by analysis of the electrode potential at a constant current density as a function of time. Data obtained from Figures 6-6a and 6-6b for the electrode potential at 100 mA/cm^2 as a function of time are plotted in Figure 6-6c. At short times, the potential of the air electrode in both CO_2-free air and CO_2-containing air are comparable. However, at longer times a higher performance is clearly evident for the air electrode in CO_2-free air. Higher concentrations of KOH are also detrimental to the life of O_2 electrodes operating with CO_2-containing air, but operating the electrode at higher temperature is beneficial because it increases the solubility of $CO_3^=$ in the electrolyte. Modifying the operating conditions can prolong electrode life, but it is clear from the results in Figure 6-6 that the life expectancy of air cathodes is lowered by the presence of CO_2. Extensive studies by Kordesch et al. (12) indicate that the operational life of air electrodes (PTFE-bonded carbon electrodes on porous nickel substrates) with CO_2-containing air in 9 N KOH at 65°C ranges from 1600 to 3400 h at a current density of 65 mA/cm^2. The life of these electrodes with CO_2-free air tested under similar conditions ranged from 4000 to 5500 h. It has been reported (1) that a lifetime of 15,000-h has been achieved with AFCs, and failure at this time is by attack of the cell frames.

6.2 Polymer Electrolyte Fuel Cell

The advantages of PEFCs are: (i) no free corrosive liquid in the cell, (ii) simple to fabricate cell, (iii) able to withstand large pressure differentials, (iv) materials corrosion problems are minimal, and (v) demonstrated long life. On the other hand, the disadvantages of PEFCs are: (i) fluorinated polymer electrolyte is traditionally expensive, (ii) water management in the membrane is critical for efficient operation, and (iii) long-term high performance with low catalyst loadings in the electrodes needs to be demonstrated. Other advantages and disadvantages of PEFCs are presented in Chapter 1.

The early efforts to about the mid 1960s which led to the development of PEFCs were reviewed by Maget (13) and Liebhafsky and Cairns (14). Based on the experience with ion-exchange membrane polymers for PEFCs, these materials should have the following properties:

- high H^+ conductivity to obtain low internal resistance and high current density;
- H^+ transport number of unity and low electroosmotic H_2O transport rates to prevent large concentration gradients;
- zero solubility of the polymer in H_2O but high solubility of H_2O in the polymer;
- low O_2 and H_2 permeability to achieve high current efficiency;
- rapid H_2O transport and reversible hydration to maintain nearly uniform H_2O content or to prevent localized drying;
- adequate mechanical integrity and structural strength to ensure dimensional stability under tension;
- adequate chemical and electrochemical stability in the presence of electrocatalysts and in the cell environment;
- suitability for bonding catalyzed electrodes to the polymer surface.

The use of organic cation-exchange membrane polymers in fuel cells was originally conceived by Grubb (15) in the 1950s. The early membranes tested in PEFCs include the hydrocarbon-type polymers such as cross-linked polystyrene-divinylbenzene-sulfonic acids and sulfonated phenolformaldehyde. The U.S. Gemini Space Program (fuel cell module: 31.7-cm diameter, 63.5-cm high, 30 kg, 1 kW at 23.3-26.5 V; cell operated at 37 mA/cm^2 at 0.78 V on pure H_2 and O_2 at 20-30 psia and ~35°C) in the 1960s employed membranes of polystyrene-divinylbenzene-sulfonic acid crosslinked within an inert fluorocarbon film. It was observed that the life of PEFCs was limited by oxidative degradation of the polymer electrolyte. Hydrocarbon-type polymers are unstable due to the cleavage of the C-H bonds, particularly the α-H where the functional group is attached. When these polystyrenes were replaced with fluorine-substituted polystyrenes (e.g., polytrifluorostyrene sulfonic acid), the life of PEFCs was extended by four to five fold. However, the operating temperature of PEFCs with the fluorinated polystyrenes was limited to less than 75°C. Research started in the early 1960s led to the development of Nafion (registered trademark of E.I. DuPont de Nemours for perfluorocarbon sulfonate membranes), which are perfluorosulfonic acid membranes that are electrochemically stable in PEFCs at temperatures up to about 100°C. This polymer consists of the following ionomer units,

$$-[(CF_2-CF_2)_n-CF_2-\underset{\displaystyle [OCF_2-CF(CF_3)]_m-OCF_2-CF_2-SO_3H}{\underset{|}{CF}}]-$$

where n = 6-10 and m $\geq$ 1. Nafion and its derivatives all have two features in common: (i) polymer chains consist mainly of a PTFE backbone, which statistically form segments several units in length, and (ii) perfluorinated vinyl polyether, a few ether links long, which joins these segments to form a flexible branch pendant to the main perfluoro-chain and carries a terminal acidic group to provide the cation-exchange capacity. These perfluorinated ionomer membranes with sulfonic acid groups meet all the required characteristics of ion-exchange membranes for use in fuel cells, as well as for use in H_2O and alkali hydroxide electrolysis cells. Nafion was first used in fuel cells in 1966, and it is still the most widely tested ion-exchange membrane in PEFCs.

The typical physicochemical properties of Nafion membranes are summarized in Table 6.1 (16). The Nafion membranes, which are fully fluorinated polymers, exhibit exceptionally high chemical and thermal stability, i.e., stable against chemical attack in strong bases, strong oxidizing and reducing acids, H_2O_2, Cl_2, H_2 and O_2 at temperatures up to 125°C (17). A high degree of dissociation and a high concentration of mobile H^+ ions (>4 molal) ensure good ionic conductivity in Nafion; a conductivity of >0.05 ohm^{-1}cm^{-1} at 25°C is considered to be acceptable for use in fuel cells. A review on the conductivity properties of Nafion is presented by Yeo (18). The range of equivalent weights[b] for Nafion that is of greatest interest in PEFCs is 1100 to 1350, which provides a highly acidic environment (i.e., comparable to a 10 wt% H_2SO_4 solution) in a hydrated membrane.

The porous electrodes in PEFCs are bonded to the surface of ion-exchange membranes (0.12- to 0.25-mm thick) by pressure and at a temperature usually between the glass transition temperature and the thermal degradation temperature of the membrane. These conditions provide the necessary environment to produce an intimate contact between the electrocatalyst and the membrane surface. The early PEFCs contained Nafion membranes and about 4 mg/cm^2 of Pt black in both the cathode

[b] Defined as the weight of polymer which will neutralize one equivalent of base, and is inversely proportional to the ion-exchange capacity.

Table 6.1 Physicochemical Properties at 25°C of a Typical Nafion Membrane (equilibrated with H_2O at 100°C)

Thickness	~0.3 mm
Equivalent weight	1200
Ion-exchange capacity	0.83 meq/g dry polymer
Ionic resistance	0.46 ohm-cm^2
Tensile strength at break	2500 psi
Elongation at break	150%
Mullen burst strength	150 psi
Water content (based on dry polymer)	28%
H_2 permeability	5.6×10^{-4} cm^3–cm/cm^2h-atm
O_2 permeability	3.0×10^{-4} cm^3–cm/cm^2h-atm
Hydrodynamic H_2O permeability	2.7×10^{-5} cm^3–cm/cm^2h-atm
Electroosmotic permeability	7.5×10^{-4} cm^3/coulomb

Source: (Table 1, p. 356) A.B. LaConti, A.R. Fragala and J.R. Boyack, in *Proceedings of the Symposium on Electrode Materials and Processes for Energy Conversion and Storage,* Edited by J.D.E. McIntyre, S. Srinivasan and F.G. Will, The Electrochemical Society, Inc., Pennington, NJ (1977).

and anode. Such electrode/membrane combinations, with the appropriate current collectors and supporting structure in PEFCs and water electrolysis cells, are capable of operating at pressures up to 3000 psi, differential pressures up to 500 psi, and current densities of 2000 mA/cm^2 (19).

In a H_2/O_2 PEFC, H_2 is oxidized at the anode to H^+ ions, which are transported through the membrane to the cathode. During operation of the fuel cell, water is also transported through the Nafion membrane with H^+ ions because of the electroosmotic effect. At 100°C, about 3.5 to 4 H_2O molecules are transported with each H^+ ion (16). The transport of substantial amounts of water through the membrane presents a water-management problem. There is a tendency for the anode side to dehydrate, resulting in a reduction in ionic conductivity and a decrease in the power output from the cell. One solution to this problem is to humidify the fuel gas entering the cell, but the addition of too much H_2O can be detrimental because it may form a liquid film on the electrocatalyst and prevent rapid H_2 oxidation from occurring. At the cathode H_2O is produced which must be rapidly removed to avoid "flooding" of the electrode.

A summary of the performance levels achieved with PEFCs since the mid 1960s is presented in Figure 6-7 (6). Because of the changes in the operating conditions involving pressure, temperature, reactant gases, etc., a wide range of performance levels can be obtained. The performance of the

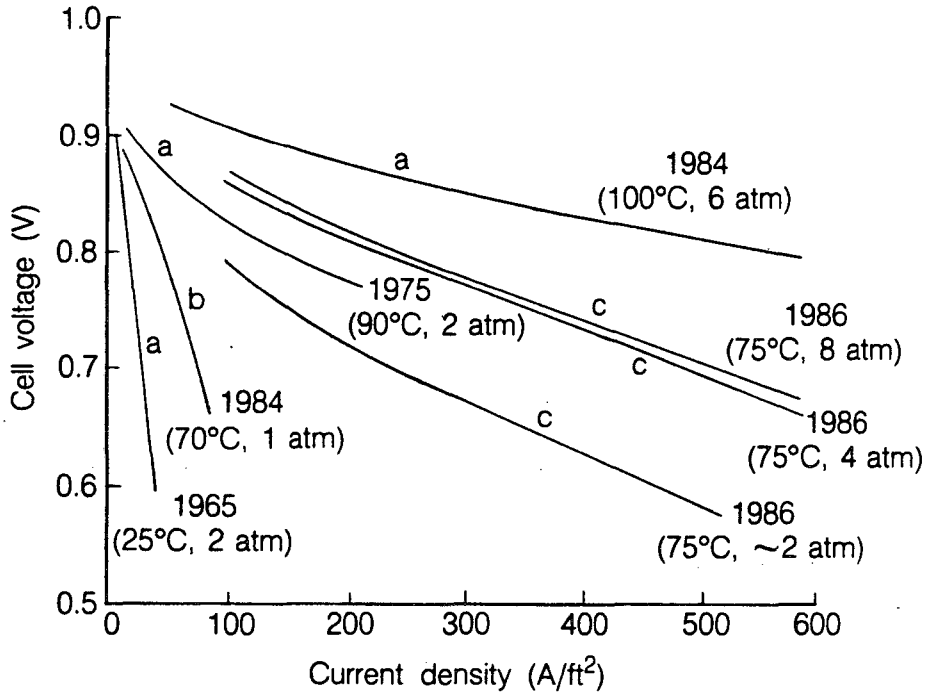

Figure 6-7. Evolutionary changes in the generic performance of PEFCs. (a) H_2/O_2, (b) reformate fuel/air, (c) H_2/air.

Source: J.R. Huff, paper presented at the 1986 Fuel Cell Seminar, October 26-29, 1986, Tucson, AZ.

PEFC in the U.S. Gemini Space Program was 37 mA/cm^2 at 0.78 V in a 32-cell stack that typically operated at 50°C and 2 atm (3). It is evident from Figure 6-7 that the current technology yields performance levels that are vastly superior. Recent unpublished results from Los Alamos National Laboratory show that a performance of 0.78 V at about 200 mA/cm^2 (3-atm H_2 and 5-atm air) can be obtained at 80°C in PEFCs containing a Nafion membrane and electrodes with a Pt loading of 0.4 mg/cm^2. Further details on the recent developments in the performance of PEFCs with Nafion membranes are presented by Watkins et al. (20).

Currently the major focus of R&D on PEFC technology is to develop a fuel-cell system for terrestrial transportation applications, which require the development of low-cost cell components. Reformed methanol is expected to be a major fuel source for PEFCs in transportation applications. Because the operating temperature of PEFCs is much lower than that of PAFCs, poisoning of the anode electrocatalyst by CO from steam-reformed methanol is a concern. The performances achieved with a proprietary anode in a PEFC at various temperatures and with two concentrations of CO in the fuel gas are shown in Figure 6-8 (21). The CO tolerance of the anode increases as the cell temperature increases to 104°C. The anode polarization in the presence of 0.17% CO is 100 mV at 240 and 340 mA/cm^2 at 82 and 93°C, respectively. In 0.3% CO the corresponding current densities at an anode polarization of 100 mV are 170 and 245 mA/cm^2, respectively. The anode polarization at 82°C with the fuel containing 0.17% CO is not affected by a reduction in the electrocatalyst loading from 4 to 2 mg/cm^2. This result suggests that a lower-cost anode with acceptable CO tolerance can be obtained by reducing the electrocatalyst loading. The CO-tolerance of Pt elec-

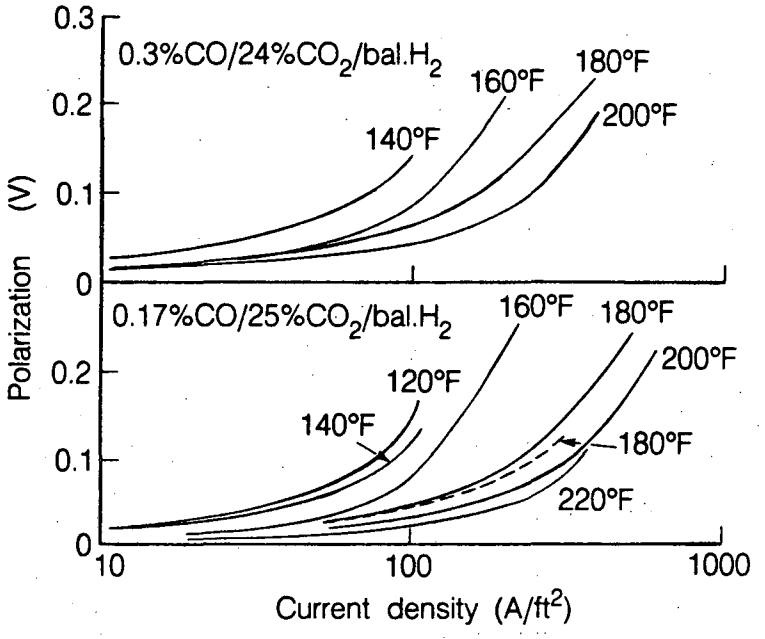

Figure 6-8. Influence of CO on the anode performance loss of PEFCs at various temperatures. Electrode loadings of 4 mg/cm^2 Pt at anode and cathode, except for one case with 2 mg/cm^2 at anode. Oxidant: 135 psig O_2; reformed fuel: 30 psig.

Source: (Figure 26, p. 46) A. LaConti, G. Smarz and F. Sribnik, "New Membrane-Catalyst for Solid Polymer Electrolyte Systems," final report prepared by Electro-Chem Products, Hamilton Standard for Los Alamos National Laboratory under Contract No. 9-X53-D6272-1 (1985).

trocatalysts is also improved by increasing the cell operating temperature. This temperature is limited by the high vapor pressure of water in the ion-exchange membrane which is susceptible to dehydration and loss of ionic conductivity.

The influence of O_2 pressure on the performance of PEFCs at 93°C is illustrated in Figure 6-9 (21). An increase in the O_2 pressure from 30 to 135 psig produces an increase of 0.042 V in the cell voltage at 200 A/ft^2. According to the Nernst equation, the increase in the reversible cathode potential that is expected for this increase in O_2 pressure is about 0.012 V, which is considerably less than the measured value. When the temperature of the cell is increased to 104°C, the cell voltage increases by 0.054 V for the same increase in O_2 pressure. Thus, these results demonstrate that an increase in the pressure of O_2 results in a significant reduction in the polarization at the cathode.

Several recent developments have been reported that improve the prospects for PEFCs in terrestrial applications. These developments are expected to result in the reduction of noble-metal electrocatalyst in the electrodes and an improvement in the properties of ion-exchange membranes for PEFCs. Recent studies (22, 23) demonstrated that the interfacial area available for electrochemical reaction can be extended beyond the three-phase contact region of the gas/electrocatalyst/membrane in PEFCs. The practical consequence is that electrodes with low loadings of Pt electrocatalyst (i.e., Pt-supported-on carbon) can be used instead of the high Pt loadings of earlier PEFCs. Raistrick (23) showed that electrodes with 0.35 mg Pt/cm^2 have activity for H_2 oxidation and O_2 reduction at room temperature comparable to that for conventional electrodes with about 10 times higher loading

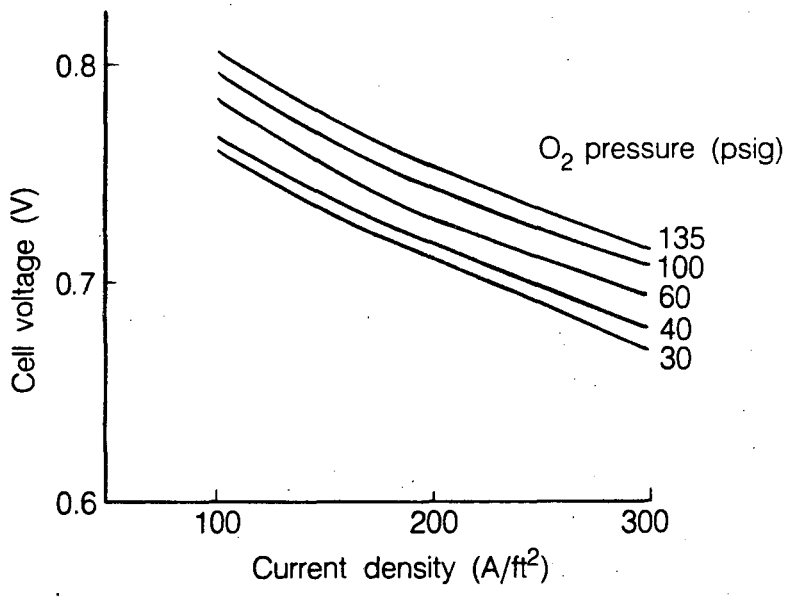

Figure 6-9. Influence of O_2 pressure on the performance of PEFCs at 93°C. Electrode loadings of 2 mg/cm^2 Pt. Oxidant: 30 to 135 psig O_2; fuel: 30 psig H_2.
Source: (Figure 29, p. 49) A. LaConti, G. Smarz and F. Sribnik, "New Membrane-Catalyst for Solid Polymer Electrolyte Systems," final report prepared by Electro-Chem Products, Hamilton Standard for Los Alamos National Laboratory under Contract No. 9-X53-D6272-1 (1985).

of noble metal. The electrodes with low Pt loadings are obtained by using Pt supported on carbon, which is more effective for enhancing the utilization of platinum. An electrode with a loading of 0.35 mg/cm^2 Pt is capable of achieving an O_2-reduction rate (at ambient temperature and 1 atm) of 600 mA/cm^2 at 570 mV (IR-free, vs RHE). Single-cell tests (20) at 55°C with reduced Pt loadings (anode with 0.5 mg/cm^2 and cathode with 2 mg/cm^2) yielded 0.67 V at 215 mA/cm^2 with air and hydrogen after 120 h operation. These results are encouraging and demonstrate the prospects for achieving PEFCs with low-loading electrodes.

A new series of perfluorinated ionomers has recently become available from Dow Chemical Company, which provides an attractive alternative to Nafion in PEFCs (24, 25). The major thrust of their program on ion-exchange membranes is to develop an improved membrane for the chlor-alkali industry, and the results to date indicate that these membranes have demonstrated promising performance in improving the efficiency of chlor-alkali production compared to Nafion membranes (25). Their new polymer has a PTFE-like backbone similar to those of Nafion, but the pendant side chain containing the sulfonic acid group is shorter. Instead of the long side chain of Nafion shown above, the Dow polymer has a side chain consisting of $-OCF_2-CF_2-SO_3H$. This polymer possesses ion-exchange properties similar to that of Nafion, and it is also available with higher acid strength and lower equivalent weights (i.e., 600-950). Even at these low equivalent weights the Dow membrane has good mechanical strength and does not hydrate excessively, whereas Nafion of comparable equivalent weight would form a highly gelled polymer, having poor or no mechanical integrity. The physical and transport properties of ion-exchange membranes are largely determined by the amount

of absorbed H_2O. For a given equivalent weight,[c] and in an environment such as that in chlor-alkali cells, the Dow polymer absorbs less water (~ 50%) than Nafion, but it has comparable ionic conductivity and lower permeability. The Dow polymer has a higher glass transition temperature (165 vs 110°C for Nafion), thus PEFCs containing this material should be capable of operating at high temperatures (>100°C). A summary of the physicochemical properties of the Dow polymer is discussed by Eisman (24) and Ezzell et al. (25). This polymer is currently being evaluated in PEFCs.

6.3 Alternative Electrolytes

The ideal liquid electrolyte for fuel-cell applications should have characteristics which include:

- high ionic conductivity
- good solvent for reactant species (i.e., high solubility and diffusivity of H_2 and O_2)
- good medium for transport of reactants and reaction products
- chemically and electrochemically stable over the temperature and operating voltage range of the fuel cell
- possess suitable physical properties, e.g., viscosity, vapor pressure
- should not interfere with electrocatalytic reactions (i.e., low adsorption of electrolyte on electrode surface)
- should not be strongly reactive to cell components

In addition, it is desirable for the electrolyte to be low cost and to have a high contact angle on PTFE. These characteristics, as well as others, serve as guidelines in the search for alternative electrolytes to those currently utilized in fuel cells.

6.3.1 Acidic Electrolytes

Considerable effort has been directed towards finding alternative acid electrolytes to H_3PO_4 for fuel cells operating at temperatures up to about 200°C, and some of these electrolytes are discussed by Foley (26) and Appleby (27). A list of several alternative acid electrolytes that were considered is presented in Table 6.2 (28-53). It is the intent of the present discussion to provide only a brief overview on these electrolytes; interested readers should consult the references provided in the table for more details.

The inorganic acids such as $HClO_4$, H_2SO_4, HF and HCl have been evaluated in laboratory-scale fuel cells, and the results are summarized by Foley (26). Compared to H_3PO_4, these acids have lower thermochemical stability and higher vapor pressure, and therefore are not acceptable at the typical operating temperatures of PAFCs. For these reasons, H_3PO_4 is the only inorganic acid that is being developed for use in fuel cells by utility, commercial and industrial companies.

Of the many acids listed in Table 6.2, trifluoromethane sulfonic acid (TFMSA) has probably received the most thorough scrutiny in laboratory tests. TFMSA, which was first discovered in 1954 (54), is a strong acid (55, 56) with many desirable characteristics for fuel-cell applications, i.e., high ionic conductivity (56, 57) and good thermal stability (58). However, TFMSA in concentrated form (>6 M) wets PTFE (53, 59). Furthermore, vapor pressure data (60) indicate this electrolyte is not suitable for long-term use above about 80°C; pure TFMSA boils at 162°C at 760 Torr (54).

[c] The relative amount of absorbed H_2O increases with a decrease in the equivalent weight of an ion-exchange membrane, and for a given equivalent weight the amount of absorbed H_2O increases with an increase in temperature.

Table 6.2 Alternative Acid Electrolytes for Fuel-Cell Applications

Acid	Formula	Reference
Methane sulfonic	CH_3SO_3H	28-31
Methane disulfonic	$CH_2(SO_3H)_2$	28,30
Methane trisulfonic	$CH(SO_3H)_3$	29,32
Dichloromethane disulfonic	$CCl_2(SO_3H)_2$	29,32
Chloromethane trisulfonic	$CCl(SO_3H)_3$	29,32
Trifluoromethane sulfonic	CF_3SO_3H	27,33-45
Difluoromethane disulfonic	$CF_2(SO_3H)_2$	42,46
Ethane sulfonic	$CH_3CH_2SO_3H$	30,31
Ethane disulfonic	$SO_3H–CH_2CH_2–SO_3H$	30
Tetrafluoroethane disulfonic	$SO_3H–CF_2CF_2–SO_3H$	42,47-49
Hexafluoropropane disulfonic	$SO_3H–CF_2CF_2CF_2–SO_3H$	42
Octafluorobutane disulfonic	$SO_3H–CF_2(CF_2)_2CF_2–SO_3H$	47,50
Benzoic	C_6H_5COOH	28
Benzene sulfonic acid hydrate	$C_6H_5SO_3H \cdot xH_2O$	28
Perfluorobenzene sulfonic	$C_6F_5SO_3H$	30
Difluoromethane diphosphonic	$CF_2(OP(OH)_2)_2$	46
Pentafluoropropanoic	CF_3CF_2COOH	28
Perfluorobutyric	$CF_3CF_2CF_2COOH$	51
Dichloroacetic	$HCCl_2COOH$	52
Trichloroacetic	CCl_3COOH	28
Chlorodifluoroacetic	$ClCF_2COOH$	28
Sulfoacetic	$SO_3H–CH_2COOH$	31
Hexafluorophosphoric	HPF_6	53
Hexafluoroantimonic	$HSbF_6$	53

Some interesting results were obtained with TFMSA at temperatures less than 150°C (28, 33-38, 43, 45). These studies indicate that the kinetics for O_2 reduction (28, 33-38, 45), methanol oxidation (36) propane oxidation (34, 35) and H_2 oxidation (28, 38) are faster in TFMSA than in H_3PO_4. The overpotential for O_2 reduction is about 50 mV lower in TFMSA than in H_3PO_4 (27); at room temperature and 1-atm pressure, the exchange current density for O_2 reduction on Pt is about two orders of magnitude higher in 1.1 M TFMSA than in 85% H_3PO_4 (37). The enhanced electrocatalytic activity observed with Pt electrodes in TFMSA is attributed, in part, to low specific anion adsorption (32, 43) and the high O_2 solubility-diffusivity product (45) in this acid. The solubility of O_2 is 1.2 x 10^{-6} moles/cm^3 in 6 M TFMSA and 1 x 10^{-7} mole/cm^3 in 98% H_3PO_4, both at 100°C. The corresponding diffusivities are 1.73 x 10^{-4}cm^2/s and 1.05 x 10^{-5}cm^2/s, respectively.

Besides TFMSA, numerous other organic acids have been evaluated as alternative electrolytes for H_3PO_4 in fuel cells (see Table 6.2). Experiments by Rebert et al. (28) show that the halogenated fatty acids (methane disulfonic, trichloroacetic, chlorodifluoroacetic and pentafluoropropanoic acids) and aromatic acids (benzoic and benzene sulfonic acids) listed in Table 6.2 are not suitable candidates for fuel-cell electrolytes. Of the many acids investigated by Rebert et al., only methane sulfonic acid (MSA) showed promise as a fuel-cell electrolyte; H_2 oxidation currents at 0.5 V obtained with this acid at 35°C are comparable to those obtained in 85% H_3PO_4 at 135°C. A more recent report by Ahmad et al. (31) confirmed that H_2 oxidation on Pt in MSA is rapid. However, MSA and the other two acids (ethane disulfonic and sulfoacetic acids) investigated by Ahmad et al. decompose at temperatures above 100°C. Furthermore, sulfonic acids containing terminal methyl groups that are not completely fluorinated are readily susceptible to thermal decomposition, and they strongly adsorb on the surface of Pt electrodes. Fluorinated acids with a longer chain length of molecular carbon and with more than one sulfonic acid group were synthesized to overcome the problems encountered with TFMSA and other non-fluorinated sulfonic acids. It was found that acids which do not have terminal $-CF_3$ groups do not wet PTFE (27). With the exception of perhaps difluoromethane disulfonic acid, tetrafluoromethane disulfonic acid, difluoromethane diphosphonic acid and dichloromethane disulfonic acid, the acids in Table 6.2 do not appear to be suitable for use at temperatures above 150°C in fuel cells because of their high vapor pressure and/or poor thermal stability. Unfortunately, the ionic conductivity of the most stable acids is relatively poor at temperatures in the range 100 to 200°C.

Despite the limited success with the alternative acid electrolytes at the typical operating temperature of PAFCs for utility applications, there still exists some interest in this type of electrolyte, with the Gas Research Institute supporting research programs in this area (61-66). Electrolytes from the families of perfluorinated-organosulfonic acids [e.g., $HO_3S(CF_2)_nSO_3H$], perfluoro-organophosphonic acids [e.g., $(HO)_2P(O)R$, R = $CF_3(CF_2)_n$], perfluoroorganophos- phinic acid [e.g., $(HO)P(O)R_2$, R = $CF_3(CF_2)_n$], and perfluoro-sulfonimides [e.g., $(RSO_2)_2NH$, R = $(CF_2)_n$] are being evaluated. Oxygen reduction on Pt in trifluoromethylphosphonic acid, for instance, shows comparable performance at 0.05 to 500 mA/cm^2 to that obtained in H_3PO_4. More recently, Razaq et al. (67) reported that the cathodic polarization for oxygen reduction on platinum in bis(trifluoromethanesulfonyl)imide at 70°C was lower than that observed in H_3PO_4 (i.e., 40 mV more positive at 100 mA/cm^2).

6.3.2 Alkaline Electrolytes

AFCs were the first fuel cells employing a liquid electrolyte to demonstrate a practical application, i.e., in the U.S. Space Program. The advantages and disadvantages of AFCs are described in the preceding discussion in this chapter and in Chapter 1. The major problem with AFCs for terrestrial applications is carbonation (see Equation 6-1) of the electrolyte by CO_2 that is present in practical reactant gases (i.e., reformed hydrocarbon fuel and air oxidant). Several studies (68-72) have demonstrated that alkali carbonate electrolytes have some interesting possibilities for use in fuel cells.

The results obtained by Cairns and Bartosik (68) indicated that a strong electrolyte of cesium or rubidium carbonate (or bicarbonate) at 100 to 140°C is capable of sustaining the anodic oxidation of methanol to CO_2 at Pt electrodes, while still maintaining an invariant electrolyte. The high solubility of Cs_2CO_3 and Rb_2CO_3 in H_2O allows fuel-cell operation up to about 200°C with these electrolytes, and CO_2 rejection by these alkali carbonate electrolytes results from the instability of the corresponding bicarbonates above about 100°C.

It is well-known that oxygen reduction is more rapid in alkaline electrolytes than in acid electrolytes. The fact that NaOH and KOH do not reject CO_2 has effectively restricted alkaline electrolytes to AFCs utilizing pure hydrogen. However, as mentioned above, several alkali carbonate electrolytes are capable of rejecting CO_2. Recent experiments by Striebel et al. (71, 72) demonstrate that oxygen reduction kinetics on Pt disk electrodes in carbonate-containing electrolytes (e.g., Cs_2CO_3, K_2CO_3, K_2CO_3 + KOH) are comparable to or higher than that obtained in KOH. However, oxygen reduction on PTFE-bonded Pt electrodes in 2 M K_2CO_3 showed increasing polarization (~200 mV at 23°C) because of an increase in pH that occurs from the generation of hydroxyl ions in the electrode pores. This behavior is less extreme at higher carbonate concentrations and temperatures. These interesting results demonstrate that fuel-cell reactions can be sustained in alkaline CO_2-rejecting electrolytes. However, further studies are required to verify the viability of these electrolytes in fuel cells.

Preliminary results obtained by Huggins and co-workers (73) indicate that a hydroxide ion conductor from the Li-Al-O-H system is a possible electrolyte for intermediate-temperature fuel cells. In a humid environment at 500°C, Li_5AlO_4 exhibits ionic conductivity that is attributed to OH^- transport. At 500°C Li_5AlO_4 reacts with H_2O according to the reaction

$$Li_5AlO_4 + 2H_2O \rightarrow 4LiOH + LiAlO_2 \qquad (6\text{-}2)$$

The formation of LiOH and the OH^- that is produced is believed to be responsible for the observed conductivity (~0.1 $ohm^{-1}cm^{-1}$). In the absence of H_2O the conductivity is only 10^{-4} to 10^{-3} $ohm^{-1}cm^{-1}$ at 500°C. These findings suggest LiOH incorporated in a matrix of Li_5AlO_4 and $LiAlO_2$ deserves further consideration for use as an alkaline electrolyte in fuel cells, but the significant (1-50%) contribution of electronic conductivity from these materials (74) is a definite problem that must be eliminated.

6.3.3 Solid State Proton Conductors

Fast-proton conducting solids could have practical applications in solid electrolytes for moderate-temperature fuel cells. Ideally, a proton conductor for this application should be thermodynamically stable up to about 400°C, exhibit negligible electronic conductivity, and have satisfac-

tory chemical and electrochemical compatibility with electrode materials over the temperature range from 100 to 400°C. A reasonable number of materials are available which possess proton conductivity but many of them do not satisfy the properties necessary for use in fuel cells. Discussions on the properties of various proton conductors are found in References 75 and 76.

One of the most interesting proton conductors for fuel cells is hydrogen uranyl phosphate, $HUO_2PO_4 \cdot 4H_2O$ (HUP), which has a conductivity of 4×10^{-3} $ohm^{-1}cm^{-1}$ at 25°C. HUP belongs to a large class of compounds of the general formula $M^{m+}_{1/m}\ UO_2XO_4 \cdot nH_2O$, where M can be a mono-, di-, or some tri-valent cation, and X can be P, As or V (77). In HUP, which is a layered compound, the layers are connected by hydrogen bonds from water molecules and H_3O^+ ions in intervening layers. This network forms a continuous but unsaturated hydrogen-bonded network where the proton vacancies probably facilitate rapid proton migration, but the exact mechanism for proton conduction in HUP has been disputed (78). It appears that water is necessary to prevent drying of the HUP and its gradual transformation to the less-proton-conducting HUO_2PO_4. Other solid electrolytes from the phosphate family that have potential use in fuel cells are dodecamolybdphosphoric acid, $H_3Mo_{12}PO_{40} \cdot 29H_2O$ and dodecatungstophosphoric acid, $H_3W_{12}PO_{40} \cdot 29H_2O$, both of which have a conductivity of 0.2 $ohm^{-1}cm^{-1}$ at 25°C (79).

Proton conductors that are stable at the high temperatures of operation of conventional SOFCs have also been investigated (80-85). Some sintered oxides based on $SrCeO_2$ (i.e., $SrCe_{0.95}Yb_{0.05}O_{3-x}$, $SrCe_{0.90}Sc_{0.10}O_{3-x}$, and $SrCe_{0.90}Y_{0.10}O_{3-x}$, where x is the number of the oxygen deficiencies per perovskite-type oxide unit cell) exhibit appreciably high proton conductivity in hydrogen-containing atmosphere at high temperatures. At 1000°C, the conductivity of $SrCe_{0.95}Yb_{0.05}O_{3-x}$ in a partial pressure of 0.05 atm H_2O and 0.21 atm O_2 (balance N_2) is about 10^{-2} $ohm^{-1}cm^{-1}$. These ceramic materials have only p-type electronic conductivity in a hydrogen-free atmosphere, but on introducing water vapor or hydrogen, electronic conduction decreases and protonic conduction appears. However, under the typical operating conditions of SOFCs, oxide ions as well as protons might be conducting. Thorough evaluation of these materials for solid electrolytes in fuel cells is not complete.

References

1. J. O'M Bockris and A.J. Appleby, *Energy,* **11,** 95 (1986).
2. E.J. Taylor and S. Srinivasan, in *Power Sources for Electric Vehicles,* Edited by B.D. McNicol and D.A.J. Rand, Elsevier Science Publishers B.V., Amsterdam, The Netherlands, (1984) p. 839.
3. A.J. Appleby and E.B. Yeager, *Energy,* **11,** 137 (1986).
4. F.T. Bacon, *Electrochim. Acta,* **14,** 569 (1969).
5. D.W. Sheibley and R.A. Martin, *Prog. Batteries Solar Cells,* **6,** 155 (1987).
6. J. Huff, paper presented at the 1986 Fuel Cell Seminar, October 26-29, 1986, Tucson, AZ.
7. A.J. Appleby, *Energy,* **11,** 13 (1986).
8. K.F. Blurton and E. McMullin, *Energy Conversion,* **9,** 141 (1969).
9. M.B. Clark, W.G. Darland and K.V. Kordesch, *Electrochem. Tech.,* **3,** 166 (1965).
10. K. Tomantschger, F. McClusky, L. Oporto, A. Reid and K. Kordesch, *J. Power Sources,* **18,** 317 (1986).

11. J. McBreen, G. Kissel, K.V. Kordesch, F. Kulesa, E.J. Taylor, E. Gannon and S. Srinivasan, in *Proceedings of the 15th Intersociety Energy Conversion Engineering Conference,* Volume 2, American Institute of Aeronautics and Astronautics, New York, NY (1980) p. 886.
12. K. Kordesch, J. Gsellmann and B. Kraetschmer, in *Power Sources 9,* Edited by J. Thompson, Academic Press, New York, NY (1983) p. 379.
13. H.J.R. Maget, in *Handbook of Fuel Cell Technology,* Edited by C. Berger, Prentice-Hall, Inc., Englewood Cliffs, NJ (1968) p. 423.
14. H.A. Liebhafsky and E.J. Cairns, *Fuel Cells and Fuel Batteries,* John Wiley, New York, NY (1968) p. 587.
15. W.T. Grubb, *Proceedings of the 11th Annual Battery Research and Development Conference,* PSC Publications Committee, Red Bank, NJ (1957) p. 5; U.S. Patent No. 2,913,511 (1959).
16. A.B. LaConti, A.R. Fragala and J.R. Boyack, in *Proceedings of the Symposium on Electrode Materials and Processes for Energy Conversion and Storage,* Edited by J.D.E. McIntyre, S. Srinivasan and F.G. Will, The Electrochemical Society, Inc., Pennington, NJ (1977) p. 354.
17. W.G.F. Grot, G.E. Munn and P.N. Walmsley, paper presented at the 141st National Meeting of the Electrochemical Society, Inc., Houston, TX, May 7-11, 1972; Abstract No. 154.
18. R.S. Yeo, in *Proceedings of the Symposium on Transport Processes in Electrochemical Systems,* Edited by R.S. Yeo, T. Katan and D.T. Chin, The Electrochemical Society, Inc., Pennington, NJ (1982) p. 178.
19. T.G. Coker, A.B. LaConti and L.J. Nuttall, in *Proceedings of the Symposium on Membranes and Ionic and Electronic Conducting Polymers,* Edited by E.B. Yeager, B. Schumm, K. Mauritz, K. Abbey, D. Blankenship and J. Akridge, The Electrochemical Society, Inc., Pennington, NJ (1983) p. 191.
20. D. Watkins, K. Dircks, E. Epp and A. Harkness, *Proceedings of the 32nd International Power Sources Symposium,* The Electrochemical Society, Inc., Pennington, NJ (1986) p. 590.
21. A. LaConti, G. Smarz and F. Sribnik, "New Membrane-Catalyst for Solid Polymer Electrolyte Systems," Final Report prepared by Electro-Chem Products, Hamilton Standard for Los Alamos National Laboratory under Contract No. 9-X53-D6272-1 (1986).
22. J. McBreen, *J. Electrochem. Soc.,* **132,** 1112 (1985).
23. I.D. Raistrick, in *Proceedings of the Symposium on Diaphragms, Separators, and Ion-Exchange Membranes,* Edited by J.W. Van Zee, R.E. White, K. Kinoshita and H.S. Burney, The Electrochemical Society, Inc., Pennington, NJ (1986) p. 172.
24. G.A. Eisman, in *Proceedings of the Symposium on Diaphragms, Separators, and Ion-Exchange Membranes,* Edited by J.W. Van Zee, R.E. White, K. Kinoshita and H.S. Burney, The Electrochemical Society, Inc., Pennington, NJ (1986) p. 156.
25. B.R. Ezzell, W.P. Carl and W.A. Mod, in *Industrial Membrane Processes,* AIChE Symposium Series Vol. 82, No. 248, American Institute of Chemical Engineers, New York, NY (1986) p. 45.
26. R.T. Foley, "On the Properties of a Fuel Cell Electrolyte," Final Technical Report prepared by The American University for the U.S. Army Mobility Equipment Research and Development Command, Fort Belvoir, VA under Contract No. DAAK70-78-C-0128 (February 1979).
27. A.J. Appleby, *Prog. Batteries & Solar Cells,* **5,** 246 (1984).
28. N. Rebert, B.G. Ateya, T. Poweigha and L.G. Austin, *J. Electrochem. Soc.,* **127,** 2641 (1980).
29. S.B. Brummer, J. McHardy, J. Foos and J. McVeigh, "New Electrolytes for Direct Methane Fuel Cells," Quarterly Progress Report for Period July 10, 1978 - October 9, 1978, prepared

by EIC Laboratories for the U.S. Department of Energy under Contract No. EY-76-C-03-1363 (October 1978).
30. R.N. Camp and B.S. Baker, "Electrolyte for Hydrocarbon Air Fuel Cells," Semi-annual Technical Report prepared by Energy Research Corp. for the U.S. Army Mobility Equipment Research and Development Command, Fort Belvoir, VA under Contract No. DAAK02-73-C-084 (July 1973).
31. J. Ahmad, T.H. Nguyen and R.T. Foley, *J. Electrochem. Soc.*, **128,** 2257 (1981).
32. S.B. Brummer, J. Foos, J. McHardy, and J. McVeigh, paper presented at the National Fuel Cell Seminar, June 26-28, 1979, Bethesda, MD.
33. A.A. Adams, R.T. Foley and H.J. Barger, *J. Electrochem. Soc.*, **124,** 1228 (1977).
34. A.A. Adams and H.J. Barger, *J. Electrochem. Soc.*, **121,** 987 (1974).
35. A.A. Adams and R.T. Foley, *J. Electrochem. Soc.*, **126,** 775 (1979).
36. V.B. Hughes, B.D. McNicol, M.R. Andrew, R.B. Jones and R.T. Short, *J. Appl. Electrochem.*, **7,** 161 (1977).
37. A.J. Appleby and B.S. Baker, *J. Electrochem. Soc.*, **125,** 404 (1978).
38. G.W. Walker and R.T. Foley, *J. Electrochem. Soc.*, **128,** 1502 (1981).
39. P.N. Ross, E.J. Cairns, K. Striebel, F. McLarnon and P.C. Andricacos, *Electrochim. Acta,* **32,** 355 (1987).
40. K.L. Hsueh, H.H. Chang, D.T. Chin and S. Srinivasan, in *Proceedings of the Symposium on The Chemistry and Physics of Electrocatalysis,* Edited by J.D.E. McIntyre, M.J. Weaver and E.B. Yeager, The Electrochemical Society, Inc., Pennington, NJ (1984) p. 558.
41. H.C. Maru and D.N. Patel, paper presented at the Fifth U.S. Department of Energy Battery and Electrochemical Contractors' Conference, December 7-9, 1982, Crystal City, VA.
42. W.E. O'Grady and C.E. Shea, paper presented at the 1985 Fuel Cell Seminar, May 19-22, 1985, Tucson, AZ; W. O'Grady, "Fuel Cell Reactions in Super Acid Electrolytes," Final Report GRI-86/0058 prepared by Brookhaven National Laboratory for the Gas Research Institute, Chicago, IL under Contract No. 5081-260-0584 (January 1986).
43. P. Zelenay, B.R. Scharifker, J. O'M. Bockris and D. Gervasio, *J. Electrochem. Soc.*, **133,** 2262 (1986).
44. T. Sarada, R.D. Granata and R.T. Foley, *J. Electrochem. Soc.*, **135,** 1899 (1978).
45. M.A. Enayetullah and J. O'M Bockris, in *Proceedings of the 22nd Intersociety Energy Conversion Engineering Conference,* Volume 2, American Institute of Aeronautics and Astronautics, New York, NY (1987) p. 1028.
46. M. Walsh, paper presented at the National Fuel Cell Seminar, July 14-16, 1980, San Diego, CA.
47. R.N. Camp and B.S. Baker, "Electrolyte for Hydrocarbon Air Fuel Cells," Second Interim Technical Report prepared by Energy Research Corp. for the U.S. Army Mobility Equipment Research and Development Command, Fort Belvoir, VA under Contract No. DAAK02-73-C-084 (February 1974).
48. M. Walsh, paper presented at the National Fuel Cell Seminar, June 23-25, 1981, Norfolk, VA.
49. K.A. Striebel, P.C. Andricacos, E.J. Cairns, P.N. Ross and F.R. McLarnon, *J. Electrochem. Soc.*, **132,** 2381 (1985).
50. R.N. Camp and B.S. Baker, "Electrolyte for Hydrocarbon Air Fuel Cells," Third Interim Technical Report prepared by Energy Research Corp. for the U.S. Army Mobility Equipment Research and Development Command, Fort Belvoir, VA under Contract No. DAAK02-73-C-084 (June 1974).

51. A.A. Adams, R.T. Foley and R.M. Goodman, "Research on Electrochemical Energy Conversion Systems," Interim Technical Report prepared by The American University for the U.S. Army Mobility Equipment Research and Development Command, Fort Belvoir, VA under Contract No. DAAK02-72-C-084 (February 1974).
52. A.A. Adams, R.T. Foley and R.M. Goodman, "Research on Electrochemical Energy Conversion Systems," Interim Technical Report prepared by The American University for the U.S. Army Mobility Equipment Research and Development Command, Fort Belvoir, VA under Contract No. DAAK02-72-C-084 (June 1973).
53. J.P. Ackerman and R.K. Stuenenberg, Interim Report for January-December 1973 prepared by Argonne National Laboratory for the U.S. Army Mobility Equipment Research and Development Command, Fort Belvoir, VA under Contract No. MERDC A3101 (November 1974).
54. R.N. Hazeldine and J.M. Kidd, *J. Chem. Soc.*, 4228 (1954).
55. R.D. Howells and J.D. McCoun, *Chem. Rev.*, **77,** 69 (1977).
56. R.L. Benoit and C. Brisson, *Electrochim. Acta,* **18,** 105 (1973).
57. D.G. Russell and J.B. Senior, *Canad. J. Chem.*, **58,** 22 (1980).
58. L. Fabes and T.W. Swaddle, *Canad. J. Chem.*, **53,** 3053 (1973).
59. T. Sarada, R.D. Granata and R.T. Foley, *J. Electrochem. Soc.*, **125,** 1899 (1978).
60. T. Gramstad and R.N. Hazeldine, *J. Chem. Soc.*, 173 (1956).
61. "Physical Science Program Area, 1986 Research Status Report," Gas Research Institute, Chicago, IL (July 1986) p. 180.
62. J.L. Adcock, "Synthesis of Novel Acid Electrolytes for Phosphoric Acid Fuel Cells," Annual Report, May 1985 to April 1986, prepared by the University of Tennessee for the Gas Research Institute, Chicago, IL (June 1986).
63. D.J. Burton, "Synthesis of Novel Fluorinated Phosphonic and Phosphinic Acid Electrolytes for Phosphoric Acid Fuel Cells," Annual Report, May 1985 to April 1986, prepared by the University of Iowa for the Gas Research Institute, Chicago, IL (May 1986).
64. D.D. DesMarteau, "Novel Fluorinated Acids for Phosphoric Acid Fuel Cells," Annual Report, April 1985 to March 1986, prepared by Clemson University for the Gas Research Institute, Chicago, IL (June 1986).
65. G.L. Gard, "Improved Acid Electrolytes - The Synthesis and Structure of Fluorine-Containing Sulfonic Acids," Annual Report, July 1985 to July 1986, prepared by Portland State University for the Gas Research Institute, Chicago, IL (July 1986).
66. J.M. Shreeve, "Improved Acid Electrolytes for Fuel Cells," Annual Report, July 1985 to July 1986, prepared by the University of Idaho for the Gas Research Institute, Chicago, IL (July 1986).
67. M. Razaq, A. Razaq, E. Yeager, D.D. DesMarteau and S. Singh, *J. Appl. Electrochem.*, **17,** 1057 (1987).
68. E.J. Cairns and D.C. Bartosik, *J. Electrochem. Soc.*, **111,** 1205, (1964).
69. E.J. Cairns and D.I. Macdonald, *Electrochem. Tech.*, **2,** 65, (1964).
70. H.A. Liebhafsky and E.J. Cairns, *Fuel Cells and Fuel Batteries,* John Wiley, New York, NY (1968) p. 476.
71. K.A. Striebel, F.R. McLarnon and E.J. Cairns, in *Extended Abstracts,* Volume 85-1, Abstract No. 658, Spring Meeting of the Electrochemical Society, May 12-17, 1985, Toronto, Canada.
72. K.A. Striebel, F.R. McLarnon and E.J. Cairns, paper presented at the 38th Meeting of the International Society of Electrochemistry, September 14-18, 1987, Maastricht, The Netherlands.

73. L.Y. Cheng, S. Crouch-Baker and R.A. Huggins, paper presented at the 172nd National Meeting of the Electrochemical Society, Inc., Honolulu, HI, October 18-23, 1987; Abstract No. 1005.
74. R.M. Biefeld and R.T. Johnson, *J. Electrochem. Soc.*, **126,** 1 (1979).
75. *Solid State Protonic Conductors I for Fuel Cells and Sensors,* Edited by J. Jensen and M. Kleitz, Odense University Press, Odense, Denmark (1982).
76. *Solid State Ionics - 83, Part II,* Edited by M. Kleitz, B. Sapoval and D. Ravaine, North-Holland Publishing Co., Amsterdam, The Netherlands (1983).
77. F. Weigel and G. Hoffmann, *J. Less-Common Metals,* **44,** 99 (1976).
78. E. Skou, I.G. Kroug Andersen, K.E. Simonsen and E. Kroug Andersen, *Solid State Ionics,* **9/10,** 1041 (1983).
79. O. Nakamura, T. Kokama, I. Ogino and Y. Miyake, *Chem. Lett.,* 17 (1979).
80. H. Iwahara, H. Uchida, K. Ono and K. Ogaki, *J. Electrochem. Soc.,* **135,** 529 (1988).
81. H. Iwahara, T. Esaka, H. Uchida and N. Maeda, *Solid State Ionics,* **3/4,** 359 (1981).
82. H. Iwahara, N. Maeda and H. Iwahara, *J. Appl. Electrochem.,* **12,** 645 (1982).
83. H. Uchida, N. Maeda and H. Iwahara, *Solid State Ionics,* **11,** 117 (1983).
84. H. Iwahara, H. Uchida and N. Maeda, *Solid State Ionics,* **11,** 109 (1983).
85. H. Uchida, S. Tanaka and H. Iwahara, *J. Appl. Electrochem.,* **15,** 93 (1985).

7. FUEL CELL SYSTEMS

Fuel-cell technology has evolved from small laboratory cells to fuel-cell systems that are in the early stages of commercialization. A rough estimate of the progress in the scale up of fuel-cell stacks from the mid 1960s to the mid 1980s is summarized in Table 7.1 (1). The table suggests that an order-of-magnitude increase in the size of cell stacks and an order-of-magnitude increase in demonstrated stack durability have occurred over the intervening twenty years. Over the same time period, approximately one order-of-magnitude improvement in fuel-cell performance, as measured by the practical power density of fuel-cell stacks, has also occurred (1). A chronology of the progress in the size of the largest stack and the longest life of the fuel cells listed in Table 7.1, and examples of selected highlights, are presented in Figure 7-1. The information presented in the figure was compiled by Huff (2), and it complements but does not necessarily agree with the data summarized in Table 7.1. It is evident in the figures that the stack size of the five types of fuel cells reached a plateau in the mid 1980s. These fuel cells are now showing signs of a dramatic increase in size, and the duration of the longest stack test has shown steady progress from the mid 1970s.

The recent status of stack tests for the three major fuel-cell systems, PAFC, MCFC and SOFC, is summarized in this paragraph. Thirty-cell stacks (0.34 m^2 electrode area) of PAFCs have operated at 205°C and 8.2 atm for 16,000 h at 216 mA/cm^2 (3). Even larger electrodes (0.98 m^2) have been tested in stacks, without a decrease in performance. A 20-cell PAFC stack with the larger electrodes operated for over 1000 h (205°C and 8.2 atm) with a decay of only 3 to 4 mV per 1000 h. Both the performance and decay rate were within the accepted goal (i.e., performance at 1000 h of 0. 76 V at 216 mA/cm^2, end-of-life performance of 0.73 V, decay rate of <6 mV/1000 h) for PAFCs for utility applications. The largest fuel-cell power plant that has been demonstrated to date is a 4.8 MW PAFC (4.5-MW AC net power) which was installed in Japan. This power plant started operation in April 1983 and generated 5428 MWh (total operating time of 2887 h) before the test was completed in December 1985. The performance achieved was 0.65 V/cell at 250 mA/cm^2 (190°C, 3.4 atm), which corresponds to an efficiency (HHV) of 37% on natural gas (3). Tests of MCFC stacks have not reached the endurance achieved with PAFC stacks. Small stacks (0.09 m^2 electrode, 20 cells) have been operated for over 5000 h, and single cells have been tested for over 13,000 h. MCFC stacks (20 cells) with larger electrodes (0.74 m^2) have operated successfully for over 1700 h (4). A three-cell (20.5-cm length, 1.6-cm diameter) SOFC stack has achieved over

Table 7.1 Progress in Scale-up of Fuel-Cell Stack Technology

Fuel Cell	Early 1960s		Mid 1980s	
	Largest Stack[a] (kW)	Stack Life[a] (h)	Largest Stack[b] (kW)	Stack Life[b] (h)
PEFC	0.1	100	10[a]	10,000[a]
AFC	10	1,000	10[a]	10,000[a]
PAFC	1	1,000	700	2,000
PAFC	—	—	~15	15,000
MCFC	0.1	100	24	1,700
SOFC	0.01	100	3	3,700
SOFC	—	—	5	500

[a] Order-of-magnitude estimate

Source: (Table 1, p. 3) A.P. Fickett and E.A. Gillis, *Abstracts 1985 Fuel Cell Seminar,* May 19-22, 1985, Tucson, AZ (1985).

[b] Recent data, unless otherwise noted.

Source: W. Huber, Morgantown Energy Research Center (May 1988).

9000 h of operation at 1015°C at 252 mA/cm^2 (5). Except for a slight fluctuation in stack voltage after 7000 h, the performance remained steady to 9000 h even after 23 thermal cycles. More recently, a 24-cell[a] SOFC stack operated for about 2000 h at 200 mA/cm^2 and the initial stack voltage of ~5.26 V decayed by 0.7 V at the end of the test (6).

The technical (e.g., efficiency, performance, life) and economic (e.g., hardware cost, cost of electricity generated) factors of various designs of fuel-cell power plants have been extensively analyzed, and numerous fuel-cell system studies have been conducted. The comprehensive Energy Conversion Alternatives Study (ECAS) and Cogeneration Conversion Alternatives Study (CTAS) sponsored by the U.S. Department of Energy, as well as several studies sponsored by the Electric Power Research Institute, are summarized by Warshay (7). Another major study (8) was sponsored by the Jet Propulsion Laboratory (JPL) to investigate and screen advanced technology concepts for integrated gasifier/fuel cell systems. Another purpose of this study was to identify and recommend R&D areas that have the potential for contributing significant performance and cost improvements to fuel-cell technology. An extensive discussion on the numerous fuel-cell system studies is outside the scope of this chapter. Instead, the discussion will focus on selected examples of fuel-cell systems that have been proposed and their energy efficiencies. In particular, only the PAFC and MCFC will be considered in this chapter because they have received the greatest scrutiny in the

[a] See Figures 5-2 and 5-3 for cell design and arrangement for interconnection between cells.

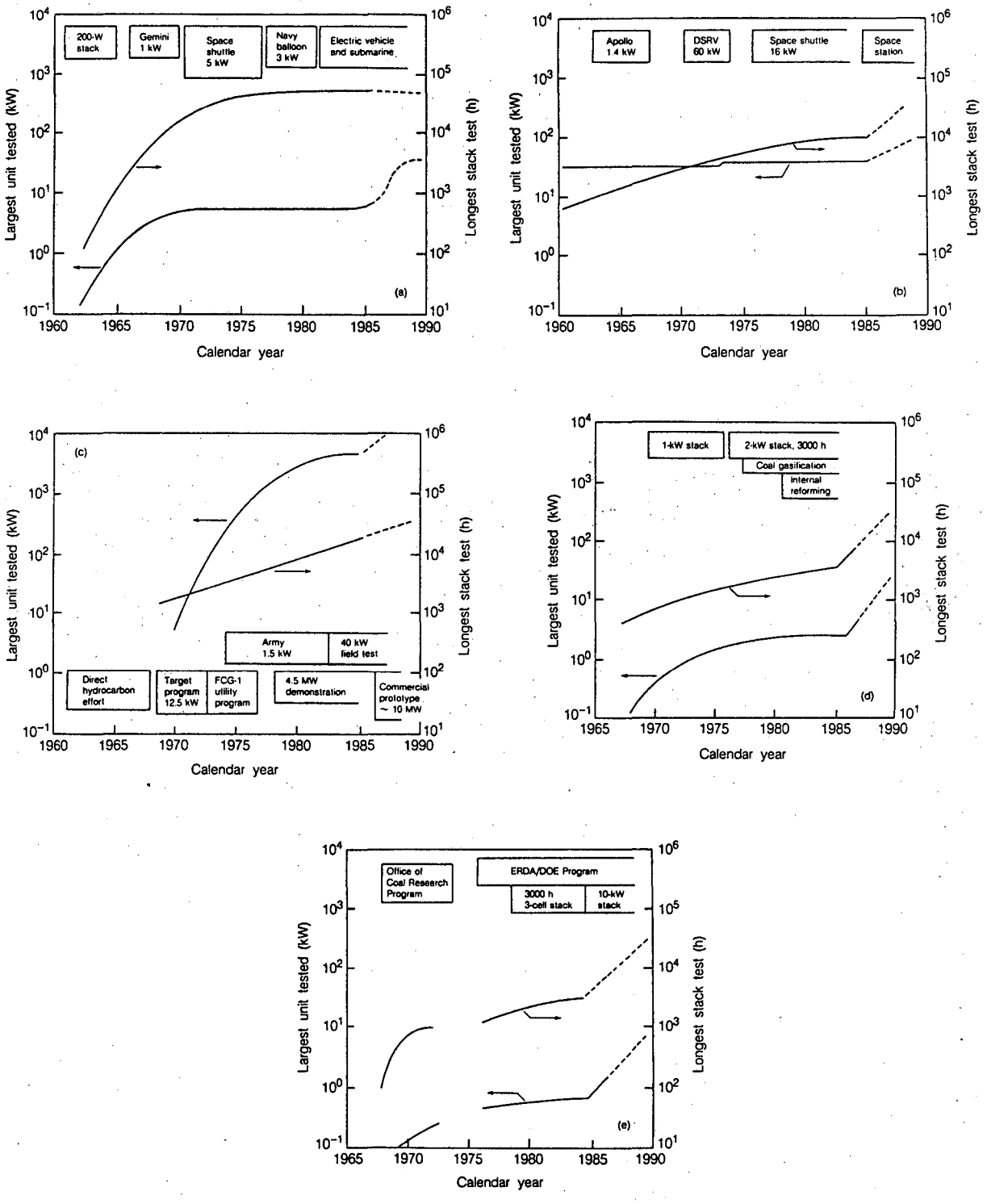

Figure 7-1. Chronology of the longest stack test and the largest unit tested. The projected change is noted by the dashed lines. (a) PEFC, (b) AFC, (c) PAFC, (d) MCFC, (e) SOFC.

Source: J.R. Huff, paper presented at the 1986 Fuel Cell Seminar, October 26-29, 1986, Tucson, AZ.

assessment studies. The intent of the discussion is to provide a brief overview of several systems, rather than to provide in-depth descriptions, which can be obtained from the original literature.

Benjamin et al. (9) presented a method to calculate the efficiency of fuel cells and the equations required for the calculation. In addition Benjamin et al. discussed various examples that illustrated the integration of a fuel cell with the fuel processing and ancillary system required for thermal management and waste heat recovery. The examples presented were:

- MCFC integrated with an air-blown coal gasifier and a bottoming cycle
- MCFC integrated with an oxygen-blown coal gasifier and a bottoming cycle
- PAFC integrated with a methanol reformer and export steam for a bottoming cycle or process heat
- PAFC integrated with a fuel processor for No. 2 fuel oil and export steam used for a bottoming cycle or process heat
- PAFC integrated with a naphtha reformer

An analysis of these systems provided information on heat and mass balances in the systems as well as their efficiencies. Since these analyses were completed, additional fuel-cell data have become available, which were used in recent assessments of fuel-cell technologies by Krumpelt and co-workers (10-12). In their assessments they applied the same ground rules in comparing various fuel-cell systems and competing technologies. The results of their assessment, as well as the results from the JPL studies, are briefly reviewed.

The characteristics of various fuel-cell systems evaluated by Krumpelt et al. (10) are summarized in Table 7.2. Eight conceptual designs for fuel-cell power plants were analyzed; five were for utility baseload power applications (150-1430 MW) utilizing coal and the other three were considered for dispersed power applications (1.8-11 MW) using natural gas. The cost of electricity[b] (COE, mid-1982 dollars) and system efficiency for the different power plants are computed for the specified operating conditions and fuel and oxidant utilizations listed in the table. These data provide interesting insight into the projected COE of fuel-cell power plants. Fairly detailed engineering design and analysis have been reported for 150-MW PAFC and 675-MW MCFC, and a meaningful comparison of COE between these two systems is possible. The MCFC appears to have a cost advantage over that of the PAFC, but a comparison of COE with the other fuel-cell systems would be speculative because of the differences in the maturity of the technology or the preliminary state of the engineering design, particularly in the case of SOFC.

The results in Table 7.3 provide another comparison of various fuel-cell technologies (8). In this analysis, PAFC, MCFC and SOFC of the same power rating, 675 MW, were considered with different options for the coal gasifier and cleanup. If MCFCs with internal reforming are not included, the analysis indicates that the COE for a 675-MW MCFC is less than that of a comparable-sized PAFC. The summaries in Tables 7.2 and 7.3 show that SOFC and IR-MCFC power plants have higher projected system efficiencies (i.e., >50%) than conventional MCFC and PAFC power plants. Furthermore, the projected COE for a SOFC power plant is lower than that for both PAFC and MCFC power plants.

In the following three sections, examples of systems designs of PAFC, MCFC, and SOFC power plants that are integrated to coal gasifiers are discussed. These examples illustrate the distribution of the sources of energy generation and loss in an integrated fuel-cell power plant. In the following system designs, electrical power is derived from the fuel cell, gas turbine and steam turbine. The distribution of electrical power that is obtained from these sources varies with changes in the operating parameters (i.e., current density, fuel utilization) of the fuel cell.

[b] See Appendix 9.5 for a description of the parameters considered in the the calculation of COE.

Table 7.2 Characteristics of Various Fuel-Cell Systems

System	Fuel	Operating Conditions V @ mA/cm^2	Operating Conditions psia/°C	COE	Utilization (%) Fuel	Utilization (%) Oxidant	ε_S[a] (%)	E_{FC} (%)
150-MW PAFC • steam turbine • turboexpanders	C	0.725 @ 200	120/205	81.2	85	70	35.5[b]	89
675-MW MCFC • steam turbine • gas turbine	C	0.77 @ 160	100/650	73.3	85	46	49.0	68
635-MW MCFC • steam turbine • turboexpanders	C	0.85 @ 160	150/600 to 700	51.4	85	50	49.6	68
1430-MW MCFC • steam turbine • turboexpanders	C	0.75 @ 210	150/600 to 700	62.0	90	58	47.9	70
675-MW SOFC • steam turbine	C	0.66 @ 294	165/526 to 877	46.7	62	31	58.4	41
11-MW PAFC	NG	0.73 @ 202	120/205	NA	86	NA	41.1	100
7.5-MW PAFC • steam turbine	NG	0.68 @ 325	50/191	81	80	50	40	100
1.8-MW IR-MCFC	NG	0.73 @ 160	14/650	83.2	90	78	52.9	100

[a] HHV fuel

[b] HHV coal minus Btu credit for by-products

C = coal
COE = Cost Of Electricity, mills/kWh in mid-1982 dollars
NA = not available
NG = natural gas

ε_S = fuel-cell system efficiency

E_{FC} = per cent of total electrical energy derived from fuel cell

Source: M. Krumpelt, V. Minkov, J.P. Ackerman and R.D. Pierce, "Fuel Cell Power Plant Designs, A Review," ANL-85-39, DOE/MC/49941-1833, prepared by Argonne National Laboratory for the U.S. Department of Energy, Morgantown, WV (November 1985).

Table 7.3 Comparison of Various 675-MW Fuel-Cell Systems

System	COE[a]	Power Output (% of Plant Feed HHV)				ε (%)
		Fuel Cell	Steam Turbine	Net Gas Turbine	Plant Consumption	
1. MCFC, entrained bed gasifier, LT cleanup	86.6	34	10	12	-7	49[b]
2. MCFC, fluidized bed gasifier, LT cleanup	90	32	12	10	-9	45
3. MCFC, fluidized bed gasifier, HT cleanup (IGT)	83.1	32	13	12	-9	48
4. IR-MCFC, fluidized bed gasifier, LT cleanup	91.1	41	8	10	-7	52
5. IR-MCFC, catalytic LT gasifier, HT cleanup (zinc ferrite)	104.4	48	0	11	-1	58
6. PAFC, catalytic-acceptor gasifier, LT cleanup	100.8	28	10	7	-1	44
7. SOFC, fluidized bed gasifier, HT cleanup (zinc ferrite)	79.0	23	13	21	-2	55

[a] Cost Of Electricity, mills/kWh in 1981 dollars

[b] DOE reference design

ε = net system efficiency
HT = high temperature
IGT = Institute of Gas Technology
IR = internal reforming
LT = low temperature
Source: H.P. Stevens, "Coal-Based Fuel-Cell Powerplant," NPO-16543/6046, Jet Propulsion Laboratory, California Institute of Technology, Pasadena, CA (July 1986).

7.1 Phosphoric Acid Fuel Cell

A flow diagram for a design of a PAFC integrated with an oxygen-blown Texaco coal gasifier[c] and a bottoming cycle (steam turbine and gas turbine) for a 575-MW baseload power plant (15, 16) is presented in Figure 7-2. The upper diagram shows the various components for fuel processing, thermal management, and oxidant feed to the fuel-cell stack. Cleanup of H_2S is performed by the Selexol (17), Claus (18) and SCOT (19) processes. An organic solvent such as the dimethyl ether of polyethylene glycol is used in the Selexol process to physically absorb H_2S. The organic solvent is stripped of H_2S, and the Claus process is used for recovering elemental sulfur from H_2S. The SCOT (*S*hell *C*laus *O*ff-gas *T*reatment) process, which uses catalytic hydrogenation over a Co-Mo catalyst to convert sulfur compounds to H_2S and selective amine absorption (usually diisopropanolamine), treats the tail gases from the Claus process. The tail gas that is treated by this process goes to an incinerator where residual sulfur-containing compounds are converted to SO_2 before venting to the atmosphere. The fuel processing system is designed to reduce CO to less than 1 mol% in intermediate- and low-temperature shift reactors, and the fuel stream enters the fuel cell at about 160°C and 127 psi. The depleted fuel stream from the anode and the depleted oxidant from the cathode of the fuel cell are catalytically reacted, and then expanded in a gas turbine which compresses the air for the oxidant feed stream and which generates electrical energy. The lower diagram in Figure 7-2 shows the steam-turbine bottoming cycle that is integrated to the fuel cell. Water is used to remove heat from the fuel-cell stacks, which is recovered to produce high-pressure steam for the integrated steam cycle to produce electrical energy.

An energy flow diagram for the power plant shown in Figure 7-2 is given in Figure 7-3. In this analysis the fuel cell is operated at 180 mA/cm^2 (0.737 V/cell) and with a fuel utilization of 70%, and an overall system efficiency of 42.4% (based on HHV) is projected. The energy utilized in the gas and steam turbines is obtained from the coal gasifier and the fuel cell, and no distinction is made in Figure 7-3 as to the source of the thermal energy utilized in the turbines. According to the energy balance in Figure 7-3, ~55% of the total output of electrical energy is obtained from the fuel cell, whereas ~21 and 24% are obtained from the gas turbine and steam turbine, respectively. The efficiency achieved with this system design is higher than any reported for coal-based PAFC systems, partly because of the extensive heat recovery system which enhances the power output from the bottoming cycle (i.e., gas and steam turbines).

7.2 Molten Carbonate Acid Fuel Cell

A flow diagram for a design of a MCFC integrated with an oxygen-blown Texaco coal gasifier and a steam-turbine bottoming cycle for a 575-MW baseload power plant (15, 16) is presented in Figure 7-4. Except for the high-temperature shift converter, the fuel processing for the MCFC system design is similar to that of the PAFC system design in Figure 7-2. The MCFC does not require a shift converter because it is not poisoned by CO. After the gas passes the cleanup section and the expansion turbine, it enters the fuel cell at 537°C and about 100 psi. The CO_2 required for the cathode reaction is obtained by recycling CO_2 from the anode exhaust stream to the cathode inlet. Part of the cathode exhaust stream is expanded in the gas turbine which compresses the air for the oxidant feed stream and which generates electrical energy. High-pressure steam for the integrated

[c] See Appendix 9.6 for a brief description of the Texaco coal gasifier. References 13 and 14 provide a summary of various coal gasification processes and gas cleanup systems.

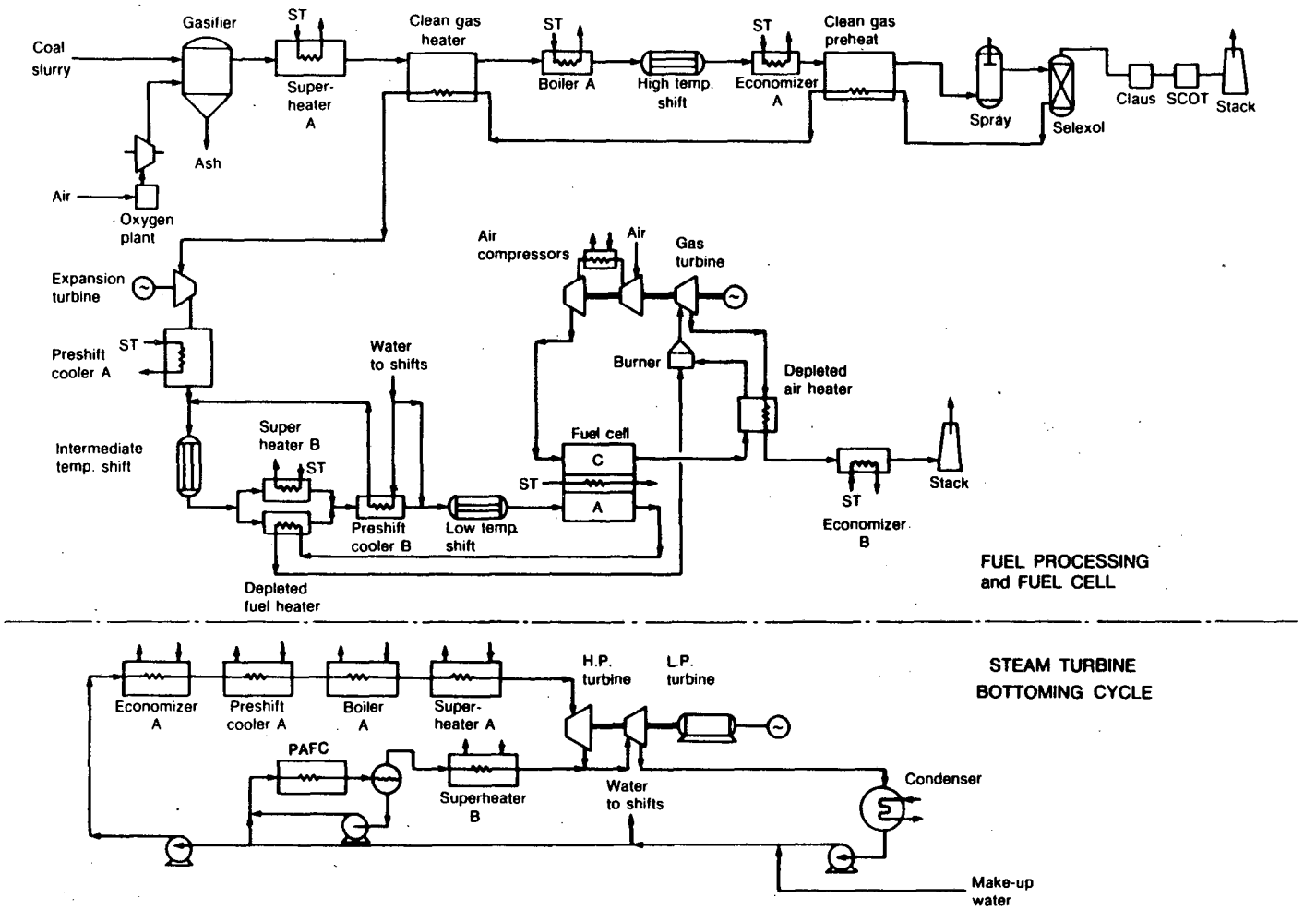

Figure 7-2. Flow diagram for design of a PAFC integrated to coal gasifier and steam-turbine bottoming cycle. Fuel cell is operated at 180 mA/cm^2 (0.737 V/cell) and 70% fuel utilization.

Source: V. Minkov, E. Daniels, C. Dennis and M. Krumpelt, paper presented at the 1986 Fuel Cell Seminar, October 26-29, 1986, Tucson, AZ.

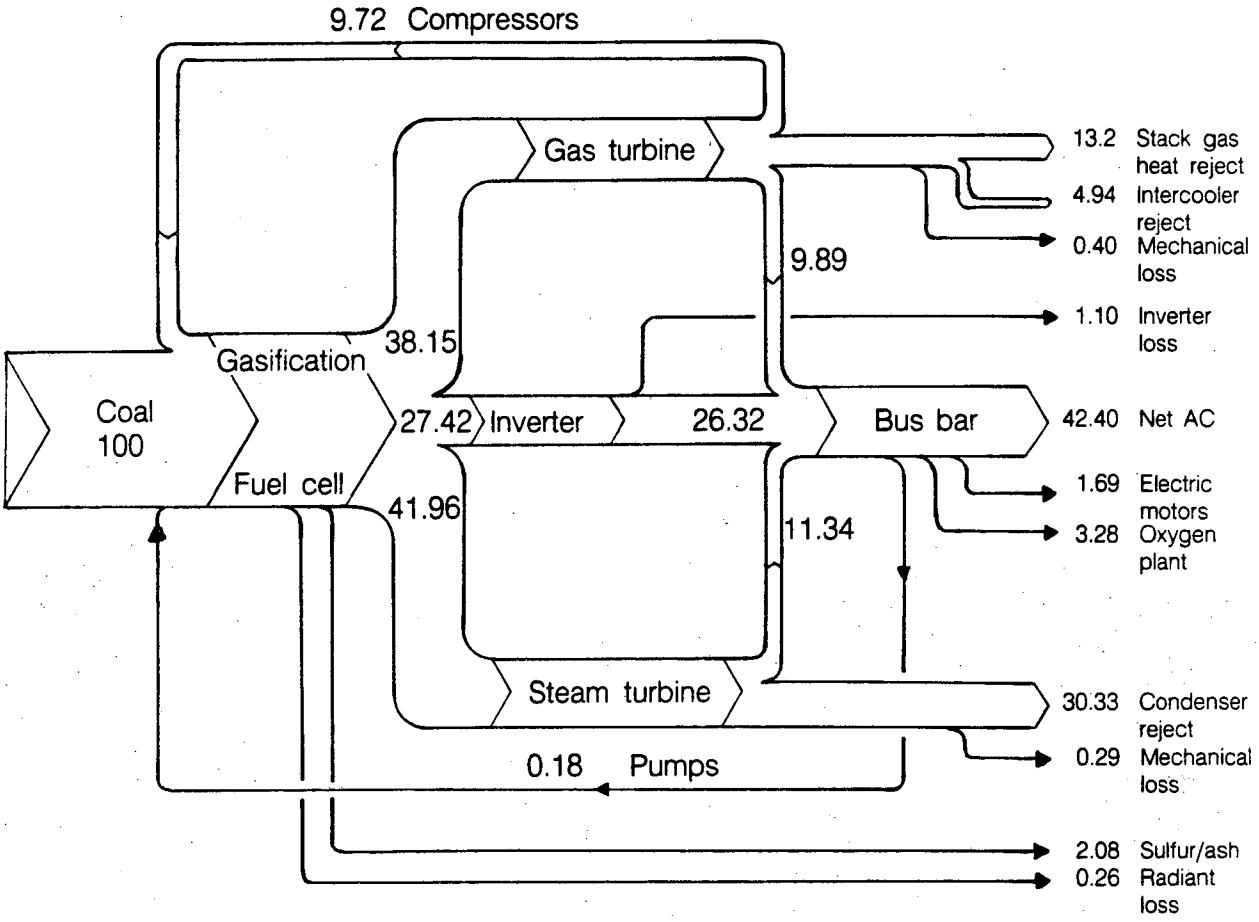

Figure 7-3. Energy balance for fuel-cell system presented in Figure 7-2.
Source: M. Krumpelt, Argonne National Laboratory, Argonne, IL, private communication (April 30, 1987).

steam cycle is produced by the heat recovered from the gasification section and the cathode recycle streams. The corresponding energy flow diagram for the system in Figure 7-4 is presented in Figure 7-5. The overall system efficiency for such a plant design is projected to be 46.7% (based on HHV) when the fuel cell is operated at 380 mA/cm^2 (0.623 V/cell) and with a fuel utilization of 55%. According to the energy balance in Figure 7-5, ~38% of the total output of electrical energy is obtained from the fuel cell, whereas ~46 and 16% are obtained from the gas turbine and steam turbine, respectively.

The relative amounts of electrical energy obtained from the fuel cell, steam turbine and gas turbine in the system designs in Figures 7-2 and 7-4 will depend on the operating conditions of the fuel cell. These aspects, as well as the economics of fuel cell power plants for utility central stations, are discussed by Minkov et al. (11). The fuel utilization and cell voltage are two parameters that affect system efficiency and COE. By varying these two parameters, the contribution of the fuel cell and the bottoming section to the total electrical power output from the power plant can be changed. According to the analysis by Minkov et al., the COE is minimized when the fuel cell operates at low fuel utilization where it provides a smaller fraction of the total electrical output from the power plant.

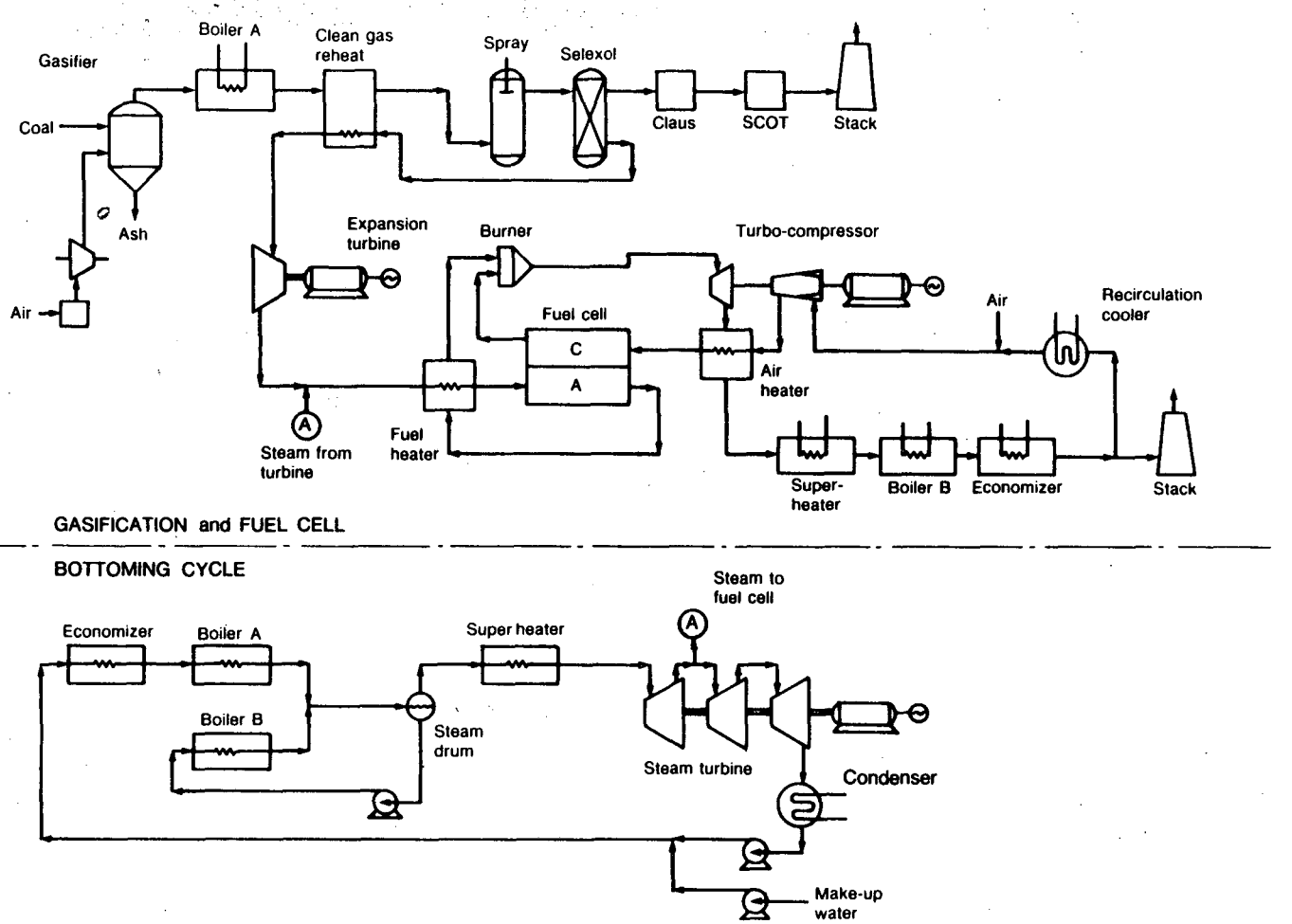

Figure 7-4. Flow diagram for design of a MCFC integrated to coal gasifier and steam-turbine bottoming cycle. Fuel cell is operated at 380 mA/cm^2 (0.6223 V/cell) and 55% fuel utilization.
Source: V. Minkov, E. Daniels, C. Dennis and M. Krumpelt, paper presented at the 1986 Fuel Cell Seminar, October 26-29, 1986, Tucson, AZ.

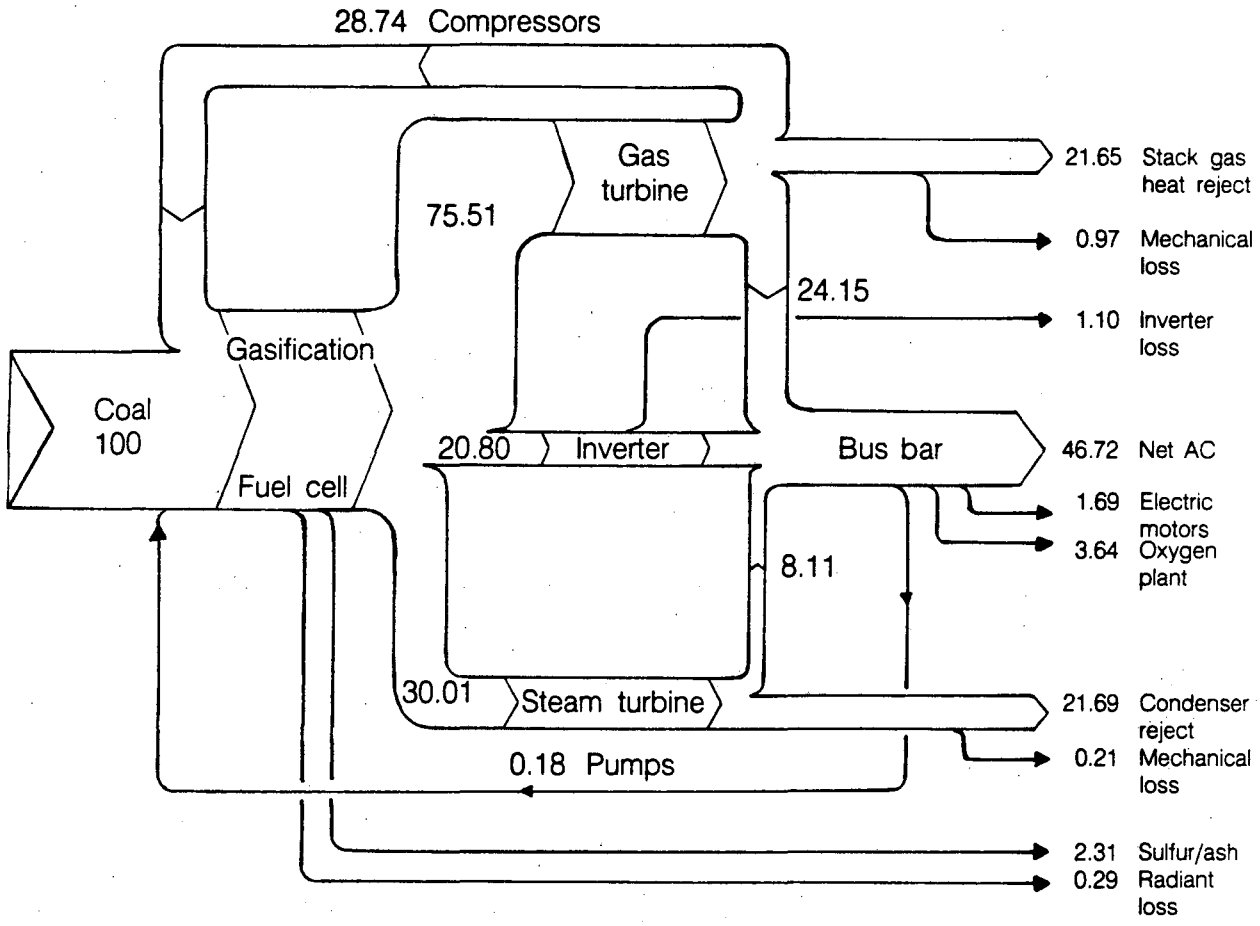

Figure 7-5. Energy balance for fuel-cell system presented in Figure 7-4.
Source: M. Krumpelt, Argonne National Laboratory, Argonne, IL, private communication (July 20, 1987).

7.3 Solid Oxide Fuel Cell

A flow diagram for a design of a pressurized (11 atm) SOFC integrated with an air-blown coal gasifier (Westinghouse fluidized-bed gasifier) and a steam-turbine bottoming cycle for a 637-MW baseload power plant is presented in Figure 7-6 (8). This system employs a hot-gas cleanup subsystem (zinc ferrite absorption bed at about 650 to 700°C) for H_2S absorption, which means a wet scrubbing process such as the type used in the PAFC (Figure 7-2) and MCFC (Figure 7-4) power plants are not required. The corresponding energy flow diagram for the system in Figure 7-6 is presented in Figure 7-7. Because the SOFC operates at 11 atm, about 18% of the input energy is required for an air compressor. The overall system efficiency is projected to be 55.2% at 294 mA/cm^2 (0.66 V/cell), with a fuel utilization of 62% and an oxygen utilization of 32%. The net power output from the fuel cell and the gas turbine are nearly equal, which is similar to the situation obtained with the MCFC system in Figure 7-4. The efficiency of the pressurized SOFC system does not appear to depend heavily on fuel-cell output, and thus it can be designed to operated at a lower fuel utilization in the fuel cell.

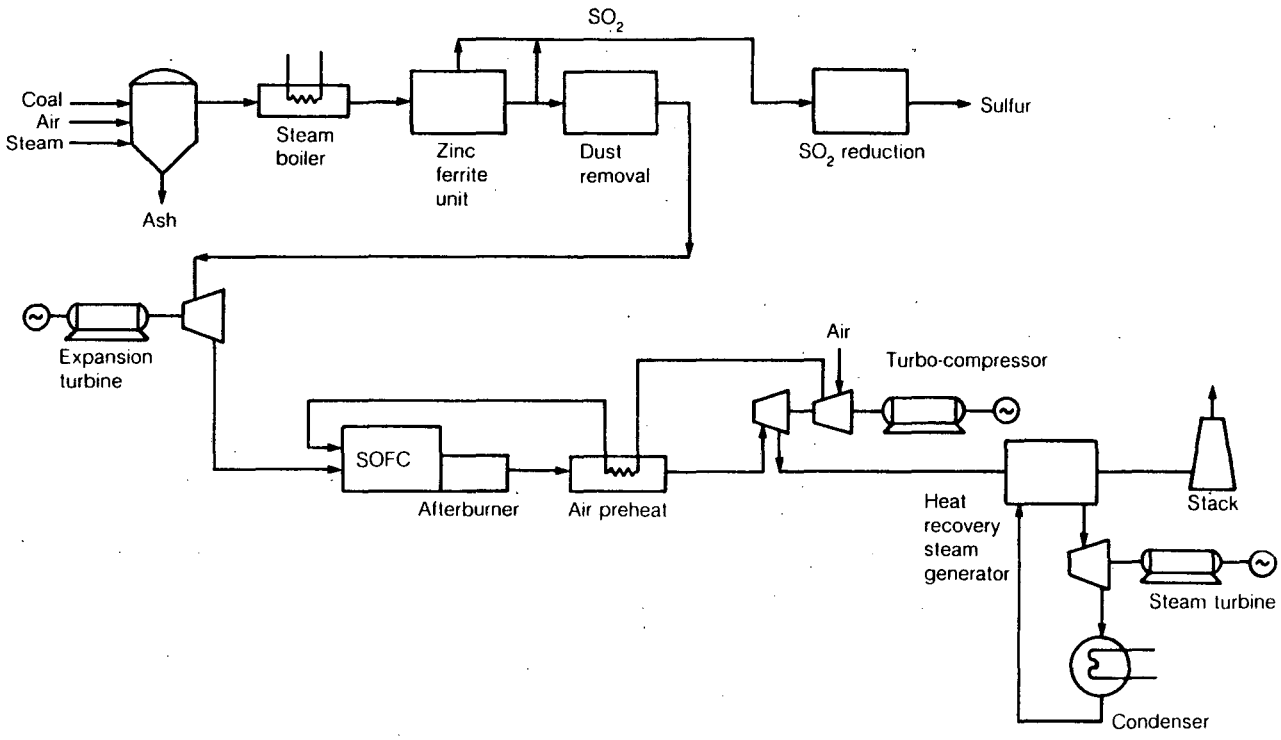

Figure 7-6. Flow diagram for design of a pressurized SOFC integrated to coal gasifier and steam-turbine bottoming cycle. Fuel cell is operated at 11 atm and at 294 mA/cm^2 (0.66 V/cell) and 62% fuel utilization.
Source: H.P. Stevens, "Coal-Based Fuel-Cell Powerplant," NPO-16543/6046, Jet Propulsion Laboratory, California Institute of Technology, Pasadena, CA (July 1986).

The discussion in this chapter has briefly touched upon the relationship between the factors relevant to the economics (i.e., capital cost, COE, operating and maintenance costs) and performance (i.e., current density, cell voltage, efficiency, fuel utilization) of fuel-cell power plants. The brief discussion presented above illustrates the complexity involved in assessments of fuel-cell power plants. A more detailed discussion on these topics is outside the scope of this handbook, but is available in the cited references.

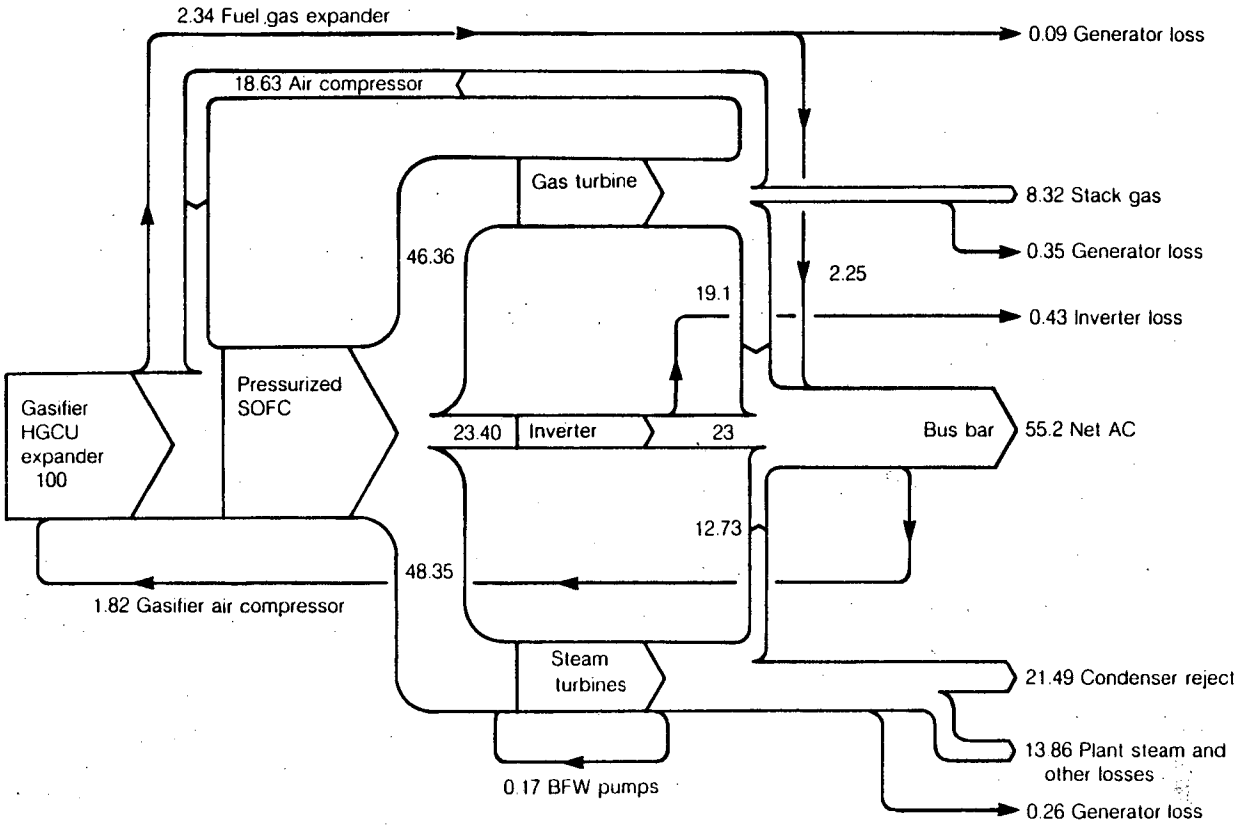

Figure 7-7. Energy balance for fuel-cell system presented in Figure 7-6.
Source: H.P. Stevens, "Coal-Based Fuel-Cell Powerplant," NPO-16543/6046, Jet Propulsion Laboratory, California Institute of Technology, Pasadena, CA (July 1986).

References

1. A.P. Fickett and E.A. Gillis, paper presented at the 1985 Fuel Cell Seminar, May 19-22, 1985, Tucson, AZ; *Abstracts 1985 Fuel Cell Seminar* (1985) p. 1.
2. J.R. Huff, paper presented at the 1986 Fuel Cell Seminar, October 26-29, 1986, Tucson, AZ.
3. *Assessment of Research Needs for Advanced Fuel Cells,* Edited by S.S. Penner, DOE/ER/30060-T1, prepared by the DOE Advanced Fuel Cell Working Group for the U.S. Department of Energy under Contract No. DE-AC01-84ER30060 (November 1985); *Energy,* **11,** 1 (1986).
4. R.H. Goldstein, *EPRI Journal,* 40 (September 1987).
5. A.O. Isenberg, paper presented at the 1985 Fuel Cell Seminar, May 19-22, 1985, Tucson, AZ; *Abstracts 1985 Fuel Cell Seminar,* (1985) p. 102.
6. P. Reichner and J.M. Makiel, paper presented at the 1986 Fuel Cell Seminar, October 26-29, 1986, Tucson, AZ; *Abstracts 1986 Fuel Cell Seminar,* (1986) p. 32.
7. M. Warshay, in *The Science and Technology of Coal and Coal Utilization,* Edited by B.R. Cooper and W.A. Ellingson, Plenum Press, New York, NY (1984) p. 339.
8. H.P. Stevens, "Coal-Based Fuel-Cell Powerplant," NPO-16543/6046, Jet Propulsion Laboratory, California Institute of Technology, Pasadena, CA (July 1986).

9. T.G. Benjamin, E.H. Camara and L.G. Marianowski, *Handbook of Fuel Cell Performance,* prepared by the Institute of Gas Technology for the U.S. Department of Energy under Contract No. EC-77-C-03-1545 (May 1980).
10. M. Krumpelt, V. Minkov, J.P. Ackerman and R.D. Pierce, "Fuel Cell Power Plant Designs, A Review," ANL-85-39, DOE/MC/49941-1833, prepared by Argonne National Laboratory for the U.S. Department of Energy, Morgantown, WV (November 1985).
11. V. Minkov, E. Daniels, C. Dennis and M. Krumpelt, paper presented at the 1986 Fuel Cell Seminar, October 26-29, 1986, Tucson, AZ; *Abstracts 1986 Fuel Cell Seminar,* (1986) p. 255.
12. M. Krumpelt, V. Minkov, E. Daniels and C. Dennis, paper presented at the 1986 Fuel Cell Seminar, October 26-29, 1986, Tucson, AZ; *Abstracts 1986 Fuel Cell Seminar,* (1986) p. 308.
13. "Development of Molten Carbonate Fuel Cell Power Plant," Final Report, DOE/ET/17019-20, prepared by the General Electric Co. for the U.S. Department of Energy, Morgantown, WV, under Contract No. DE-AC02-80ET17019 (March 1985).
14. J.C.W. Kuo, in *The Science and Technology of Coal and Coal Utilization,* Edited by B.R. Cooper and W.A. Ellingson, Plenum Press, New York, NY (1984) p. 163.
15. *Fuel Cell Technology Status Report,* DOE/METC-86/0241, prepared by Morgantown Energy Research Center, Morgantown, WV (1985).
16. M. Krumpelt, private communication (May 13, 1987).
17. *Coal Gasification Processes,* Edited by P. Nowacki, Noyes Data Corporation, Park Ridge, NJ (1981) p. 311.
18. *Coal Gasification Processes,* Edited by P. Nowacki, Noyes Data Corporation, Park Ridge, NJ (1981) p. 330.
19. *Coal Gasification Processes,* Edited by P. Nowacki, Noyes Data Corporation, Park Ridge, NJ (1981) p. 336.

8. CONCLUDING REMARKS

The types of fuel cells discussed in this Handbook have attained different levels of acceptance as viable candidates for terrestrial and space applications. The PAFC is currently on the verge of commercialization for baseload electric power generation, whereas MCFCs and SOFCs are at earlier stages of development. The AFC is an integral part of the United States Space Program (i.e., currently used in the Space Shuttle Orbiter), and the PEFC is now receiving attention for possible use in transportation applications. Despite the interesting possibilities for fuel cells in transportation (propulsion), space and military applications, only in space applications has the fuel cell been clearly demonstrated as a viable technology. Recent efforts with fuel cells for transportation applications offer promise, but their high cost is a definite disadvantage compared to internal combustion engines. On the other hand, cost is not a major consideration for fuel cells in space and military applications, and thus these markets are expected to be well-served by fuel-cell technology.

Dramatic improvements in technology have shown promise for reducing the cost of fuel-cell power plants. One of the early examples is the demonstration that porous gas electrodes for PAFCs can operate effectively with low loadings of Pt electrocatalysts supported on carbon black. The use of carbon-based materials in low-temperature fuel cells is expected to lead to the development of low-cost components. New concepts are also under investigation; two such examples are the new cell (stack) designs for SOFCs and the discovery of promising novel electrolytes for fuel cells.

The utilization of fuel-cell power plants by the gas and electric utilities and industry will require resolution of the following issues (1): (i) manufacturer's willingness to risk capital and/or forward pricing, (ii) utilities' willingness to assume risk and/or premium cost for early units, and (iii) government and other institutions' willingness to support (subsidize) early units. Currently these issues are being discussed, and hopefully they will lead to a positive result for the penetration of fuel cells into the marketplace. The turnkey price for the initial 11-MW PAFC power plants[a] (available for operation in 1990), which are not mass produced, is estimated to be about $37 to $40 million each, or $3360 to $3630/kW (2). As expected, this cost range is higher than that of a mature technology such as conventional fossil-energy power plants, which cost about $1000/installed kW. However, if the system efficiency can be increased to 43.8% (HHV) or higher, then even at the high cost mentioned above the fuel cell should be able to compete with proposed advanced combustion turbine, combined-cycle units (3). Various estimates for the projected cost of MCFC and SOFCs for utility applications are available, and several studies are summarized by Appleby (4).

[a] Heat rate (HHV) on natural gas is projected to be 8300 Btu/kWh, corresponding to 41.1% system efficiency.

These fuel cells are expected to be commercialized after PAFCs achieve a mature state in the marketplace.

The intent of this Handbook is to focus on the various types of fuel cells and their current technical status, and only to a lesser extent on their applications. As described in the preceding chapters (Chapters 3-6), the various fuel cells have undergone dramatic changes in the past two decades, and research continues to improve the technology. Optimization of parameters such as pressure, temperature, reactant composition and utilization are important to obtain the maximum performance from fuel cells. Because the fuel cell must be integrated with other subsystems involving fuel processing, thermal management and power conditioning, a systems approach to utilizing fuel cells is needed, and several examples are provided in Chapter 7. Finally, it is apparent that there are numerous markets where fuel cells can play a prominent role if certain economic and technical issues are resolved. If these issues and the institutional barriers confronting fuel cells are overcome, then fuel-cell technologies should penetrate the commercial and industrial marketplaces.

Since the pioneering efforts by F.T. Bacon in the 1930s, the development of various fuel cell systems has flourished. The published literature describing various aspects of fuel-cell technology has also proliferated, and lists of pertinent books, proceedings publications and bibliographies are included in Appendix 9.7. A list of fuel-cell publications from periodicals is not presented because these citations can be found in the bibliographies.

References

1. A.P. Fickett, in *Advances in Energy Systems and Technology,* Volume 5, Edited by P.L. Auer and D. Douglas, Academic Press, New York, NY (1986) p. 1.
2. G.L. Hagey, paper presented at the International Seminar on Fuel Cell Technology and Applications, October 26-29, 1987, The Hague, Holland.
3. A.J. Appleby, paper presented at the 38th Meeting of the International Society of Electrochemistry, September 14 - 18, 1987, Maastricht, The Netherlands, *Extended Abstracts,* (1987) p. 474.
4. A.J. Appleby, "Advanced Fuel Cells and Their Future Market," to be published in *Energy Conservation Strategies,* Edited by W.E. Murphy and L.H. Fletcher, American Society of Aeronautics and Astronautics, New York, NY (1987).

9. APPENDIX

9.1 Heat Capacity Correlation

The thermodynamic data (e.g., ΔG, ΔH, ΔS) required to calculate the efficiency parameters (see Chaper 2) for fuel cells must be available for temperatures (T) other than the standard temperature, usually 298°K. ΔH and ΔS at a given T are obtained by the use of the equations presented in Chapter 2 and the heat capacity correlation such as the one given in Table 9.1 (1).

Reference

1. H.M. Spencer, *J. Amer. Chem. Soc.*, **67**, 1858 (1945).

9.2 Reactant Gas Utilization in Molten Carbonate Fuel Cells

The electrochemical reactions occurring in a MCFC are

$$\text{Anode:} \qquad H_2 + CO_3^{=} \rightarrow H_2O + CO_2 + 2e^- \tag{9-1}$$

and

$$\text{Cathode:} \qquad \tfrac{1}{2}O_2 + CO_2 + 2e^- \rightarrow CO_3^{=} \tag{9-2}$$

The overall cell reaction is

$$H_2 + \tfrac{1}{2}O_2 + CO_2\ (\text{cathode}) \rightarrow H_2O + CO_2\ (\text{anode}) \tag{9-3}$$

and the corresponding reversible cell potential is computed from the Nernst equation[a]

[a] The activity gradient for $CO_3^{=}$ is assumed to be zero through the cell.

Table 9.1 Heat Capacities of Gases (273-1500°K)

$$C_p = a + bT + cT^2 \ (C_p \text{ in cal/mol–deg K})$$

Gas	a	b x 10^3	c x 10^7
H_2	6.9469	-0.1999	4.808
O_2	6.148	3.102	-9.23
N_2	6.524	1.250	-0.01
CO	6.420	1.665	-1.96
H_2O	7.256	2.298	2.83
CO_2	6.214	10.396	-35.45
CH_4	3.381	18.044	-43.00

Source: H.M. Spencer, *J. Amer. Chem. Soc.*, **67,** 1858 (1945).

$$E = E^o + \frac{RT}{2F} \ln [P_{H_2} P_{O_2}^{1/2} / P_{H_2O}] + \frac{RT}{2F} \ln [(P_{CO_2})_c / (P_{CO_2})_a] \tag{9-4}$$

In an operating fuel cell, the cell voltage changes in response to the utilization of the reactant gases, as well as other processes that result in polarization. The influence of reactant utilization on the MCFC cell voltage can be determined, and this calculation is discussed here.

In the following analysis, the fuel gas composition at the anode inlet is assumed to correspond to the equilibrium composition established by the water-gas shift reaction. This is a reasonable assumption since the water-gas shift reaction reaches equilibrium rapidly in MCFCs. Thus, H_2 that electrochemically reacts at the anode can originate from the H_2 present in the inlet gas stream [moles H_2 (in)] and from H_2 obtained from CO [moles CO (in)] by the water-gas shift reaction in the cell. In other words, the total H_2 available for electrochemical oxidation is equal to the moles H_2 (in) + moles CO (in).

Fuel Utilization: The utilization of H_2 (β) is defined as

$$\beta = \frac{\text{moles } H_2 \text{ consumed}}{\text{moles } H_2 \text{ (in)} + \text{moles CO (in)}} = \frac{f_{in}[X_{H_2} + X_{CO}]_{in} - f_{out}[X_{H_2}]_{out}}{f_{in}[X_{H_2} + X_{CO}]_{in}} \tag{9-5}$$

where $[X_{H_2} + X_{CO}]$ corresponds to the sum of the mole fraction of H_2 and CO, and subscripts in and out refer to the inlet and outlet of the cell, respectively. The total gas flow rate at the inlet and

outlet is given by f_{in} and f_{out}, respectively. When H_2 electrochemically reacts at the anode, an equivalent amount of CO_2 and H_2O are formed, i.e.,

$$\beta f_{in}[X_{H_2} + X_{CO}]_{in} = CO_2 \text{ (produced)} = H_2O \text{ (produced)} \tag{9-6}$$

Thus, there is a net increase in the amount of gas at the outlet

$$CO_2 \text{ (produced)} + H_2O \text{ (produced)} - H_2 \text{ (consumed)} = \beta f_{in}[X_{H_2} + X_{CO}]_{in} \tag{9-7}$$

and

$$\text{total gas flow (out)} = \text{total gas flow (in)} + \beta f_{in}\,[X_{H_2} + X_{CO}]_{in} \tag{9-8}$$

$$= f_{in}\,(1 + \beta[X_{H_2} + X_{CO}]_{in})$$

The mole fraction of H_2 + CO at the anode outlet $[X_{H_2} + X_{CO}]_{out}$ is obtained from Equations 9-5 and 9-8,

$$[X_{H_2}]_{out} = \frac{(1 - \beta)[X_{H_2} + X_{CO}]_{in}}{1 + \beta[X_{H_2} + X_{CO}]_{in}} \tag{9-9}$$

A net gain in CO_2 is obtained at the anode outlet,

$$CO_2 \text{ (out)} = CO_2 \text{ (in)} + CO_2 \text{ (produced)} = f_{in}[X_{CO_2}]_{in} + f_{in}\,\beta[X_{H_2} + X_{CO}]_{in} \tag{9-10}$$

The mole fraction of CO_2 at the anode outlet $[X_{CO_2}]_{out}$ is given by

$$[X_{CO_2}]_{out} = \frac{[X_{CO_2}]_{in} + \beta[X_{H_2} + X_{CO}]_{in}}{1 + \beta[X_{H_2} + X_{CO}]_{in}} \tag{9-11}$$

Similarly, the mole fraction of H_2O at the anode outlet $[X_{H_2O}]_{out}$ is given by

$$[X_{H_2O}]_{out} = \frac{[X_{H_2O}]_{in} + \beta[X_{H_2} + X_{CO}]_{in}}{1 + \beta[X_{H_2} + X_{CO}]_{in}} \tag{9-12}$$

The mole fraction $[X_{inert}]_{out}$ of inert gases (e.g., N_2), if present, is given by

$$[X_{inert}]_{out} = \frac{[X_{inert}]_{in}}{1 + \beta[X_{H_2} + X_{CO}]_{in}} \tag{9-13}$$

The mole fraction of CO at the anode outlet $[X_{CO}]_{out}$ is obtained from the equilibrium gas composition at the anode outlet, taking into account the water-gas shift reaction, i.e.,

$$K = \frac{[X_{H_2O}]_{out}[X_{CO}]_{out}}{[X_{H_2}]_{out}[X_{CO_2}]_{out}} \tag{9-14}$$

Oxidant Utilization: The utilization of oxidant (γ) can be defined in terms of the quantity of CO_2 consumed,

$$\gamma = \frac{\text{moles } CO_2 \text{ consumed}}{\text{moles } CO_2 \text{ (in)}} = \frac{f_{in}[X_{CO_2}]_{in} - f_{out}[X_{CO_2}]_{out}}{f_{in}[X_{CO_2}]_{in}} \tag{9-15}$$

where the terms f and X have been defined above. The cathode reaction involves the consumption of 2 moles of CO_2 for each mole of O_2. Thus,

$$CO_2 \text{ reacted} = \gamma f_{in} [X_{CO_2}]_{in} \tag{9-16}$$

and

$$O_2 \text{ reacted} = \tfrac{1}{2}\gamma f_{in} [X_{CO_2}]_{in} \tag{9-17}$$

At the cathode, the reaction of 0.5 mole of O_2 with 1.0 mole of CO_2 produces a net loss of 1.5 $\gamma f_{in} [X_{CO_2}]_{in}$ moles of oxidant, and therefore,

$$\text{total gas (out)} = \text{total gas (in)} - 1.5\ \gamma f_{in} [CO_2]_{in} \tag{9-18}$$

or

$$f_{out} = f_{in} - 1.5\ \gamma f_{in} [X_{CO_2}]_{in} \tag{9-19}$$

From Equations 9-15 and 9-19, the mole fraction of CO_2 at the outlet is given by

$$[X_{CO_2}]_{out} = \frac{(1 - \gamma)\ [X_{CO_2}]_{in}}{1 - 1.5\ \gamma[X_{CO_2}]_{in}} \tag{9-20}$$

In the case of O_2, the amount that is present at the cathode outlet is given by

$$O_2 \text{ (out)} = O_2 \text{ (in)} - 0.5\ \gamma f_{in} [X_{CO_2}]_{in} \tag{9-21}$$

and,

$$[X_{O_2}]_{out} = \frac{[X_{O_2}]_{in} - 0.5\ \gamma[X_{CO_2}]_{in}}{1 - 1.5\ \gamma[X_{CO_2}]_{in}} \tag{9-22}$$

The mole fraction of inert gases $[X_{inert}]_{out}$ is given by

$$[X_{inert}]_{out} = \frac{[X_{inert}]_{in}}{1 - 1.5\ \gamma[X_{CO_2}]_{in}} \tag{9-23}$$

Nernst Potential: The mole fraction of specie i (X_i) is related to its partial pressure by

$$X_i = \frac{P_i}{P_T} \tag{9-24}$$

or upon rearrangement

$$P_i = X_i P_T \tag{9-25}$$

where P_T is the total gas pressure. Substituting for P_i in the Nernst Equation (9-4) yields the reversible potential at the outlet of a MCFC, i.e.,

$$E = E^o + \frac{RT}{2F} \ln \frac{[X_{H_2}][X_{O_2}]^{1/2}[X_{CO_{2,c}}]P^{1/2}}{[X_{H_2O}][X_{CO_{2,a}}]} \tag{9-26}$$

where $P_c = P_a = P$ is assumed.

9.3 Equilibrium Constants

The temperature dependence of the equilibrium constants for the water-gas shift reaction

$$CO_2 + H_2 = CO + H_2O \tag{9-27}$$

carbon deposition (Boudouard reaction) reaction

$$2CO \rightarrow C + CO_2 \tag{9-28}$$

methane decomposition reaction

$$CH_4 \rightarrow C + 2H_2 \tag{9-29}$$

and methane formation reaction

$$CO + 3H_2 \rightarrow CH_4 + H_2O \tag{9-30}$$

are presented in Figure 9-1, using data from Rostrup-Nielsen (1).

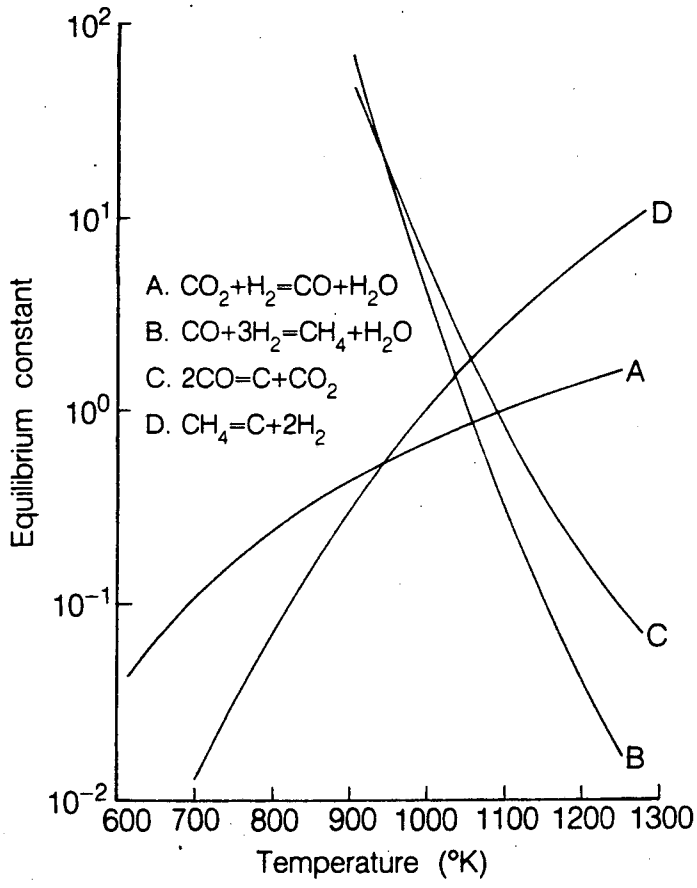

Figure 9-1. Equilibrium constants (partial pressures in MPa) for: (A) water-gas shift, (B) methane formation, (C) carbon deposition (Boudouard reaction), and (D) methane decomposition. See text, Appendix 9.3 for chemical reactions.
Source: J.R. Rostrup-Nielsen, in *Catalysis Science and Technology*, Edited by J.R. Anderson and M. Boudart, Springer-Verlag, Berlin, GDR (1984) p.1.

Reference

1. J.R. Rostrup-Nielsen, in *Catalysis Science and Technology,* Volume 5, Edited by J.R. Anderson and M. Boudart, Springer-Verlag, Berlin, German Democratic Republic (1984) p. 1.

9.4 Contaminants from Coal Gasification

A list of contaminant levels that result from various coal gasification processes are presented in Table 9.2 (1). The contaminant levels obtained after a first stage of hot-gas cleanup with zinc ferrite are also listed.

Reference

1. A. Pigeaud, Progress Report prepared by Energy Research Corporation for U.S. Department of Energy, Morgantown, WV under Contract No. DE-AC21-84MC21154 (June 1987).

Table 9.2 Typical Contaminant Levels obtained from Various Coal Gasification Processes

Parameters	Coal Gasification Process				
	HYGAS Fluidized Bed	Koppers-Totzek Entrained Bed	LURGI Fixed Bed	METC (raw gas) Fixed Bed	Cleaned Gas
Max. Product Temp. (°C)	940	1900	750	1300	<800
Gasification	O_2 blown	O_2 blown	O_2 blown	Air blown	Regenerative
Pressure (psi)	1165	15	435	220	150
Product Gas (°C)	NS[a]	1500	600	650	<700
Methane (vol%)	18.6	0.1	11	3.5	3.5
Coal type	Pittsburgh #8	Bituminous Eastern	Sub-bitum. Navajo	Sub-bitum. New Mexico	(Humidified Output)
Particulates (g/l)	NS	0.015	0.016	0.058	0.01 est.
Sulfur (ppm) (Total H_2S, COS, CS_2, mercaptans)	12,000	3,500	2,000	5,300	<10
NH_3 (vol%)	0.5	0.11	0.4	0.44	0.25
Trace metals (ppm)					
As	0.8	5	2	NS	NS
Pb	5	2	0.8	2	1.7
Hg	0.1	NS	0.4	NS	NS
Zn	13	NS	0.4	NS	140
Halogens (ppm)	300-4000	366	200	700	500
Hydrocarbons (vol%)					
C_2H_6	0.7-1.6	NS	1	NS	NS
C_2H_4	0.7-1.6	NS	1	0.3	NS
C_2H_2	0.7-1.6	NS	1	NS	NS
Oil tar	NS	NS	0.09	NS	NS

[a] Not specified

Source: A. Pigeaud, Progress Report prepared by Energy Research Corporation for U.S. Department of Energy, Morgantown, WV under Contract No. DE-AC21-84MC21154 (June 1987).

9.5 Cost of Electricity

Three major contributors are considered in the computation of the cost of electricity (COE) for a fuel-cell power plant: (i) capital cost, (ii) fuel cost and (iii) operation and maintenance costs. The cost of electricity ($/KW-yr) can be calculated using these parameters as follows (1):

$$COE = 0.2CC + \frac{3413H}{\varepsilon_S}\frac{FC}{10^6} + OM \tag{9-31}$$

where 0.2 is a fixed charge rate, CC is the capital cost ($/kW), FC is the fuel cost ($/$10^6$ Btu), 3413 is the theoretical heat rate for 100% efficiency (Btu/kWh), ε_S is the efficiency, H is the h/yr operated, and OM is the operating and maintenance costs ($/kW-yr).

Reference

1. A.P. Fickett, *Int. J. Hydrogen Energy,* **8,** 617 (1983).

9.6 Texaco Coal Gasifier

The Texaco coal gasifier is an entrained-bed gasifier that produces either a low- or medium-Btu synthesis gas, using either air or oxygen (1, 2). Gasification of coal takes place by the following sequence of reactions. The combustion reaction

$$C + O_2 \rightarrow CO_2 \tag{9-32}$$

provides the heat energy needed to drive the endothermic reactions involving H_2O/C and CO_2/C:

$$C + H_2O \rightarrow CO + H_2 \tag{9-33}$$

and

$$C + CO_2 \rightarrow 2CO \tag{9-34}$$

Other reactions such as the water-gas shift reaction and methanation reaction also occur in the gasifier.

In this process, ground coal of a carefully controlled size (<3.8 cm) is mixed with water, and the slurry (0.24-0.43 steam/carbon weight ratio) is then fed to the gasifier. The gasifier operates in the temperature range of 1260 to 1430°C and at a pressure of about 600 psig (41 atm). Because of the high operating temperatures, no oils, tars, coal fines or ash are present in the gas. Ammonia and hydrogen sulfide are the principal impurities to be removed. The Texaco gasifier functions equally well with air or oxygen, but the product gas composition is considerably higher in nitrogen and lower in hydrogen in an air-blown gasifier than that in an oxygen-blown gasifier. In addition, the presence of nitrogen in the gases from air-blown gasifiers requires the use of larger, more-expensive components in the gas cleanup subsystem. A typical composition for Illinois No. 6 coal is listed in Table 9.3 (3), and the typical gas composition obtained from an oxygen-blown Texaco gasifier, using Illinois No. 6 coal in a pilot plant, is listed in Table 9.4 (3).

Table 9.3 Typical Composition of Illinois No. 6 Coal

Proximate Analysis, Wt. %	
Moisture	4.2
Ash	9.6
Fixed carbon	52.0
Volatile matter	34.2
Total	100.0
Ultimate Analysis[a], Wt. %	
Carbon	77.26
Hydrogen	5.92
Oxygen	11.14
Nitrogen	1.39
Sulfur	4.29
Total	100.0
Heating Value[b], Btu/lb	
Higher heating value	12,235
Net heating value	11,709

[a] Dry, ash-free basis

[b] As received

Source: E.C. Mangold, M.A. Muradaz, R.P. Ouellette, O.G. Farah and P.N. Cheremisinoff, *Coal Liquefaction and Gasification Technologies*, Ann Arbor Science, Ann Arbor, MI (1982) p. 213.

Table 9.4 Typical Gas Composition from Oxygen-Blown Texaco Gasifier with Illinois No. 6 Coal

Gas composition, vol%	
CO	44.62
CO_2	17.97
H_2	35.78
CH_4	0.03
H_2O	1.02
COS	0.05
N_2 + Ar	6.48
HHV of gas, Btu/scf	~320

Source: E.C. Mangold, M.A. Muradaz, R.P. Ouellette, O.G. Farah and P.N. Cheremisinoff, *Coal Liquefaction and Gasification Technologies,* Ann Arbor Science, Ann Arbor, MI (1982) p. 213.

References

1. E.C. Mangold, M.A. Muradaz, R.P. Ouellette, O.G. Farah and P.N. Cheremisinoff, *Coal Liquefaction and Gasification Technologies,* Ann Arbor Science, Ann Arbor, MI (1982) p. 209.
2. *Coal Gasification Processes,* Edited by P. Nowacki, Noyes Data Corporation, Park Ridge, NJ (1981) p. 254.
3. E.C. Mangold, M.A. Muradaz, R.P. Ouellette, O.G. Farah and P.N. Cheremisinoff, *Coal Liquefaction and Gasification Technologies,* Ann Arbor Science, Ann Arbor, MI (1982) p. 213.

9.7 Fuel Cell References

Books on Fuel Cells

1. A.J. Appleby, ed., *Fuel Cells: Trends in Research and Applications,* Hemisphere Publishing, NY, 1987.
2. A.J. Appleby, ed., *Proceedings of the DOE/EPRI Workshop on Molten Carbonate Fuel Cells,* Electric Power Research Institute, Palo Alto, CA, 1979.
3. V.S. Bagotskii and Y.B. Vasil'ev., eds., *Fuel Cells. Their Electrochemical Kinetics,* translated from Russian by Consultants Bureau, NY, 1966.

4. B.S. Baker, ed., *Hydrocarbon Fuel Cell Technology,* Academic, NY, 1965.
5. B.S. Baker, ed., *Fuel Cell Systems-II,* Advances in Chemistry Series, No. 90, American Chemical Society, Washington, D.C., 1969.
6. T.G. Benjamin, E.H. Camara and L.G. Marianowski, *Handbook of Fuel Cell Performance,* prepared by the Institute of Gas Technology for U.S. Department of Energy under Contract No. EC-77-C-03-1545, May 1980.
7. C. Berger, ed., *Handbook of Fuel Cell Technology,* Prentice-Hall, Englewood, NJ, 1968.
8. J. O'M. Bockris and S. Srinivasan, *Fuel Cells and Their Electrochemistry,* McGraw-Hill, NY, 1969.
9. M.W. Breiter, *Electrochemical Processes in Fuel Cells,* Springer-Verlag, NY, 1969.
10. E.H. Camara, ed., *Symposium Proceedings on Fuel Cells: Technology Status and Applications,* Institute of Gas Technology, Chicago, IL, 1982.
11. K.J. Euler, *Entwicklung der Elektrochemischen Brennstoffzellen,* Thieme Taschenbucher 62, Munchen, 1974. In German.
12. Editors of Chemical Engineering Progress, *Fuel Cells, A Technical Manual,* American Institute of Chemical Engineers, NY, 1963.
13. R.F. Gould, ed., *Fuel Cell Systems,* Advances in Chemistry Series, No. 47, American Chemical Society, Washington, D.C., 1965.
14. A.B. Hart and G.J. Womack, *Fuel Cells: Theory and Application,* Chapman and Hall, London, 1967.
15. J.P. Hoare, *The Electrochemistry of Oxygen,* Interscience, NY, 1968.
16. J. Jensen and M. Kleitz, eds., *Solid State Protonic Conductors I for Fuel Cells and Sensors,* Odense University Press, Odense, Denmark, 1982.
17. E.W. Justi and A.W. Winsel, *Cold Combustion. Fuel Cells,* Franz Steiner Verlag, Wiesbaden, 1962. In German.
18. E.W. Justi, M. Pilkuhn, W. Scheibe and A.W. Winsel, *High Drain Hydrogen Diffusion Electrode Operating at Ambient Temperature and Low Pressure,* Mainz: Akademie der Wissenschaften und der Literature, 1959. English translation by T.E. Burton, Published by Research Information Service Division, Pergamon International Corporation, NY.
19. H.A. Liebhafsky and E.J. Cairns, *Fuel Cells and Fuel Batteries,* John Wiley, NY, 1968.
20. D. Linden, ed., *Handbook of Batteries and Fuel Cells,* McGraw-Hill, NY, 1983.
21. D.G. Lovering and E.W. Lees, *Fuel Cells: An Update,* ETSU N-104, Harwell Laboratory, Oxfordshire, England, June 1987.
22. A. McDougall, *Fuel Cells,* John Wiley, NY, 1976.
23. J.D.E. McIntyre, S. Srinivasan and F.G. Will, eds., *Proceedings of the Symposium on Electrode Materials and Processes for Energy Conversion and Storage,* The Electrochemical Society, Inc., Pennington, NJ, 1977.
24. B.D. McNicol and D.A.J. Rand, eds., *Power Sources for Electric Vehicles,* Elsevier, Amsterdam, 1984
25. W. Mitchell, Jr., ed., *Fuel Cells,* Academic, NY, 1963.
26. W.E. O'Grady, P.N. Ross and F.G. Will, eds., *Proceedings of the Symposium on Electrocatalysis,* The Electrochemical Society, Inc., Pennington, NJ, 1982.
27. W.E. O'Grady, S. Srinivasan and R.F. Dudley, eds., *Proceedings of the Symposium on Electrocatalysis of Fuel Cell Reactions,* The Electrochemical Society, Inc., Pennington, NJ, 1979.

28. L. Oniciu, *Fuel Cells,* Abacus Press, Kent, England, 1976. English translation by A. Nana and V. Vasilescu of the Romanian work Pile de Combustie by L. Oniciu, published by Editura Stintifica, Bucharest, Romania in 1971.
29. S.S. Penner, ed., *Assessment of Research Needs for Advanced Fuel Cells,* DOE/ER/30060-T1, prepared for U.S. Department of Energy under Contract No. DE-AC01-84ER30060, November 1985; *Energy* **11(1/2),** 1 (1986).
30. N.W. Ranney, *Fuel Cells - Recent Developments,* Noyes Development Corp., Park Ridge, NJ, 1969.
31. F.J. Salzano, ed., *Proceedings of the Conference on High Temperature Solid Oxide Electrolytes, August 16-17, 1983,* BNL 51728, Brookhaven National Laboratory, Upton, NY, October 1983.
32. G. Sandstede, ed., *From Electrocatalysis to Fuel Cells,* University of Washington Press, Seattle, 1972.
33. J.R. Selman and H.C. Maru, eds., *Proceedings of the Symposium on Electrochemical and Thermal Modeling of Battery, Fuel Cell and Photoenergy Conversion Systems,* The Electrochemical Society, Inc., Pennington, NJ, 1986.
34. J.R. Selman and T.D. Claar, eds., *Proceedings of the Symposium on Molten Carbonate Fuel Cell Technology,* The Electrochemical Society, Inc., Pennington, NJ, 1984.
35. S. Srinivasan, S. Wagner and H. Wroblowa, eds., *Proceedings of the Symposium on Electrode Materials and Processes for Energy Conversion and Storage,* The Electrochemical Society, Inc., Pennington, NJ, 1987.
36. W. Vielstich, *Brennstoffelemente (Fuel Cells),* Verlag Chemie, Weinheim, 1965. In German. English translation, published by Wiley, NY, 1970.
37. H. Von Döhren and K.J. Euler, *Der Heutige Stand der Brennstoffelemente,* Varta, Frankfurt, 1966. In German.
38. K. Wiesener, J. Garche and W. Schneider, *Elektrochemische Stromquellen (Electrochemical Power Supply Systems),* Akademie-Verlag, Berlin, 1981. In German.
39. K.R. Williams, ed., *An Introduction to Fuel Cells,* Elsevier, NY, 1966.
40. G.J. Young, ed., *Fuel Cells,* Volume 1, Reinhold, NY, 1960.
41. G.J. Young, ed., *Fuel Cells,* Volume 2, Reinhold, NY, 1963.
42. *Les Piles à Combustible,* French Petroleum Institute, Paris, 1964. In French.

Bibliographies on Fuel Cells

1. *Bibliography on Fuel Cells,* Central Electricity Generating Board, United Kingdom, 1947. Bibliography containing over 500 citations.
2. M. von Stackelberg and W. Vielstich, *Russian Research in Fuel Cells and Alkaline Type Batteries,* University of Bonn, Bonn, 1961. A report on Communist-bloc research.
3. *Fuel Cell Bibliography,* College of Ceramics, Alfred University, State University of New York, Alfred, NY, 1962. Bibliography containing over 1000 citations.
4. L.G. Austin, *Fuel Cells,* NASA SP-120, National Aeronautics and Space Administration, Washington, 1967. Bibliography of citations for government-sponsored research covering the period from 1950 to 1964.
5. *Fuel Cells, A Bibliography,* TID-3359, Office of Scientific and Technical Information, U.S. Department of Energy, Oak Ridge, TN, June 1977. Bibliography containing 3273 citations covering the period from mid 1960s to June 1977.

6. R.C. Chudacek, *Batteries, Fuel Cells, and Related Electrochemistry: Books, Journals, Periodicals, and Other Information Sources, 1950-1979,* NTIS, PC A04/MF A01, National Technical Information Service, Springfield, VA, April 1980. Bibliography containing 130 citations from NTIS data base.
7. *Fuel Cells, A Bibliography,* TID-3359 (Suppl. 1), Office of Scientific and Technical Information, U.S. Department of Energy, Oak Ridge, TN, June 1980. Bibliography containing 1067 citations covering the period June 1977 to June 1980.
8. D.M. Cavagnaro, *Fuel Cells. 1979-June 1980,* NTIS, PC N01/MF N01, National Technical Information Service, Springfield, VA, July 1980. Bibliography containing 139 citations from NTIS data base.
9. D.M. Cavagnaro, *Fuel Cells. 1977-1978,* NTIS, PC N01/MF N01, National Technical Information Service, Springfield, VA, August 1980. Bibliography containing 193 citations from NTIS data base.
10. D.M. Cavagnaro, *Hydrocarbon Fuel Cells. 1967-July 1980,* NTIS, PC N01/MF N01, National Technical Information Service, Springfield, VA, October 1980. Bibliography containing 130 citations from NTIS data base.
11. *Fuel Cells, A Bibliography,* DOE/METC-85/15, Office of Scientific and Technical Information, U.S. Department of Energy, Oak Ridge, TN, April 1985. Bibliography containing approximately 1900 citations covering the period July 1977 to February 1985.
12. D.H. Nochumson, J.H. Altseimer, K.D. Williamson, J.A. Frank, A.T. Peaslee, A.J. Martinez and C.A. Stroup, *Fuel Cell Applications Literature Review,* NTIS, PC A07/MF A01, National Technical Information Service, Springfield, VA, March 1985. Bibliography containing over 600 citations were entered into a fuel-cell applications computerized data base. Also includes 157 references.

Proceedings and Abstracts from Fuel Cell Meetings

1. *Proceedings of the International Power Sources Symposium,* PSC Publications Committee, Red Bank, N.J. Meetings are held biennially in Cherry Hill, NJ (33rd meeting held on June 13-16, 1988). These proceedings are published biennially. The bulk of the fuel-cell papers have appeared in the later volumes, starting with the 11th conference (1957).
2. *Proceedings of the International Power Sources Symposium,* University Press, Cambridge, England. Meetings are held biennially in England (16th meeting held in Bournemouth, England on September 26-29, 1988). These proceedings are published biennially.
3. *Proceedings of the Intersociety Energy Conversion Engineering Conference.* Sponsorship of meeting rotates among seven Technical Societies. Meetings are held annually (usually in August) in different cities in the United States (23rd meeting held in Denver, CO on August 1-5, 1988)
4. *Extended Abstracts International Society of Electrochemistry,* Meetings are held annually (usually in August or September) in different cities (39th meeting held in Glasgow, Scotland on September 5-10, 1988).
5. *Abstracts Fuel Cell Seminar,* Sponsored by the National Fuel Cell Coordinating Group. Meetings are held approximately every two years in different US cities (meeting will be held in Long Beach, CA on October 23-26, 1988).

6. P. Zegers, ed., *Potential, State of the Art and R&D Requirements for Fuel Cells in the European Community,* Report EUR 10595, Office for Official Publications of the European Communities, Luxenbourg, 1986. Proceedings of the Commission of the European Communities Fuel Cell Workshop held on October 7-8, 1985 in Noordwijkerhout, The Netherlands.
7. *Second International Symposium on Fuel Cells,* (Deuxieme Journees Internationales D'etudes des Piles à Combustible), Presses Academiques Europeennes, Brussels, 1967. Proceedings of conference held under the joint sponsorship of SERAI and COMASCI, Brussels, June 19-23, 1967.
8. *Third International Symposium on Fuel Cells,* (Troisiemes Journees Internationales D'etudes des Piles à Combustible), Presses Academiques Europeennes, Brussels, 1969. Proceedings of conference held under the joint sponsorship of SERAI and COMASCI, Brussels, June 16-20, 1969.

LAWRENCE BERKELEY LABORATORY
TECHNICAL INFORMATION DEPARTMENT
1 CYCLOTRON ROAD
BERKELEY, CALIFORNIA 94720